MASTER COPY

UNIVERSITY OF SOUTHAMPTON

AN INVESTIGATION INTO THE PHENOMENON OF HELICOPTER BLADE SAILING

by

Simon James Newman

Doctor of Philosophy

DEPARTMENT OF AERONAUTICS AND ASTRONAUTICS

March 1995

This thesis has been completed as a requirement for a higher degree of the University of Southampton

UNIVERSITY OF SOUTHAMPTON

ABSTRACT

DEPARTMENT OF AERONAUTICS AND ASTRONAUTICS

Doctor of Philosophy

AN INVESTIGATION INTO THE PHENOMENON OF HELICOPTER BLADE SAILING

by

Simon James Newman

This thesis has been completed as a requirement for a higher degree of the University of Southampton.

Blade sailing is an aeroelastic phenomenon affecting helicopter rotors when rotating at low speeds in high wind conditions. This is a potentially dangerous blade motion and the excessive flapwise tip deflections generated endanger the airframe, the flight crew and any personnel working close to the aircraft. This phenomenon is particularly applicable to naval helicopters or those operating off exposed sights such as oil rigs. The research covered an experimental investigation into the effect of an abeam wind flow over a simulated flight deck of a Rover Class Royal Fleet Auxiliary vessel on a Westland Lynx sized helicopter. A theoretical rigid blade method was derived to allow blade sailing to be predicted and a comparison with the experimental results was used as the verification. Blade sailing was obtained and the influence of the deck location of the helicopter was found to be of paramount importance. Agreement of the theory was only possible when a detailed Laser Doppler Anemometer (LDA) survey of the deck flows was performed and used as an input to the theory.

The helicopter rotor system, in reality, is far more complicated than the model used for the wind tunnel tests and the verified simpler theory was extended. Blade flexibility and rotor hub mechanical features were introduced into the theory and the resulting method applied to the Westland Lynx and Sea King aircraft. The semi-rigid rotor is relatively well controlled but the rotor hub construction of an articulated rotor and the interaction with the flexing blades allows blade tip deflections to be generated of an order to strike the fuselage. Results of this analysis was compared with data from a rotor engagement and disengagement of a full scale Puma aircraft.

The present study described in the thesis has lead to an improved understanding of the blade sailing phenomenon. This potentially violent rotor blade aeroelastic behaviour has been investigated in the past but to no great degree considering its importance. Research work has addressed the origins of the aerodynamic forcing and examined simple approximations to the blade dynamic motion. However, the research described herein, to the author's knowledge, is the first time that a detailed qualitative and quantitative survey of the airflow over a ship's flight deck has been married to detailed aeroelastic modelling of the helicopter rotor blade. A rigid blade teetering rotor and ship's flight deck have been tested in wind tunnels and the behaviour of the rotor blades has been accurately predicted using a theoretical model developed for this research. The effect of blade flexibility has been introduced to the theoretical model and the results concur with the reports of the blade sailing occurrences and the operational conditions which are likely to trigger this phenomenon. The development of theoretical models may be used to assess the importance or otherwise of this effect on future rotor designs or the operational limitations of the aircraft.

TABLE OF CONTENTS

LIST OF FIGURES

LIST OF TABLES

LIST OF PLATES

PREFACE

The way to do research is to attack the facts at the point of greatest astonishment.

Celia Green

It all began when I was requested to visit the Royal Aircraft Establishment at Farnborough to discuss a future research contract. Representatives from Westland Helicopters, the R.A.E. and the University of Southampton were present and the subject was blade sailing. Having been steeped in the insular nature of Somerset man this trip was akin to Amundsen's jaunt to the South Pole and was therefore to be taken particularly seriously! Suffice it to say that the work was given to me and my association with the Department of Aeronautics and Astronautics moved from alumni to business partner. Over the years much collaborative work has been achieved and the results are presented in this thesis. Whilst it carries my name, there are many other colleagues involved and who I should like to mention.

The initial work was located in the Dynamics Department at Westland Helicopters in Yeovil and I am indebted to David Balmford, Steve King, Phil Juggins, Eddie Vickers, Len Wilkes and Tom Beddoes from the Aerodynamics Department. I received much support from the R.A.E., particularly Johnnie Johnson and Colin Handley of Bedford together with Alan Jones of Farnborough. The University of Southampton began as collaborators but ended up as my employers. I am grateful to Dave Hurst for his help in conducting the initial wind tunnel tests, particularly his willingness to kipper himself in smoke tracer when determining the flow over a ship's flight deck. To provide the models for the wind tunnel tests and to actually complete them on time I must thank John Mason, Tony Edgeley, Doug Clayton, Bob Stansbridge, Mike Bartlett, Colin Bielby, Jeff Baldwin, Geoff Thomas and Ian McKnight. My technical monitors were Ron Walker and Dick Davies at Farnborough who shouldered much of the load in keeping me on the straight and narrow. Their contribution to the final results has varied between willingly giving their technical expertise to showing considerable restraint in not strangling me when I provided reports a little late!

I offer my sincere thanks to Robin Langley for agreeing to be my internal supervisor. I only hope he does not regret it....too much.

Finally to my dear wife Stella for encouraging me to complete the research and to submit the thesis. She has had to endure considerable periods of loneliness with my disappearing to the study to write some more down and has always come up smiling carrying a cup of tea! To her I dedicate this thesis.

GLOSSARY OF TERMS

A glossary of the definitions used in Chapter 3 are presented below:

V_W	Wind velocity
F_H	Wind - horizontal component factor *(positive from starboard - Figure III.1)*
F_V	Wind - vertical component factor *(positive upward on starboard side & downward on port side - Figure III.2)*
ρ	Air density
a	Lift curve slope
θ_0	Collective pitch angle
A_1	Laterally applied cyclic pitch angle
B_1	Longitudinally applied cyclic pitch angle
c	Blade chord
R	Rotor radius
N	Number of blades
Ω_N	Maximum rotor speed
T_1	Rotor acceleration time
T_2	Constant rotor speed period
T_3	Rotor deceleration time
V_i	Rotor induced velocity
ψ	Rotor blade azimuth angle
K_{ROT}	Blade flapping velocity factor used for teetering rotor
I_2	Moment of inertia of a single blade/cuff combination

I_3 Moment of inertia of a balance weight

U_T Inplane velocity component at a blade section *(positive leading edge to trailing edge)*

U_P Normal to rotor plane velocity component at a blade section *(positive downwards)*

CHAPTER I

INTRODUCTION

It is an interesting thought that the design of the conventional helicopter rotor hub owes much to the design of bridge trusses. The disparaging remarks sometimes made about helicopters being "agricultural in appearance" seem therefore to have justification. In fact, and this is a totally biased view, the helicopter rotor is a most sophisticated example of the aerodynamicists and dynamicists work[1]. In forward flight a section of a helicopter rotor blade passes from high to low Mach number whilst the incidence can vary from stalling angles to the flow approaching from the wrong direction of the trailing edge. This happens several times every second. So to condemn is not to fully understand.

In order to amplify the opening statement it is necessary to consider briefly the aerodynamic environment surrounding a helicopter main rotor. The most noticeable feature of helicopters is the ability to hover. The combination of airspeed over the blades due to rotation about the rotor shaft and the application of pitch to the blades generates the aerodynamic forces necessary to lift the airframe off the ground and to sustain it in a hovering condition. If this were all that was required then the design of the aircraft would be much simpler. The problems arise when the aircraft is required to leave the hovering state and move in a horizontal manner. It cannot possibly be considered in the same context as a propeller since the propeller moves in a direction parallel to the shaft allowing the blades to experience an axisymmetric flow pattern. The helicopter fuselage must move in a horizontal direction which requires the main rotor to move in an essentially edgewise manner. There will be a tilting forward of the plane of the rotor towards the line of flight, but the predominant flight state is an edgewise translation. The rotor now naturally divides into two halves. The advancing side is the semicircle of rotation on one side of the rotor disc where the blades and the airframe are moving in the same direction. The other, retreating, side of the disc has the blades and airframe moving in opposite senses. The advancing side of the rotor disc will therefore have greater flow velocity, and hence dynamic head, than the retreating side giving a disparity in the lift. With a rotor

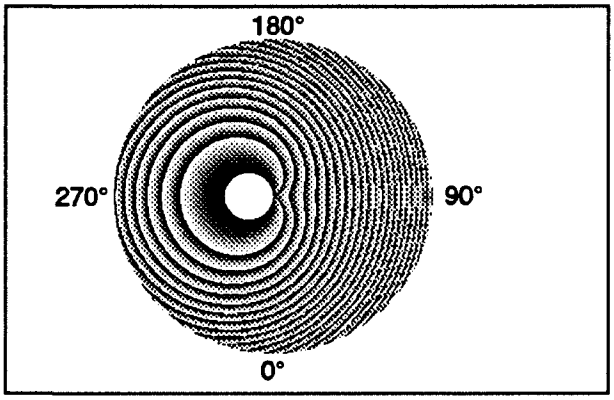

Figure I.1 - Contours of Constant Dynamic Pressure on an Untrimmed Rotor

consisting of blades rigidly attached to the hub, this will cause a rolling moment to be generated. Without any further attention the aircraft cannot sustain flight and will roll onto its back and will be lost. The variation in dynamic pressure is shown in Figure I.1 as a set of contours. The figure indicates an azimuth convention where the zero datum is taken to be over the aircraft's tail boom and increases in the direction of rotor rotation.

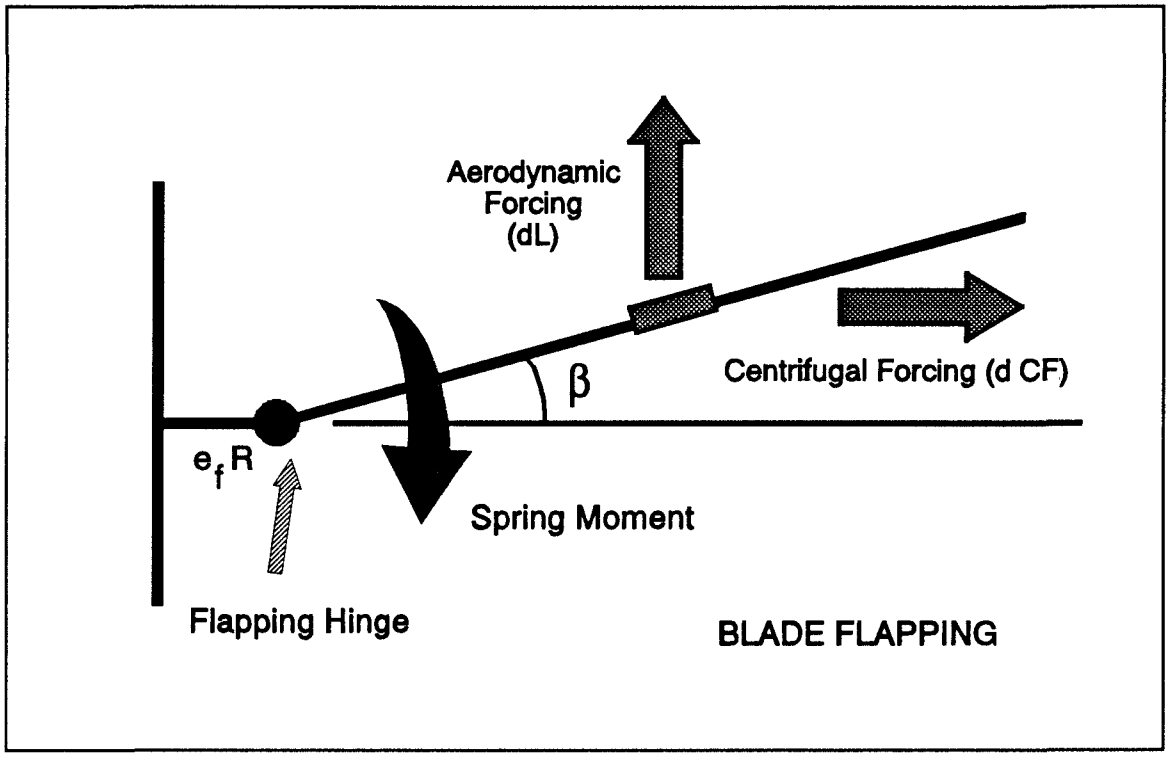

Figure I.2 - The Forces and Moments on a Flapping Rotor Blade

This phenomenon was first encountered with autogyros, an early pioneer being the Spaniard Juan de la Cierva. In his earlier career he was a structural engineer and in his work on bridges he was aware of the use of pinned bridge trusses to support parts of a structure but isolate them from any bending moments. This principle is an ideal solution to the problem of the rolling moment of the helicopter rotor. The blades are attached to the rotor hub using either a bearing assembly, or in recent designs flexible elements and the fuselage is then isolated from the rolling moment. This allows the blades to move out of the plane of the rotor disc under the influence of aerodynamic and centrifugal forces as shown in Figure I.2. The isolation is two way and the blades are not able to be directly controlled from the rotor hub. The forward flight velocities over the rotor disc now require the rotor disc to be controlled in attitude. This can only be accomplished by adjusting the balance between the aerodynamic forces trying to move the blades out of the plane of rotation and the centrifugal forces working in the opposite sense to return the blades to the rotation plane. A change in the blade pitch angle, particularly a once per revolution sinusoidal variation, will cause the blades to flap in such a way as to tilt the rotor disc plane. The use of this so called cyclic pitch in forward flight amends the contours of Figure I.1 to those of Figure I.3.

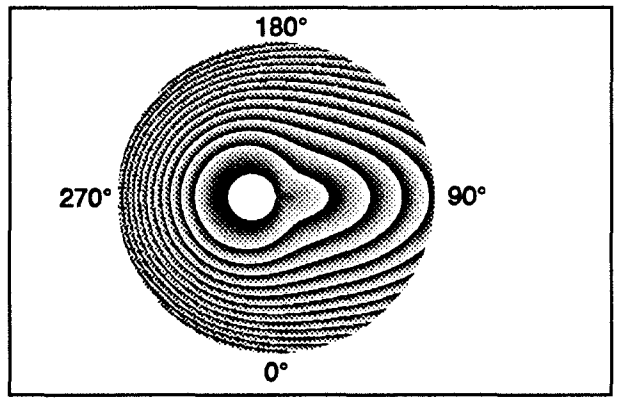

Figure I.3 - Contours of Constant Dynamic Pressure on an Trimmed Rotor

Even though the rotor blades are not rigidly connected to the rotor hub, the considerable centrifugal accelerations found on rotor blade tips (a typical figure is 500-750G) maintains the rotor in an almost flat plane. A small coning angle is seen where the two moments (aerodynamic and centrifugal) are in balance. Provided the rotor speed is maintained at a high level this situation will remain. Under flight conditions, engine governors assure this feature and in the event of an engine failure, piloting techniques allow the aircraft to autorotate keeping the rotor speed to the required level. There are two parts of an aircraft's sortie where a high rotor speed cannot be achieved, those being rotor engagement and disengagement. The rotor must be spun up to speed from rest at the beginning and slowed to rest at the end. Should

the weather be calm then as the rotor speed varies the centrifugal and aerodynamic flapping moments are dependent on the square of the rotor speed. The balance between them is maintained and the blade flapping remains under control. However, if the weather is inclement then the wind speed will rise and the aerodynamic forcing will increase. Since the centrifugal restoring moment is wholly dependent on rotor speed the two effects will go out of balance and the blade flapping can grow quite markedly. When the airframe experiences a horizontal wind then the blade flapping is not too alarming. However, if a vertical wind component is generated through the disc the blade flapping motion will become excessive and the fuselage, flight crew and any ground personnel are under a distinct threat. This uncontrolled blade behaviour is known as *blade sailing*. The rotor disc attitude can be controlled by the use of cyclic pitch but its effectiveness is dependent on dynamic pressure being present over the blades. At low rotor speed this may not be sufficient to prevent the blades sailing.

The dynamics of a helicopter rotor blade can often be achieved by considering the blades as rigid only being connected to the rotor hub by means of a pinned hinge (articulated) or a flexure (semi-rigid). This enables the rotor engineer to locate the rotor disc relative to the aircraft and thereby determine the trim conditions. However, in order to conduct a precise investigation into rotor aeroelastics, the rotor operational envelope, or a study of vibration, the flexing of the blades is an important feature. It is normal practice for a rotor dynamicist to use natural blade vibratory modes for these calculations. Because modern rotor speed governing keeps such a tight control on the rotational speed of the hub and blades, the blade modes will have a fixed set of frequencies and shapes. This enables a set of equations of motion to be set up for them providing a solution for the blade motion.

This thesis maps out a research programme of analysing the blade sailing phenomenon with the aim of creating a reliable predictive technique of its occurrence and the influence on the outside conditions governing its severity. The order of the discussion takes the reader from the initial building of relatively simple blade flapping models under acceleration or deceleration to more sophisticated methods which consider the influence of blade flexibility and the dynamic aspects of the rotor hub construction. The order of the presentation is of increasing complexity, however, it does not in any way reflect the chronological order of conducting the research. To allow the reader an insight into the

progression of the work programme the following section outlines the milestones.

The work was initiated in the late 1970's when the author was a principal dynamicist at Westland Helicopters in Yeovil. The use of helicopters on board ships was becoming common and the effects of the harsh environment in which a naval helicopter is expected to operate were very apparent. Figure I.4 shows typical locations for helicopters on ship's flight decks. As can be seen, they are very exposed and therefore vulnerable to high winds. The EH101 project was in its formative years and the design concept was to operate this large airframe on board a small frigate when the size ratio was leaning ever heavier on the main rotor. The EH101 was to be the replacement for the Westland Sea King, a development of the Sikorsky S61 aircraft, and there were fears that such a large airframe on such a small vessel would create many problems one of which was the occurrence of blade sailing. This phenomenon was well known though, as it turned out, extremely sparsely discussed in technical documents. It has the potential to be fatal, many instances being quoted in various safety journals. The large blade deflections can cause tremendous damage to the tail boom, and with the modern use of weapon sights mounted above the cockpit (the Hughes TOW missile is an example) damage to these areas is now a consideration. The operation of the Boeing Vertol Chinook tandem helicopter in the Falkland Islands conflict of 1982 showed the danger of blade sailing when attempting to operate the helicopter in catabatic winds of the order of 70 knots. The triggering of blade sailing was feared and, until the wind speed dropped below an acceptable level, the rotors were kept turning with crew changes "on the fly" as necessary. The author has heard of instances of rescue helicopters operating in the South West of England which had to spin the rotors up within the hangars because of the ferocious winds which are typical of this coastal area. It was considered necessary to have a predictive model available to aid the design of the future helicopter requirements. The problem was addressed by immediately pursuing a full flexible blade modal analysis[2], gradually bringing in more detailed and sophisticated

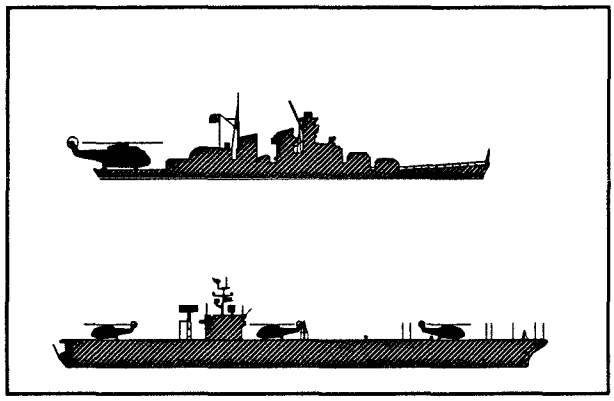

Figure I.4 - Typical Helicopter Flight Deck Locations

theories as they became available. Burton[2] provided the launch pad for this research and a modal model was derived with the purpose of predicting the blade tip flapwise deflection. It was a stepwise integration of the equations of motion with respect to time and a linear, unstalled, aerodynamic theory was incorporated. The model was developed to examine the blade sailing behaviour of the then new composite main rotor blade for use on the Westland Sea King naval helicopter. This blade was designed with approximately one half of the flapwise stiffness of the conventional metal blade. The reduction in stiffness would allow the overtone flapping modes to be more easily triggered. As was discovered during the blade sailing research under discussion herein, these overtone modes, the second flap in particular, are very important to the interaction of the blade cuff with the droop and anti-flap mechanical stops. The results were of use but the main worry of the author was the absence of cold, hard facts on blade sailing occurrences to provide the acid test of the methods.

The lack of test data was not surprising in that the potential severity of this phenomenon demanded that avoidance procedures should be written into the flight manuals and so any occurrence was not deliberately sought. Indeed a recent conversation with a senior naval pilot indicated that blade sailing can be very insidious in nature since a seemingly benign rotor engagement or disengagement can suddenly become a potentially hazardous one as the blades unexpectedly begin the large deflections so typical of this phenomenon. It was apparent that any suitable test data must be obtained from a model testing in the controlled environment of a wind tunnel.

Of the various types of main rotor, the semi rigid rotor found on the Westland Navy Lynx aircraft and the articulated rotor found on the Westland Sea King were those used for the investigation. The semi rigid rotor has distinct advantages as regards analysis as the flexible flapping elements provide the support for the blades at low and zero rotor speed[3,4]. The blade dynamic characteristics remain unaltered apart from the effects of rotational speed. The articulated rotor is more common and at first sight may seem more tractable as the hub does not play a direct part in the blade flapping behaviour. The problem arises when the rotor is rotating slowly and the blades require support to overcome the effects of their own weight. This is supplied by extending physical stops from the hub to act as props for the blades. These devices are called droop stops and as the blade makes contact the dynamic behaviour is of a cantilever blade. In normal

flapping positions the blades are pinned and so the dynamic characteristics of the blades changes with flapping amplitude as they make contact with the stops. Additional restraint is also provided by the anti-flap assembly which prevents upward vertical movement of the blade. Finally, these stops are only required at low rotor speed and are an encumbrance at normal rotor speeds. For this reason they are retracted or extended at preset rotor speeds. The point at which the blade dynamic model must change from cantilever to pinned and vice versa will alter with rotor speed. As is now apparent the modelling of the articulated rotor is much more problematic[5].

In 1985 the author moved to the Department of Aeronautics and Astronautics, University of Southampton and the research obtained two important checks. The first, described by Hurst and Newman[6-9], looked at the wind velocities over a full size naval vessel and comparative tests in the wind tunnel with a 1/120nd scale model. Because of operational limitations the only vessel available for this work was a Rover Class Royal Fleet Auxiliary. All future work on the ship effects were therefore based on this type of ship. The flow over the flight deck of the full size ship was conducted by the Royal Navy and produced essentially data on the frequency spectrum of the turbulence over the deck. The ship had a wind direction of 20° to port and two deck locations were examined. One point lay in the turbulent wake off the ship's superstructure whilst the other lay in relatively clean incident air. The anemometer used was of the golf ball type which is rugged but suffers from a maximum frequency limit of 4 Hz. The comparative wind tunnel tests commenced with a smoke flow survey followed by a quantitative flow velocity survey. This used a triple axis hot wire probe which has a much greater frequency range but suffers from the problem of a cone of acceptance. The probe possesses a solid cone inside of which a flow direction can be reliably measured. With the amount of turbulence found over the model deck, only winds from the rear quarter provided sufficient data to use with any confidence. The forward quarter had a very high proportion of rejected measurements so these conditions were abandoned. However, with the limits on frequency of the golf ball anemometer excepted the frequency spectra obtained at full and model scale agreed satisfactorily. The two sets of results were scaled using Strouhal Number as a basis and both possessed a peak level at 4 Hz. The full size test spectrum declined above 4 Hz more rapidly than the model test results but this is consistent with the golf ball anemometer behaviour. In addition to the power spectral

analysis, mean values of velocity component were also obtained. This showed that with an incident wind at right angles to the ship's centreline, a vertical component of 30% freestream was obtained on the windward side whilst a figure of 10% was appropriate to the leeward side. The influence of deck location indicated by this result is reflected in comments such as those found in Porteous[10].

The second set of information was obtained on 21st July 1988 [5] when the fully instrumented Puma aircraft of the Royal Aircraft Establishment at Bedford performed a rotor engagement and disengagement in a 10 knot wind. This aircraft was pointing directly into wind and so a light wind in a horizontal direction gave a very mild blade flapping behaviour. Since, at that time, no other data existed it provided a welcome comparison with the theoretical model which had been created. The agreement was very acceptable but the victory was not total since the violent essence of blade sailing was not approached.

At this point it was decided to perform a computer database search for published papers on blade sailing however, there seemed to be no papers existing of any use. In due course the keywords were changed to tunnel strikes which is that used in the United States. The subsequent computer search again provided virtually nothing but a short M.Sc. project conducted at the Naval Postgraduate Centre in Monterey California. However, this reference provided the trigger for a series of references which describe the work conducted in analysing the problem of blade sailing for a shipborne helicopter with particular emphasis on the effect of the wind flow over the ship on the rotor blade behaviour[11-19].

Carico et al[11] describes a study of flight testing and simulation. It discusses the problem of blade strikes and the somewhat ad hoc method of fuselage protection using the so called *"greasy board"*. This comprises a wooden framework placed above the top surfaces of the fuselage and physically deflects the blades over the structure should they fly too low. Hofman and Fang[12] discusses, generally, the operation of helicopters on ships whilst Roades and Val Healey[13] investigates the airflow characteristics over ship's flight decks and the interaction with a helicopter rotor. Roades and Val Healey[13] describes the changes in gross flow behaviour with the effects of separation and reattachment. It also studies the possibility of using flow deflectors placed above the hangar doors. Johnston[14] is a general discussion of shipborne helicopter operations featuring interference of hangar

doors, recirculation, vortex ring state and the danger of high winds triggering blade sailing. The influence of the flow over the ship's superstructure is tested in Johns and Val Healey[15] using a wind tunnel. The results show the importance of the yaw orientation of the wind to the ship's centre line and the influence of the ship superstructure over the flight deck. The flow over the ship's deck is the main thrust of the work described in Narveson[16] and Val Healey[17]. Narveson[16] is interesting in that the blade sailing phenomenon is discussed at length. The Boeing Vertol H-46, Sea Knight, tandem rotor helicopter has suffered considerable problems with blade sailing with the rear rotor blades striking the top of the fuselage. The problem is exacerbated since the built-in shaft tilt angle moves the forward half of the rear rotor disc downwards and therefore closer to the fuselage. It states that up to the middle of 1989, this type of helicopter had suffered from over 100 mishaps due to tunnel strikes. The damage suffered has varied from superficial to the complete loss of the aircraft. It should be noted that this aircraft is now out of production and therefore cannot be replaced. The rotor speed at which blade sailing is likely to occur is quoted as 20% NR (NR is the conventional notation for rotor speed, i.e. 100%NR is normal operating rotor speed.). This is a higher value than the research described in this thesis but not by very much. He used a C.F.D. method (Phoenix code) to examine the flow over the flight deck, the roof of the hangar in particular, in an attempt to expand the flight envelope of the H-46 by reducing the turbulence level and the size of the flight deck separation zones. The effect of Reynold's number on the comparison between a full size flight deck and the codes were discussed. The method appeared to assume that the flow left the hangar parallel to the roof line. He cites Val Healey[17] as a study of simulating the helicopter ship interface as an alternative to current methods of determining safe operating envelopes. The Phoenix code was applied, Woolman[18], to optimise the performance of the deflectors. Moran[19], took the flow over the ship as an input to a method of analysing the blade sailing behaviour of a rotor. This was a rare occurrence of the combination of ship flow data and the ensuing rotor blade behaviour. The blade dynamics was modelled using a DYSCO code (DYnamic System COupling program) provided by Kaman Aerospace. It uses a Runge Kutta time marching method to integrate the equations of motion including those of the undercarriage. The blade droop stops were modelled using damping elements. Convergence problems resulted in a rigid blade model being used but only bending

moments were discussed and blade tip deflection results were absent. The importance of blade torsional effects was highlighted. Lloyd[20] is a paper which also discusses the operational problems of a shipborne helicopter, but makes the interesting comment that ship motions are relatively unimportant.

The other area which produced a reasonable number of references[21-23] is that of the Dynamic Helicopter/Ship Interface. This is concerned with the operation of a helicopter when flying close to a ship's flight deck, together with the take-off and landing phases of a sortie. The wind flow over the ship's flight deck is important to this topic as well as blade sailing. These references tend to concentrate on the effects along the flight line of the helicopter to and from a ship using hot wire anemometers for the test sensors[21].

It became apparent that the only way to obtain comparative results for the developing theories was accurate model data of a rotor blade placed in the most adverse situation which could be expected in operation. To accomplish this, a model kit helicopter was purchased and suitably modified. This was mounted on a wooden simulation of the flight deck of a Rover Class Royal Fleet Auxiliary vessel with the wind from an abeam direction. The detailed discussion of the wind tunnel model and its testing is described in the technical reports[24-26] and papers[27-31]. The hot wire tests[6] had shown that an abeam wind direction gives the greatest value of vertical wind component. Different deck locations were tested together with differing rotor speed variations. The rotor and hub of these types of kit are of a two blade teetering type and the blades can be sensibly regarded as stiff. (For later testing one blade was removed and replaced by a counterbalance weight.) Because of this a second theoretical model was developed to predict the blade behaviour of this type of rotor. The wind data was based on a horizontal component over the ship's deck with appropriate vertical components superimposed on the windward and leeward sides of the deck. The comparison was good in some instances but completely in error in others. A brief tuft study showed that the simplistic model of wind flow over the ship's deck was not sufficient and that more detailed and quantitative data should be sought. The cone of acceptance of a hot wire anemometer precluded its use in mapping the ship flow. The only viable alternative was the Laser Doppler Anemometer installed in the largest wind tunnel of the Department. A reduced ship model was required and a detailed survey completed. The data was then used as input to the theoretical model with good agreement over all conditions and rotor configurations.

Amongst the various papers highlighted by the literature search, one paper, which did not show up on the search, was obtained, Willmer[32]. This paper discusses the development of a blade sailing model and its application to contemporary aircraft operating off ships. It provides an interesting comparison with the methods used in the present research and the results obtained. The discussion of this paper[32] encompasses the unconventional approach that must be taken to sensibly model blade sailing.

A normal aerodynamic model of a helicopter rotor makes use of the fact that the rotational speed of the blades is mainly high, especially compared to the induced downflow. The incidences are normally below the stall angles of the blade aerofoil section and so unstalled aerodynamic theories can be invoked. The rotor speed is usually governed closely to avoid vibration problems and blade flapping motion is normally small, 5° being a typically large deflection. The forward speed is normally much smaller than the rotor tip speed, as reflected in the advance ratio, so the reverse flow region on the retreating side of the disc is normally within 30% of the rotor radius, much of which is taken up by the rotor hub and blade attachments. The aerodynamic complication of the reverse flow region is therefore small and can often be neglected. The high degree of centrifugal force generated on the blades usually allows the weight of the blades to be ignored. The constancy of the rotor speed permits the tension forces in the blades to remain essentially constant as should the aeroelastic behaviour of the blades. With the variation of the rotor speed during engagement and disengagement all of these assumptions require careful justification, and in many cases can only be justified because of furnishing a tractable solution. Indeed at very low rotor speeds and high wind speeds, the reverse flow region extends to virtually the entire retreating side.

The equations of motion of the rotor blades are set up in Willmer's paper assuming that they are articulated and remain in contact with the droop stops at all times and therefore behave as a cantilever. The blade is considered unstalled at all times and a constant value of lift curve slope is adopted. The reverse flow region is handled by assuming that the retreating side of the rotor disc generates no lift. These assumptions are made to allow a solution to be obtained by analytic techniques. In the full blade sailing analysis to be described in this thesis no simplifying assumption was felt to be justified and a closed form solution was therefore out of the question. For this reason a numerical integration method was adopted from the outset.

Willmer's investigation involved two contemporary aircraft. They were the Westland Whirlwind, a derivative of the Sikorsky S55 and the P531, originally a Saunders Roe design which eventually became the Westland Wasp. The analysis commenced with the blade response to a horizontal wind. As previously mentioned this produced small blade tip deflections of the order of 12-24 inches for the P531 and 24-36 inches for the Whirlwind. This was a 30 knot horizontal wind and a rotor speed of 2 rpm. Considering the static deflection of the Whirlwind blade tip is of the order of 42 inches these blade deflections are not hazardous. For each calculation the rotor speed was held constant.

The effect of the rolling of the ship was next considered. The effect was limited to the horizontal wind now having a component in the vertical sense. From results of this research a vertical wind is known to be worse than a horizontal one, and so not unsurprisingly greater tip movement of the blades was predicted.

The influence of the ship's deck and hull on the incident wind flow was next discussed. This is dominated by the "cliff edge effect" caused by the wind impinging on the windward side of the ship's hull. The flow is forced up over the deck creating the upflow and hence the vertical component of the wind through the rotor disc. The flow was assumed to be symmetrical in that the upflow on the windward side was matched by a corresponding downflow on the leeward side. A cylinder was used as a model for this flow. The P531 had comparatively well controlled blade flapping of 12 inches with a 15° roll angle and a 25 knot incident wind speed. However, the Whirlwind achieved blade tip deflection of the order of 48-60 inches, and the existence of blade sailing is predicted. The use of cyclic pitch to control this excessive flapping was seen to have merit.

The discussion then progressed to examine effect of the wind on the rotor thrust. Whilst this was not a major component of the paper one comment as very pertinent to the wind tunnel test results. The behaviour of a P531 aircraft when operating from the ship H.M.S. Dauntless was examined in the light of the upward wind component generated by the cliff edge effect on the windward side and the corresponding downflow to leeward. The thrust increase to windward was as expected but the thrust decrease to leeward was not as apparent in comparison. This immediately indicates the fact that whilst an appreciable upflow is created to windward, the flow leaves the deck in a more horizontal direction and the flow is definitely not symmetric. *(This conclusion, drawn from an ancillary observation, is borne out by the two sets of wind tunnel tests carried out in the*

present research.)

The final piece of analysis, conducted by Willmer[32], was of a more realistic appraisal of an accelerating rotor. The blade was again considered as a cantilever which indicates that it remains permanently on the droop stop. The effect of changing rotor speed on the blade dynamic characteristics is achieved by a variation in the EI value applied to the acceleration term in the equation of motion. A time marching technique was used where during each time step all variables were held constant allowing integration of the equations. A time step of 0.02 seconds was used. The results of the study were confined to the Whirlwind and very severe blade flapping excursions were predicted. At a rotor speed of 2 rpm a tip deflection of 108 inches was obtained although this value dropped considerably to 36 inches at 4 rpm. This analysis has hence obtained strong evidence of the existence of blade sailing and its potential severity.

This reference was revisited after the completion of the research programme and it is very interesting to see how many of the conclusions of the present work tie in with Willmer's remarks. The susceptibility of articulated rotors to vertical winds in particular and the asymmetry of the flow over the deck of the ship. The effect of this asymmetry was amplified by Porteous[10] in the importance of aircraft placement on a deck.

This is corroborated by King[33] where blade tip deflections of 35"-45" are predicted for a Lynx type semi-rigid rotor, whilst figures of 130"-180" are obtained for an articulated rotor like the Sea King. In view of the later results, the Sea King figures are considered high but the analysis in King[33] used a simple rigid blade with a linear, unstalled, aerodynamic model.

If the conclusions of the literature search are distilled, then the overall impression is of a known and documented problem and attempts to predict it have occurred. The difficult aerodynamic conditions for deck operation of a helicopter have been observed and attempts to theoretically model the phenomenon have been made. However, it is felt that the present research, described herein, attacks the problem directly and mathematical tractability has not been allowed to interfere with the modelling of the physics of the problem.

The influence of the ship on the air flow surrounding the flight deck is shown in the results of the wind tunnel tests. They highlighted the change in character of the blade flapping motion as the helicopter location on the flight deck moved from windward to

leeward. The theoretical model using wind data from the LDA traverses produces very good agreement of the blade behaviour and the wind tunnel data and the theoretical modelling are seen as a combined package. The more demanding flexible blade method takes this theory and observes the effect of blade structural properties and the influence of the hub restraint geometry.

As already mentioned in this introduction, there is a scarcity of published research on the blade sailing phenomenon which is surprising considering the unease with which it is acknowledged by pilots. This thesis provides a statement of results and conclusions of a broad attack on the problem. It answers many questions but some avenues still need to be pursued. It is the author's intention to continue to investigate the problems highlighted and still unanswered. It is hoped that recent contacts with the Aeronautical Research Laboratory in Melbourne, Australia and the University of Pennsylvannia will bear fruit. The thesis is not the bible on the subject but it is fondly hoped that it will provide a springboard for research in the near future.

MODELLING PHILOSOPHY

The thesis will describe the assembly of a theoretical model and the conducting of wind tunnel tests. However, to discuss these features one by one will not set the scene as to the particular problems posed by modelling the blade sailing phenomenon. Therefore to introduce these special difficulties and place them in context a brief outline of the philosophy behind the methods used is presented here.

The helicopter rotor blade undergoes a complicated set of aerodynamic conditions during flight. Much of this is due to the conflicting requirements of a rotor which can both hover and translate in an essentially edgewise direction. The rotor blade experiences a periodic variation in inflow velocity, and executes a series of rotations about the rotor hub hinges or flexible elements. All of these make the derivation of the equations of motion for the rotor blades complicated and requires a high degree of sophistication. In simpler aerodynamic models, closed form solutions can be achieved, but if any amount of difficulty is introduced, the analysis cannot be solved exactly. So it is apparent that some form of numerical integration of the equations of motion must be used.

Because of the rotational speeds normally encountered with helicopter rotors and the corresponding aerodynamic and dynamic forces generated, it is permissible to make a number of simplifying assumptions. However, in the study of blade sailing the analysis of a rotor during acceleration or deceleration requires that certain assumptions, valid for normal rotor speed operation, are no longer admissible. The centrifugal accelerations felt by a rotor blade during normal rotor speed operation allow the effect of the blade weight to be sensibly ignored. With low rotor speed operation, this approximation is unacceptable and blade weight must be accounted for in the equations of motion and is included in the right hand side forcing term.

The use of blade modes for the description of the blade deflections has no problems for normal rotor speed operation as the reference speed for the modes is usually chosen to be the operating rotor speed and no corrections need be applied. However, as the rotor speed changes, the effect of variations in the blade tension need to be included to correct for this in the equation of motion.

Under normal operating circumstances, the rotor speed is held within a close region about the design value. This allows a small angle approximation for the incidence to be justified

and the ignorance of the reverse flow region to be defensible for all but the highest forward speeds. The incident wind direction is from ahead with a comparatively small downflow through the rotor disc. The blade flapping motion is kept to within typically 5° of amplitude with a period of once per revolution without any influence from the rotor hub. If the rotor engagement/disengagement manoeuvres are examined then many of these factors do not apply and the approximations which could be justified are not now applicable. The blade flapping behaviour is now at the potential mercy of a large aerodynamic forcing without the controlling influence of a substantial centrifugal force field. Large blade flapping excursions must now be envisaged. At low rotor speeds the rotational inflow velocity will be relatively small. If this is coupled with the severe wind velocities which are to be examined, the advance ratio becomes extremely large, exceeding unity in the worst situations, and therefore the reverse flow region can become virtually the entire retreating side of the disc. This cannot be ignored and the reverse flow region must be catered for by the aerodynamic theory. In consequence the aerodynamic model must cater for aerofoil sections in separated conditions from the point at which the flow breaks away on the suction side to conditions of deep stall. The difficulty of the aeroelastic analysis is therefore exacerbated. For these reasons, any attempt to obtain a closed form of solution was not contemplated and the solution of the equations of motion was numerical virtually from the outset. Various attempts at a more mathematically precise method were tried but the amount of realistic analysis which had to be discarded rendered the analysis untrustworthy at best and meaningless at worst.

As already mentioned, under normal rotor operation, the rotor speed keeps the blade flapping excursions to a small level of the order of 5°. This, when transferred to modal displacements also means that the various modal responses are small. It is therefore relatively easy to justify the use of a linear combination of modes for the overall blade deflection because the necessary linearity of the method can be successfully argued.

With the amount of blade movement and deformation generated with an occurrence of blade sailing the justification for linearity becomes a more difficult point of discussion. The large blade deflections will cause not only the difficulties of non linearity but also the limitation of blade length. By using only the flapwise deflections the modal approach will always put a point of a blade at the same radial position which is not possible for a large tip deflection and a fixed blade length (along the arc). Therefore the method

generated in Chapter 6 assumes that an individual point of the blade moves perpendicular to the rotation plane. To give scale to this assumption, the largest blade tip deflections produced by the theory (for the Westland Sea King) will give a 2.5% error in the blade length measured along the arc. Therefore, the approximation is relatively small and it is considered justified to use only the flapwise component of the modes in the development of the analysis.

Another important factor is the influence of blade torsion during these large blade tip deflections. The blade data was derived using a coupled blade mode program. Each blade mode will have flap, lag and torsion components, however, the modes can be identified as predominantly one of these three degrees of freedom. Up to the first four flapping blade modes were taken, the lag motion was ignored but the torsion in each mode was used during the program operation.

Each occurrence of this feature is described in the appropriate section but the type of rotor hub configuration plays an important part in the incorporation of the blade torsion motions. For a semi-rigid rotor head the blade deflections are not interfered with in any way and the amount of blade torsion is factored appropriately. With an articulated rotor the contact of a blade cuff with a mechanical flap restrainer causes a change in the kinematics of the blade pitch control system. With the blade free to flap any blade pitch/flap coupling (δ_3) will be generated by the geometry of the control linkages. When contact is mode with a stop, the control system mechanically locks up and the blade then flexes in an elastic manner. This will normally cause the blade pitch/flap coupling to become virtually zero, which is the position taken with the theory. The program allows for a specified amount but for all the calculations in this thesis, the δ_3 was set to zero for a blade in contact with a stop.

Therefore, any blade sailing method must address these extra requirements.

Although the thesis will describe the rigid blade modelling first, the decision to go for a time marching technique was determined by the more complicated flexible blade aeroelastic model. There are several time marching techniques available but the choice of fourth order Runge Kutta[34,35] was made on the basis of two points:

(i) It is a well tried and tested method. It is acknowledged that it has limitations but these are well known and can be circumvented.

(ii) The exact method used is not the important fact. It is a means to an end with the final resulting predictions of the blade behaviour, and their accuracy, being the ultimate goal.

Once this decision was made the blade flapping equations can be assembled.

The research developed aeroelastic models to predict the blade motion. However, it must be made clear that the modelling used to compare with the wind tunnel tests described in Chapter 3 were of a blade or blades freely hinged at the rotor centre line and assumed to be elastically rigid. This is to accurately model the Kalt Cyclone rotor head and blades used in the tests. When the method is applied to the Westland Lynx, Sea King and Aerospatiale Puma helicopters, blade flexibility is included in the analysis.

The development of these for the rigid blade is shown in Chapter 3. Even thought the blade flapping motion is simplified by the assumption of rigidity, the aerodynamic model must be capable of handling grossly separated flow conditions. An empirical model was available as outlined in Beddoes[36] whereby the attached and stalled aerodynamic lift coefficient variation with both incidence and Mach number could be recreated. Naturally each set of data only applies to a specific aerofoil section but that available was of NACA 0012 which is a typical aerofoil section for helicopter rotor blades of the 60's and 70's.

The severity of blade deflections with a fully articulated rotor has been cited. The freedom of the blades in flap are restricted, at the lower rotor speeds, by means of mechanical stops, see Schafer[37]. The contact of rotor blades with these stops changes the blade from articulated to built-in. Hence the interaction between the blades and the stops requires careful consideration. Leone[38,39] investigates this problem. In[38] an attempt is made to simulate an incident with an H-46 helicopter. *(This reference shows the concern of helicopter designers in the potential damage to articulated rotor blades and hubs caused by repeated and heavy contact of blade cuffs with droop or anti flap stops.)* It is situated on the flight deck of an oil rig positioned at an angle of 35° to the deck centre line and the wind coming from the rear of the aircraft. The wind was considered to approach the deck at a vertical inclination angle of 15°. The blade was considered to flap up and contact the upper (anti-flap) stop and then descend to contact the lower (droop) stop. The blade tip movement was calculated to be 81" upwards followed by 65" downward. A 62" tip deflection will give a tunnel strike. Only the fundamental bending flexural mode was used. Moran[19] cites this reference but regards the use of an oil rig

model to be of no use in the modelling of the flow over a ship because of the absence of the vertical sides of the hull.

In Leone[39] a theoretical and experimental appraisal of the effect of blade/droop stop contact was considered. The contact was achieved by means of high values of cyclic pitch coupled with a low collective pitch setting. Differences between the results was considered to be due to not including the second flapwise mode. (This provides interesting supportive evidence to the results of chapter 6.) A linear aerodynamic model was used which allows for full separation of modes and the blade characteristics change between pinned-free and cantilever-free as the blade flapping is free or constrained by a stop respectively. The rotor motion was considered at successive rotational speeds and a periodic solution for each speed obtained.

LAYOUT OF THESIS

The technical content of the thesis commences with Chapter 2 where the description of the sets of wind tunnel tests is made. The first set was used to determine the blade behaviour of a model rotor placed on a simulation of a ship's flight deck. The helicopter model was based on a Westland Lynx sized airframe and the ship was scaled to a Rover Class Royal Fleet Auxiliary. Blue Rover was used for the deck size, this being important as Gold and Black Rover have different deck sizes to the rest of the fleet. The model construction is described together with the instrumentation used and the calibration results. The results are presented highlighting the importance of deck location. Preliminary calculations were undertaken which showed that a simplification of the flow pattern over the ship's flight deck could give acceptable results for a very limited number of deck positions. For the remainder, the agreement was totally unacceptable. For this reason a detailed survey of the flow over the deck simulation was advisable. An initial attempt was made with the ship model being used but the degree of flow separation over the deck and the ensuing turbulence rendered pitot tubes and hot wire anemometers of little use. The only viable solution was Laser Doppler Anemometry and use was made of the Department's largest tunnel which has this equipment. However, the size of the existing model was scaled for use in a settling chamber whilst to use the LDA the working section of the larger tunnel must be used. For this reason a smaller scale model (2.8:1) was constructed for this experiment and flow surveys were made. Problems with flow seeding were encountered which required a second day in the wind tunnel with appropriate modifications to increase the number of samples per burst. The flow patterns and turbulence levels are then presented.

Chapter 3 begins the derivation of the aeroelastic theoretical models developed to predict blade sailing and to compare with the previous wind tunnel results. As previously mentioned, the construction of the helicopter model rotor head and blades made a rigid blade theory applicable for this part of the research. Initially, a simple one degree of freedom flapping model was constructed which enabled the two and one blade teetering results to be viewed. The results of this part of the research are then presented and the amount of agreement discussed.

Chapter 4 extends the theory to permit blade flexibility by using a modal approach. This

proved important for the semi-rigid rotor but vital for the articulated rotor. This requires the provision of droop and anti-flap restrainers being fitted to the rotor hub and therefore requiring modelling. The method of rotor speed variation and the accompanying calculations are presented.

Chapter 5 takes the modal based theory and applies it to the semi-rigid rotor of the Westland Lynx aircraft. Blade modes supplied by Westland Helicopters Ltd. are used in the calculations.

Chapter 6 uses the modal model on the articulated rotor of the Westland Sea King naval helicopter. The influence of blade flexibility is shown to be extremely important for this class of helicopter rotor hub because of the use of mechanical blade flapping restrainers. The increase in blade movement is highlighted and the interaction of the blades with the hub is discussed in detail. Again, the blade modes, supplied by Westland Helicopters Ltd., are used in the calculations.

Chapter 7 concludes the thesis with a summary of the conclusions of the complete work and the author's view of where future work is necessary. Throughout the research a strange feeling was always present where the blade sailing phenomenon was always cited as a severe operational problem, particularly for naval helicopters, whilst the amount of work being carried out seemed inappropriately small. An attempt is made to overview the knowledge base at the time of writing and to put forward the author's opinion on where the direction of future work is best placed.

CHAPTER 2
WIND TUNNEL TESTS OF THE ROTOR MODEL

2.1 INTRODUCTION

This Chapter describes the various wind tunnel tests conducted to observe the blade sailing behaviour and to determine the aerodynamic influence of the ship on the helicopter placed on its flight deck. They provide an insight into the driving forces and furnish data to use as a comparison for the predictions of the emerging theories.

There are two wind tunnel tests described in this chapter, set S1 being the first investigation. They used the rotor only in the two bladed teetering configuration and with nominally zero rotor thrust. The contribution to this chapter from the S1 tests is confined to a description of the model design and construction together with the operating procedures and test conditions completed. The second set of wind tunnel tests (S2) were conducted in the light of experiences gained with the S1 tests. The rotor was operated in one or two bladed configurations with zero rotor thrust and collective pitch of 6° settings. The description of the two sets of tests is as follows:

- The model design and operation is discussed (S1)
- The initial calibrations are presented with any changes from S1 to S2
- The rotor modifications for the S2 runs are described
- Test conditions for the S2 tests described
- Conclusions from both the S1 and S2 tests are presented after their respective test descriptions

Until the wind tunnel tests were undertaken, experimental work had been restricted to a short investigation of rotor accelerations and decelerations in mild wind conditions, using a Puma aircraft. The blade flapping excursions achieved were, not unsurprisingly, very limited and whilst this showed sensible agreement with the theory it did not cause the phenomenon to occur with its customary severity. As it is both unrealistic and foolhardy to attempt a blade sailing investigation with a full scale piloted aircraft, a wind tunnel test at model scale is the only available means of inducing the severe blade movement expected with low rotor speed and high wind conditions. As has been discussed, the most obvious situation which is likely to trigger blade sailing is shipborne operation. Previous theoretical work indicated that the wind coming from the abeam condition (horizontal and perpendicular to the ship's centre line) was likely to produce the most dramatic effects. In consequence this situation was used as the basis of the testing sequence.

The previous work on this topic described in Newman and Hurst[7,8] has examined the Rover Class Royal Fleet Auxiliary vessel as the operating platform, and for consistency this was repeated in the present wind tunnel tests. A wooden scaled mock up of the stern section of this class of ship was built and installed in the large settling chamber of the Department's 7ft x 5ft wind tunnel. Again for consistency with previous work, the Westland Lynx helicopter was the chosen aircraft on which to use as the model. The cost of scratch building a rotor model for this would have been considerable and so an alternative and more economic solution was sought. A suitable radio controlled helicopter kit was available which was of the correct relative dimensions of the Westland Lynx aircraft and which cost only £300. Modifications were necessary to enable recording of the rotor speed variation as well as the blade behaviour. The rotor, in common with most model kits, has two blades on a teetering hub. This is not the semi-rigid type of rotor hub found on the Lynx aircraft, but as this was a first examination of the blade sailing induced on a model ship's deck, this was not considered too much of an approximation. The theory can also be modified, if necessary, to look at a teetering hub.

A test sequence was devised to enable what was thought to be the most important effects to be investigated. This was completed successfully, without destruction to the model as had, at first, been feared.

2.2 FIRST WIND TUNNEL TEST (S1)

The first wind tunnel test required the design, manufacture and calibration of the ship and helicopter models. These various components are described below.

2.2.1 WIND TUNNEL

Settling Chamber

In order to use the helicopter kit for testing, the ship's flight deck must be of appropriate size to scale correctly. The sizing of the ship's carcass is discussed later in the report but suffice it to say that the use of the working section was prohibited because of the need to keep the rotor/tunnel interference to a minimum. The only practical way was to install the entire model in the settling chamber of the wind tunnel. The installation is shown in Plate II.1. Monitoring of the model operation could be achieved by using the porthole in the side of the tunnel wall, see Plate II.2, which also shows the model control system and data acquisition setup.

Wind Speeds

The rotor was operated with a collective pitch value close to the no lift angle of the blade aerofoil section. A helicopter rotor, in reality, when running up or down uses nominally zero rotor thrust conditions. Several runs of the rotor model were made before the wind tunnel tests began to establish the motor's performance in driving the rotor. At the collective pitch setting of -1.7°, which remained fixed for the entire test sequence, and zero cyclic pitch, a rotor speed of 650 rpm was achieved. It seemed sensible to use 600 rpm as the maximum, so tests were conducted at 300 and 600 maximum rotor rpm. During low speed operation in high winds, the helicopter main rotor achieves advance ratios far in excess of those occurring in normal flight. In order to keep these values in sensible agreement with a 50 knot wind, tunnel speeds of 2.5 and 5 metres per second were selected.

2.2.2 SHIP MODEL

Rover Class Royal Fleet Auxiliary

The Rover Class Royal Fleet Auxiliary vessel has been used for all work on this blade sailing investigation. The initial part of the work conducted a brief investigation into the wind and turbulence characteristics over the flight deck of a ship at full scale. The available ships were naturally chosen for us, and the Rover Class was the vessel selected.

Sizing

The Kalt Cyclone helicopter model, when fitted to the base plate, has a height/rotor diameter ratio very close to the Westland Lynx aircraft and was therefore selected. In order to maintain appropriate sizes for the ship, the Lynx on a Rover class flight deck was selected for the sizing. The model helicopter was determined by the size of the kit chosen, and the ship model size was scaled appropriately.

Table II.1 - Full and Model Scale Ship Dimensions

	SHIP/MODEL DIMENSIONS	
	Full Scale	Model Scale
Deck Length(ft)	84.65	9.26
Deck Width(ft)	52.74	5.77
Deck Height(ft)	35.43	3.88

Construction

The ship model was in essence a wooden carcass constructed from plywood using deal as corner pieces, see Figure II.1. It was required to move the helicopter across the deck in a direction perpendicular to the ship's centre line. As the case of an abeam wind was being tested, the helicopter model movement was along the axis of the settling chamber. A slot in the top of the carcass was included and the helicopter model slid within this slot on rails supporting the baseplate, see Figure II.2. A clamping arrangement was provided and secured by four Allen bolts. When the baseplate was secured, wooden panels were then fitted to blank off the unused portions of the slot leaving a complete flight deck with the model standing on it. These panels were secured with woodscrews into the rails on each side of the slot. As a fair degree of model movement was needed to complete the test programme, rapid release and refixing of the baseplate and wooden panels was necessary.

2.2.3 HELICOPTER MODEL

Requirements

The requirements of the model were to operate the rotor during both accelerating and decelerating phases whilst subjected to a wind over the deck.

The sizing of the chosen helicopter model is tabulated below, together with the Westland Lynx. The choice of the model was governed by the height/rotor diameter ratio.

Table II.2 - Comparison of Helicopter Model Size with a full size Westland Lynx Helicopter

	HELICOPTER DIMENSIONS WESTLAND LYNX/KALT CYCLONE	
	Full Scale	Model Scale
Rotor Diameter(ft)	42.0	4.74
Rotor Height Above Deck(ft)	10.5	1.2
Height/Rotor Diameter Ratio	0.250	0.253

Plate II.3 and Figure II.3 shows the modified Cyclone kit fitted to the ship model and installed in the wind tunnel.

Kalt Cyclone

The Kalt Cyclone is an off the shelf kit of a four channel radio control helicopter model. It has a two bladed teetering main rotor system, and has both collective and cyclic pitch control.

Modifications

The main fuselage, main rotor hub and controls were the essential components used. The tail boom, tail rotor assembly, and undercarriage were not required. The main fuselage frame was made from a composite material and the four bolt fixtures intended for the skid undercarriage attachment were used to attach the frame to a aluminium plate. This plate forms the part of the ship's deck immediately beneath the model and by means of the brackets fixed to the carcass of the ship's deck allowing the model to be positioned

laterally with respect to the ship by sliding it along the rails and then fixing it by tightening two bolted aluminium plates which gripped the rails. See Plate II.4. In order to record the rotor electronic signals for hub teeter and blade pitch angles, a slipring assembly had to be installed. This was fitted to an extension of the main rotor shaft below the hub and within the main fuselage frame. See Plate II.5. The model will usually be powered by a glowplug engine of about 10cc capacity. Such a powerplant is totally unsuitable for this model for various reasons. The vibration will disrupt the electronics, the pollution of the exhaust will contaminate the model instrumentation, and the power variation of the motor with speed will not possess the necessary control for the intended tests. For these reasons, electric power was chosen. The motor could not be accommodated in the fuselage body since the space reserved for the motor in the original model was occupied by the slipring assembly. This was not a problem for the tests since the motor could be fitted below the base plate, which placed it below the ship's deck level. See Plate II.6. The motor was thus placed within the wooden carcass forming the ship's flight deck. The drive was still via the model's original gear train, and an extension was fitted to the first pinion which ran via a double ball race through a hole in the aluminium base plate to connect with the electric motor via two spur gears. See Plates II.7 and II.8, and Figure II.4.

Electric Motor

An investigation was undertaken into the type of electric motors available with similar performance to the glowplug engine. A rotational speed of 10,000 rpm with a power of 0.5 HP was best provided by a standard spin-dryer motor which was purchased from a local washing machine repair shop! It also was a very economical purchase. Modifications were necessary in order to provide the necessary control, and these were a separation of the armature and electro-magnet circuits.

Rotor Speed Control

A repeatable set of runs was the intended goal of the tests, and from the outset an automated rotor speed control was designed.

The variation of the rotor speed was:

A steady run up to speed from rest (T1).

A period of constant rotor speed (T2).

A steady slowing to rest (T3).

This variation was characterised by the three time periods described above (T1, T2, T3), and the maximum rotor speed required. This variation is shown in Figure II.5.

Signal Output

The control box supplied the following data during the tests:

Rotor Speed - An RS 631-632 optical modular shaft encoder was fitted to the rotor shaft extension to provide the rotational speed of the rotor. It consists of a stainless steel disc with radial slots cut into it. A Light Emitting Diode (LED) illuminates the disc and the slots trigger photodetectors. An amplifier delivers a pulse of given width and magnitude which is then passed through a very low pass filter. This reaches a stable state giving a linear variation of voltage with rotor speed.

Rotor Azimuth - An additional single slot is cut into the disc which also triggers a second photodetector to act as a rotor azimuth marker. It is set to trigger a pulse at a rotor azimuth angle of 180°(for the master blade ‡).

Blade Teeter Angle - The hub position is measured by two linear potentiometers mounted vertically on the hub centre. The wipers are located in contact with the top faces of the pitch bearing assemblies. One potentiometer is required to record the hub teeter position, but this would bias the hub teeter position by means of the spring load on one side of the hub. To eliminate this problem a second (dummy) potentiometer is placed on a opposite side of the hub cancelling out this moment. See Plate II.9.

Blade Pitch - The pitch angle of the master blade was sensed by means of a linear potentiometer. A direct connection to the blade pitch horn is unsatisfactory since it will be affected by the hub teeter movement. To avoid this effect, the potentiometer wiper was connected directly to the control system below the rotor hub by means of a rod. See Plate II.10. This requires the use of a long throw potentiometer which can be seen above the rotor hub in Plate II.9.

The output of these four channels were recorded on a RACAL Store-4 tape recorder.

The control installation can be seen in Plate II.2.

---

‡ The master blade is on the same side as the long throw potentiometer. The blade was marked with an "M" on the blade root.

2.2.4 TESTING SEQUENCE

Calibration

Teeter Angle - The hub teeter angle was calibrated by means of a digital inclinometer. See Figure II.6. To obtain a steady reading, the master blade was rested on a stand for each position. The zero teeter position was established by temporarily securing the hub teeter by fitting the bolt which locks the hub in teeter during transit. Originally it was thought to be the zero teeter datum. However in fact it corresponds to a ½° teetering angle. This difference was included in the calibration. The calibration was repeated after the first full days testing, since much blade movement had occurred and impact with the teeter stops had occurred frequently. No noticeable change was observed. The basic model rotor hub does not include teeter stops to limit the blade motion, however the installation of the instrumentation caused limitations to the blade movement. The upward teeter of the master blade was limited by contact of the hub with the bracket holding the blade pitch (long throw) potentiometer. Downward teetering of the master blade was limited by the bottoming of the wiper on the teeter potentiometer in contact with the non master blade.

The calibration is tabulated Table II.3 and plotted in Figure II.7.

Positive teeter is master blade flapping down.

Table II.3 - Teeter Angle Calibration

Teeter Angle (°)	DVM (v)
-0.5	3.339
+0.9	3.529
+2.3	3.727
+3.7	3.906
+5.1	4.096
+6.6	4.296
+8.2	4.520
+9.9	4.744
+10.7	4.842
-16.0	1.144
-13.4	1.548
-10.8	1.949
-8.3	2.296
-5.4	2.698
-2.8	3.041
-0.9	3.263
-0.7	3.298

Pitch Angle - The blade pitch was calibrated, again using the digital inclinometer. A proprietary blade pitch setting gauge was fitted over the blade section and the inclinometer placed on its top edge. Care was necessary since the blade would easily twist elastically giving a false reading. See Figure II.8. To avoid this, the inclinometer was carefully lowered onto the upper edge of the setting gauge keeping it parallel.
The calibration values are tabulated in Table II.4 and plotted in Figure II.9.

Table II.4 - Pitch Angle Calibration

Pitch Angle (°)	DVM (v)
+10.1	2.920
+8.6	2.897
+6.8	2.797
+4.5	2.683
+2.4	2.564
+0.1	2.465
-1.7	2.334
-4.0	2.230
-6.6	2.093

Rotor Speed - The calibration of this channel was set in the electronics workshop. There was a difficulty in achieving the correct rotor speed when the electric motor was cold. This caused too much electrical power to be fed to the motor which then suffered from overheating. This in turn increased the internal resistance of the armature which caused slowing of the motor and a consequent increase in the supply current. To avoid this vicious circle, a short running in procedure was introduced into the test sequence to slowly bring the rotor speed up on the control box until the required speed was reached. A short soak period at the required rotor speed then set up the feedback circuit correctly.

Helicopter Model Positions

As previously mentioned, the position of the helicopter model was to be varied across the deck of the ship. Five positions were selected and denoted A - E. A is the nearest position to the windward deck edge, C lies on the ship's centre line, and E is nearest to the leeward deck edge. B and D lie midway between the respective points. The distance of the hub centre from the windward deck edge is tabulated Table II.5:

Table II.5 - Helicopter Model Positions from the Ship Leading Deck Edge

A	6.5 in
B	20.5 in
C	34.7 in
D	48.8 in
E	62.9 in

2.2.5 TEST SCHEDULE

As violent blade flapping behaviour was anticipated for higher wind tunnel speeds, low rotor speeds, and proximity to the windward deck edge, the testing order was arranged to start with the relatively mild conditions and progressively move toward potentially more damaging situations.

The maximum rotor speeds used were 600 and 300 rpm.

Wind tunnel speeds of 0, 2.5 and 5 metres/second were selected.

The selection of wind tunnel speeds was based on the desire to model the correct dissymmetry of flow between the advancing and retreating sides of the rotor disc. This is best accomplished by the correct value of advance ratio. Table II.6 shows the full scale wind speed which gives the same advance ratio as the wind tunnel test conditions for a Westland Lynx main rotor at full rotor speed.

Table II.6 - Helicopter Model Advance Ratios

Model Rotor Speed (rpm)	Wind Tunnel Speed (m/s)	Advance Ratio	Equivalent Wind Speed (kts)
600	2.5	.06	23
600	5	.11	47
300	2.5	.11	47
300	5	.22	93

A sequence of five run up/run down timings were used.

Each sequence has three run up or run down times of 8, 16, and 32 seconds respectively, with a 16 second central period of constant rotor speed operation.

The five combinations a - e are tabulated in Table II.7:

Table II.7 - Helicopter Model Run Timings

	T1	T2	T3
a	8	16	8
b	16	16	8
c	32	16	8
d	8	16	16
e	8	16	32

(As the testing progressed, some of the times were altered for expediency.)

To standardise the testing before starting the wind tunnel or rotor, the rotor was positioned with the master blade at an azimuth angle of 90° (i.e. pointing directly upstream) and the teeter angle set to nominally zero. (*It should be noted that the rotor rotational direction is clockwise when viewed from above*). This would often cause the master blade to flap up, as the wind tunnel accelerated, to contact the stop before the rotor was started. This is apparent in the result figures presented later in the Chapter.

Throughout the tests, the collective pitch setting of -1.7°, and zero cyclic pitch settings

were maintained. The full set of test conditions are tabulated in Table II.8:

The order of the test conditions was:-

1 - 15

31 - 40

61 - 70

91 - 100

121 - 130

41 - 45

71 - 75

101 - 105

131 - 135

Teeter angle calibration checked.

141 - 145

111 - 115

51 - 55

81 - 85

16 - 20

21 - 25

26 - 30

Table II.8 - Test Condition Numbering Scheme

DECK POSITION	ROTOR SPEED	WIND TUNNEL	a	b	c	d	e
C	600	0	1	2	3	4	5
	600	2.5	6	7	8	9	10
	600	5	11	12	13	14	† 15
	300	0	16	17	18	19	20
	300	2.5	21	22	23	24	25
	300	5	26	27	† 28	29	30
B	600	0	31	32	33	34	35
	600	2.5	36	37	38	39	40
	600	5	† 41	42	43	44	45
	300	0	46	47	48	49	50
	300	2.5	51	52	53	54	55
	300	5	56	57	58	59	60
A	600	0	61	62	63	64	65
	600	2.5	66	67	68	69	70
	600	5	71	72	73	74	75
	300	0	76	77	78	79	80
	300	2.5	81	82	83	84	85
	300	5	86	87	88	89	90
D	600	0	91	92	93	94	95
	600	2.5	96	97	98	99	100
	600	5	† 101	102	103	104	105
	300	0	106	107	108	109	110
	300	2.5	111	112	133	114	115
	300	5	116	117	118	119	120
E	600	0	121	122	123	124	125
	600	2.5	126	127	128	129	130
	600	5	131	132	133	134	135
	300	0	136	137	138	139	140
	300	2.5	141	142	143	144	145
	300	5	146	147	148	149	150

The shaded cells were not tested.
Cells marked with † are presented in the results section.

Processing of Results

The data from the four channels was recorded on a RACAL Store 4 tape recorder. The data was acquired onto an IBM PC and processed using ASYST.

The teeter angle calibration permitted a quadratic expression to be fitted to the data for conversion in the ASYST program. The resulting equation is:-

$$\beta = 23.39 - 6.38V - 0.1359V^2$$

2.2.6 RESULTS AND CONCLUSIONS ARISING FROM THE S1 WIND TUNNEL TESTS

The effect of deck location was always considered to be of major importance and the results of the S1 tests confirmed this, however the manner of this influence was unexpected. A detailed discussion of the behaviour is included in Chapter 3 but a sample of the results is shown in Figures II.10.a and II.10.b which refer to deck positions B and D, rotor speed timings (a) with a maximum rotor speed of 600 rpm and a wind tunnel speed of 5 m/s. These deck locations show the extremes of the blade behaviour and as shown in the Figures, the B position produces a violent teetering motion of the blades causing a number of impacts with the mechanical flapping stops. The tests were standardised on a maximum rotor speed of 600 rpm and a wind tunnel speed of 5 m/s, however, for reasons of completeness, and with a dash of bravado, tests were contemplated for higher wind tunnel speed of 5 metres/second and the lower rotor speed maximum of 300 rpm. The corresponding wind speed for the Lynx as previously discussed is 93 knots and is a very severe operating condition. Figure II.10.c shows the type of blade behaviour obtained and the teeter angle motion is substantial and teeter stop contact very common. The deck location is C which is, consequently, less hazardous than B, but the (c) rotor timings are used. The test shown in Figure II.10.c was considered to be the worst which could be sensibly undertaken and so deck location B was never tested for reasons of security of the rotor model. Observation of the blade motion was a cause of great concern and only five runs were performed. The test was curtailed as the only result of continuing was of severely damaging the helicopter model.

A final test was carried out to obtain an understanding of the flow patterns surrounding the rotor under the influence of the ship model. Observation of the results showed that

the deck locations A, B, and C show similar shapes to the teetering time history, whilst D and E are themselves similar but differ markedly from the other three. It is apparent that a substantial difference must exist between the external flow behaviour occurring with these two groups of deck locations.

Initially, a pitot static tube was used in an attempt to obtain flow velocity readings. The orientation of the pitot tube was adjusted using a long wool tuft as a guide. Meaningful readings were obtained for the windward deck edge location A, but elsewhere virtually no data of any use was obtainable. It was readily apparent that the level of turbulence, near the deck prevented any sensible flow speed and direction being measured by the pitot tube. For this reason, a tuft study was conducted with a traverse down the centre line of the ship model (corresponding to the helicopter model positions) to establish the region of turbulence and how it relates to the five rotor hub locations used for the tests. The flow pattern is shown diagrammatically in Figure II.11, whilst the results of the tuft study are shown in Figure II.12 with the respective hub locations plotted. The deck location B is particularly noteworthy as this corresponds to the situation where exactly one half of the rotor disc is within the turbulence and the other in the relatively undisturbed airstream deflected upwards by the cliff edge effect of the ship. Positions A and C are either mainly outside or within the turbulent region respectively. For this reason the rotor will be driven harder by the wind conditions for position B, and this explains why it is the worst condition. Positions D and E are totally within the turbulence whereby the different character of the teeter time history can be explained. Position E must be affected by the leeward deck edge flow, so position D will thus provide the most mild rotor response.

As with all experiments, more questions are posed during the work than are answered, and this wind tunnel experiment was no exception. There was no difficulty in obtaining the dramatic blade behaviour associated with blade sailing. Certain conditions were worse than others but most showed the uncontrolled behaviour of the rotor. With no restraint on the hub teeter, the flapping excursions of the rotor blades are considerable and the teetering range was covered in full with many impacts on the teeter stops observed. This range of teeter angle was from -11° to +23°, so the importance of the droop and anti-flap stops is demonstrated.

The most severe of the teeter motion was expected to occur with high wind tunnel speeds

and low rotor speeds. This was borne out by the test results. The long duration rotor accelerations and decelerations caused greater teetering motion than the shorter durations. Equivalent wind speeds (for the Lynx aircraft) of 23 knots showed blade sailing behaviour, but not of excessive nature. An equivalent wind speed of 47 knots, however, produced more violent behaviour, and the few tests conducted at an equivalent wind speed of 93 knots proved extremely violent.

The deck position of the helicopter model was an obvious influence on the response of the rotor, but the relative magnitudes of the responses, between the deck locations, was not as anticipated. The influence of deck location is a major influence and the importance of the flow states over the deck cannot be overstated. The benefit of operating the helicopter away from the windward deck edge has been described by Porteous[10] and vindicated by the results of these tests.

The five deck positions split into two distinct groups namely the windward three (A,B,C) and the leeward two (D,E). The former have a well defined teetering behaviour, whilst the latter are noticeably milder conditions. The latter group are heavily under the influence of the turbulent region, and at the central constant rotor speed phase the rotor disc is constantly "twitching". Conversely the former group are controlled by the comparatively steady flow conditions outside of the turbulence and are thus steadier at constant rotor speed, but as the aerodynamic forcing is more coherent, a greater teetering deflection is obtained.

All other things being equal, the response of the rotor to an acceleration or deceleration are very close in magnitude.

2.3 SECOND WIND TUNNEL TEST (S2)

Settling Chamber

As described in the S1 test section, the experimental helicopter rig was mounted on a simulated ship's flight deck of appropriate size and installed in the settling chamber of the wind tunnel.

Rotor Operation

The rotor for this test sequence was operated with two collective pitch values, one being close to the no lift angle of the blade aerofoil section, effectively -1.7°, the second 6° (nose up). A helicopter rotor, in reality, when running up or down uses nominally zero rotor thrust conditions, which was the condition used in the initial tests. However, the rotor was only tested in a two bladed teetering configuration, and for this series of tests one bladed operation was to be included. The effect on coning angle of collective pitch will be markedly different between a teetering rotor, and a conventional articulated rotor where each blade is individually hinged allowing it to cone up without the influence of an opposing blade. The collective pitch setting of -1.7° (2.33v DVM) was set via the calibration figures to match the zero thrust condition of the previous tests, and the 6° value (2.74v DVM) was set in a similar way. Friction in the collective pitch change mechanism made it difficult to set a given pitch value. A nominal setting of 5° was selected for the higher collective pitch, but the actual value was 6°. The tests were conducted at 300 rpm and 600 rpm rotor speed, the 600 rpm figure being the main value with some 300 rpm cases run for comparison.

Wind Tunnel Operation

The wind tunnel operation was unchanged.

Rotor Model Modifications

The model essentially remained unchanged from the previous tests. However, in order to allow single blade operation, a counterbalance weight was made to fit the jaws of the hub after removing the non master blade. A schematic diagram of the counterbalance weight is shown in Figure II.13.

The mass required was obtained by removing the non master blade, and placing a load cell under the master blade measuring the download at the blade attachment bolt position. This gives the correct first moment of mass about the teeter axle. The counterbalance

weight was designed to fit snugly in the jaws by the bolt used to secure the non master blade. It was symmetric about this point, and so the mass value read by the load cell was the design mass for the counterbalance weight.

Balancing runs were made for such operation and only a small weight adjustment was necessary. The quality of the balance was established by fitting an accelerometer to the main model structure close to the main shaft bearings. A reference test was made with the two blades fitted, and single blade runs with the adjusted balance weight obtained a lower vibration level than the reference test.

2.3.1 TESTING SEQUENCE

Calibration

Teeter Angle - The hub teeter angle calibration was checked with no change from the previous tests observed.

For reference, the recalibration values are tabulated Table II.9:

Positive teeter is master blade flapping up. (The sign is reversed from the previous S1 tests)

Table II.9 - Teeter Angle Recalibration

Teeter Angle (°)	DVM (v)
23.7	0.001
23.5	0.0285
13.7	1.513
4.6	2.800
-4.1	3.956
-11.5	4.963
-9.5	4.700
14.9	1.297
-6.1	4.235
-2.1	3.718
1.9	3.053
9.9	2.06
-0.4	3.453

Pitch Angle - The blade pitch calibration was checked, again using a proprietary blade pitch setting gauge fitted over the blade section with the inclinometer placed on its top edge. Care was necessary since the blade would easily twist elastically giving a false reading. To avoid this, the inclinometer was carefully lowered onto the upper edge of the setting gauge keeping it parallel. The calibration for this channel did not exactly match

the previous values. The difference was in the region of 0.4° and since the method of setting the angles were prone to blade twisting it was considered justified to retain the previous calibration figures.

For reference, the recalibration values are tabulated Table II.10:

Table II.10 - Pitch Angle Check Calibration

Pitch Angle (°)	DVM (v)
2.6	2.557
-1.3	2.336
-6.0	2.092
7.4	2.791
10.3	2.934
1.2	2.461

Rotor Speed - The calibration of this channel was originally set in the electronics workshop and was not checked. Subsequent analysis of the results showed the correct value of signals being returned for the rotor speed.

In order to avoid the difficulty in achieving the correct rotor speed when the electric motor was cold, the short running in procedure was again introduced into the test sequence to slowly bring the rotor speed up on the control box until the required speed was reached. A short soak period at the required rotor speed then set up the feedback circuit correctly. The rotor speed signal showed, for a period, a periodic twitching towards zero. This did not affect the interpretation of the results but made their presentation more difficult. This eventually cleared itself.

2.3.2 HELICOPTER MODEL POSITIONS

As previously tested, the position of the helicopter model was varied across the deck of the ship and denoted A - E.

2.3.3 TEST SCHEDULE

Since the S1 tests confirmed that violent blade flapping behaviour occurs with higher

wind tunnel speeds, low rotor speeds, and proximity to the windward deck edge, the testing order was arranged accordingly. This technique of approaching the violent cases was performed for both numbers of blades.

As with the S1 tests, the maximum rotor speeds used were 600 and 300 rpm, and the wind tunnel speeds of 2.5 and 5 metres/second were selected. A sequence of five run up/run down timings were used. Each sequence has three run up or run down times of 8, 16, and 32 seconds respectively, with a 4 second central period of constant rotor speed operation.

The five combinations a - e are tabulated Table II.11:

Table II.11 - Helicopter Model Amended Run Timings

	T1	T2	T3	Figure Sequence Number
a	8	4	4	(i)
b	16	4	4	
c	32	4	8	(ii)
d	8	4	16	
e	8	4	32	(iii)

(As the testing progressed, some of the times were altered for expediency.)

The rotor azimuthal starting position was with the master blade pointing directly into wind.

Throughout the tests zero cyclic pitch settings were maintained.

The order of the test conditions, as detailed in Table II.8, was:

2 Blades - θ_0=-1.7°

131 - 135

071 - 075

011 - 015

026 - 030

036 - 040

041 - 045

101 - 105

1 Blade - θ_0=-1.7°

101 - 105

036 - 040

041 - 045

071 - 075

131 - 135

011 - 015

026 - 030

1 Blade - θ_0=+6.0°

011, 013, 015

101, 103, 105

041, 043, 045

071, 073, 075

131, 133, 135

2 Blades - θ_0=+6.0°

131, 133, 135

071, 073, 075

041, 043, 045

101, 103, 105

011, 013, 015

2.3.4 RESULTS (S2)

The basic character of the results, which are repeated from the previous tests, (namely Number of blades=2, θ_0=-1.7°), is maintained. The main difference is in the central constant rotor speed period which was set at 4 seconds. However, the use of a single blade configuration and a collective pitch of 6° were performed for the first time.

The following Figures show a numbering scheme which is as follows:

The number is of the form

Wind Tunnel Test/Test Condition Number/Number of Blades/Collective Pitch

Wind Tunnel Test	S1 or S2
Test Condition Number	As detailed in Table II.8
Number of Blades	2 Blade Teetering or 1 Blade plus Counterbalance Weight
Collective Pitch	(L) Low (-1.7°) or (M) Medium (nominal 6°)

The results shown in Figures II.14.a - II.17.b show the equivalent cases to Figures II.10.a and II.10.b. Figures II.14.a and II.14.b are repeat runs of II.10.a and II.10.b and show good agreement. Figures II.15.a and II.15.b show the single blade operation. Figures II.16.a and II.16.b show the two blade rotor operating with 6° of collective pitch applied whilst Figures II.17.a and II.17.b show the equivalent single blade case. Single blade operation gives a more "lively" flapping behaviour whilst an increase in θ_0 gives a profound increase in vibratory flapping amplitude. The two blade case at 6° collective was just beyond the torque capability of the motor which shows in the rotor speed not reaching the desired maximum of 600 rpm.

In order to distil the essential character of the results and to devise a means of attributing a numerical value to the severity of the blade behaviour, two areas were examined:-

- The central steady rotor speed area was examined for mean values and vibratory amplitude (half peak to peak). The long run up time timing (ii) was used allowing the rotor the longest time to settle. This was intended to examine the normal rotor behaviour in the various deck locations and acts as a measure of local turbulence. The results are presented in Figures II.18-21.
- The longest run down timing (iii) was used to examine the number of impacts the blades made with the flapping stops during this period. This

was intended as a measure of the sailing characteristics of the blade(s). The results are presented in Figures II.22, II.23.

Figure II.18 shows the coning angle for each rotor configuration and each deck location. The two blade teetering rotor should possess nominally zero coning angle, but the figures do not show this to be the case. Since the mean value was calculated from the extreme values of flapping, the non zero coning angle results may be due to the unsteadiness in the flapping biasing one blade to fly higher. The setting of zero cyclic pitch was performed and checked before running the rig, but friction in the potentiometer connection to the swash plate may have allowed some mistracking to be present without affecting the sensor reading as the blade turned around the azimuth.

Accepting this anomaly, Figure II.18 shows the difference between a conventionally articulated rotor blade and a teetering pair of blades. The deck location for the greatest coning angle is B for the low collective case but C for the medium value. Since rotor thrust is produced with the medium collective pitch of 6°, the single blade coning, in this situation, is markedly greater than the other cases for reasons of zero thrust or the balancing effect of the teetering rotor.

Figure II.19 shows the corresponding vibratory flapping amplitude for the four rotor configurations (1 or 2 blades, low or medium collective pitch) and five deck locations (A-E).

At low collective pitch the results are consistent with the previous tests, where the deck location order, from worst to best, was BACED; although in this analysis, A and C are reversed. At medium collective pitch the order is now ABCDE for both articulated and teetering rotors. It would appear that the relatively clean air given by location A allows any collective pitch blade angle to benefit from the increase in incidence. Also Figure II.19 shows that the use of collective pitch causes a distinct increase in blade vibratory flapping, hence justifying the use of nominally zero rotor thrust for rotor engagement and disengagement in a turbulent area such as a ship's deck.

Two variations, all at low collective pitch, were also conducted, namely:

Blade Flapping, the effect of rotor speed - The run down case at position C was repeated for a reduced maximum rotor speed of 300 rpm but with the same wind tunnel speed of 5 m/s. (Locations A and B were felt to be too damaging).

Figure II.20 shows the effect of maximum rotor speed on the blade flapping behaviour

for low collective pitch at the central deck location C. The coning angles are virtually constant but the effect of lowering the rotor speed (an effective doubling of the advance ratio) on the flapping amplitude is apparent with approximately doubling of the values taking place.

Blade Flapping, the effect of wind tunnel speed - The effect of lowering the wind tunnel speed from 5 to 2.5 m/s was considered at deck location B. Since a milder blade behaviour was expected, the most precarious location could be used.

Figure II.21 shows the effect of lowering the wind tunnel speed from 5 m/s to 2.5 m/s. The coning angle for the two rotor configurations is virtually unchanged except for a single blade where the values drops by more than a half. The vibratory amplitudes are reduced consistently by about 40%.

The results of these tests are tabulated Table II.12:

Table II.12 - Summary of Blade Flapping Test Results

Number of Blades	Collective Pitch	Deck Location *(Test Number)*					
		A *(073)*	B *(043)*	C *(013)*	D *(103)*	E *(133)*	
2	Low	1.93°	2.52°	1.63°	1.63°	0.73°	Mean
		2.08°	4.07°	3.58°	1.98°	2.49°	Amplitude
1		2.32°	2.51°	1.63°	0.34°	0.93°	Mean
		3.28°	4.27°	3.77°	1.88°	2.08°	Amplitude
2	Medium	1.62°	0.54°	1.82°	1.32°	1.33°	Mean
		10.91°	9.03°	6.75°	4.07°	2.68°	Amplitude
1		4.11°	4.51°	5.10°	3.81°	3.31°	Mean
		10.02°	9.23°	6.25°	3.77°	3.28°	Amplitude

The entries surrounded by a box have been interpolated using other results as the rotor operation of this test case was found to be unsatisfactory and the steady state was not reached successfully.

The blade sailing behaviour has been quantified using the number of impacts with the

restraining stops during the extended run down of timing sequence (iii). This case was chosen as it represents the case where the rotor enters the condition from the relative calm of a controlled rotor turning at full rotor operating speed. The extended run up case (i) usually commences with a blade in contact with a stop, usually fully flapped up, and this could trigger several stop contacts purely because of the severe rotor hub condition at the start. The run down condition was felt to be more *"honest"* in terms of quantifying the severity of the blade sailing. The impact count was conducted over the run down phase only and in the following figures, the count for contact with the upward stop is positive whilst the downward contacts are negative. The data is presented in terms of bar charts.

Figure II.22 shows the results for the four rotor configurations and five deck locations, using the reference conditions of 600 rpm maximum rotor speed and 5 m/s tunnel speed. The initial observation on the distribution is the tremendous difference between the deck locations A-C where there is a reasonable number of stop contacts, whilst locations D-E have but a single stop contact occurrence between them - complementing the observations of these tests as well as those obtained in the previous test. The primary comment is how the character of the blade tip behaviour changes markedly between locations C and D. Regarding locations A-C at both collective pitch values, the two blade configuration has B as the most severe situation whilst the single blade rotor has A as its most hazardous for upward contacts but C for downward. This difference may be clouded by the fact that the single blade configuration will have a higher mean coning position biasing its movement towards the upper stop.

Figure II.22 shows an increase in upward contacts for a single blade rotor when the collective pitch is increased whilst for downward contacts the two blade rotor still has, for both collective pitch values, B as the worst location whilst the single bladed rotor has C, with a progressive increase moving from A to C. The increase in collective pitch helps both rotors in keeping away from downward contacts for the deck locations A to C.

The two variations, applied to blade stop contacts are:

Stop Impacts, the effect of rotor speed - The results are presented in Figure II.23. For the two bladed rotor (left two bars) the upper impact number doubles with increasing rotor speed, whilst the lower stop impacts remain virtually the same. The

single bladed rotor (right two bars) have the same doubling for upper stop impacts with an increase of 25% for lower stop impacts. The effect of reducing the rotor speed on upper stop contacts, is more pronounced than those for the lower stop.

Stop Impacts, the effect of wind tunnel speed - The results are presented in Figure II.24. The effect of halving the wind tunnel speed causes a dramatic reduction in the number of stop impacts for all rotor configurations. This reinforces the effect of wind speed on the blade sailing phenomenon, particularly with an unfavourable deck location for the aircraft.

The above tests S1 and S2 have shown the importance of deck location on blade sailing behaviour and provided a valuable set of results or use in assembling the rigid blade theoretical model. The final part of the tests was a brief and qualitative assessment of the flow characteristics over the ship's flight deck which went some way in explaining the variation of blade behaviour as the helicopter was moved from the windward to the leeward deck edge. To satisfactorily proceed to develop a rigid blade, blade sailing model an accurate quantitative survey of the flow over the ship's flight deck must be undertaken and this is now described.

2.4 SHIP FLOW WIND TUNNEL TESTS

The purpose of the S1 and S2 wind tunnel tests was to establish the blade sailing characteristics of a 1 or 2 bladed rotor when placed on a simulated ship's deck. A major observation was the difference in character between rotor positions towards the windward and leeward deck edges. An initial look at this effect showed that the major influence was the separation line off the windward deck edge partitioning the flow into two distinct regions. These are the essentially clean air above the separation boundary and the turbulent recirculation region between the boundary and the deck surface. The relative amount each blade spends in either region determines the difference in behaviour. On a qualitative basis, the problem is now described but initial attempts to obtain a good theoretical comparison with the test data were successful only for the situation of a blade lying wholly within clean air. To obtain sensible agreement with the test results the theoretical model must use a detailed specification of the flow patterns over the ship's deck and therefore this data must be obtained experimentally. This was accomplished by a wind tunnel test and the results incorporated into the theoretical model. This part of the work occupied two separate days of testing. A modified ship model was constructed of smaller scale, to that used in the rotor model tests [1,2], and fitted to a ground plane to avoid the tunnel working section boundary layer to interfere with the results. The initial test produced results which when inserted into the theoretical calculation showed a good comparison with the experimental results of the previous reports, [1,2]. Some differences were still present and it was felt that a more extensive survey should be conducted. This was accomplished with the second test.

2.4.1 DISCUSSION OF THE FIRST SHIP FLOW WIND TUNNEL TESTS

Since the turbulence over the deck would cause the wind velocity to have no preferred direction, complete flexibility in measuring the flow direction was essential and for this reason a laser doppler anemometer (LDA) traverse was selected. This was only available in the working section of the Department's 11 ft by 8 ft wind tunnel which created an initial problem in that the existing ship model would have created a blockage in the region of 50% which was totally unacceptable. Accordingly, a smaller ship's model (2.8:1) was built and installed on a false floor to simulate the wind tunnel flow, as shown

in Plate II.11. The false floor was raised 6 inches above the working section floor to isolate the flow from the tunnel boundary layer. A rectangular grid was specified for the test points and was defined in a vertical plane located along the centre line of both tunnel and model. The LDA traverse using a DANTEC three colour back scatter system followed this grid and the horizontal and vertical flow velocities at 51 data points were logged. The LDA installation is shown in Plate II.12. This was performed at the wind tunnel speeds of 2.5 and 5 m/s. *(During low speed operation in high winds, the helicopter main rotor achieves advance ratios far in excess of those occurring in normal flight. In order to keep these values in sensible agreement with a 50 knot wind, tunnel speeds of 2.5 and 5 metres per second were again selected, and the 5 m/s figure used for the majority of cases using the 2.5 m/s values for comparison.)*

In the first test, seeding the flow proved problematical since the flow could be virtually divided into two separate areas. The seeding generator was initially positioned a reasonable distance upstream of the model and any points outside of the turbulent region received an adequate number of particles allowing the LDA to obtain sufficient samples. Points lying within the turbulent region were virtually isolated from the seeding generator and so no reliable results were achieved. A second seeding outlet was placed close to the deck surface injecting the particles within the turbulence. This allowed a sensible number of LDA samples to be achieved but for the later testing a more thorough seeding distribution was used.

2.4.2 RESULTS OF THE FIRST TESTS

The results of the LDA tests were processed and at each grid point the two flow velocity components were statistically analysed to provide mean and standard deviation values. Attention was concentrated on the 5 m/s test cases and the mean flow direction variation around the ship's model is shown in Figure II.25. Also shown on this figure are the five rotor hub positions A to E. As can be seen, the flow divides into the externally driven flow and the turbulent region covering the deck. There is also strong evidence of a recirculating flow beyond the leeward edge of the deck. The location of rotor hub position B on the dividing line can be seen and also how the position D finds the rotor hub submerged in low speed flow causing the relatively mild flapping behaviour. The increased blade movement at position E seems to be a direct result of the recirculation in the wake of the ship's hull.

The variation in flow speed and direction over the ship's deck has now to be transferred to the rotor disc. Figure II.26 shows the flow velocity across the lateral diameter of the rotor disc (assumed horizontal) at the five deck locations. A linear interpolation method was used. The figure shows that for point A the slow build up of flow velocity as it moves over the deck rapidly drops as the turbulent region is encountered. (Each of the five graphs has the same shape only is displaced along the horizontal axis). The situation for points A-C is well indicated as more of the rotor is immersed in the turbulence but that over some of the rotor disc clean flow is encountered. Conversely, for positions D and E only the turbulent region is experienced which accounts for the complete change in character of the blade behaviour. Figure II.27 shows the equivalent plot of flow inclination angle to the horizontal. The change in flow direction when moving from location A to E shows the effect of the reversed flow along the deck in the turbulent region, also shown in Figure II.25.

The real effect of the flow over the ship however is in the change in the blade incidence induced by the wind as the rotor blade rotates about the azimuth. To examine this, Figures II.28 and II.29 show the change in incidence at the blade tip for the five deck locations and for two rotor speeds namely, 45 rpm (7.5%NR) and 90 rpm (15%NR). As can be seen considerable changes in incidence are generated, particularly around a rotor azimuth of 100° to 240° where peak changes of 120° for 7.5%NR and 50° for 15%NR are seen. This corresponds to the effective retreating blade where the rotor speeds correspond to advance ratios of 1.47 and 0.73 respectively. This will cause the major part of the retreating half of the rotor disc to lie within the reverse flow circle and hence cause these very large incidence changes. These figures also show that the constant lift curve slope model is completely inappropriate and a more sophisticated method must be used. In line with previous work, the quasi steady trailing edge stall model, Beddoes[36], was used to obtain realistic lift coefficient values for the wide range of incidences encountered in the tests.

One final comment is necessary on the modelling of the flow over the ship. With the combination of the simple flow model and a constant lift curve slope a closed form integration could be used to obtain the aerodynamic flapping moment. With the use of wind tunnel data and an empirical aerofoil method, closed form integration is not now possible. Hence the aerodynamic conditions were calculated for 11 radial positions along

the blade and the overall flapping moment obtained using a trapezoidal integration method.

2.4.3 DISCUSSION OF THE SECOND SHIP FLOW WIND TUNNEL TESTS

An initial test of this data on the theoretical model was performed and encouraging results obtained. However, it was felt that the flow close to the ship's deck surface was not defined close to the surface itself. For this reason, it was felt that the initial grid used for the LDA tests could be favourably extended particularly close to the deck surface. The recirculation area has been shown to be very important as regards the blade sailing character and an additional line of 13 points was inserted at half the grid dimension above the deck surface. Also, a traverse was made over a similar grid placed 40 mm off the centreline to investigate whether the finite span of the deck length has any influence on the wind flow patterns. The traverse grid, origin and axes in the vertical plane is shown in Figure II.30 and the plan view of these planes in Figure II.31. The lowest line of points had to be raised to avoid the LDA beams passing through a junction of the perspex wind tunnel wall. The velocity components in three axes were recorded, but the transverse component is not considered reliable and so only the vertical and horizontal components were used.

2.4.4 RESULTS OF THE SECOND SHIP FLOW WIND TUNNEL TESTS

The data was statistically analysed as in the previous tests and used an input to the blade sailing program. The flow vector plots for both speeds (5 and 2.5 m/s) and grid planes are shown in Figures II.32-35. As can be seen the same flow character behaviour is seen compared with the first set of tests. The flow velocities in the grid closest to the deck surface is seen as similar to that of the previous closest pass and the decision to include this line of 13 points is justified since the interpolation can be seen to be more reliable. The influence of tunnel speed on the results does not appear to change the overall pattern, only the magnitudes are different. The results of the traverse towards the end of the deck shows very little change in the windward part of the velocity pattern. However some changes in the recirculation behind the leeward deck edge can be seen. This part of the flow gives the increase in the turbulent blade motion from position D to E. This effect

occurs with the more benign blade sailing conditions and so this difference in flow pattern is noted but the comparison of theory and experiment is limited to the flow conditions found at the centreline being used for all blade locations. The flow is therefore assumed to be essentially two dimensional.

The two wind tunnel test, S1 and S2, produced results of blade flapping motion which confirmed conclusions previously encountered in the references. It also provided a valuable insight into the wide range of aerodynamic interference found on a ship's flight deck. These observations also explained the large disparity between the various locations on the flight deck and the appropriate influence on the blade flapping behaviour. The other result was a set of results which can be used to tests the theories which will be described in Chapter 3.

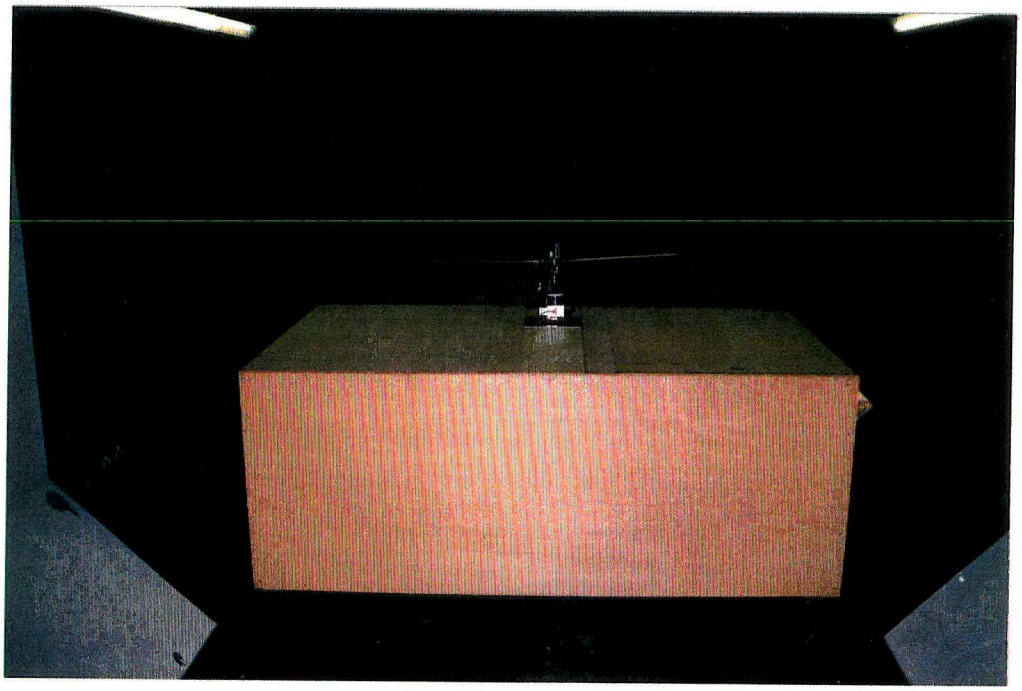

Plate II.1 - Model Installed in Wind Tunnel

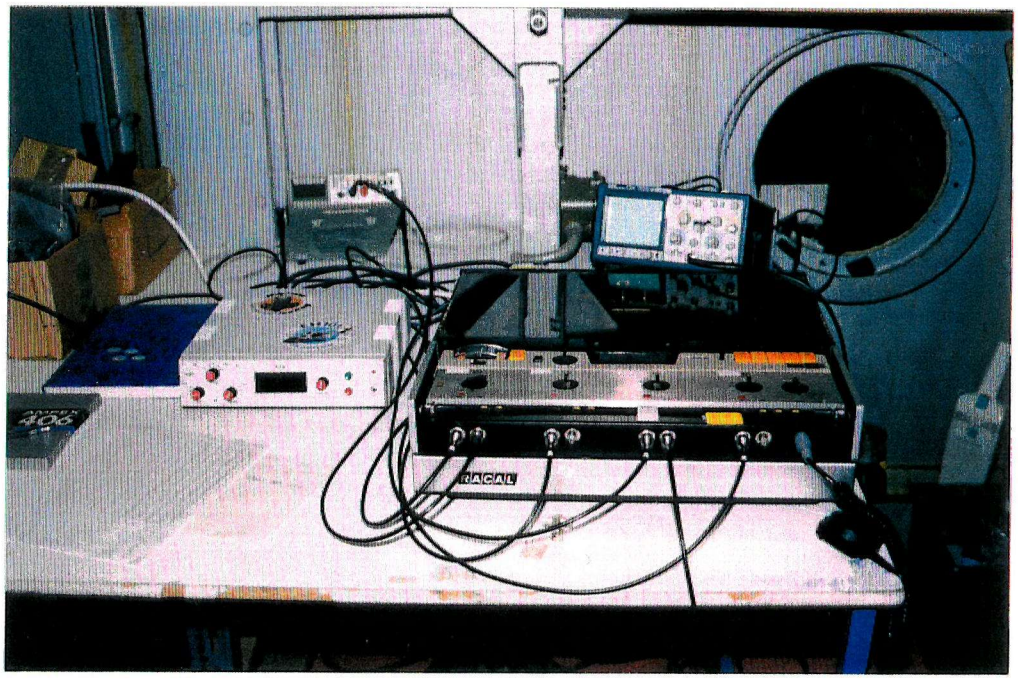

Plate II.2 - Rotor Control and Data Recording Equipment

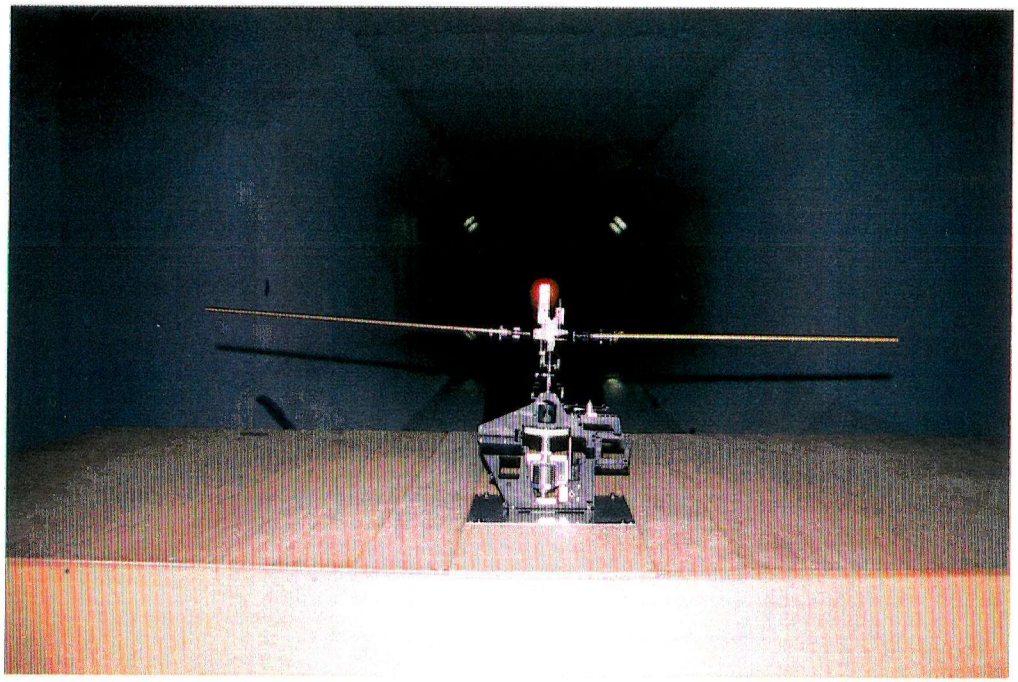

Plate II.3 - Helicopter Model on Ship Deck

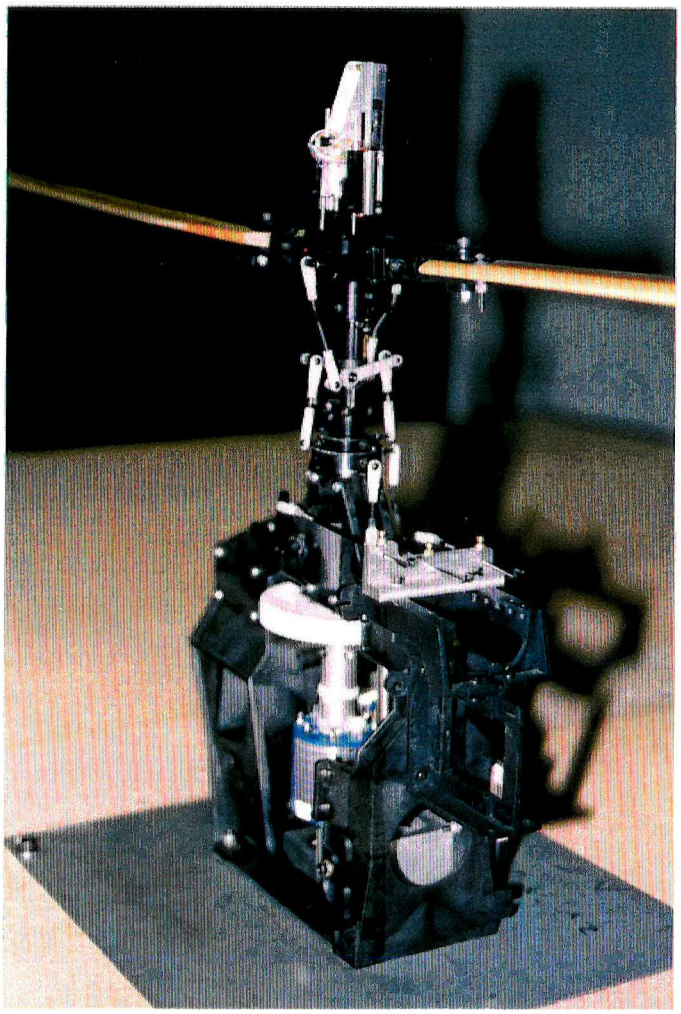

Plate II.4 - Helicopter Model, General View

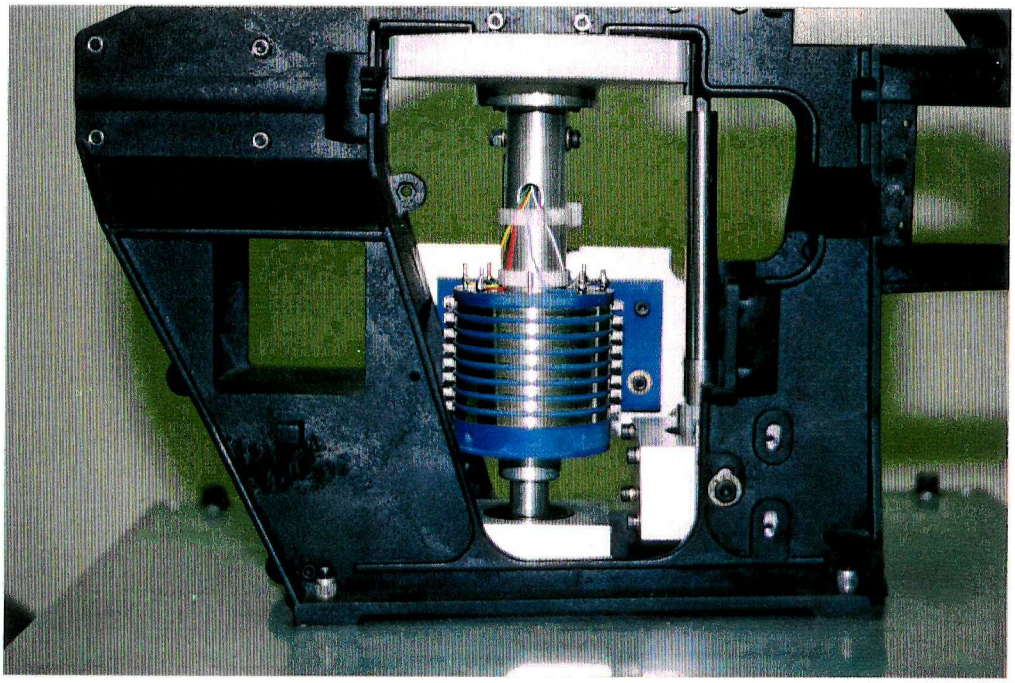

Plate II.5 - Helicopter Model, Slipring Installation

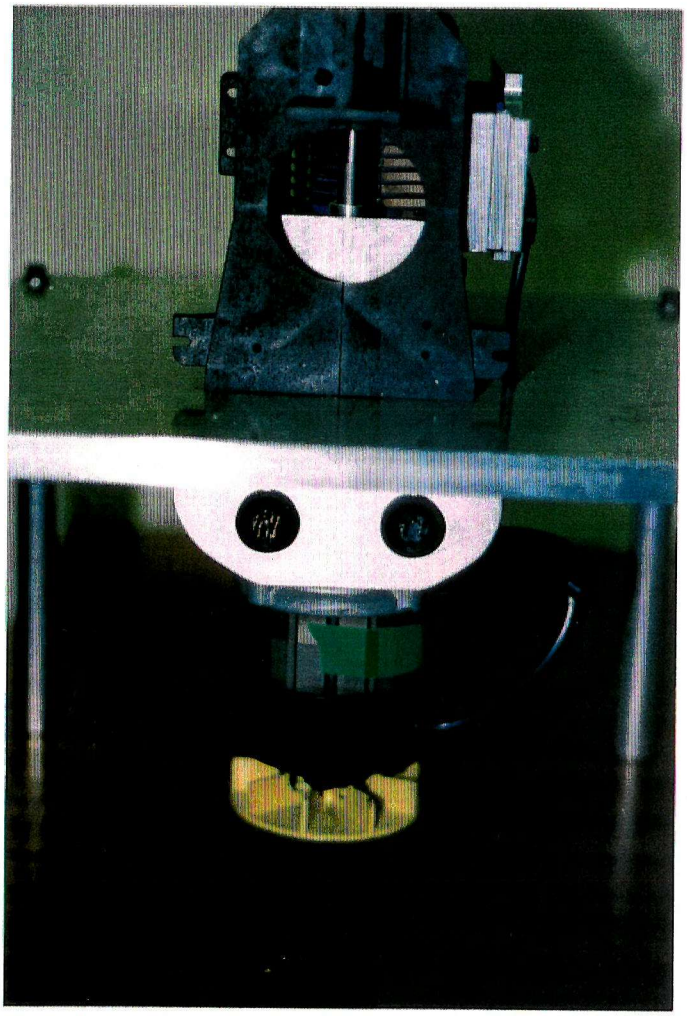

Plate II.6 - Electric Motor Installation

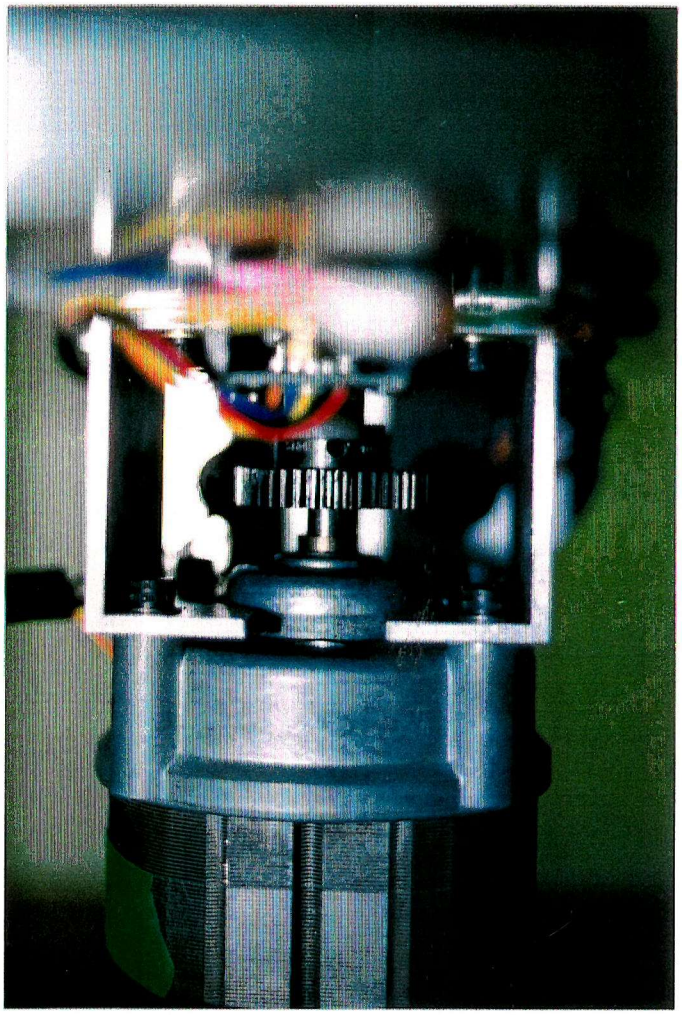

Plate II.7 - Electric Motor and Lower Drive Train

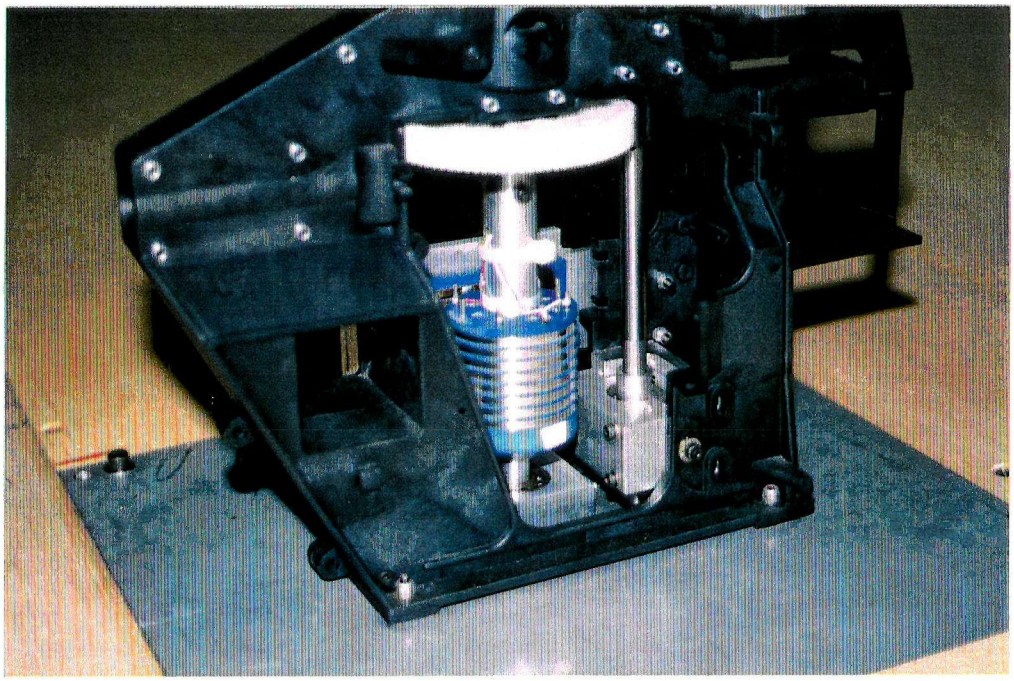

Plate II.8 - Sliprings and Upper Drive Train

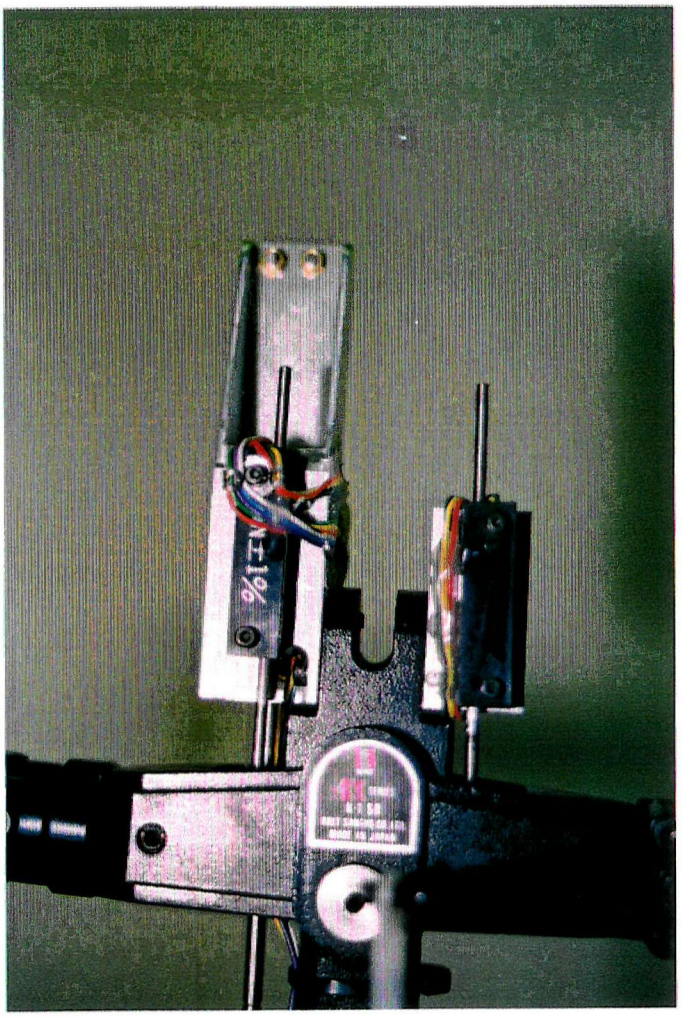

Plate II.9 - Hub Teeter Potentiometers

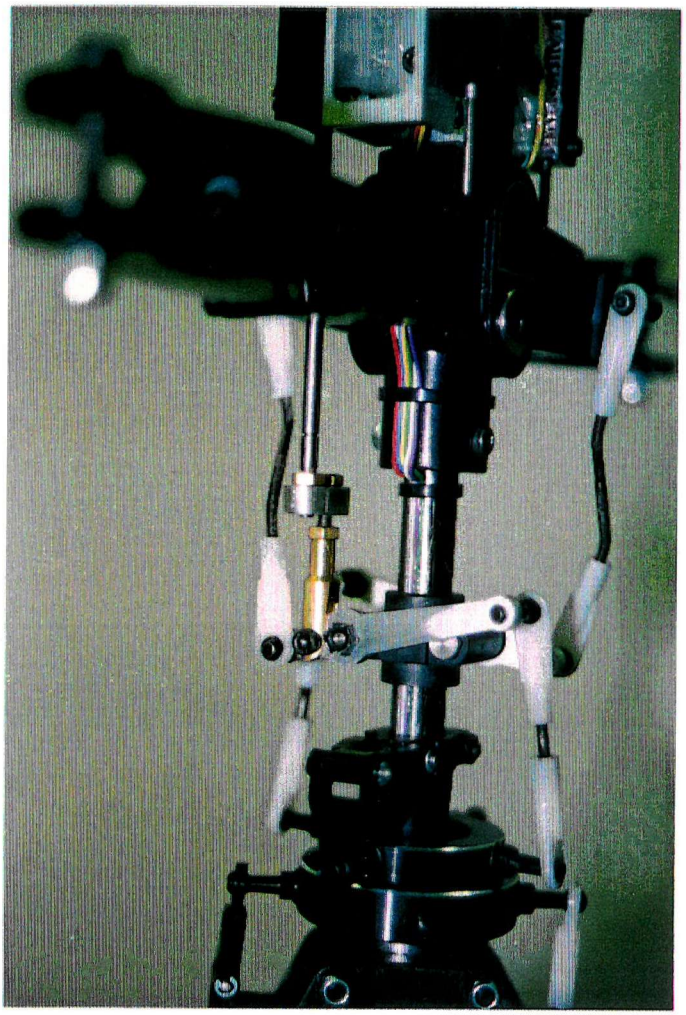

Plate II.10 - Pitch Rod Installation and Potentiometer

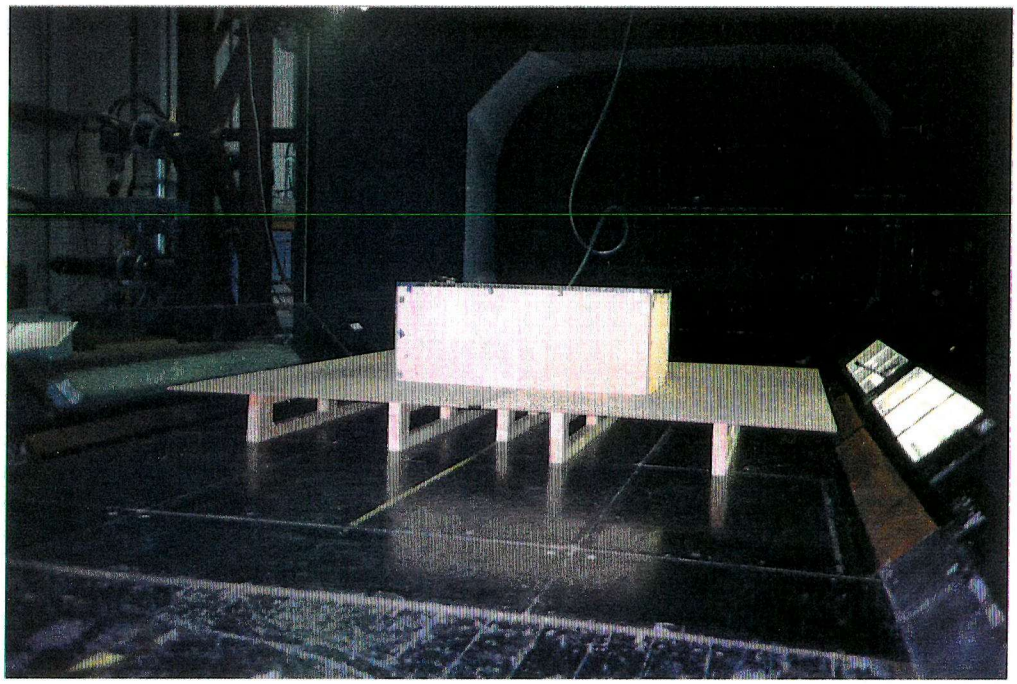

Plate II.11 - Ship Model Installed on its Ground Plane in the Working Section of the 11ft by 8 ft Wind Tunnel

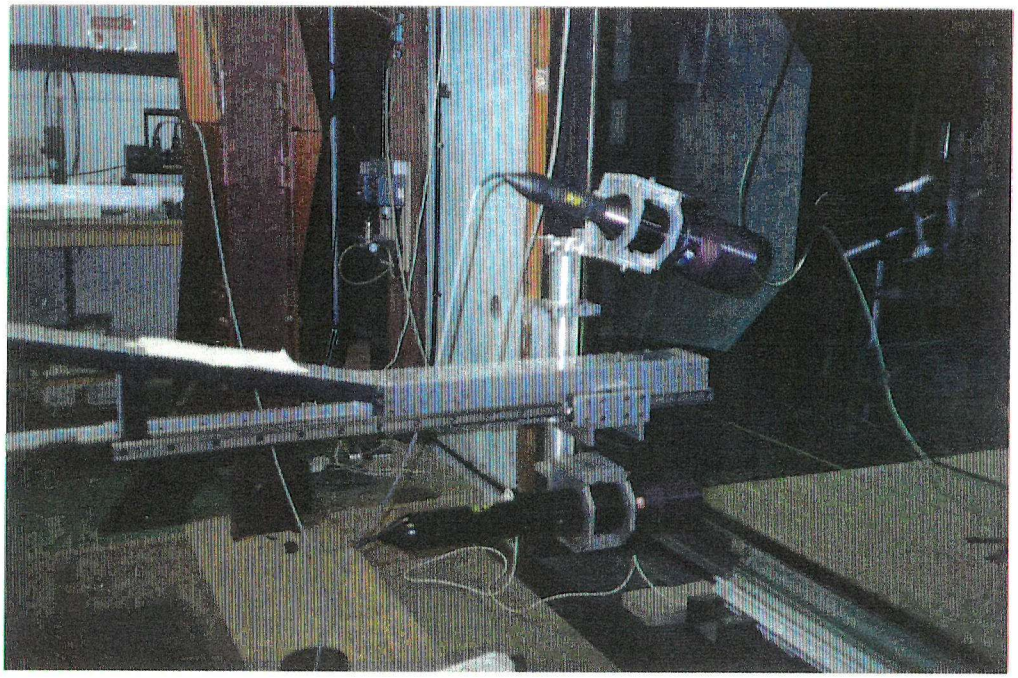

Plate II.12 - LDA Installation in the 11ft by 8ft Wind Tunnel

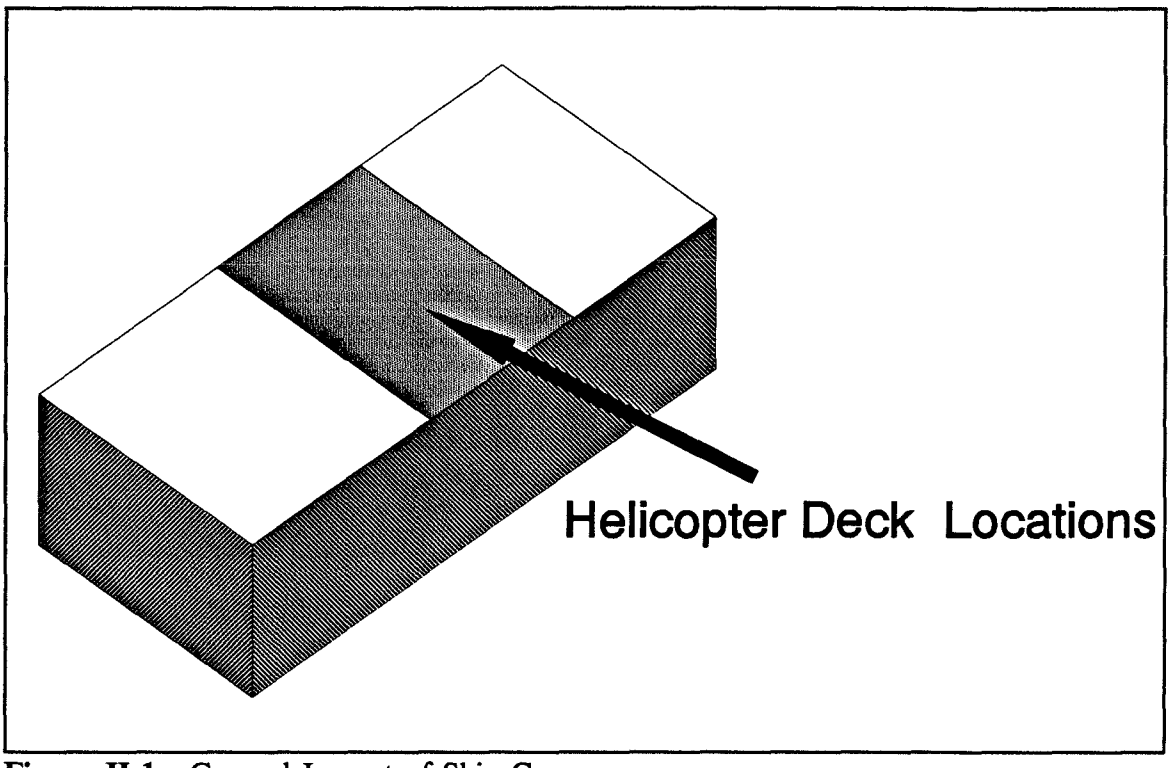

Figure II.1 - General Layout of Ship Carcass

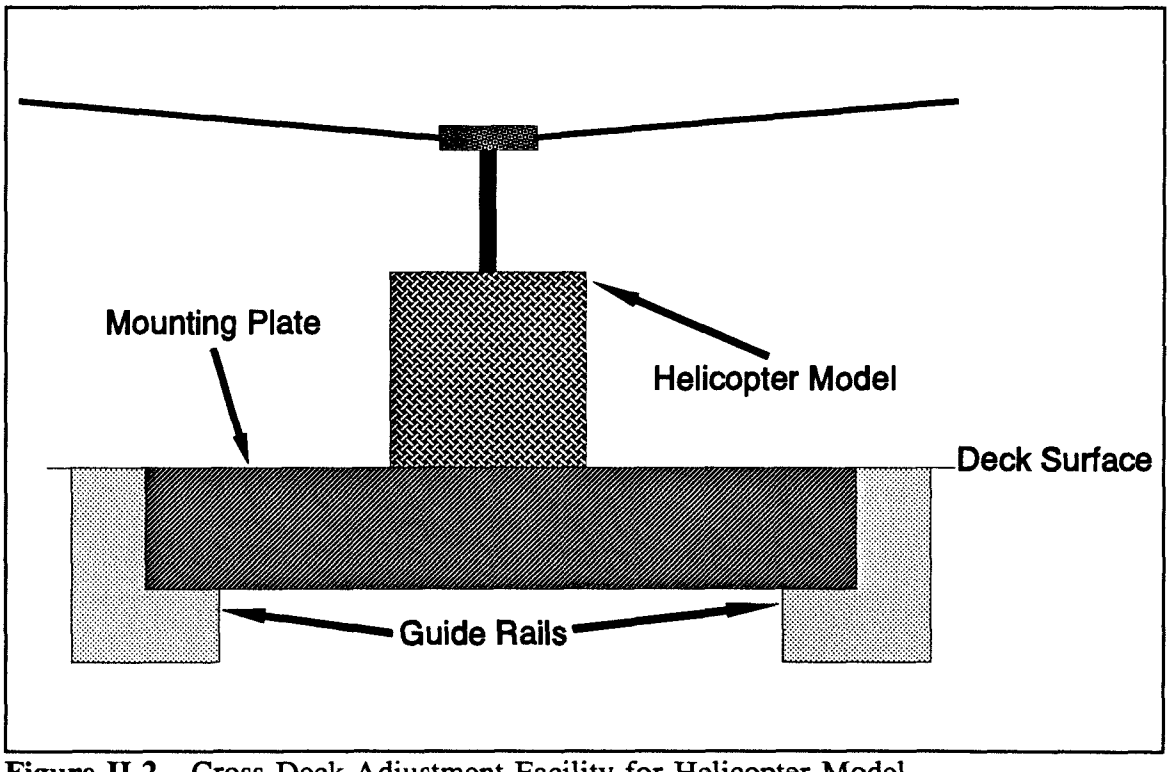

Figure II.2 - Cross Deck Adjustment Facility for Helicopter Model

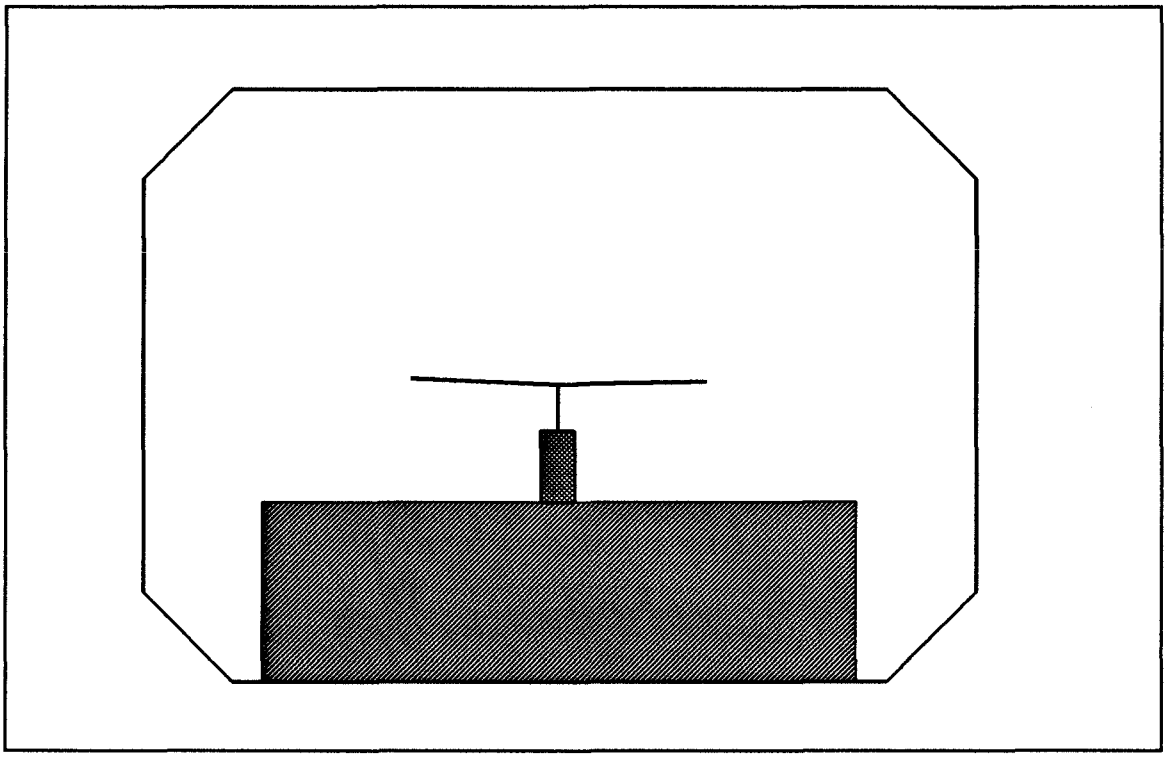

Figure II.3 - View of Model Installed In Wind Tunnel

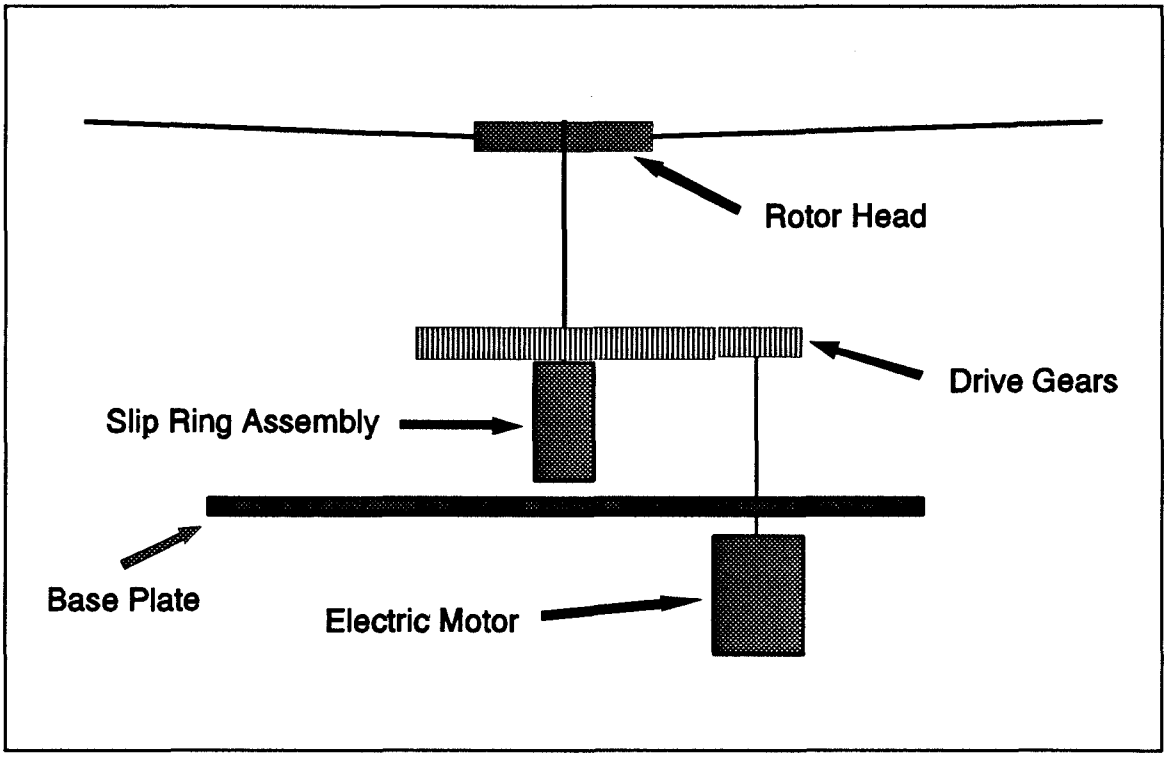

Figure II.4 - Schematic of Helicopter Model

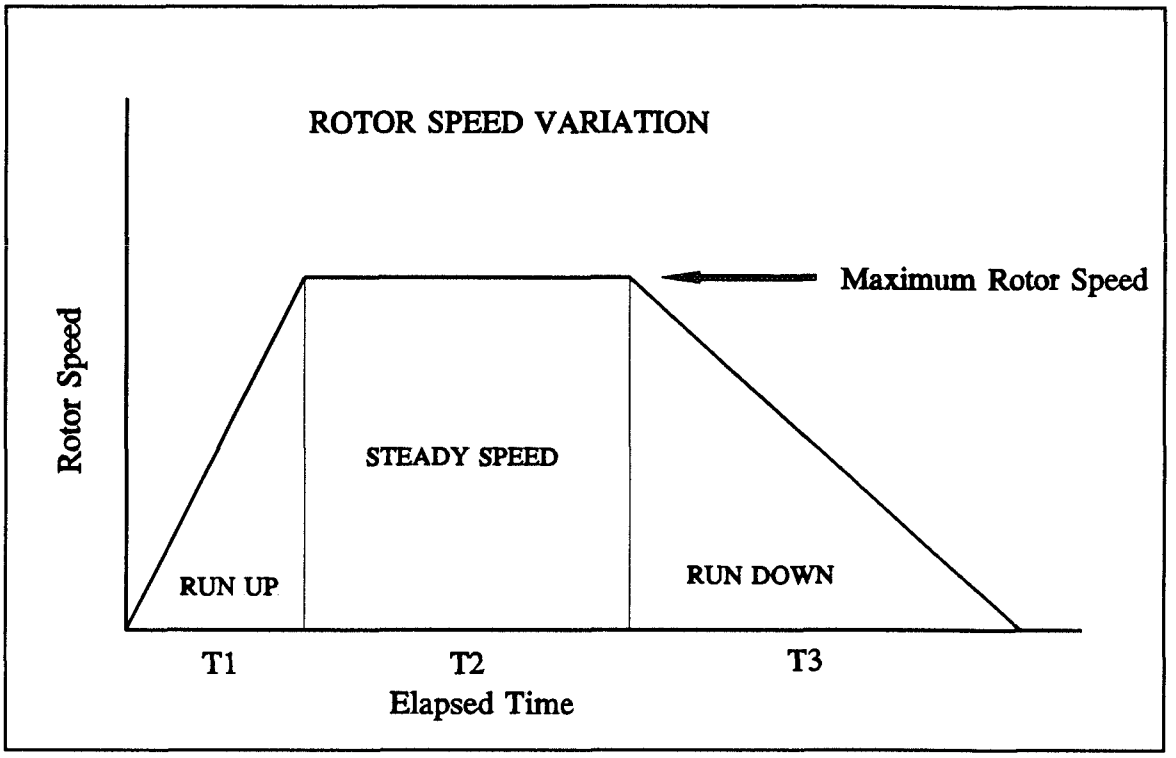

Figure II.5 - Rotor Speed Variation

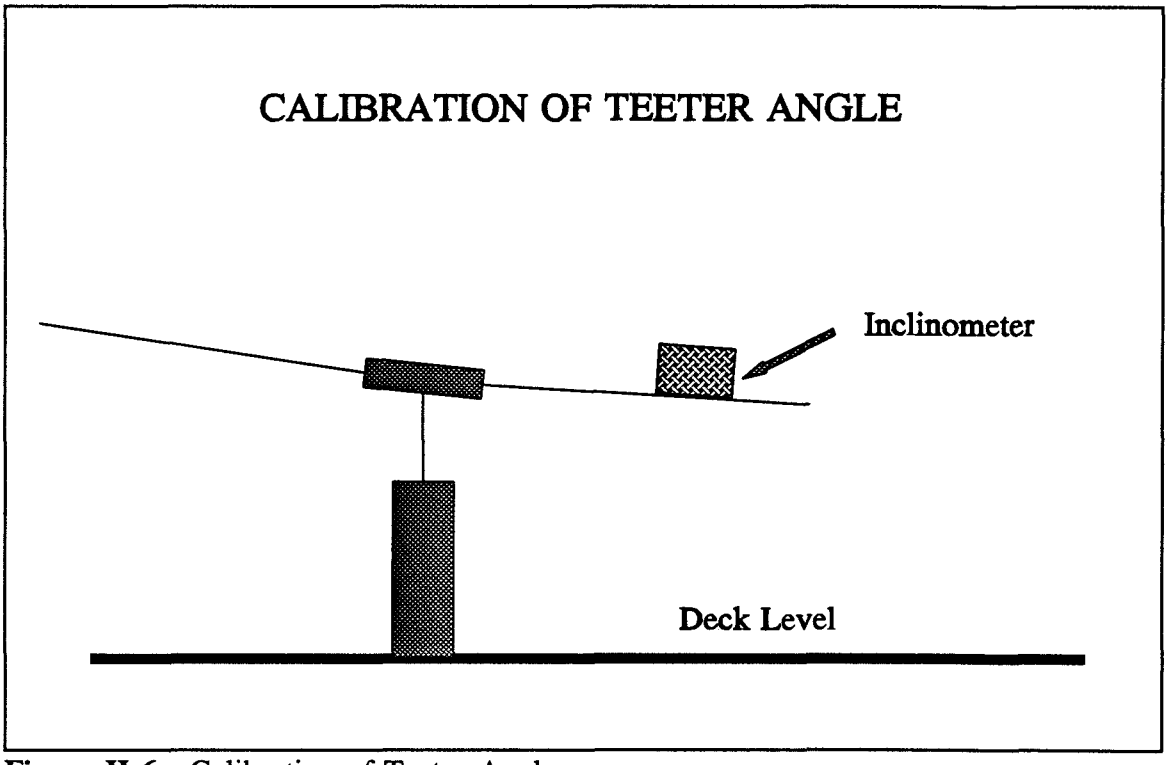

Figure II.6 - Calibration of Teeter Angle

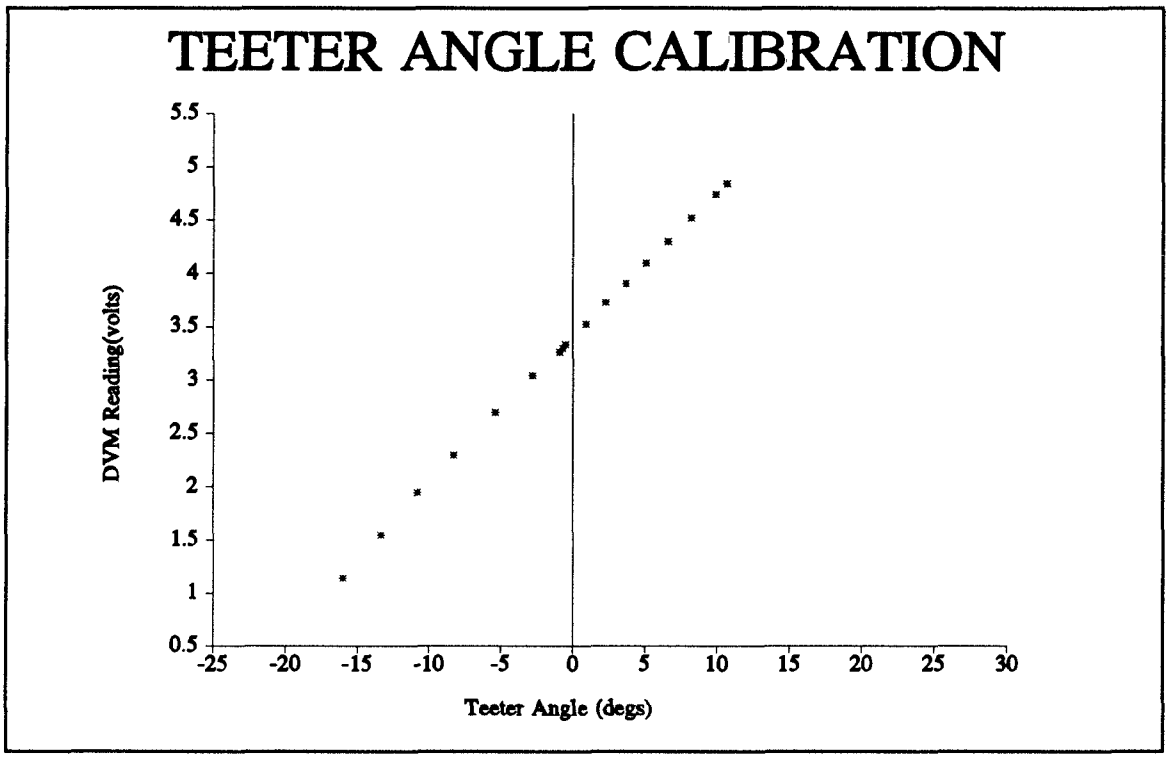

Figure II.7 - Teeter Angle Calibration Data

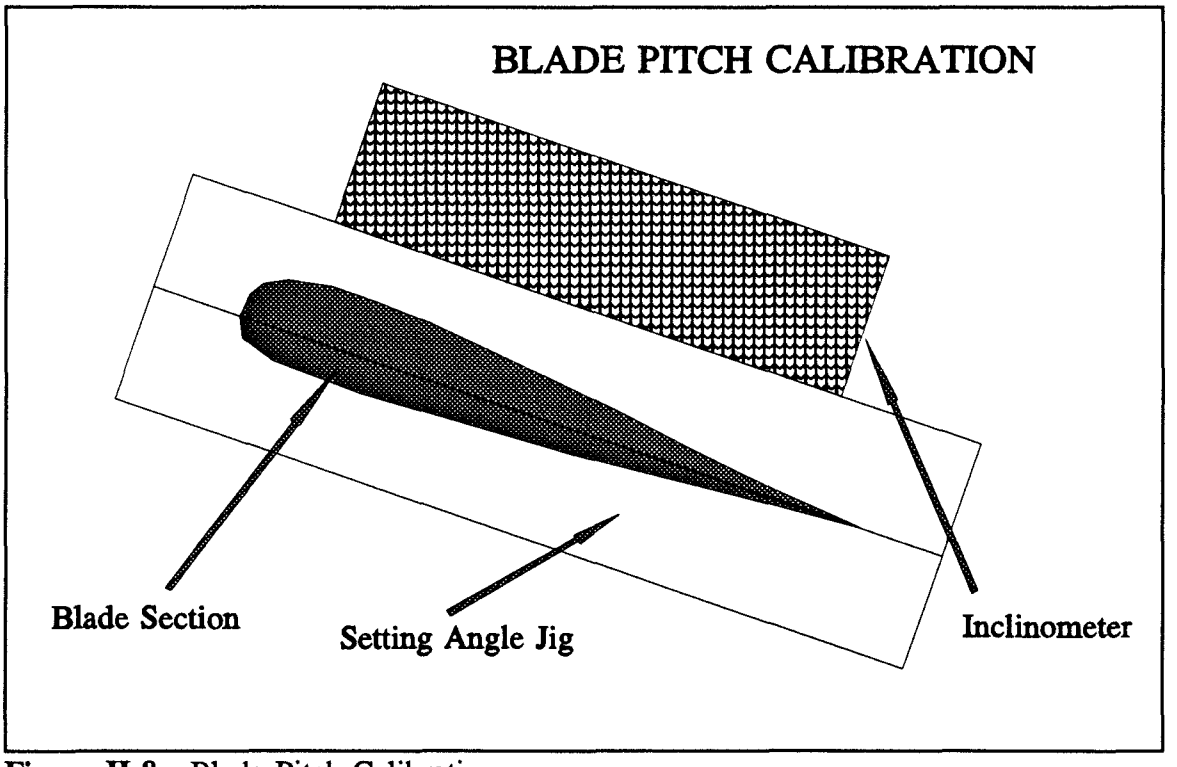

Figure II.8 - Blade Pitch Calibration

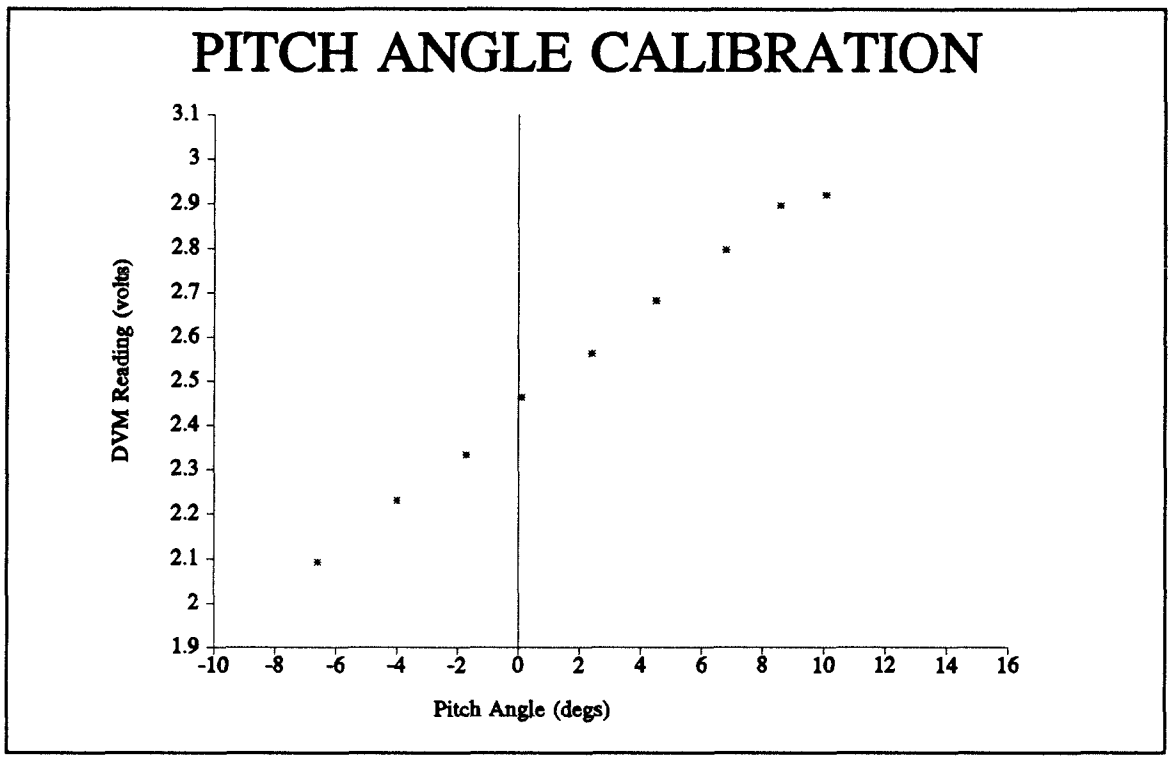

Figure II.9 - Pitch Angle Calibration Data

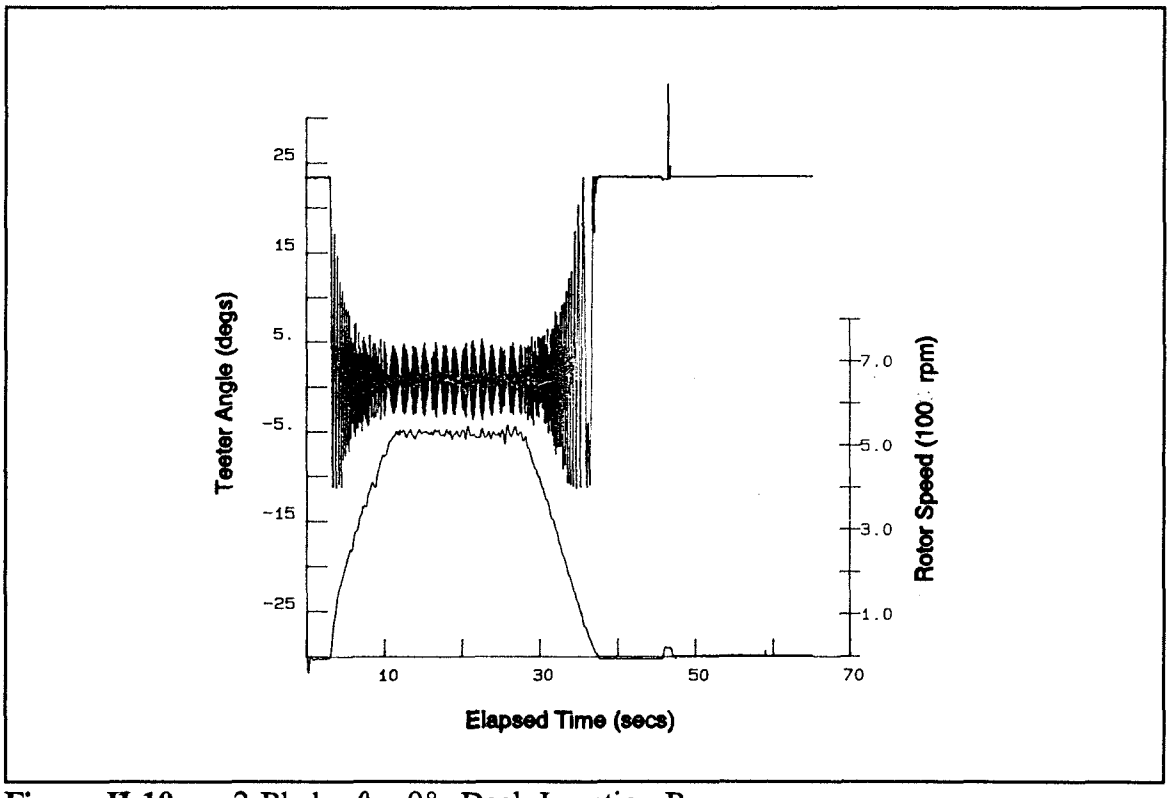

Figure II.10.a - 2 Blade, θ_0=0°, Deck Location B

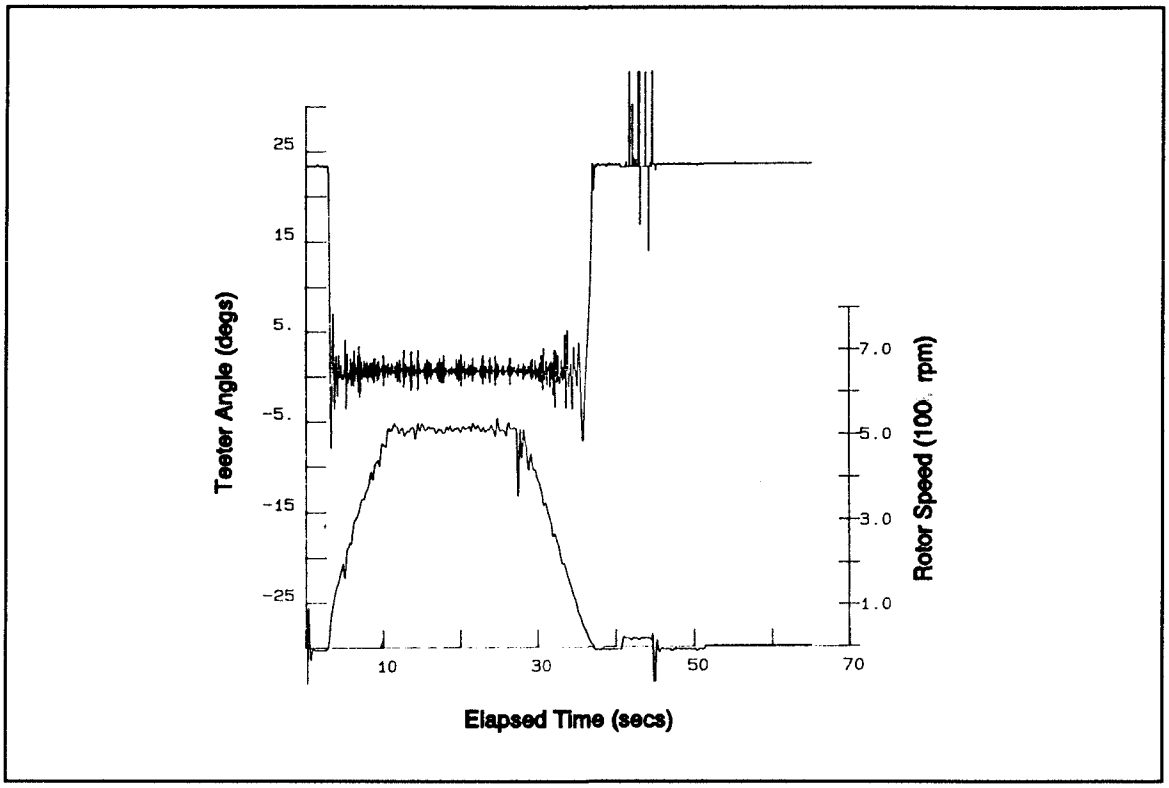

Figure II.10.b - 2 Blade, θ_0=0°, Deck Location D

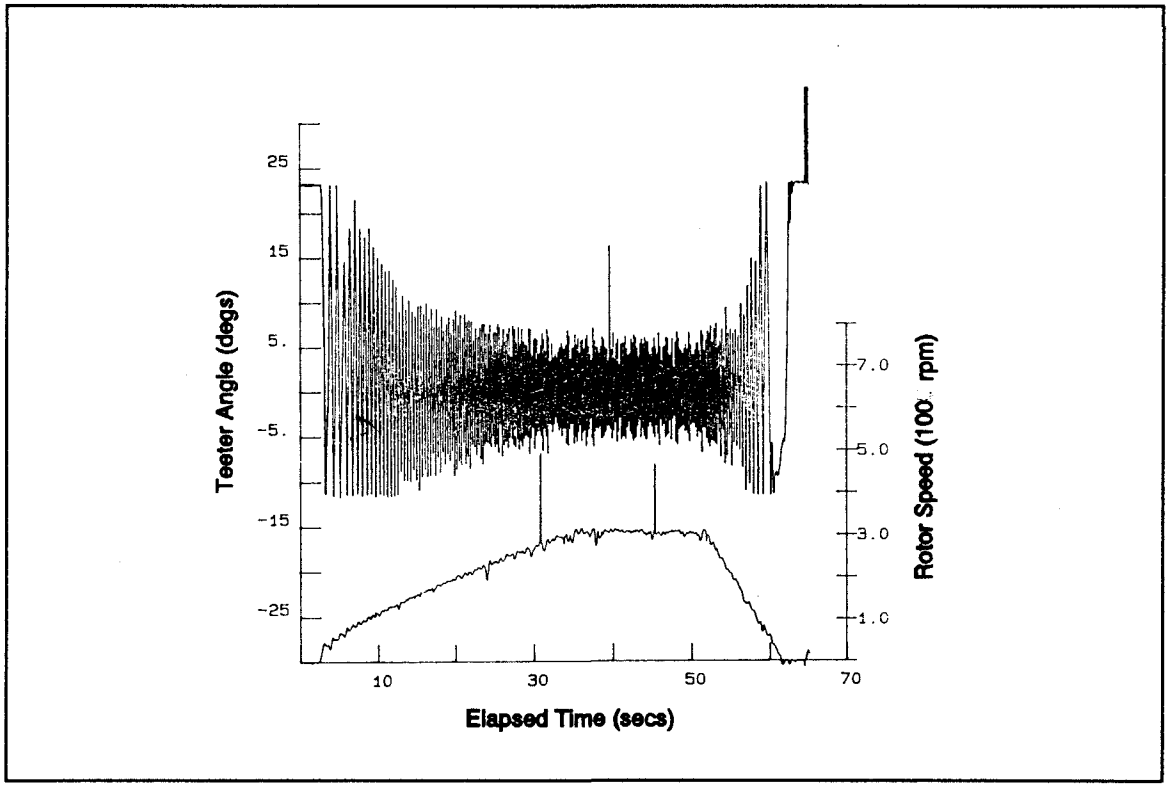

Figure II.10.c - 2 Blade, θ_0=0°, Deck Location C

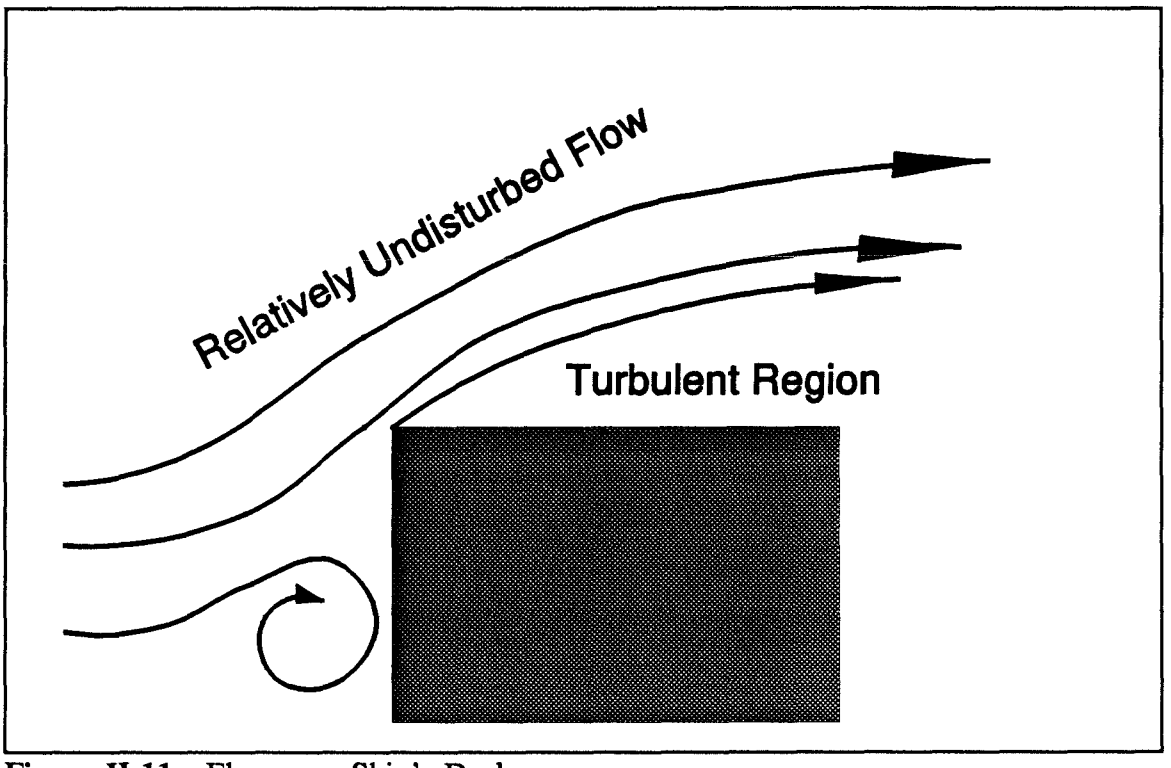

Figure II.11 - Flow over Ship's Deck

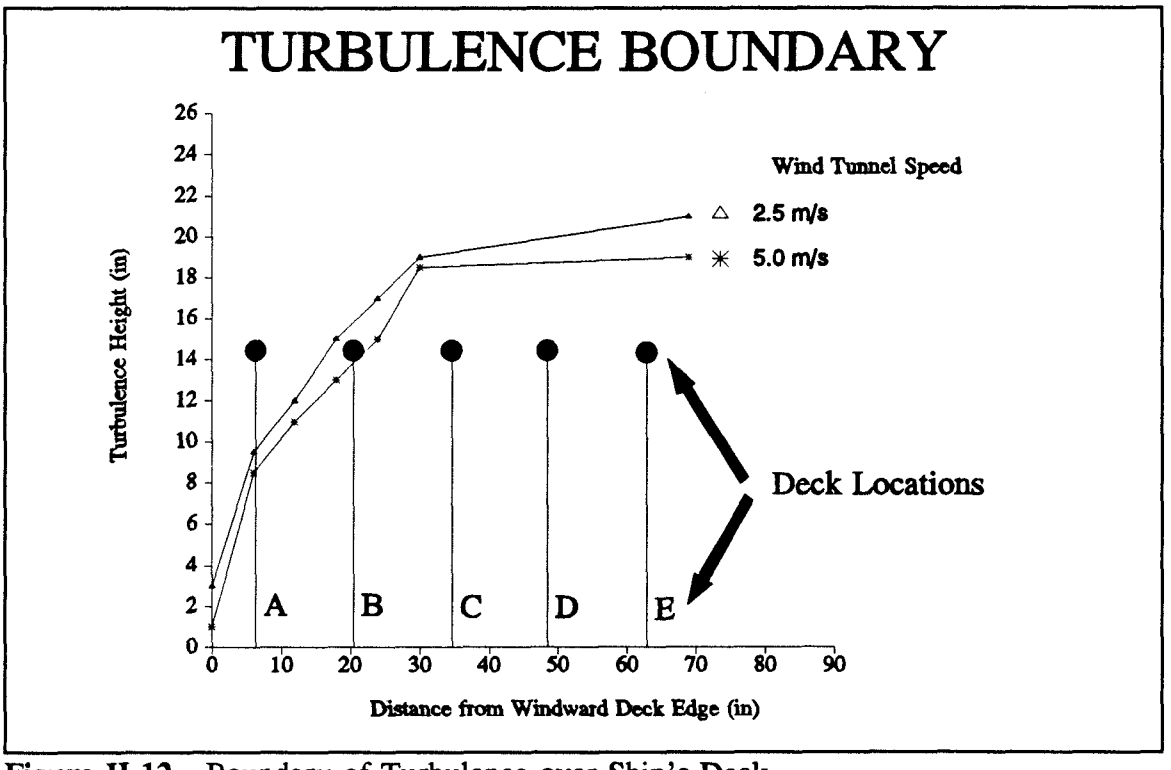

Figure II.12 - Boundary of Turbulence over Ship's Deck

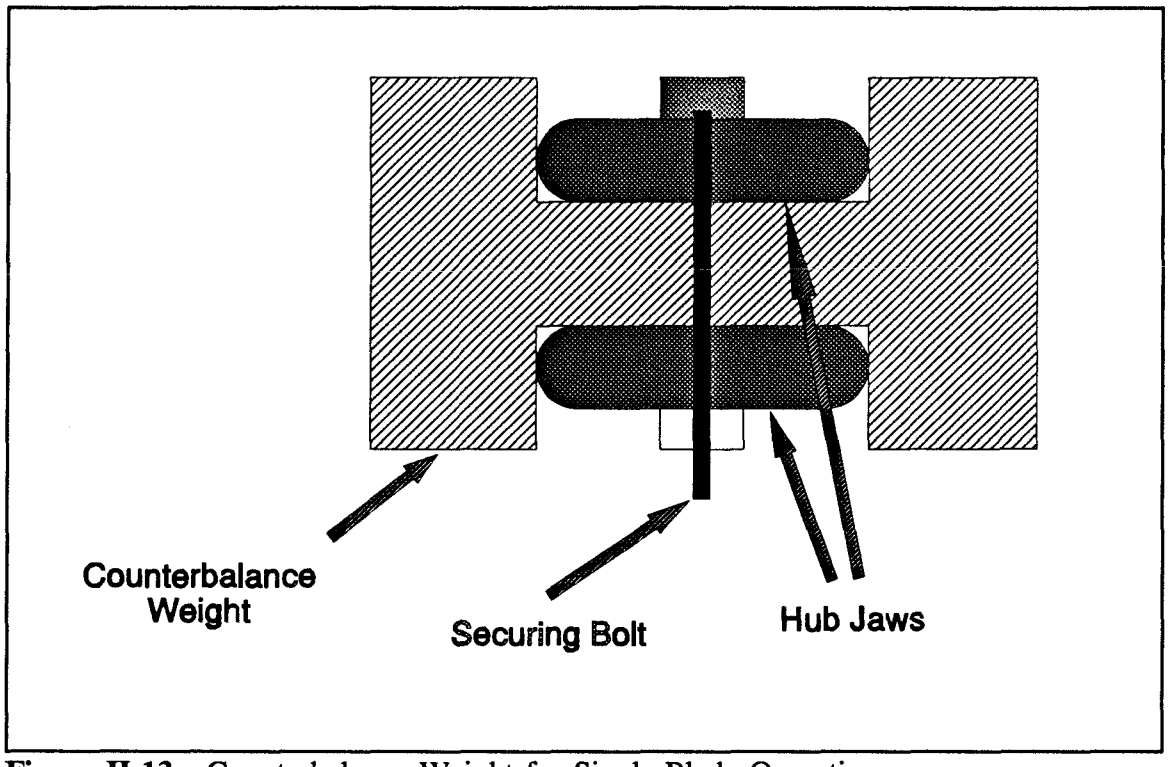

Figure II.13 - Counterbalance Weight for Single Blade Operation

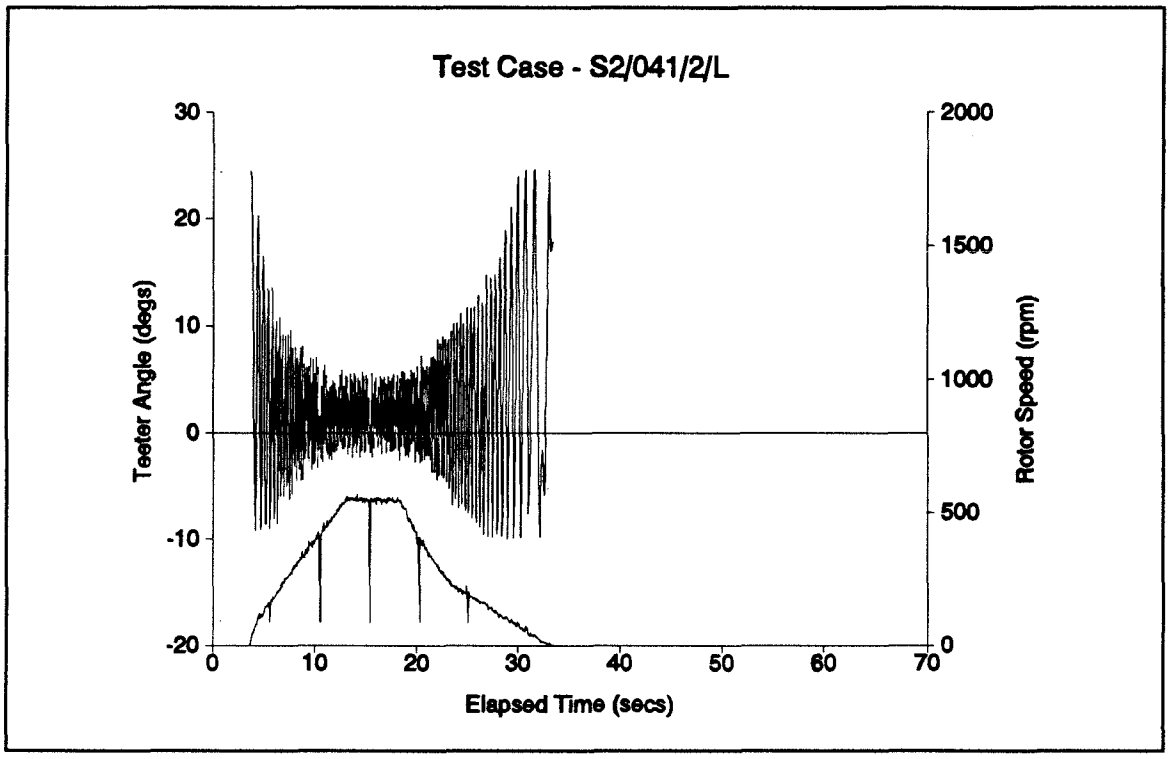

Figure II.14.a - 2 Blade, θ_0=0°, Deck Location B

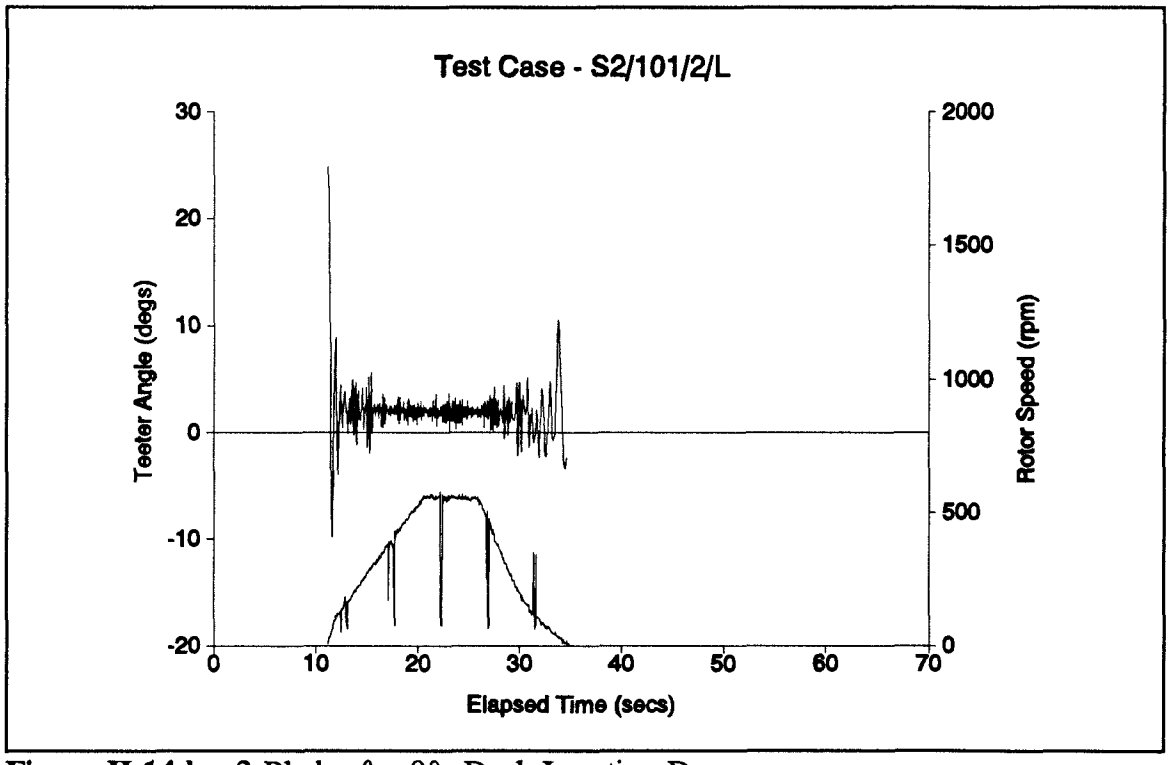

Figure II.14.b - 2 Blade, θ_0=0°, Deck Location D

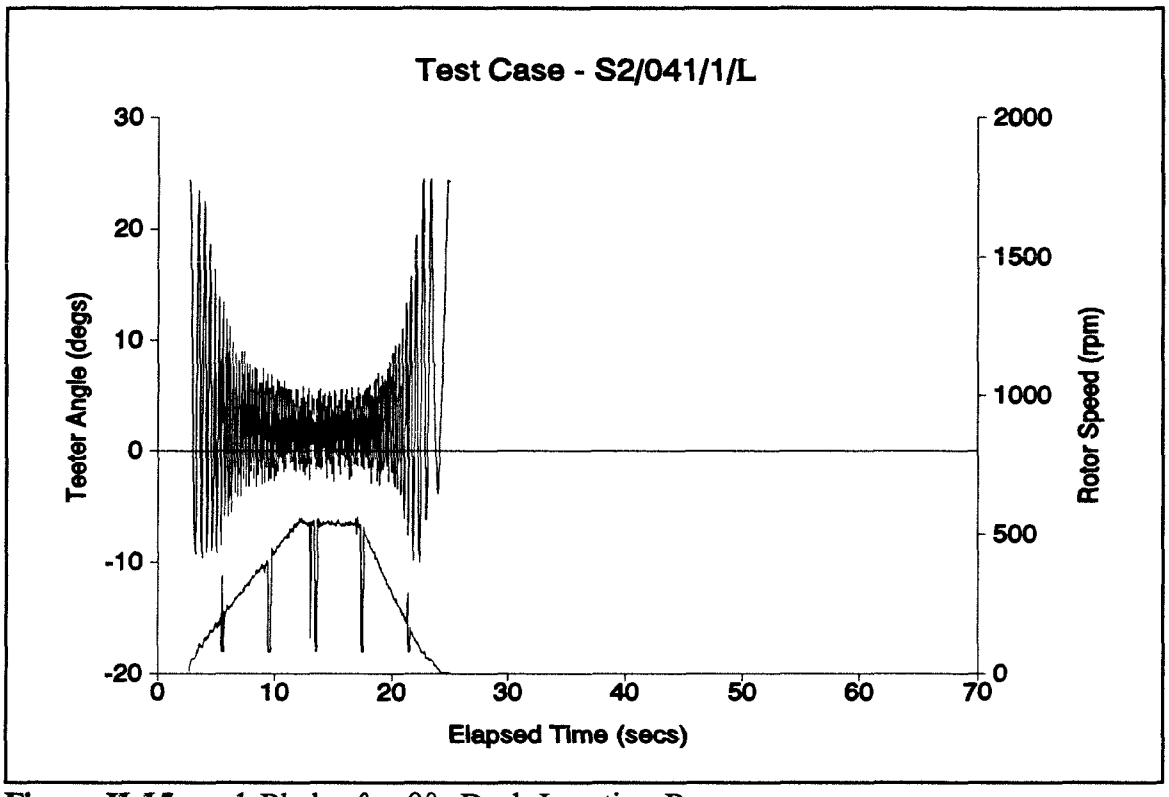

Figure II.15.a - 1 Blade, θ_0=0°, Deck Location B

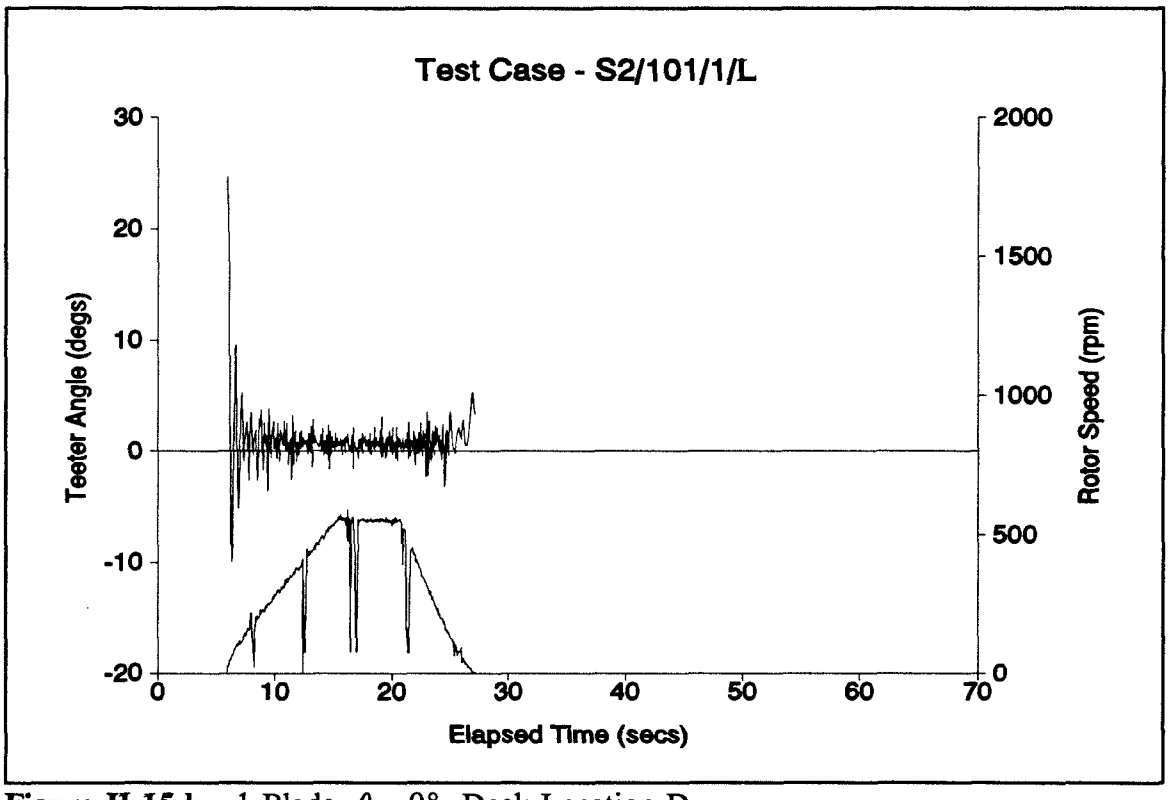

Figure II.15.b - 1 Blade, θ_0=0°, Deck Location D

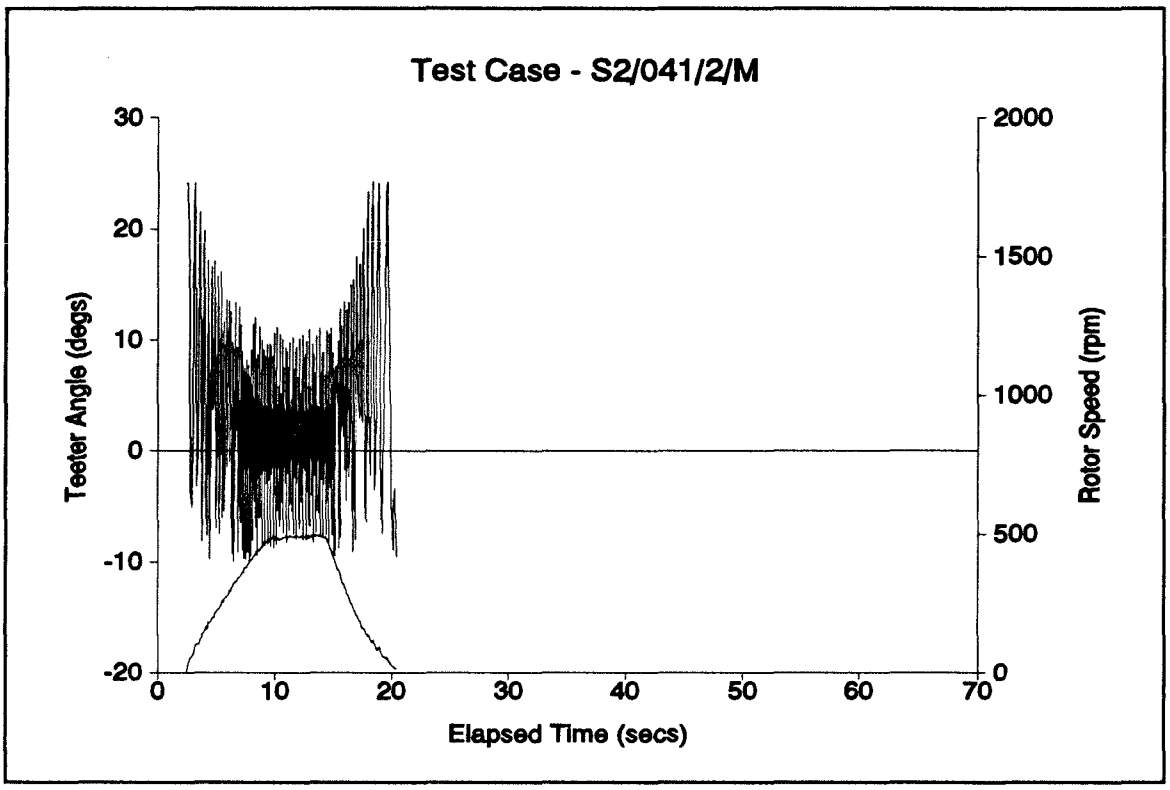

Figure II.16.a - 2 Blade, θ_0=5°, Deck Location B

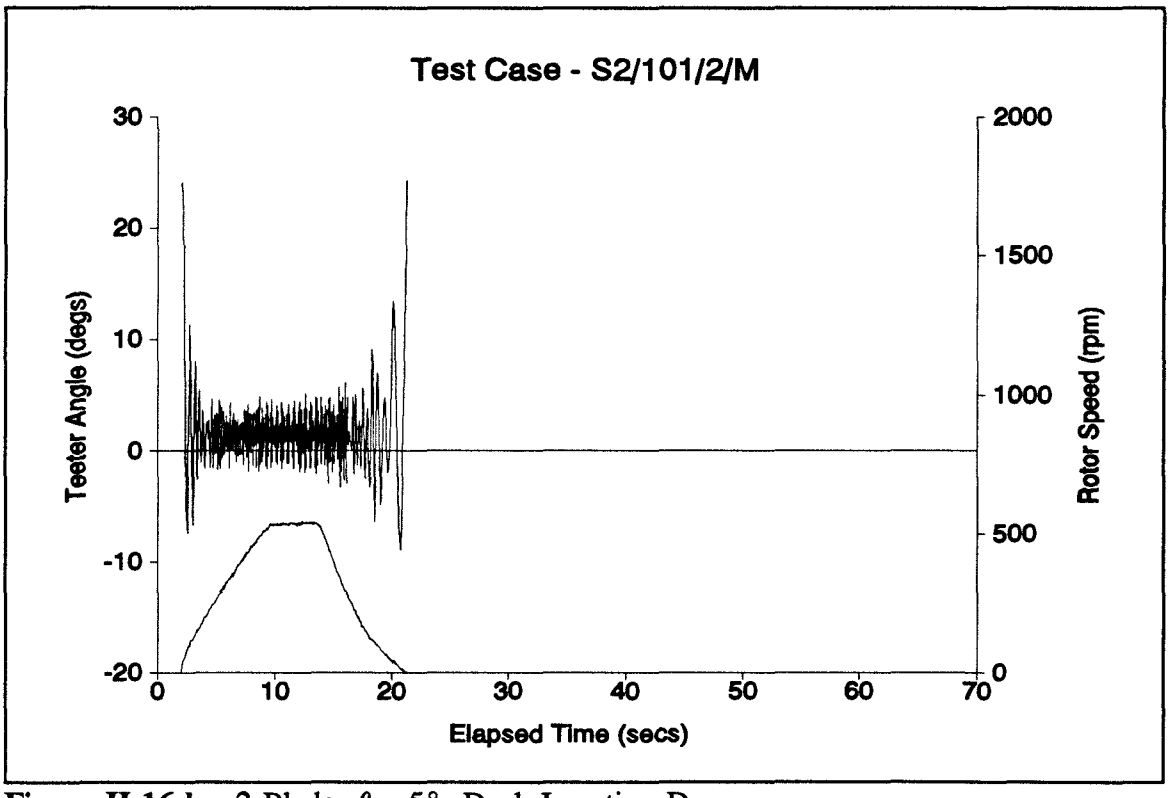

Figure II.16.b - 2 Blade, θ_0=5°, Deck Location D

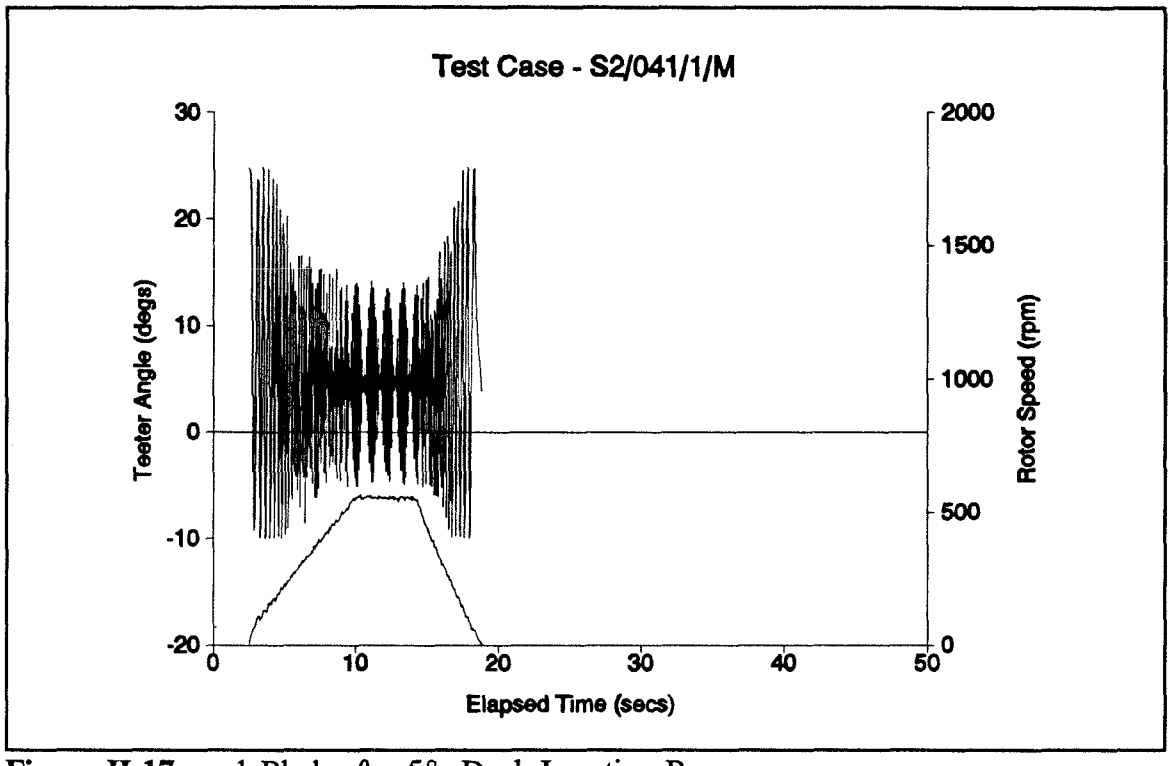

Figure II.17.a - 1 Blade, θ_0=5°, Deck Location B

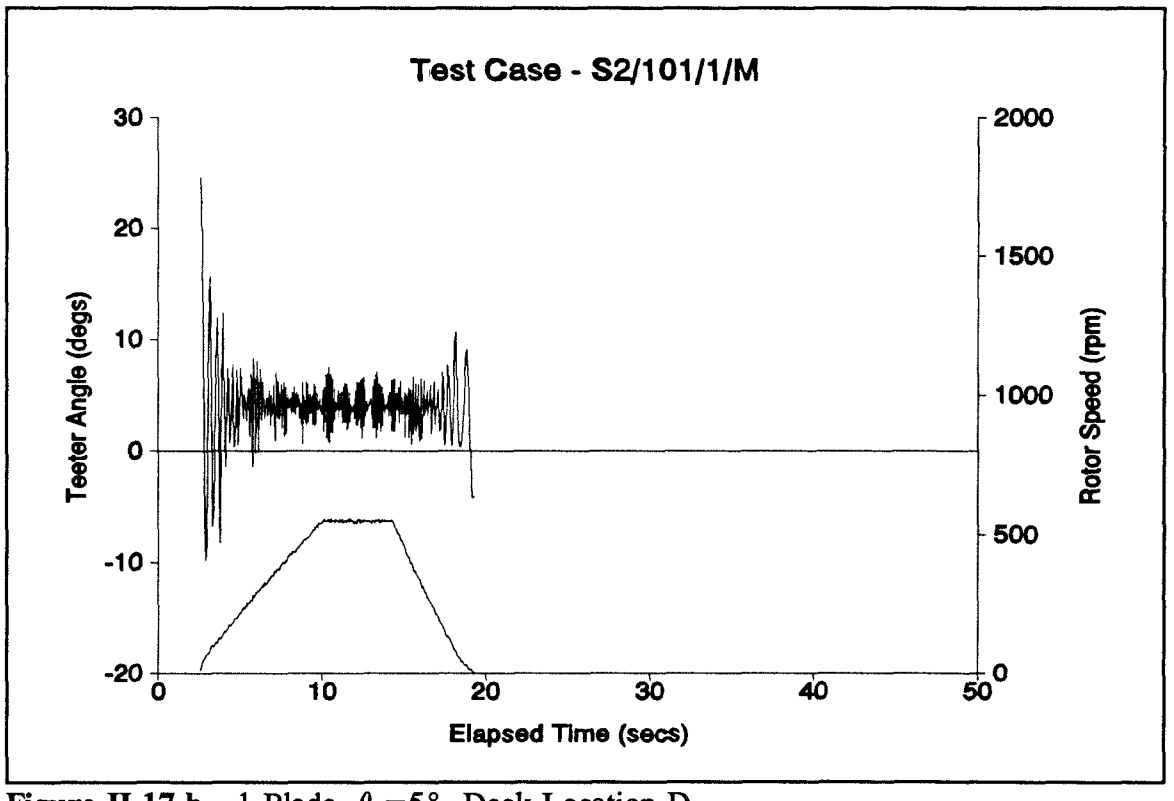

Figure II.17.b - 1 Blade, θ_0=5°, Deck Location D

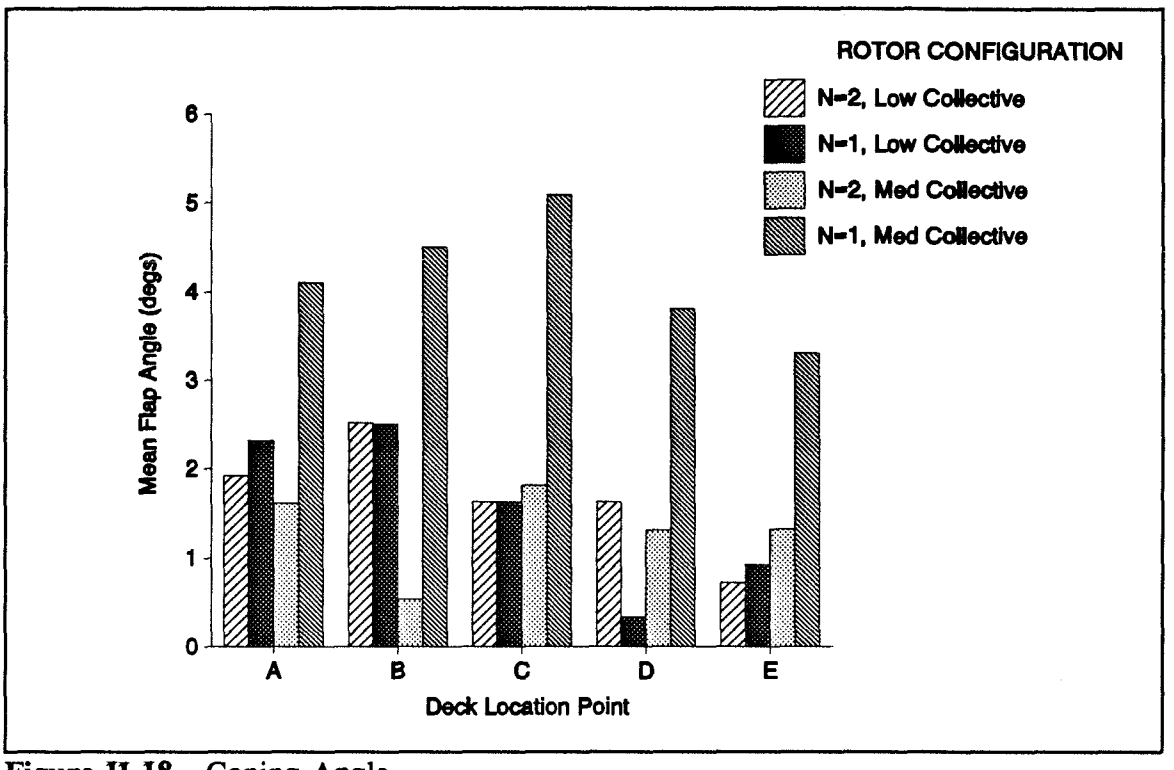

Figure II.18 - Coning Angle

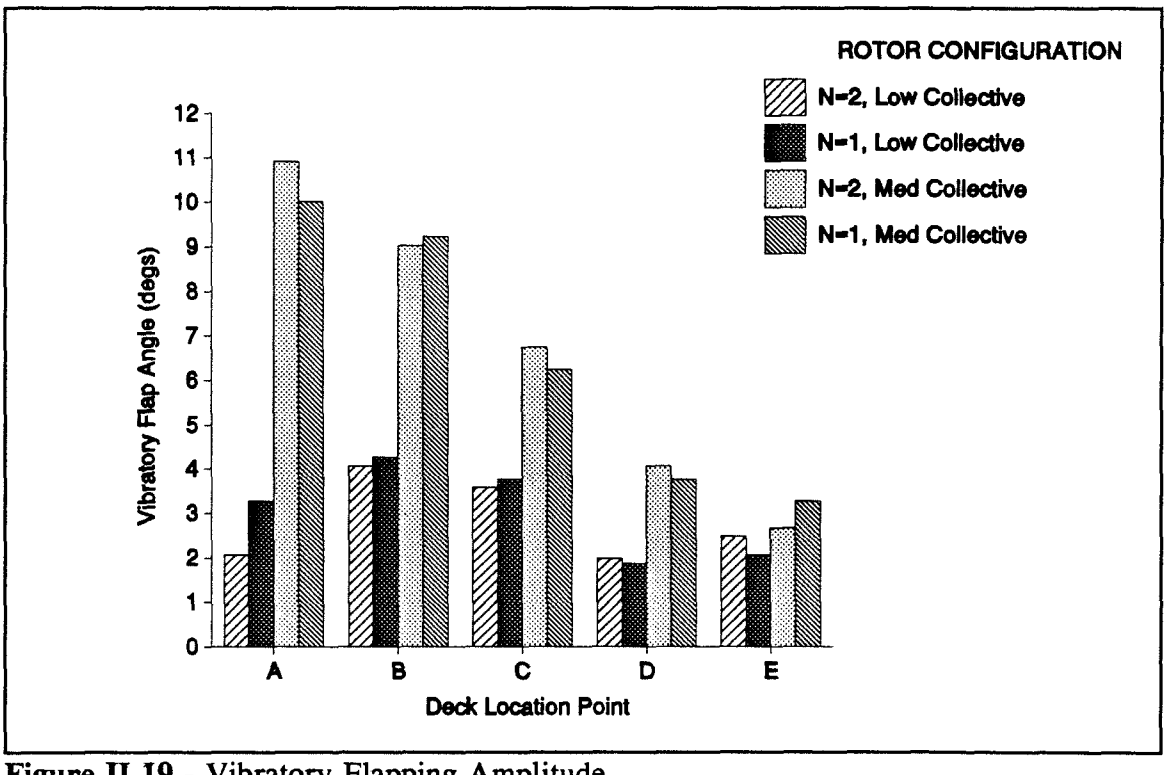

Figure II.19 - Vibratory Flapping Amplitude

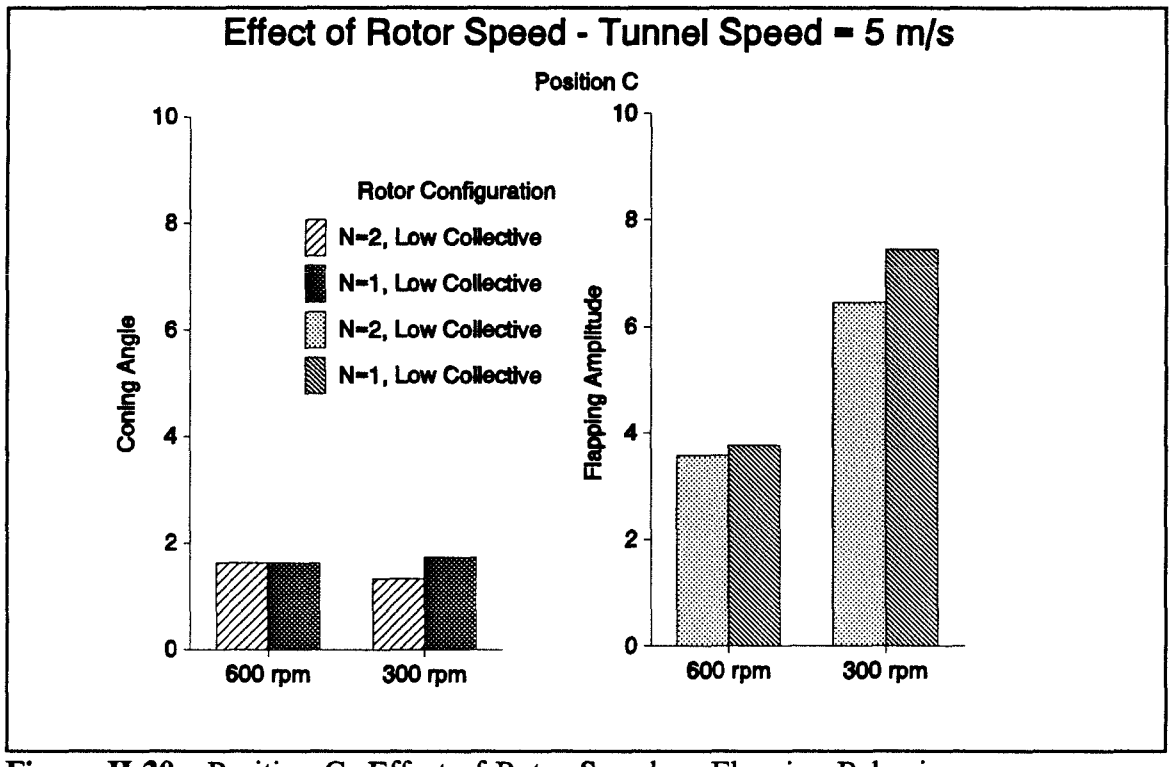

Figure II.20 - Position C, Effect of Rotor Speed on Flapping Behaviour

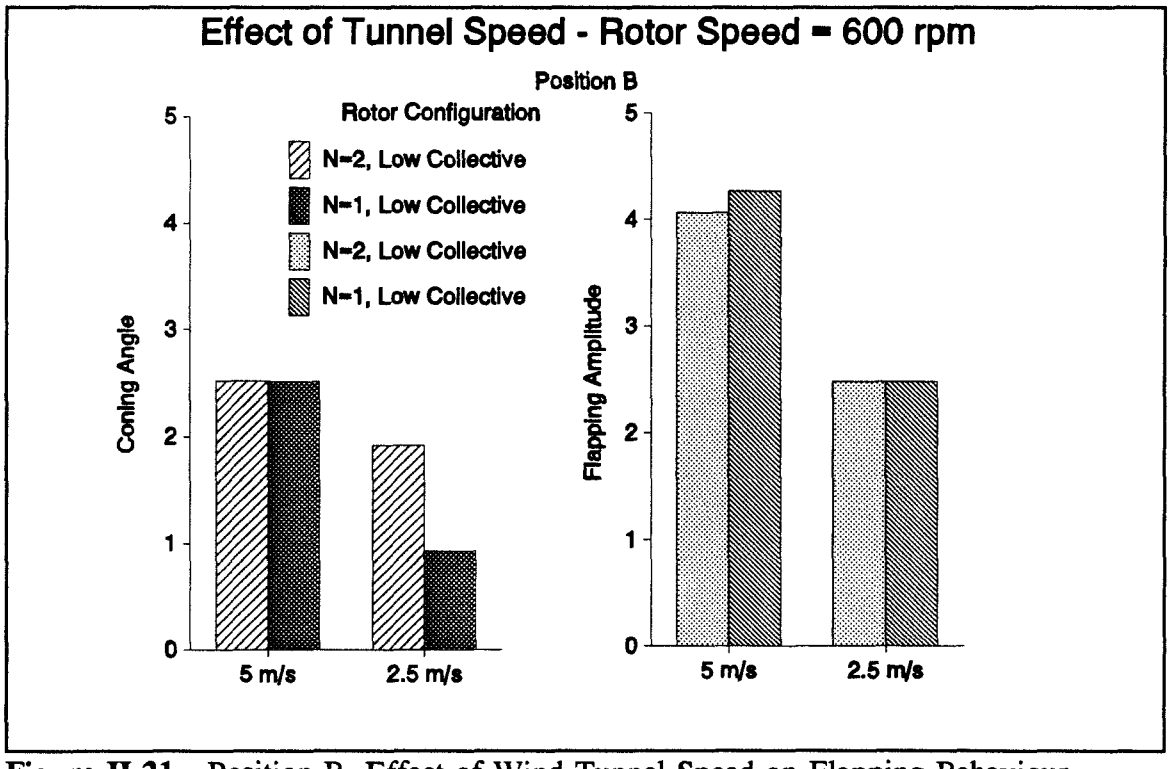

Figure II.21 - Position B, Effect of Wind Tunnel Speed on Flapping Behaviour

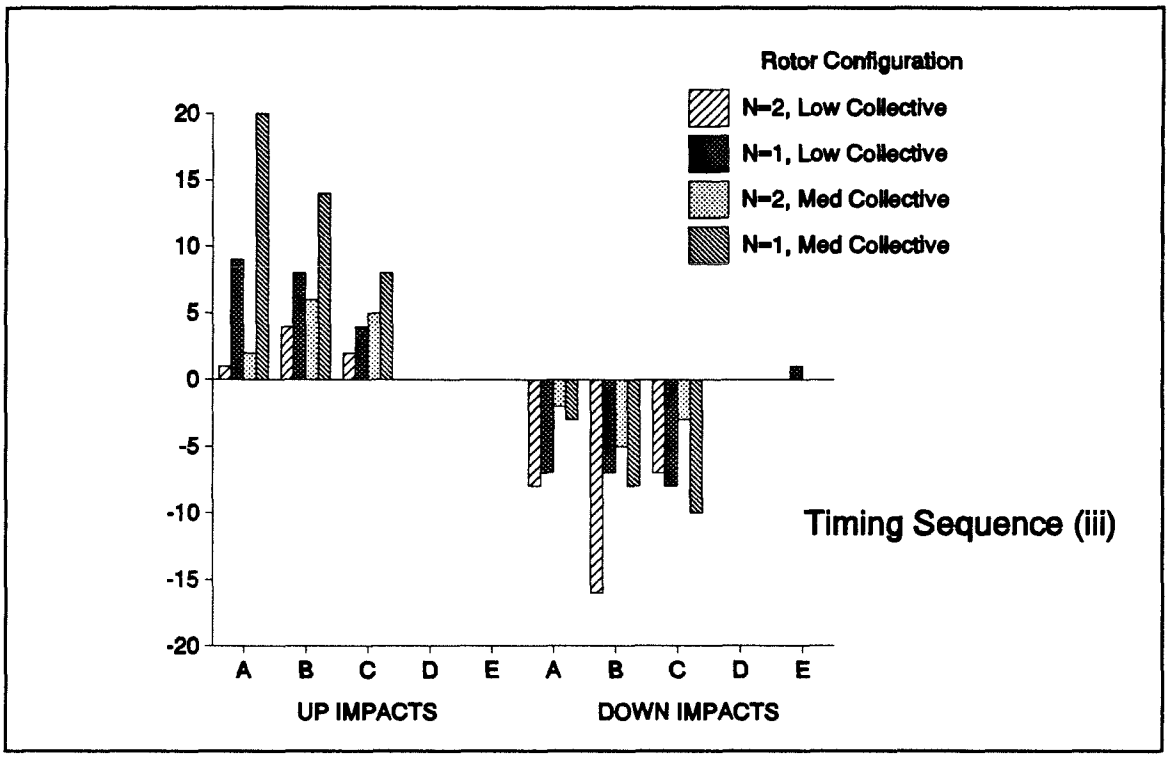

Figure II.22 - Stop Impacts with Extended Rotor Run Down

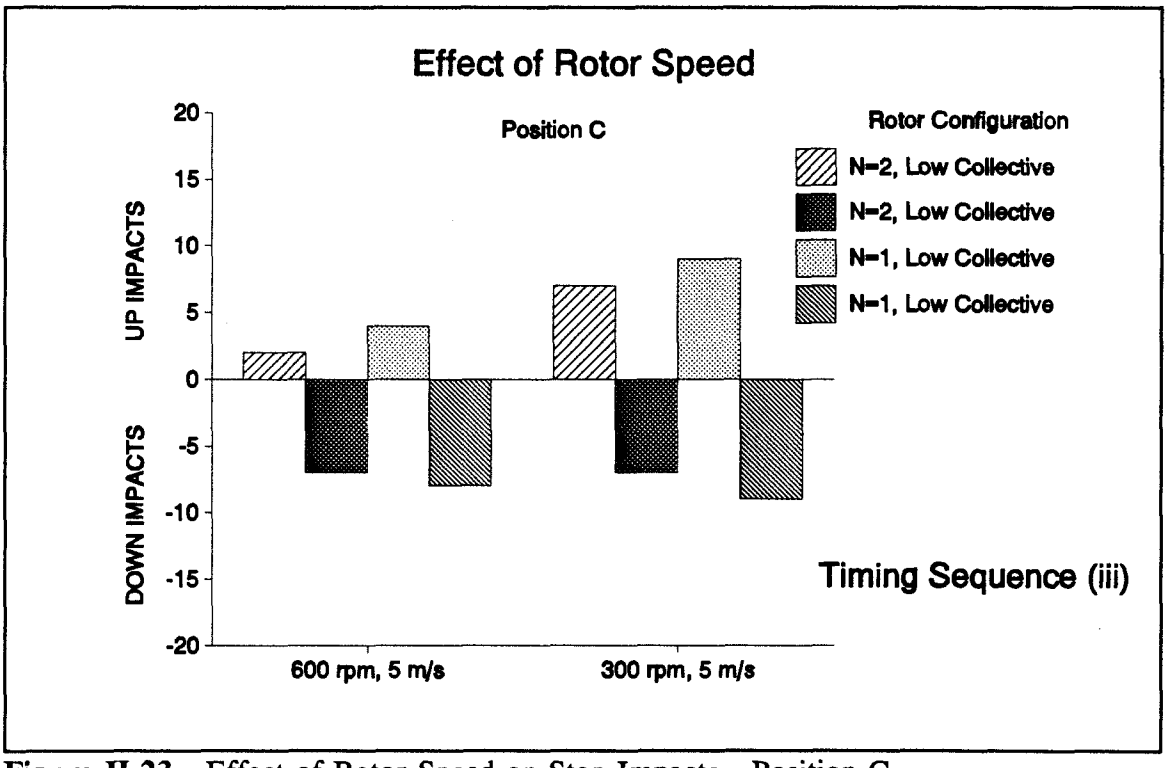

Figure II.23 - Effect of Rotor Speed on Stop Impacts - Position C

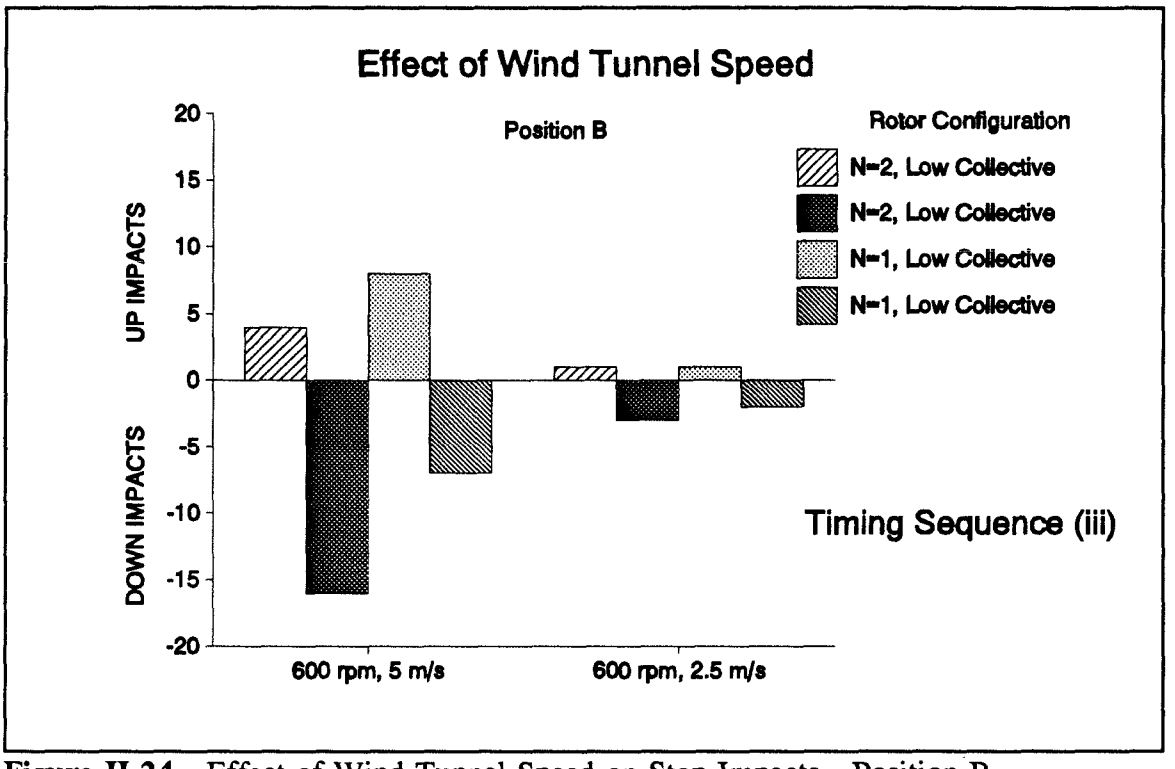

Figure II.24 - Effect of Wind Tunnel Speed on Stop Impacts - Position B

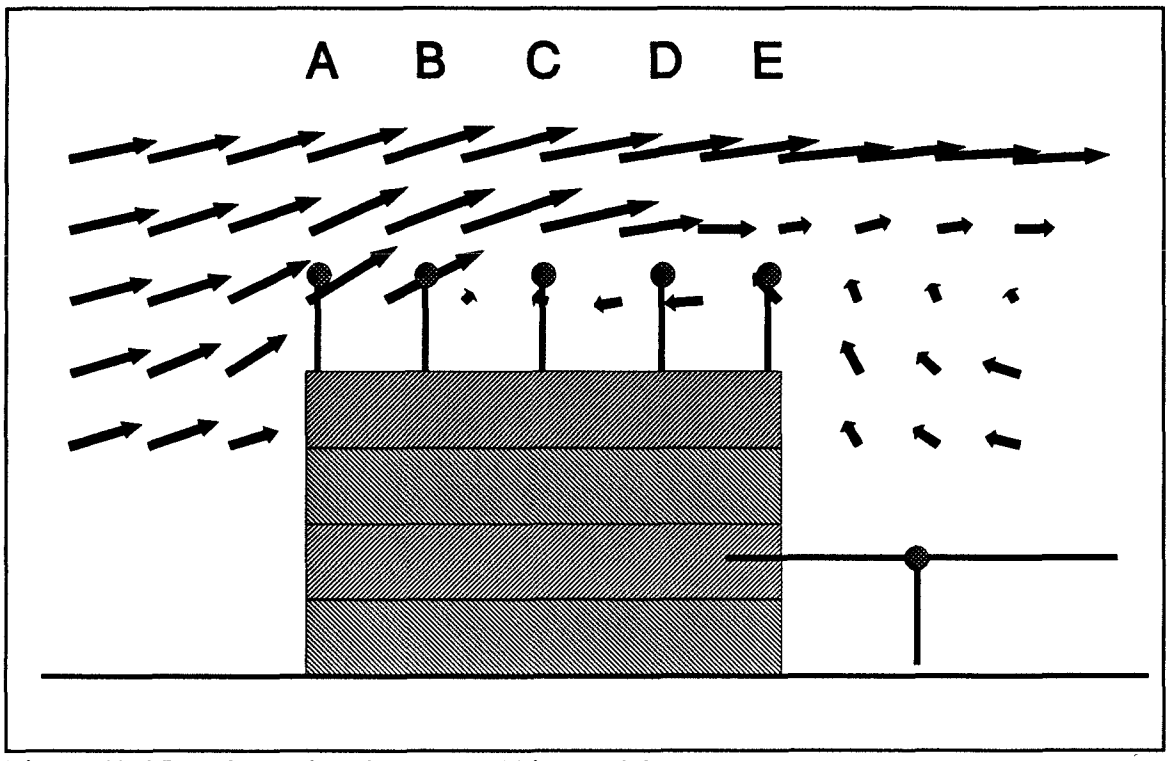

Figure II.25 - Flow Directions over Ship Model

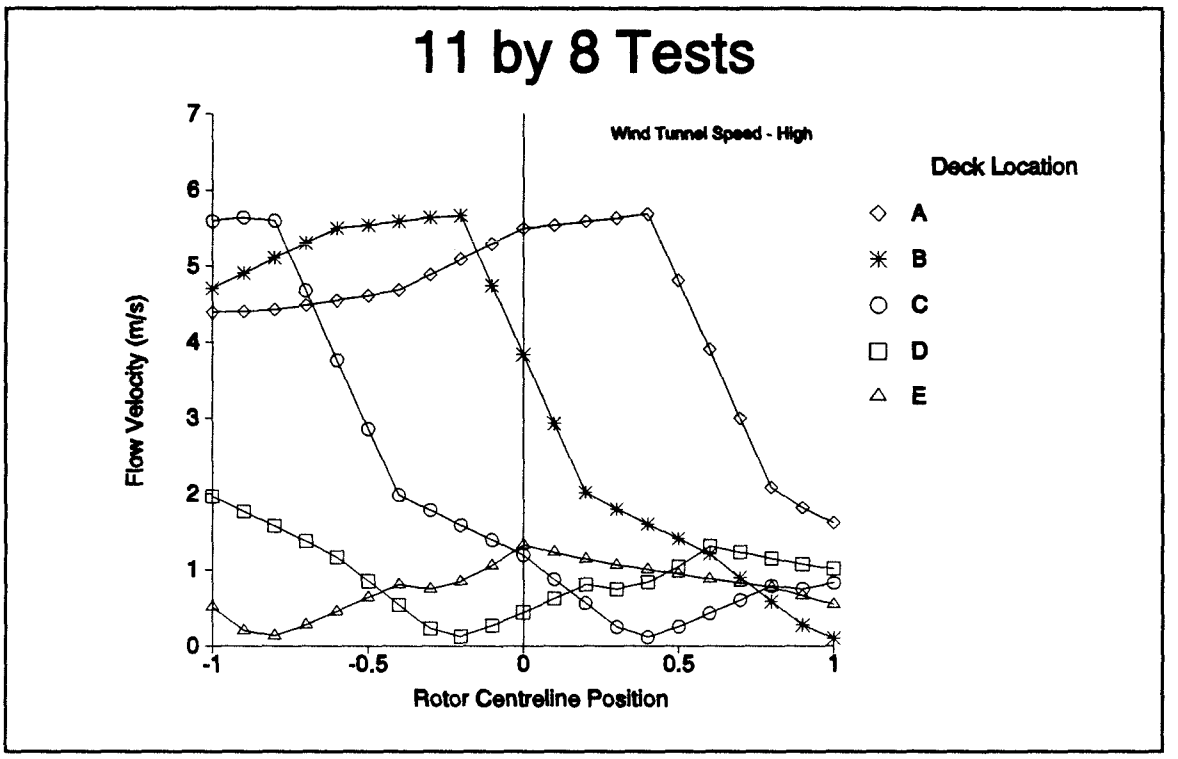

Figure II.26 - Incident Flow Velocity over Rotor Disc Centre Line

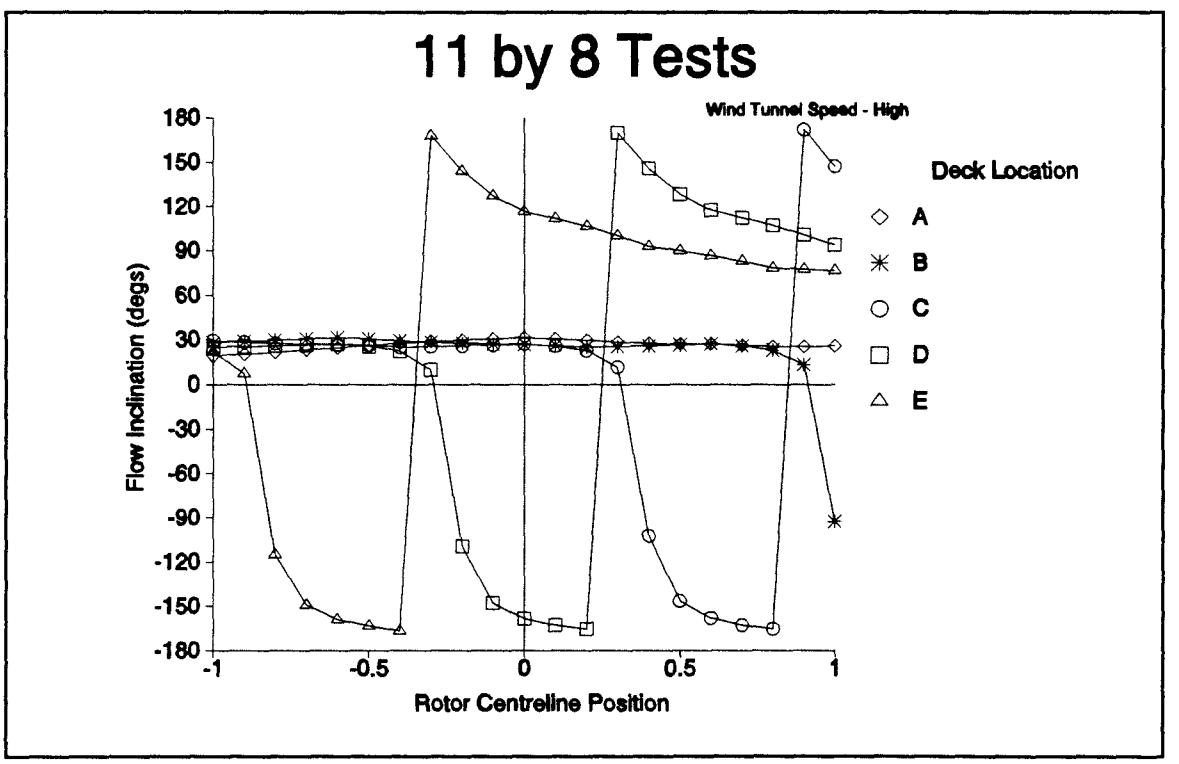

Figure II.27 - Incident Flow Inclination over Rotor Disc Centre Line

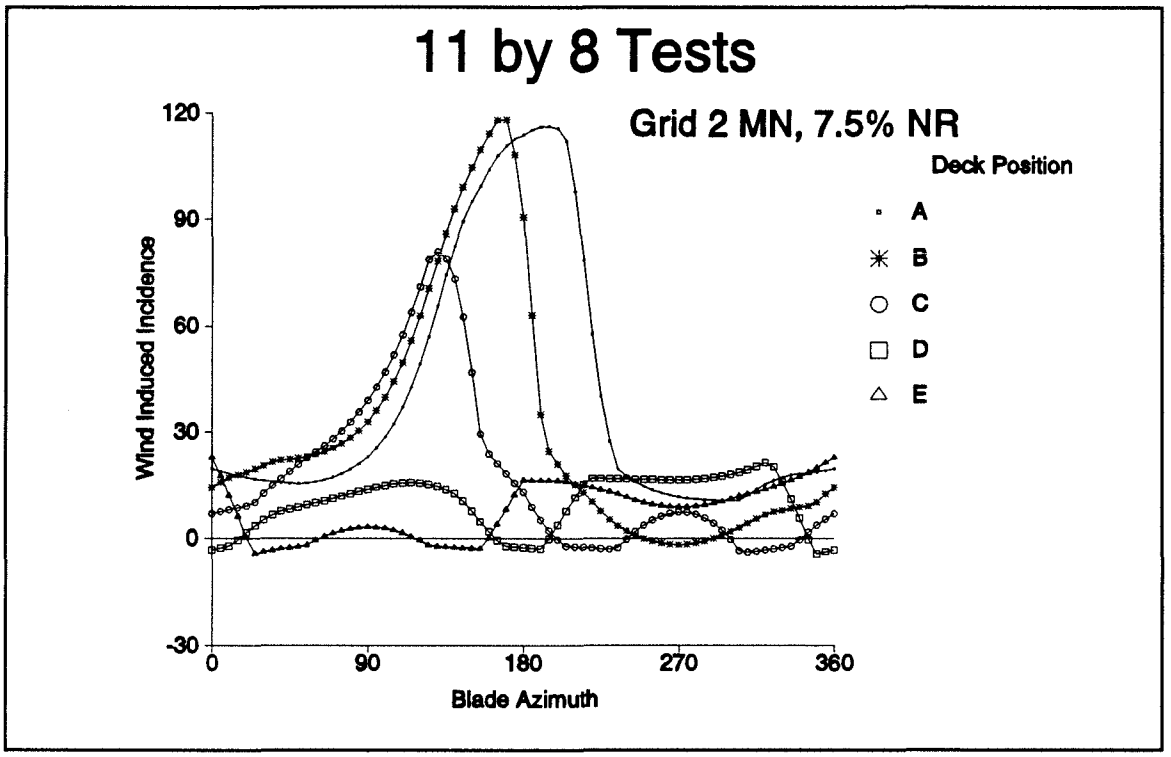

Figure II.28 - Tip Incidence Change due to Incident Wind @ 7.5% NR

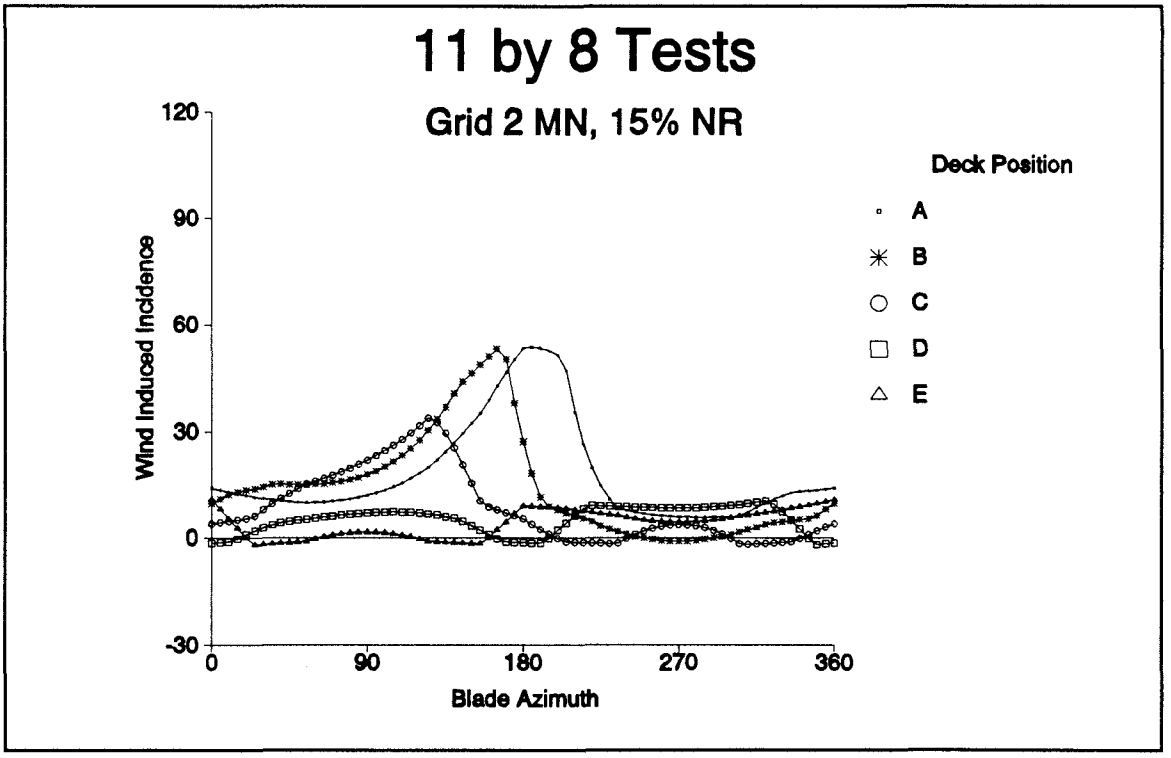

Figure II.29 - Tip Incidence Change due to Incident Wind @ 15% NR

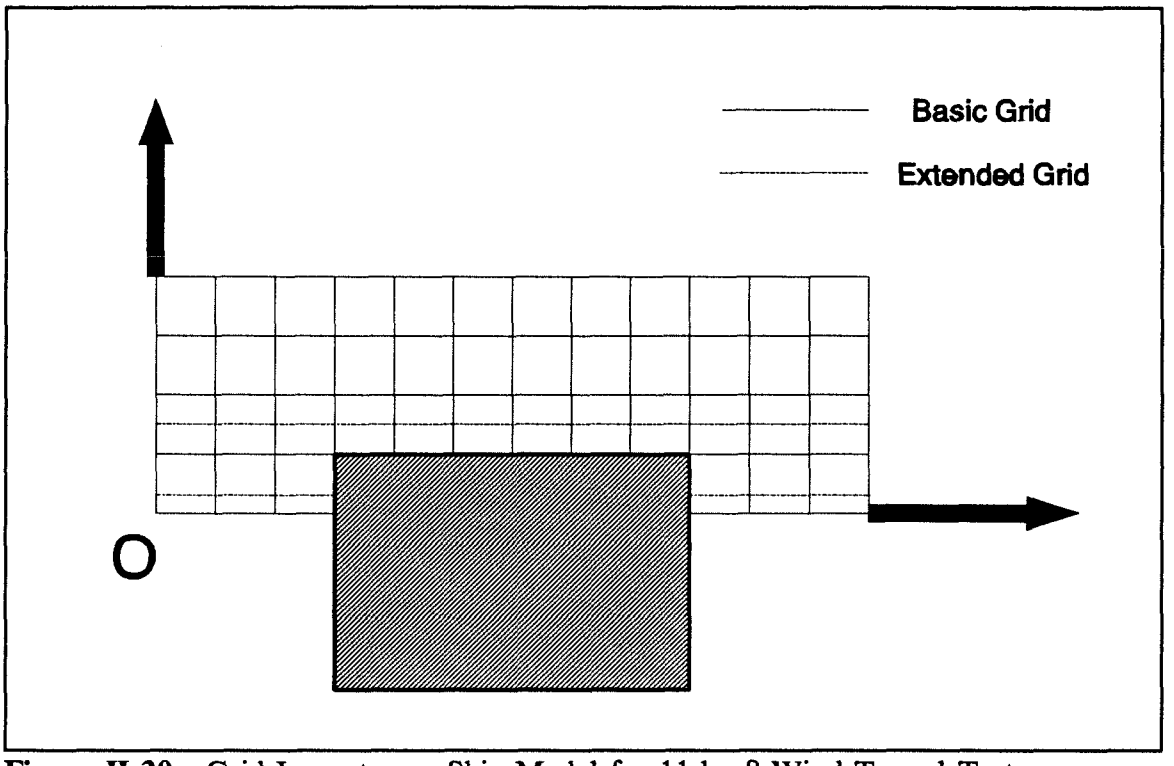

Figure II.30 - Grid Layout over Ship Model for 11 by 8 Wind Tunnel Tests

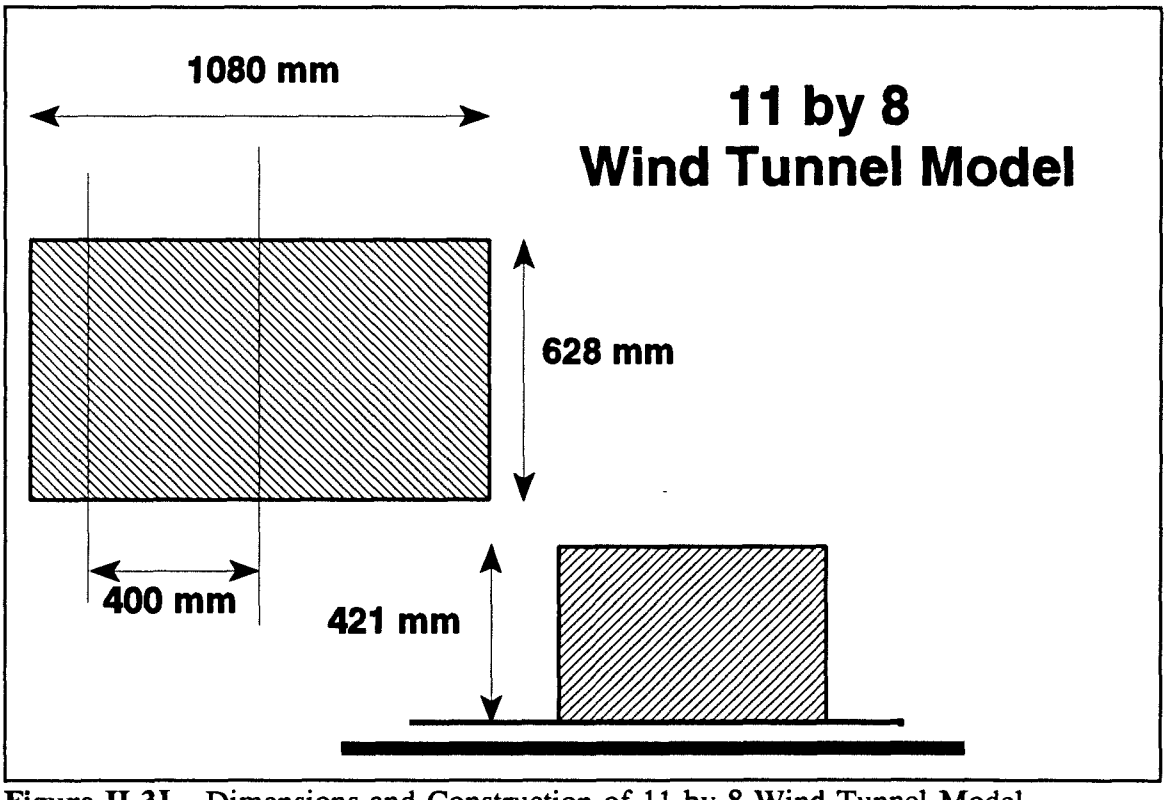

Figure II.31 - Dimensions and Construction of 11 by 8 Wind Tunnel Model

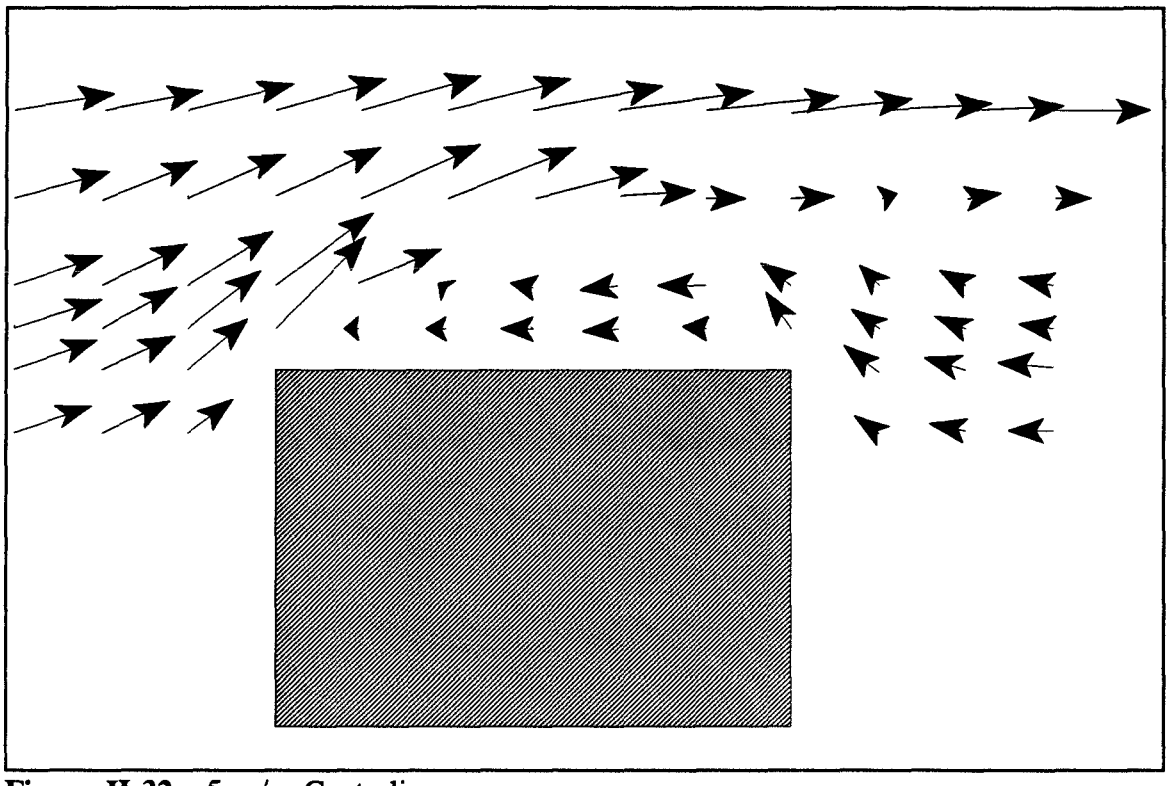

Figure II.32 - 5 m/s, Centreline

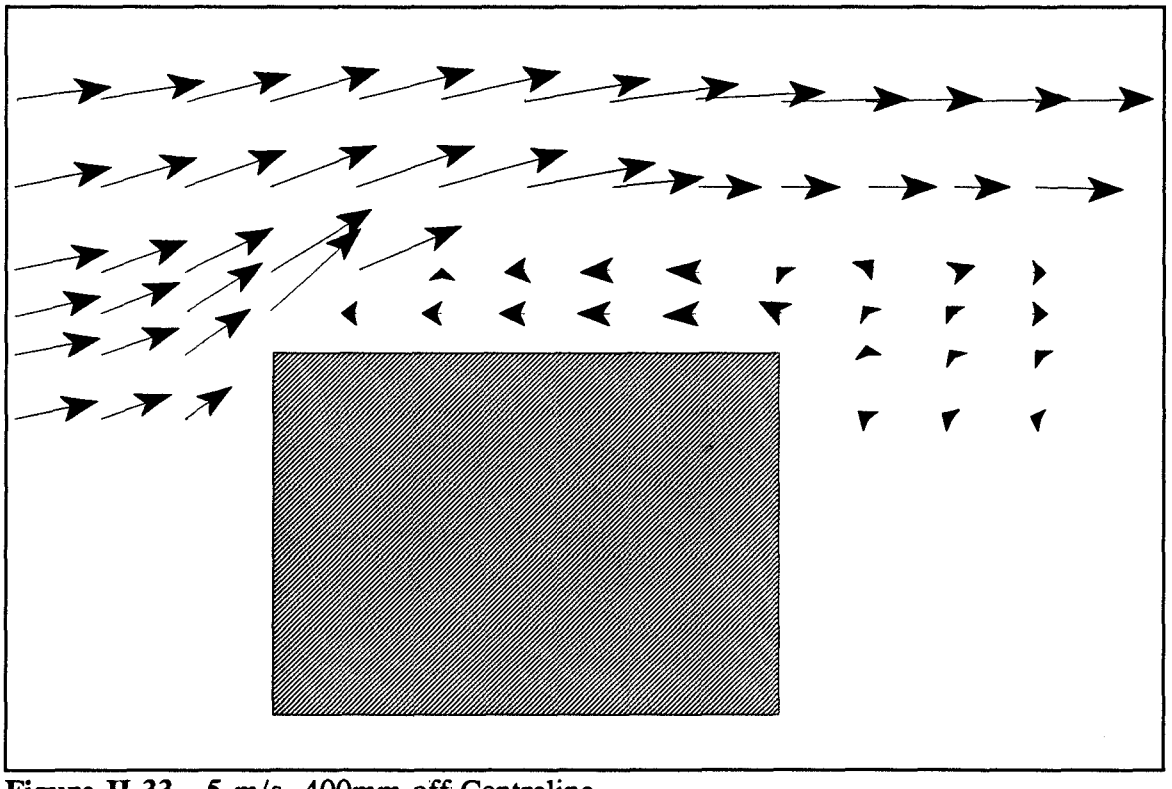

Figure II.33 - 5 m/s, 400mm off Centreline

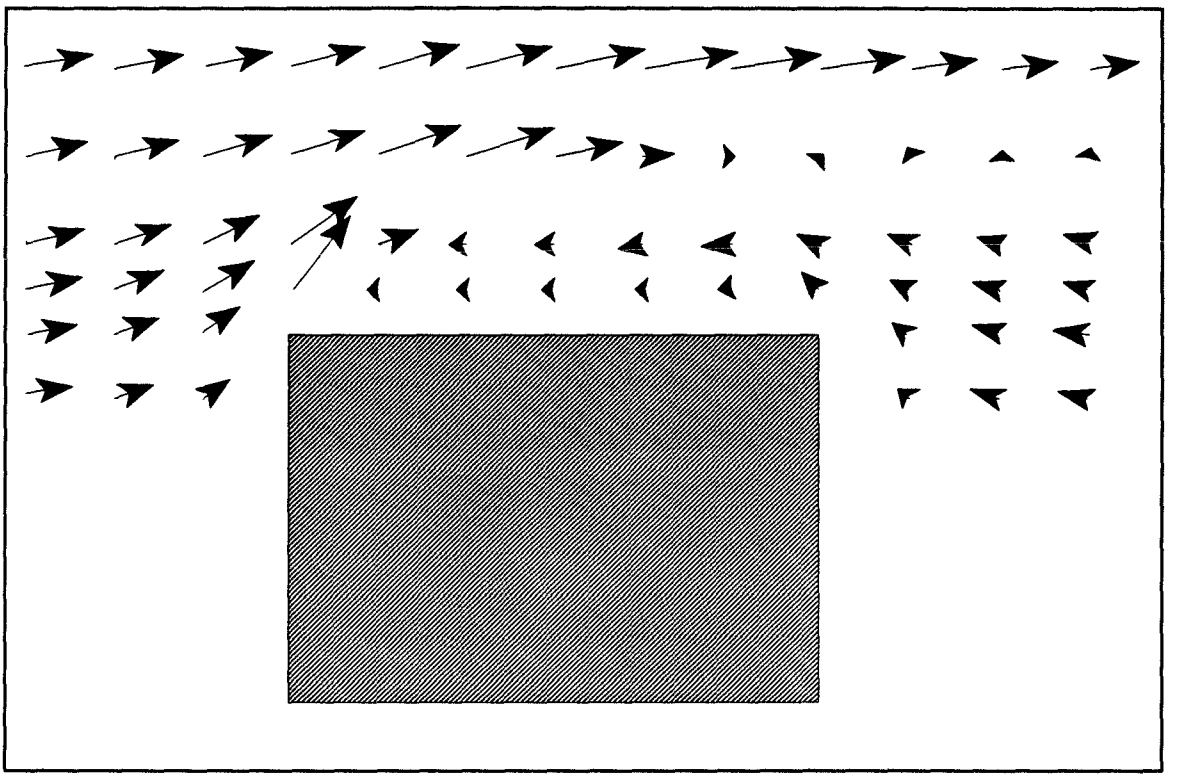

Figure II.34 - 2.5 m/s, Centreline

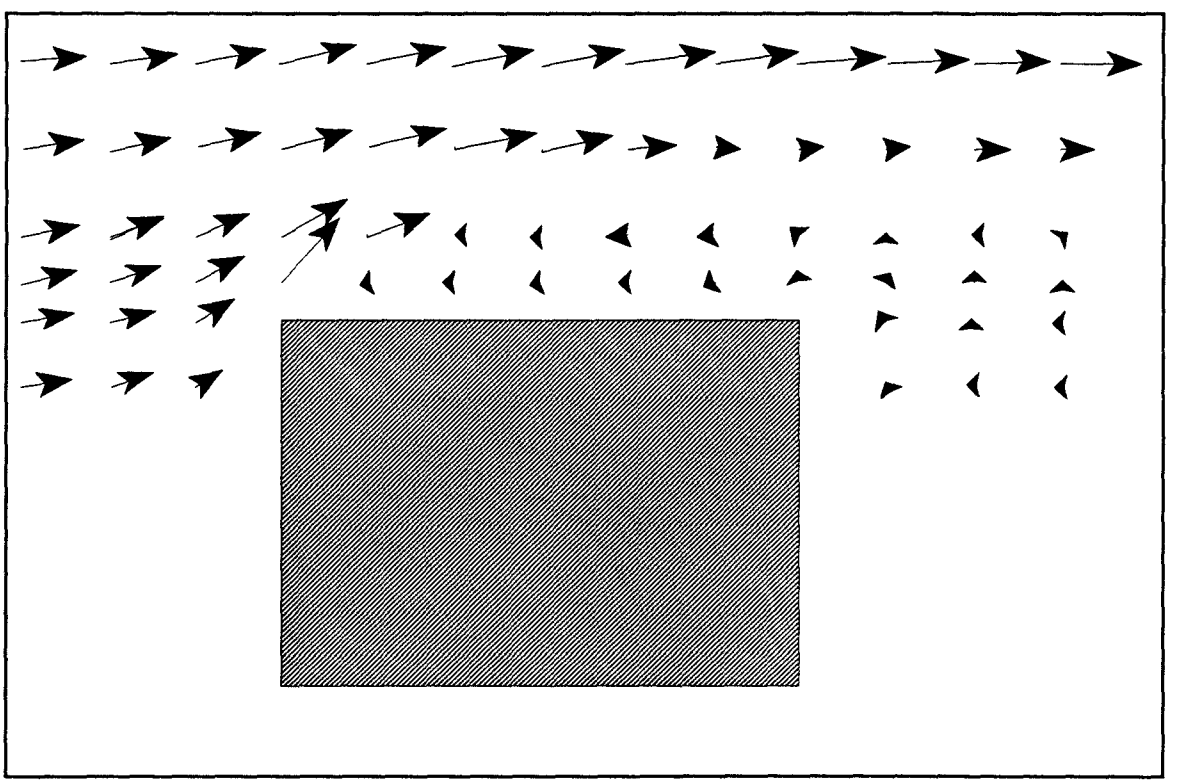

Figure II.35 - 2.5 m/s, 400mm off Centreline

CHAPTER 3

SIMPLIFIED BLADE SAILING MODEL AND COMPARISON WITH EXPERIMENTS

3.1 INTRODUCTION

This Chapter describes the development of a theoretical blade flapping model to predict the blade sailing behaviour seen in the Wind Tunnel tests presented in Chapter 2.

This theoretical model of a single or twin bladed teetering rotor was developed for two reasons:

(i) As a comparison for the wind tunnel test data

(ii) To have the use of a simpler theory to attempt to understand the characteristics of the phenomenon

The theory makes the following assumptions:

- Rigid blade/hub assembly *(only flapping/teetering motion considered)*
- No precone angle

Initially the following assumptions were used:

- Constant lift curve slope, with no stall provision
- Linear specification of vertical gust component
- Constant horizontal gust component

However, as will be explained later in the chapter, this puts a stringent limitation to the types of ship induced flow which can be modelled. These limitations only allowed any form of decent comparison with experimental results to be achieved with rotor locations on the ship's deck towards the windward edge. The behaviour over the leeward edges were completely unsuitable for a simple wind specification. The theory to be developed below assumes the simple wind description and is able to perform the integrations down the blade length to obtain closed form expressions for the aerodynamic forcing flapwise moments acting on the blade(s) and rotor hub.

3.2 DERIVATION OF THE EQUATION OF MOTION

(A Glossary of Terms is included at the front of this document.)

The actual wind components are:

$$W_H = V_W \cdot F_H$$
$$W_V = V_W \cdot F_V \qquad \text{(III.1)}$$

At a blade section we have for the velocity components:

$$\begin{aligned} U_T &= \Omega r + V_W F_H \cos\psi \\ &= \Omega r + W_H \cos\psi \end{aligned} \qquad \text{(III.2)}$$

and

$$\begin{aligned} U_P &= V_i - K_{ROT} W_H \beta \sin\psi + K_{ROT} \dot{\beta} r + W_V \left(\frac{-r \sin\psi}{R} \right) \\ &= V_i - K_{ROT} W_H \beta \sin\psi + \left(K_{ROT} \dot{\beta} - \frac{W_V}{R} \sin\psi \right) r \end{aligned} \qquad \text{(III.3)}$$

Where K_{ROT} takes the value +1 for the primary blade and -1 for the secondary blade of a teetering pair.

The aerodynamic lift is given by:

$$\begin{aligned} dL &= \frac{1}{2} \rho U_T^2 \, a \left(\theta - \frac{U_P}{U_T} \right) c \, dr \\ &= \frac{1}{2} \rho a c dr \left(\theta U_T^2 - U_P U_T \right) \end{aligned} \qquad \text{(III.4)}$$

From which the aerodynamic flapping moment is:

$$M_{AERO} = \frac{1}{2} \rho a c dr r \left(\theta U_T^2 - U_P U_T \right) \qquad \text{(III.5)}$$

From equations (III.2) and (III.3) we have the following expressions in U_P and U_T:

$$U_T^2 = \Omega^2 \cdot r^2 + 2\Omega W_H \cos\psi \cdot r + W_H^2 \cos^2\psi \qquad \text{(III.6)}$$

$$\begin{aligned} U_P U_T &= \Omega \left(K_{ROT} \dot{\beta} - \frac{W_V \sin\psi}{R} \right) r^2 \\ &+ \left[\Omega \left(V_i - K_{ROT} W_H \beta \sin\psi \right) + W_H \cos\psi \left(K_{ROT} \dot{\beta} - \frac{W_V \sin\psi}{R} \right) \right] r \\ &+ W_H \cos\psi \left[V_i - K_{ROT} W_H \beta \sin\psi \right] \end{aligned} \qquad \text{(III.7)}$$

Defining the following terms:

$$\begin{aligned} T_2 &= \Omega^2\theta - \Omega\left(K_{ROT}\dot{\beta} - \frac{W_V \sin\psi}{R}\right) \\ T_1 &= 2\Omega W_H \theta\cos\psi - \Omega\left[V_i - K_{ROT} W_H \beta \sin\psi\right] - W_H \cos\psi\left(K_{ROT}\dot{\beta} - \frac{W_V \sin\psi}{R}\right) \\ T_0 &= W_H^2 \cos^2\psi\,\theta - W_H \cos\psi\left[V_i - K_{ROT} W_H \beta \sin\psi\right] \end{aligned} \quad \text{(III.8)}$$

We have:

$$\theta U_T^2 - U_P U_T = T_2 r^2 + T_1 r + T_0 \quad \text{(III.9)}$$

Assembling the previous results gives the aerodynamic flapping moment as:

$$\begin{aligned} M_{AERO} &= \int_0^R \frac{1}{2}\rho a c r\left[T_2 r^2 + T_1 r + T_0\right] dr \\ &= \frac{1}{2}\rho a c\left[T_2\frac{R^4}{4} + T_1\frac{R^3}{3} + T_0\frac{R^2}{2}\right] \\ &= \frac{1}{24}\rho a c R^4\left[3T_2 + 4\frac{T_1}{R} + 6\frac{T_0}{R^2}\right] \end{aligned} \quad \text{(III.10)}$$

It should be noted that with the rotor azimuth at ψ_{REF},
for the primary blade:

$$\begin{aligned} K_{ROT} &= +1 \\ \psi &= \psi_{REF} \end{aligned} \quad \text{(III.11)}$$

and for the secondary blade:

$$\begin{aligned} K_{ROT} &= -1 \\ \psi &= \psi_{REF} + \pi \end{aligned} \quad \text{(III.12)}$$

The centrifugal restoring moment, for a single blade/cuff, is given by:

$$\begin{aligned} M_{CF} &= \int_0^R m\Omega^2 r\,dr\,\beta r \\ &= \Omega^2 \beta I_2 \\ \because\ I_2 &= \int_0^R m r^2 dr \end{aligned} \quad \text{(III.13)}$$

To this has to be added the restoring moment of the balance weight. By inspection this can be seen to be:

$$M_{CF(BalanceWeight)} = \Omega^2 \beta I_3 \qquad \textbf{(III.14)}$$

Finally the flapping equation of motion can be assembled with the result:

$$(NI_2 + I_3)\ddot{\beta} = M_{AERO(primary)} - \delta_{N,2}\, M_{AERO(secondary)} - N\Omega^2 I_2 \beta - \Omega^2 I_3 \beta \qquad \textbf{(III.15)}$$

where the Kronecker delta term $\delta_{N,2}$ is only non zero for the two blade teetering rotor.

3.3 APPLICATION OF THE THEORY

A selection of results is presented here. A full description of the tests and the complete set of results can be found in Newman[24,25,26]. The Figures III.3-III.6 show the model running up to and from a rotor speed of 600 rpm, whilst being subjected to a wind speed of 5 metres per second. The blade motion is mechanically limited to constrain the flapping between +23° and -11°. The figures show a progressive increase in the vertical wind component, from 10% to 100%, which is upwards on one side of the rotor disc and downward on the other. This is to model the influence of the ship's deck which acts as a bluff body causing the incident wind to climb over the windward edge of the deck and to descend over the leeward edge. As can be seen, the motion increases in magnitude with the vertical component, and at the higher values the rotor blade motion is such as to cause several impacts with the blade restraints. Figure III.6 of this sequence shows a case where the run up time has been lengthened and comparing with Figure III.4, an increased amount of contact with the flapping limits can be seen. The disadvantage of operating the rotor for overly long periods at low rotor speeds is therefore demonstrated. The middle value of 50% for the upward wind component has been used for this case.

3.4 THE DEVELOPMENT OF THE MORE DETAILED METHOD

In order to make use of the full set of wind tunnel experiments, the assumptions used for this simple method must be heavily pruned. This will involve a completely flexible method of wind specification, the use of aerodynamic effects well beyond the constant lift curve slope part of the aerofoil section performance. The W_H and W_V terms (III.1) will now be input data arrays obtained from the wind tunnel tests and the lift coefficient included in (III.4) will now be obtained by the aerodynamic trailing edge stall technique outlined in Appendix A. At a set of radial locations the inflow velocity vectors to the aerofoil section are calculated and from the resulting incidence angle the lift data can be specified. This will give a spanwise loading distribution which when integrated along the blade length(s) will result in the aerodynamic forcing flapping moment as obtained previously in (III.10). The equation of motion in (III.15) will remain essentially unaltered, however two factors were introduced into the model for greater accuracy of simulating the wind tunnel rotor rig namely precone and shaft tilt:

Precone - The rotor rig hub has a small amount of precone angle included. Therefore as the hub rotates in a teetering direction the flapping angles of the blades are biassed in one direction. The effect of this will be felt in the aerodynamic moment calculation. Looking at the primary blade, it has a flapping angle of:

$$\beta_{primary} = \beta + \beta_0 \qquad \textbf{(III.16)}$$

whilst the secondary blade has a corresponding flapping angle of:

$$\beta_{secondary} = \beta - \beta_0 \qquad \textbf{(III.17)}$$

these two results can be combined thus:

$$\beta_{blade} = \beta + K_{ROT}\beta_0 \qquad \textbf{(III.18)}$$

If these results are incorporated into the centrifugal moment terms we find for 2 blade configuration:

$$\begin{aligned} M_{primary} &= -I_2 \beta_{primary} \Omega^2 \\ &= -I_2(\beta + \beta_0)\Omega^2 \end{aligned} \qquad \textbf{(III.19)}$$

and

$$\begin{aligned} M_{secondary} &= -I_2 \beta_{secondary} \Omega^2 \\ &= -I_2(\beta - \beta_0)\Omega^2 \end{aligned} \qquad \textbf{(III.20)}$$

the sum being as before:

$$M_{primary} + M_{secondary} = -2I_2 \beta \Omega^2 \qquad \textbf{(III.21)}$$

whilst for the 1 blade/counter balance weight configuration:

$$\begin{aligned} M_{primary} &= -I_2 \beta_{primary} \Omega^2 \\ &= -I_2(\beta + \beta_0)\Omega^2 \end{aligned} \qquad \textbf{(III.22)}$$

and

$$\begin{aligned} M_{counterweight} &= -I_3 \beta_{counterweight} \Omega^2 \\ &= -I_3(\beta - \beta_0)\Omega^2 \end{aligned} \qquad \textbf{(III.23)}$$

the sum now becomes:

$$\begin{aligned} &M_{primary} + M_{counterweight} \\ &= \{-(I_2 + I_3)\beta - (I_2 - I_3)\beta_0\}\Omega^2 \end{aligned} \qquad \textbf{(III.24)}$$

The equation of motion used for the numerical solution now becomes:
for 2 blade configuration:

$$\{NI_2 + I_3\}\ddot{\beta} = M_{aero\ primary} + M_{aero\ secondary} - 2I_2 \beta \Omega^2 \qquad \textbf{(III.25)}$$

for 1 blade configuration:

$$\{NI_2+I_3\}\ddot{\beta} = M_{aero\ primary} - \{(I_2+I_3)\beta + (I_2-I_3)\beta_0\}\Omega^2 \qquad \text{(III.26)}$$

Shaft Tilt - The rotor shaft is not perpendicular to the deck surface so the plane normal to it is not parallel to the deck. If the angle of tilt *(which is lateral with respect to the incident flow direction)* is denoted by γ_s nose down then as a point of a rotor blade rotates the height of the point above the deck will vary which will need to be included with the incorporation of results from the LDA wind tunnel tests. The geometry of this is shown in Figure III.7 and the height of the point at (r,ψ) is given by:

$$h = h_{HUB} + r\cos\beta\cdot\cos\psi\cdot\sin\gamma_s + r\sin\beta\cdot\cos\gamma_s\cdot K_{ROT} \qquad \text{(III.27)}$$

The application of these amended equations to the solution method is now required. The final stage is the incorporation of the LDA ship flow data into the aerodynamic forcing terms.

3.5 TEETERING ROTOR - FINAL DEVELOPMENT AND VERIFICATION OF THEORETICAL MODEL

With the data for the flow velocity components now being used as an input to the method, the turbulence characteristics must also be simulated. As previously stated, the test data was analysed into mean and standard deviations. From this a Gaussian random number generator routine, described in Press et al[35], was used. In order to create the correct level of turbulence, this routine must be called at intervals to update the flow velocity components accordingly. As previously mentioned, the turbulence frequency was to be scaled via Strouhal number. Newman and Hurst[8] describes a full scale test conducted on the flight deck of a Rover Class RFA. The results showed a peak response for the turbulence frequency at about 4 Hz. This result is clouded by this value being the upper limit of the frequency response of the golf ball type anemometer used. A turbulence frequency value a little above 4 Hz is therefore possible. However, a 4 Hz frequency at full scale becomes 12.2 Hz for the 7ft by 5 ft wind tunnel tests. Also, further LDA testing has been conducted in the Department's larger (11ft by 8 ft) wind tunnel with an improved flow seeding arrangement. An analysis of the results has shown a fairly wide frequency range with an apparent peak at about 80 Hz. Strouhal number scaling reduces this to 29 Hz for the 7 ft by 5 ft wind tunnel tests. To account for these

findings, this initial view of the results uses a representative value of 20 Hz for the turbulence frequency. For the results which are to be presented no external rotor downwash was incorporated. Since the collective pitch is set to zero and the blades are untwisted this at first sight seems justifiable. However, with the extreme situation which the method is simulating, large incidence angles will occur over the rotor blade where lift and hence downwash will be generated. For operation at normal rotational speeds, the rotor aerodynamics are usually calculated using strip theory where two dimensional data is applied to a blade element and the incidence is determined by the downwash at that location. It is a difficult calculation in any case but with the blade sailing model an accelerating or decelerating rotor blade is under examination and the calculation of the unsteady downwash distribution over the rotor disc will require a significant investigation. The possibility of using a downwash model based on dynamic inflow was considered, but for the unconventional nature of the rotor operation was not thought appropriate. Such models are based on the complete rotor disc which must give a periodic variation of inflow with rotor azimuth angle. The calculations conducted so far have indicated that the most extreme blade excursions occur with a rotor speed of between 10%NR and 15% NR. At this condition, the rotor speed is changing appreciably and in consequence the rotor blades will be experiencing substantially different aerodynamic conditions in successive revolutions. On this basis, a rotor disc based model seems inappropriate and an individual blade approach a more realistic choice. The rapidly changing conditions experienced by an individual blade element indicate that unsteady aerodynamic effects could have important influences on the blade motion and this avenue of investigation could form a future direction for the research.

A second avenue of thought was used in this analysis whereby the lift coefficient at a blade element was calculated from the incidence without any allowance for downwash and then factored by the following equation:

$$C_{L\ MODIFIED} = C_L \frac{AR}{AR+2} \qquad \text{(III.28)}$$

where AR is the aspect ratio of the blade, see Piercy[40].

The calculation of rotor speed is elementary with the linear ramp being used but observation of the test results shows that under certain instances, the rotor tends to

undergo a jump start or a very rapid final slowing to rest. In order to give a fair comparison, this feature was built into the theoretical method.

Two Blade Experiments

The results are presented in Figures III.8-12 for the run up cases and III.13-17 for the equivalent run down cases. The test condition numbers are as described in 2.3.4 and the theoretical predictions similarly , except the **S2** test designation is replaced by **SPE** for no cyclic predictions and **SB1** if cyclic is applied. Each Figure number corresponds to the wind tunnel test (a), and the theoretical predictions (b & c). As can be seen the agreement is very encouraging although there is a small difference in the steady flapping angle. The hub behaviour is a uniform, once per revolution, blade behaviour superimposed on a steady flapping angle. There is no obvious reason for this mean position since the calibration seemed very stable. It is possible that the two blades were not perfectly tracked with one blade tending to fly higher than the other. The amount measured during the constant speed centre section of the trace is of the order of 2° and does not seem to vary unduly over the five deck positions. The basic behaviour has been accurately reproduced particularly the change in character between deck positions A,B,C to D,E. The degree of impacts with the flapping stops is accurate and the manner in which the rotor behaviour transfers to a controlled disc tilt at full rotor speeds agrees well with the test results. There is a small discrepancy in the flapping amplitude at maximum rotor speed which could be attributed to a small amount of cyclic pitch being present, of the order of 1°. The rotor was set up with the intention of cyclic pitch being absent. This was checked by slowly rotating the blade by hand and observing the output from the blade pitch sensor and ensuring that it remained constant. It is possible, however, that the small amount of backlash present in the control system could have concealed an appropriate amount of cyclic pitch (i.e 1° to 2°). The theoretical prediction method was again run only with -1.4° of B_1 cyclic pitch added, and the corresponding results are shown in the same Figure number sequence only are the third of each set labelled (c). The improvement in accuracy can be readily seen.

Single Blade Experiments

The wind tunnel results for the single bladed rotor during rotor run ups are presented in Figures III.18-III.27. The blade flapping behaviour can be seen to be more "lively" when compared to the two blade equivalent condition. There is an increased number of impacts

with the flapping stops and an increase in the flapping amplitude at full rotor speed. The corresponding cases with the -1.4° of B_1 cyclic are included as before. In the test results the coning angle stays relatively constant but for deck positions A and B, the theory predicts a reduction in the coning angle as the rotor speed increases, which is not unreasonable under normal circumstances. Position C compares well, and positions D and E which are dominated by turbulence show particularly good agreement in character, in fact better than those achieved with the two blade result.

The predicted blade behaviour follows closely that obtained during the tests, both from a comparison of the results but also from observation of the general character of the tests. One feature not immediately apparent from the flapping time histories is the orientation of the rotor disc as the rotor speed changes. It appeared that at low rotor speeds, the disc was tilted both rearwards and towards the retreating side. As the rotor accelerated, the orientation rotated, not unlike a precessing gyroscope, to a position pointing towards the advancing side. It is difficult to define a rotor disc attitude when successive maximum blade flapping amplitudes occur at differing rotor speeds, however an approximate interpretation of the disc attitude is shown in Figure III.28, obtained from the test results, and the manner in which it moves between the retreating to the advancing side. It shows the blade azimuth location for maximum upward flapping angle against rotor speed.

A rigid blade method has been developed to model the blade sailing behaviour of the Helicopter model used in the Wind Tunnel Tests S1 and S2. The LDA survey results have been included in the calculations and the agreement is very encouraging. One feature which initially caused some concern was the steady state response of the rotor blades at the maximum rotor speed condition. However, a small amount of cyclic pitch of the order of 1° to 2° enabled this difference to be overcome. The construction of the helicopter model rotor head gave a small amount of backlash which could encompass this amount of cyclic pitch. A theoretical model now exists which can accurately predict the blade behaviour of a helicopter placed on a ship's flight deck in an abeam wind. The next phase of the research work is to include blade flexibility into the theory and to observe the effect of blade flapwise elastic bending and the interaction with flap restrainers.

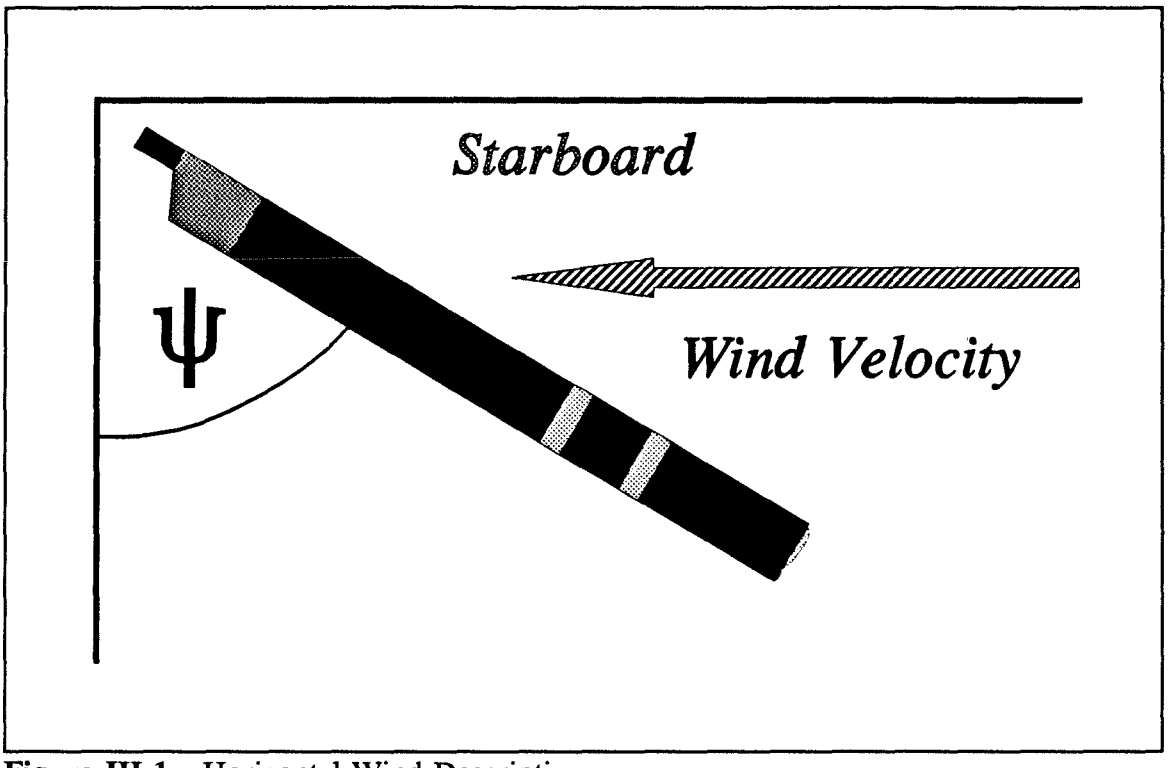

Figure III.1 - Horizontal Wind Description

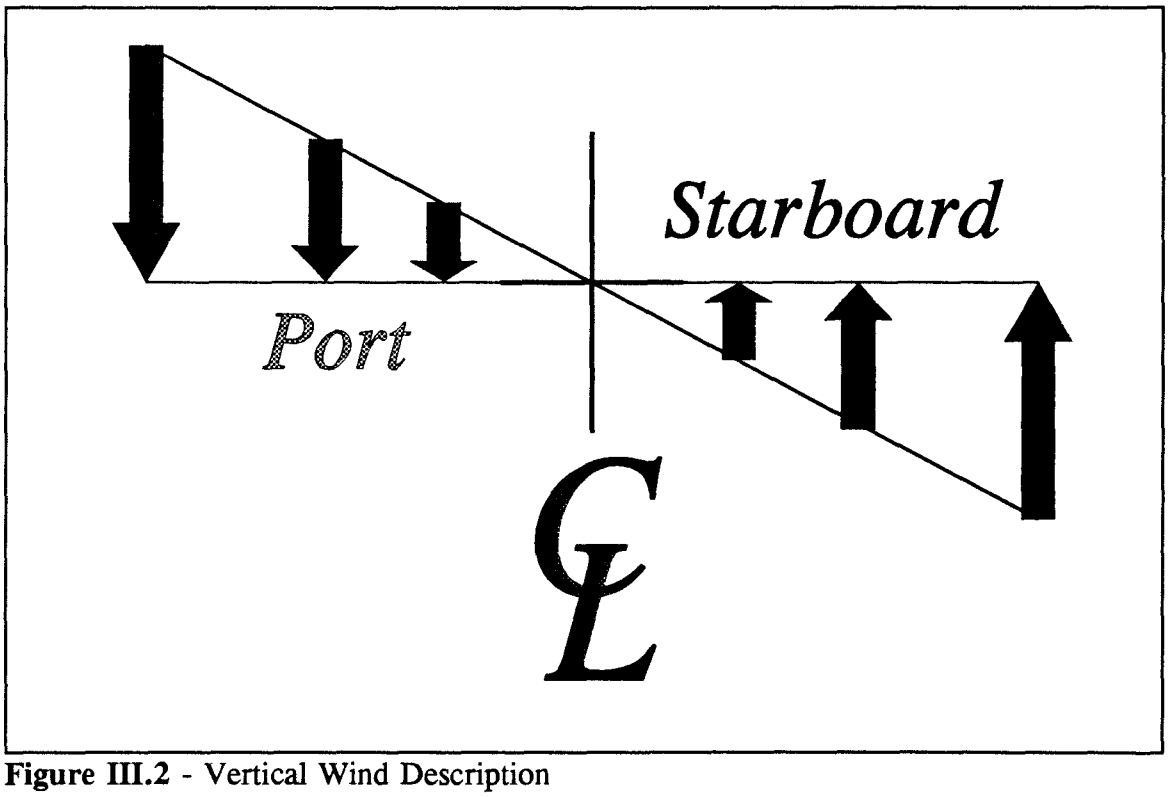

Figure III.2 - Vertical Wind Description

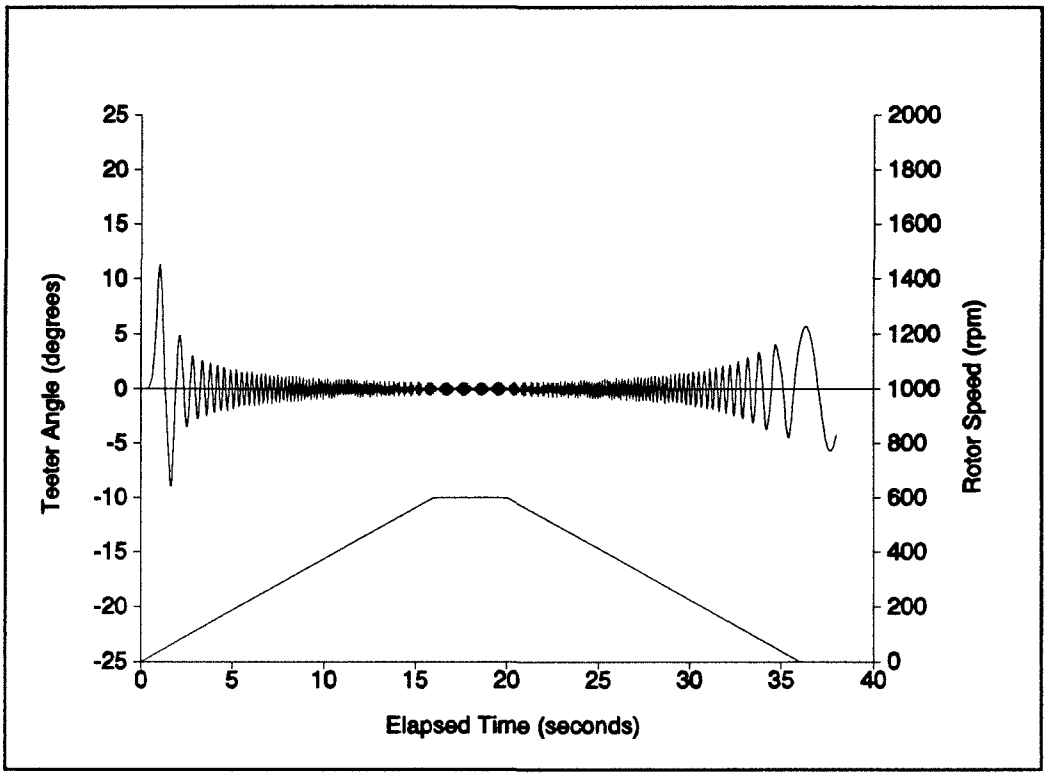

Figure III.3 - Teetering Rotor - Vertical Wind Component=10%

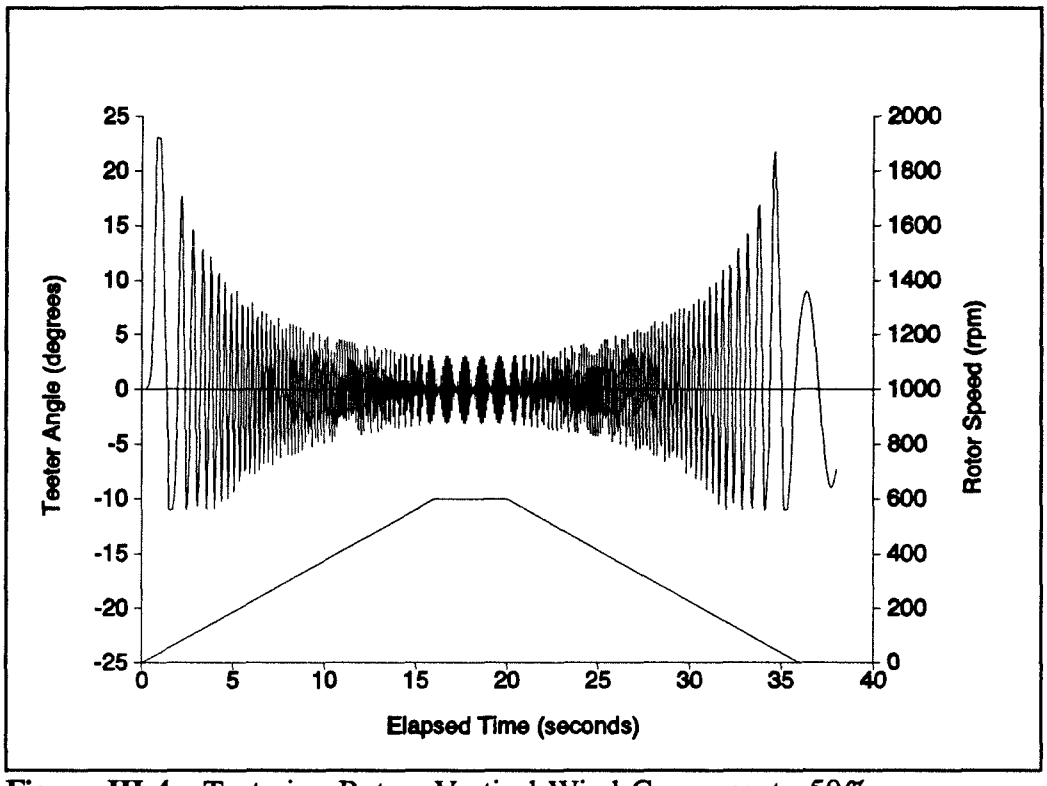

Figure III.4 - Teetering Rotor, Vertical Wind Component=50%

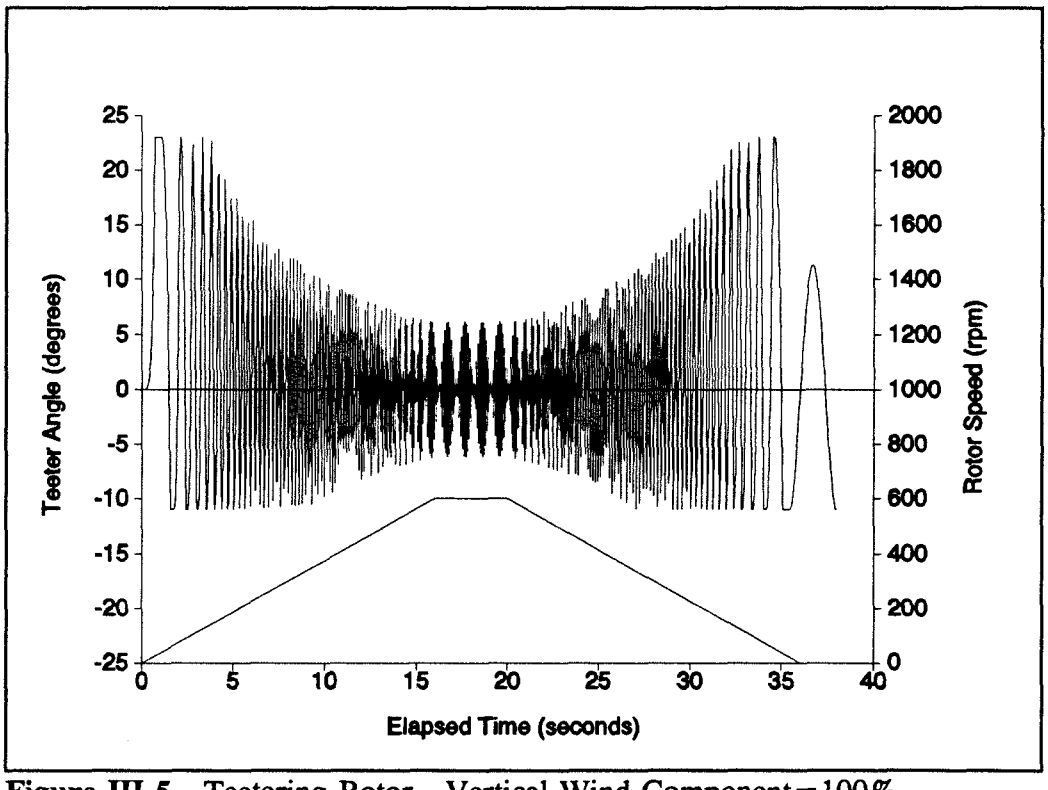

Figure III.5 - Teetering Rotor - Vertical Wind Component=100%

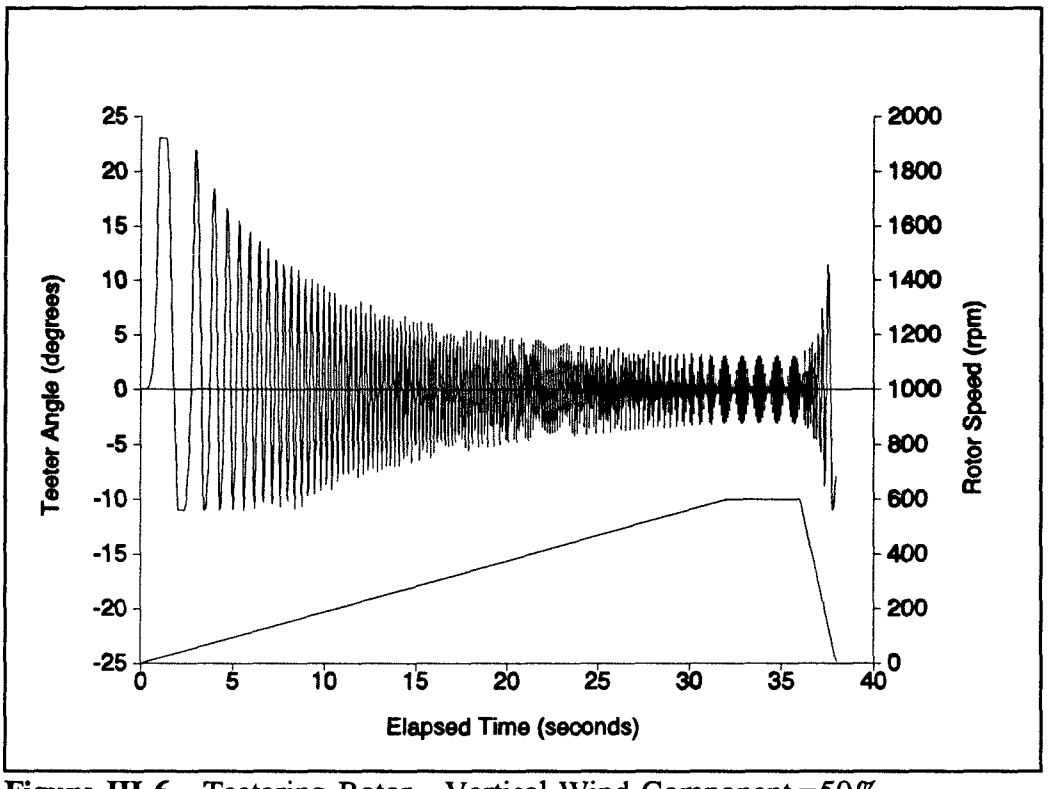

Figure III.6 - Teetering Rotor - Vertical Wind Component=50%

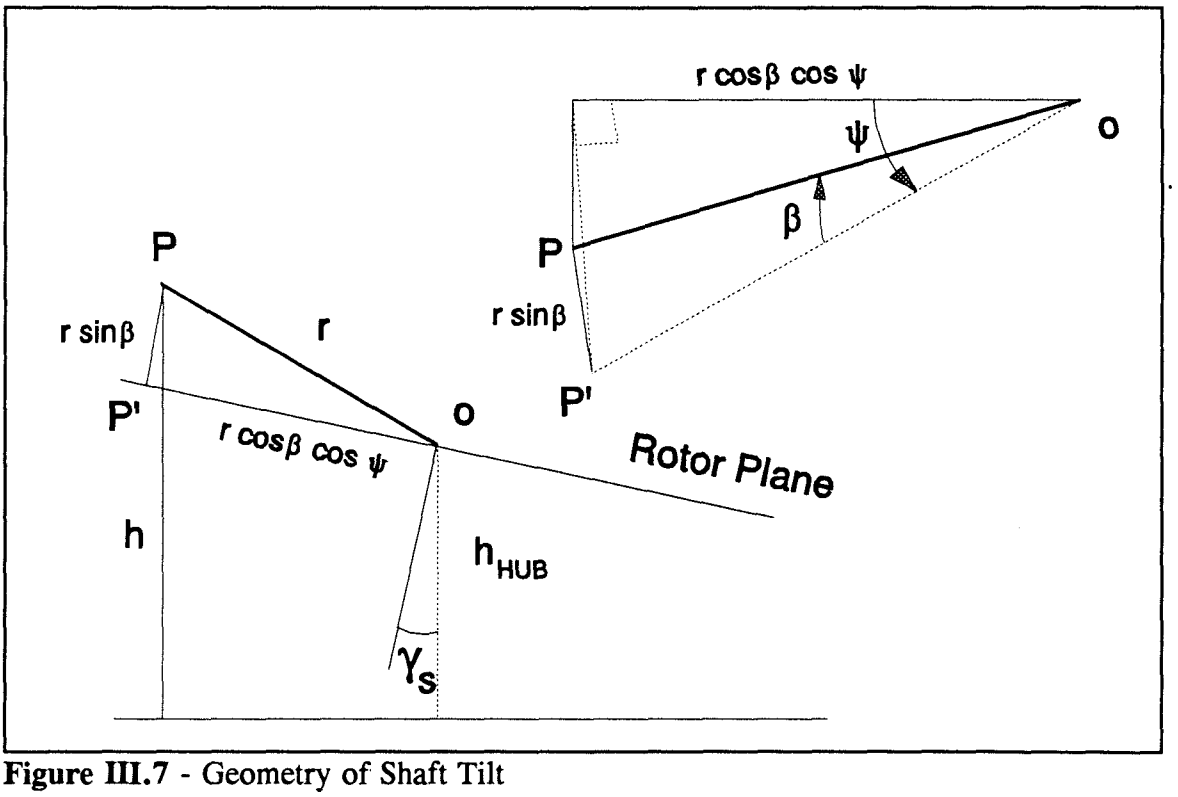

Figure III.7 - Geometry of Shaft Tilt

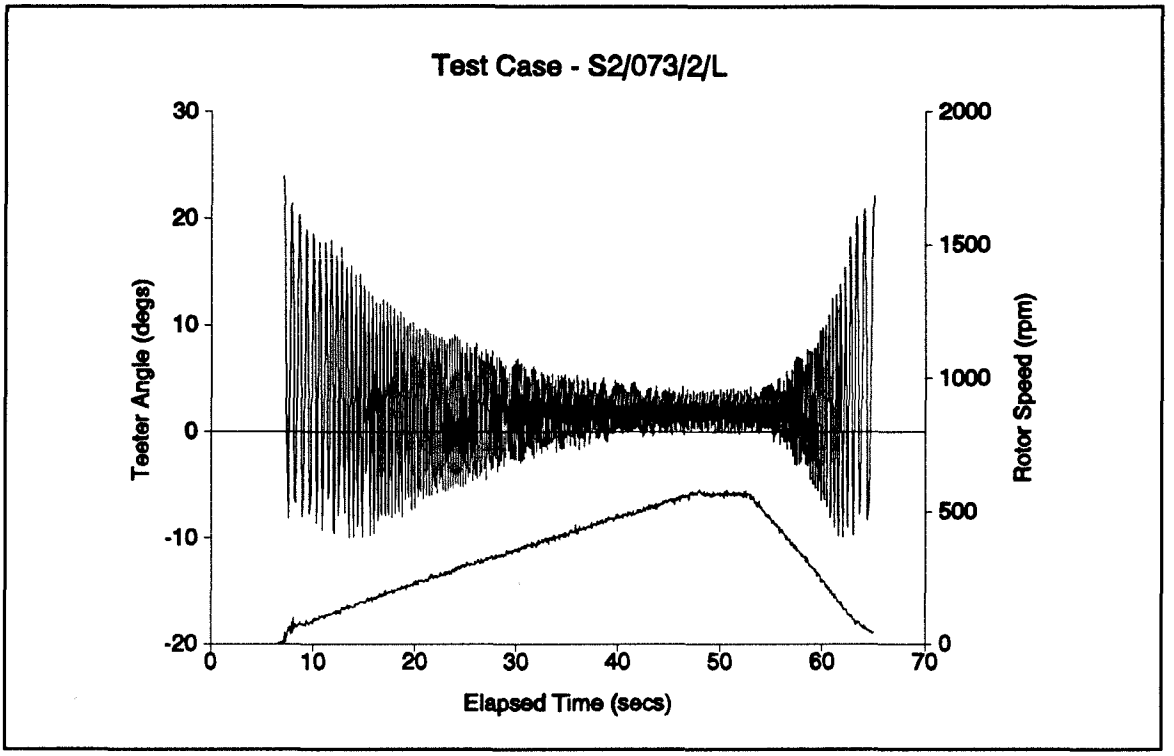

FigureIII.8.a - Wind Tunnel Test, 2 Blade, Deck Position A

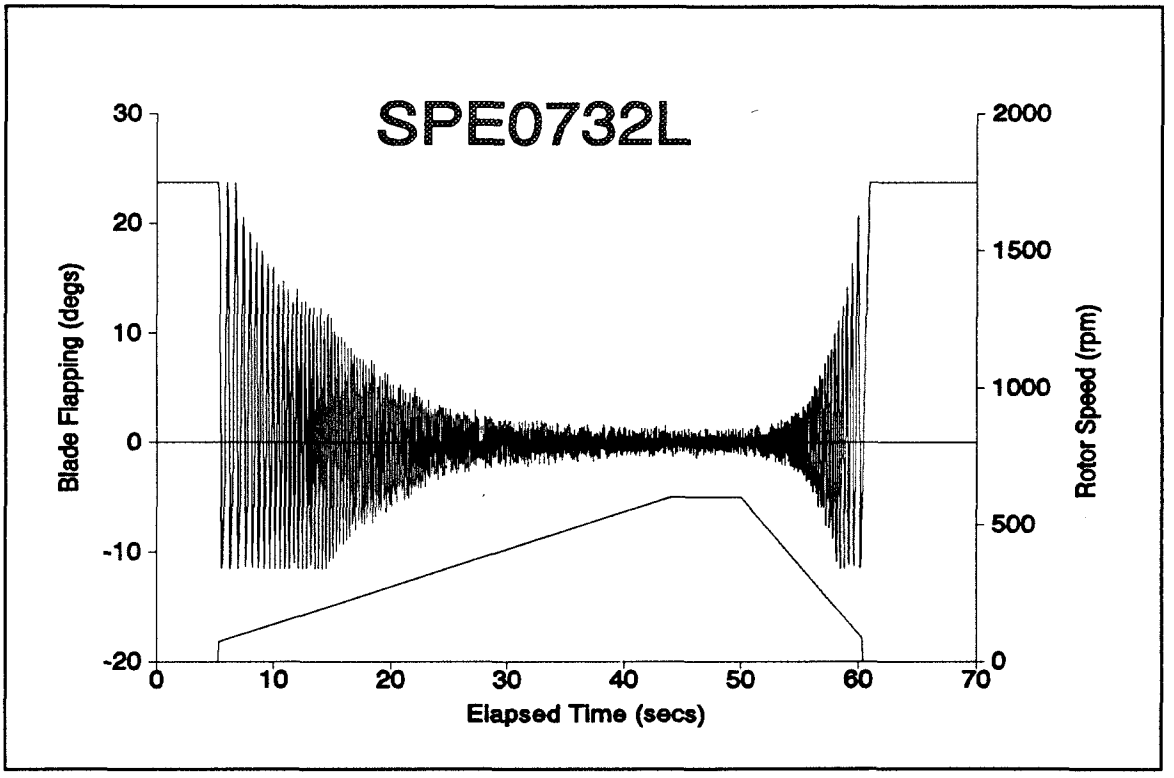

FigureIII.8.b - Theoretical Prediction, 2 Blade, Run Up, Deck Location A

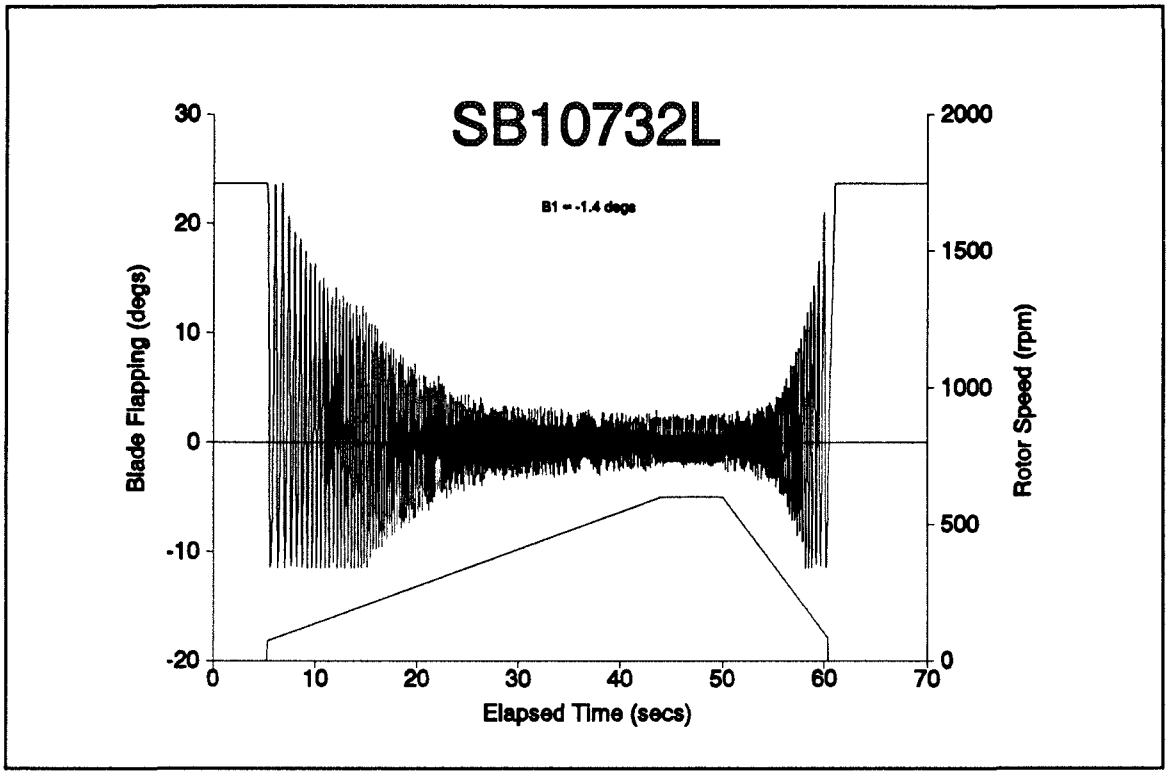

FigureIII.8.c - Theoretical Prediction. 2 Blade, Run Up, Deck Location A, B_1=-1.4°

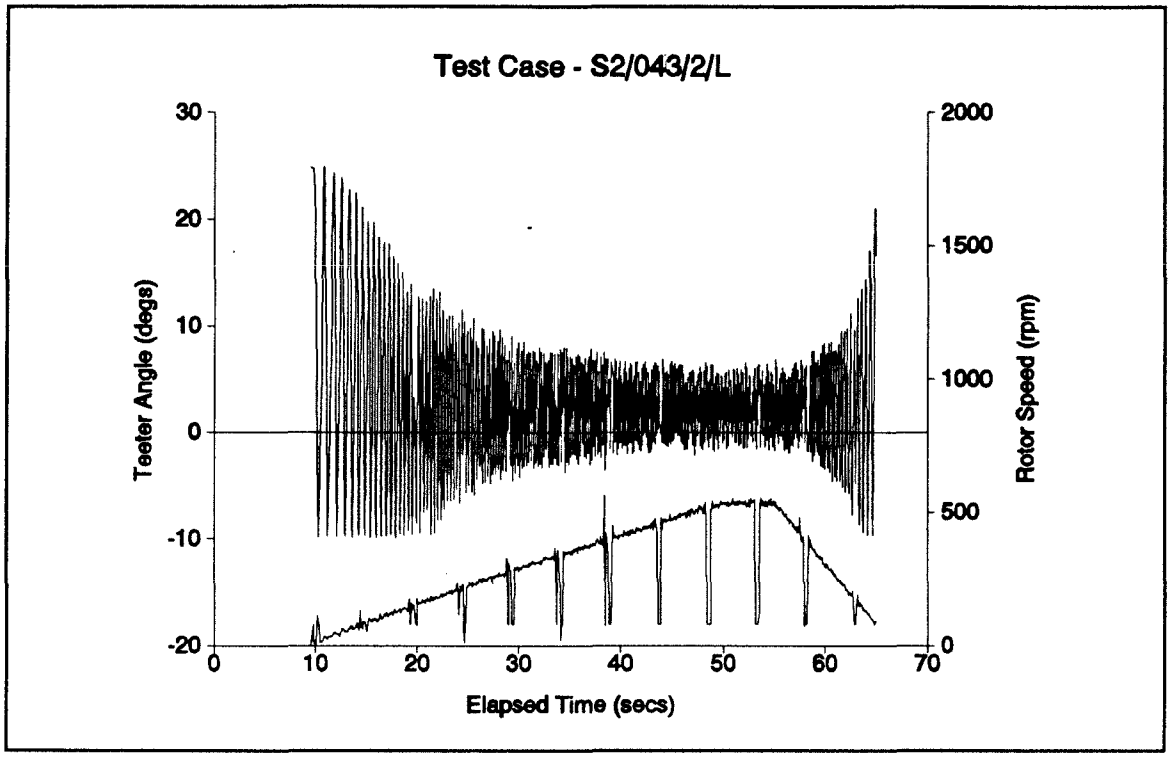

FigureIII.9.a - Wind Tunnel Test, 2 Blade, Deck Position B

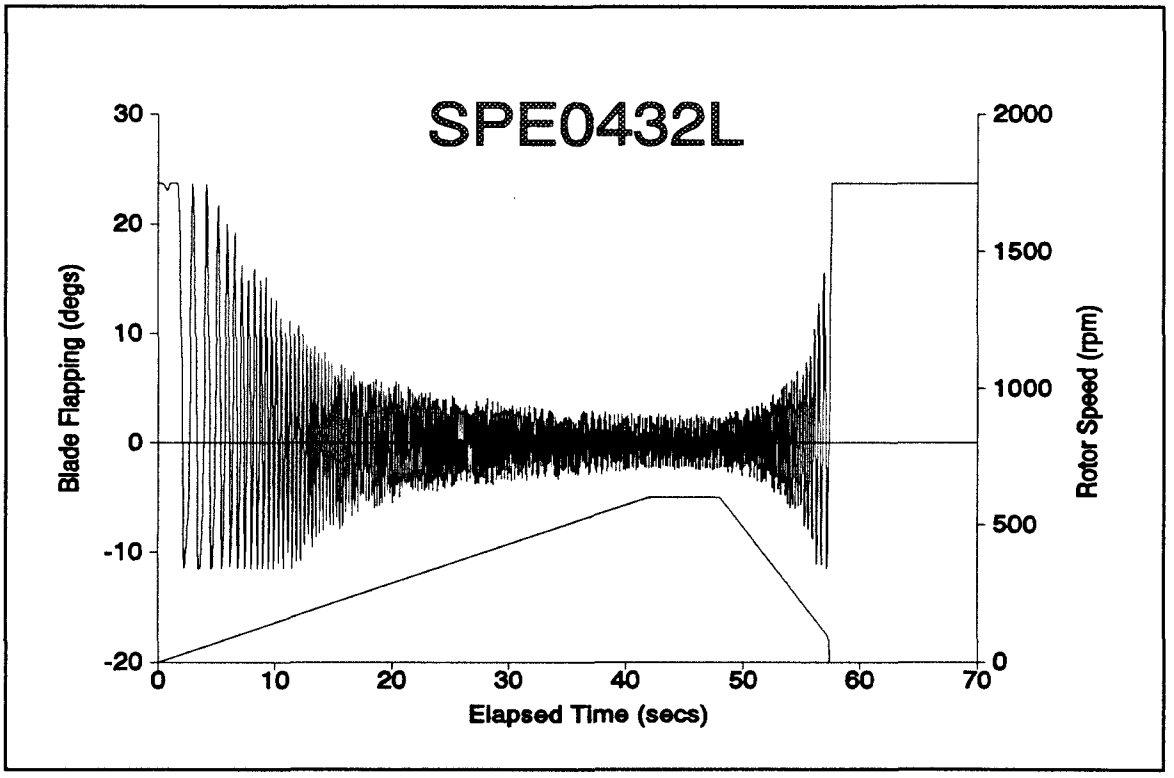

FigureIII.9.b - Theoretical Prediction, 2 Blade, Run Up, Deck Location B

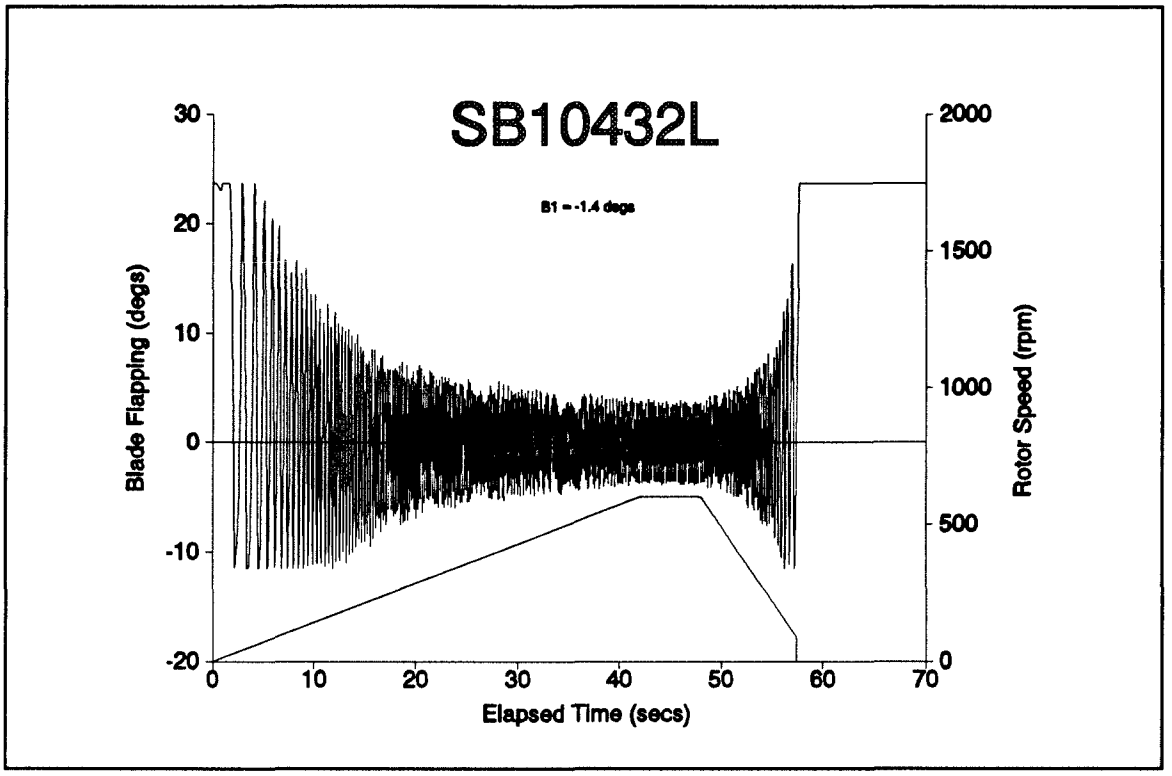

FigureIII.9.c - Theoretical Prediction. 2 Blade, Run Up, Deck Location B, B_1=-1.4°

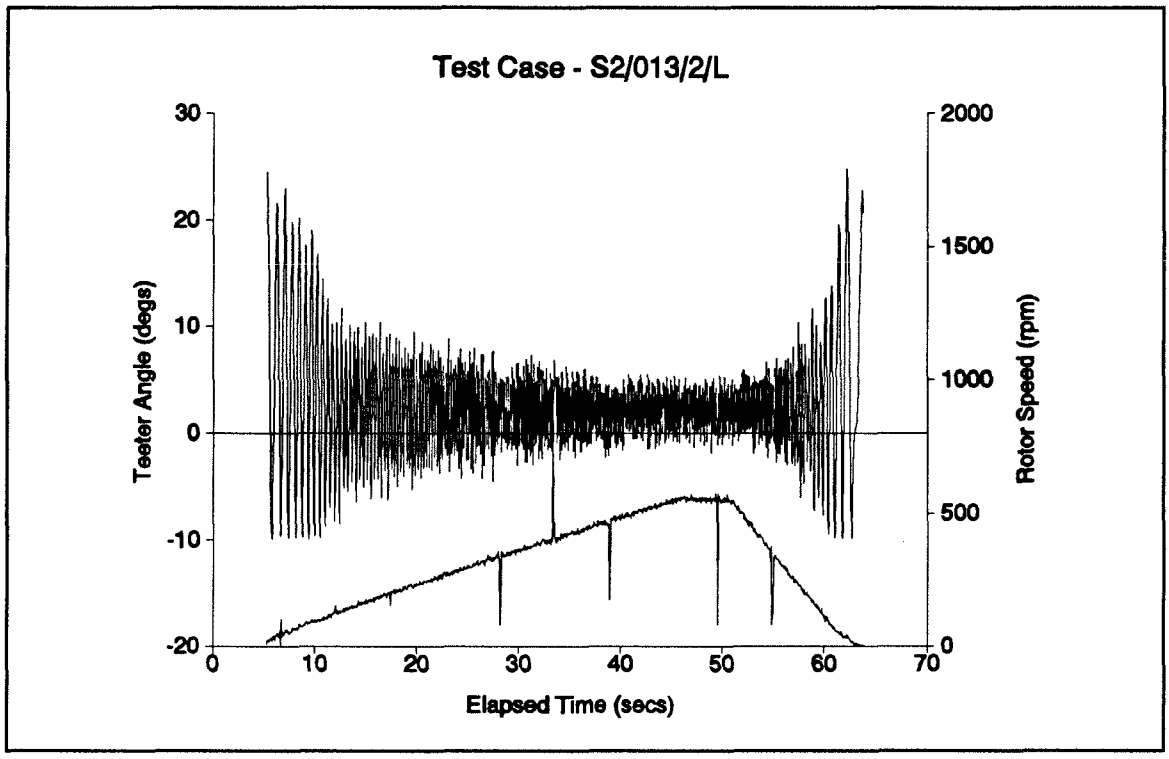

FigureIII.10.a - Wind Tunnel Test, 2 Blade, Deck Position C

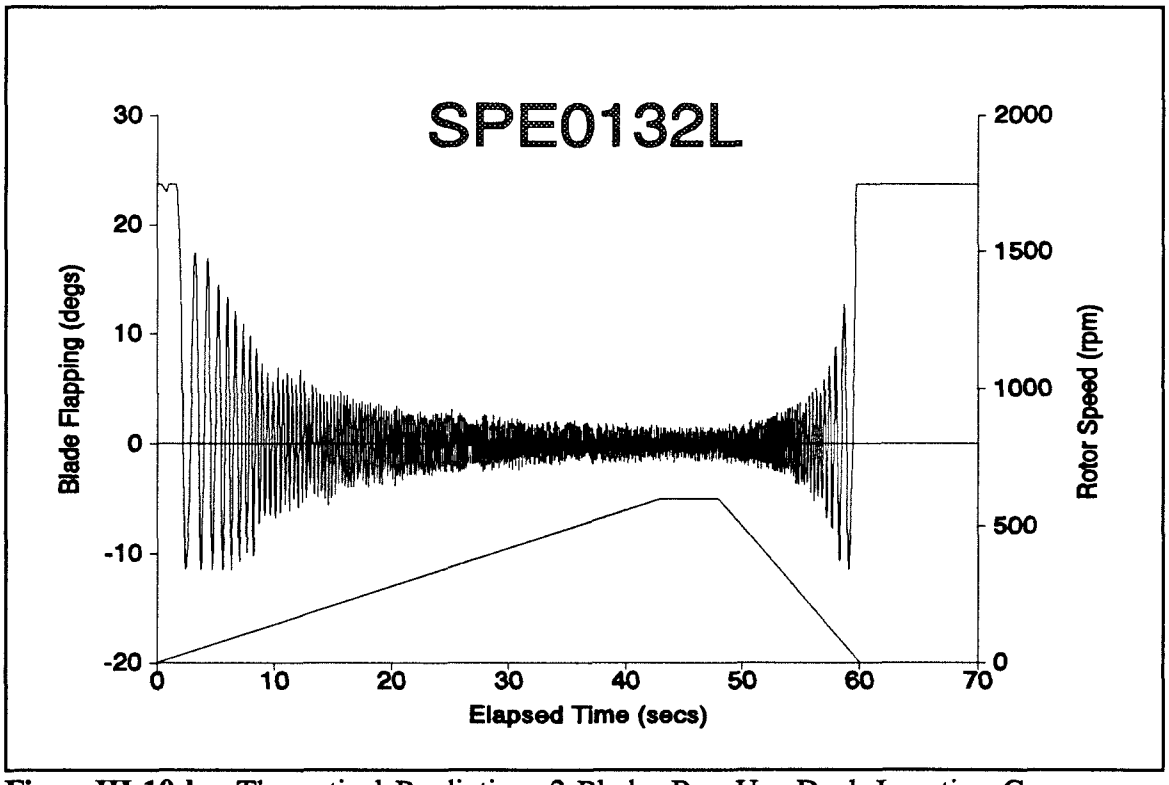

FigureIII.10.b - Theoretical Prediction, 2 Blade, Run Up, Deck Location C

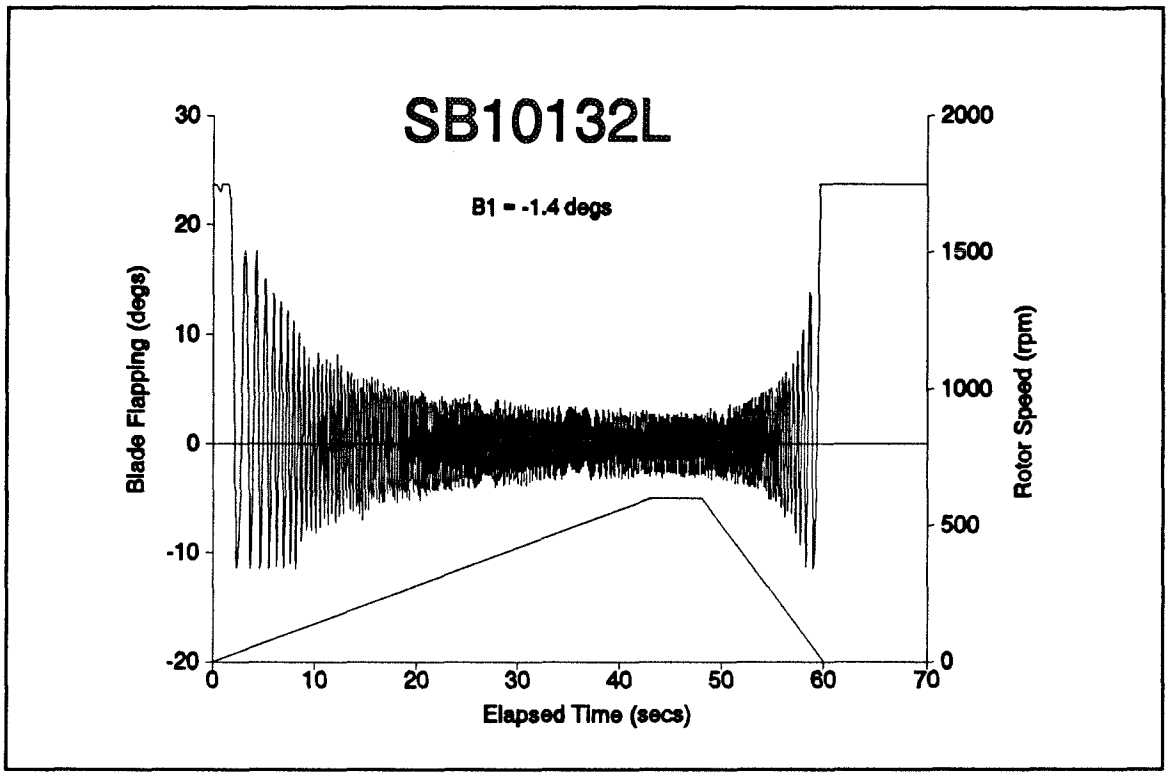

FigureIII.10.c - Theoretical Prediction. 2 Blade, Run Up, Deck Location C, B_1=-1.4°

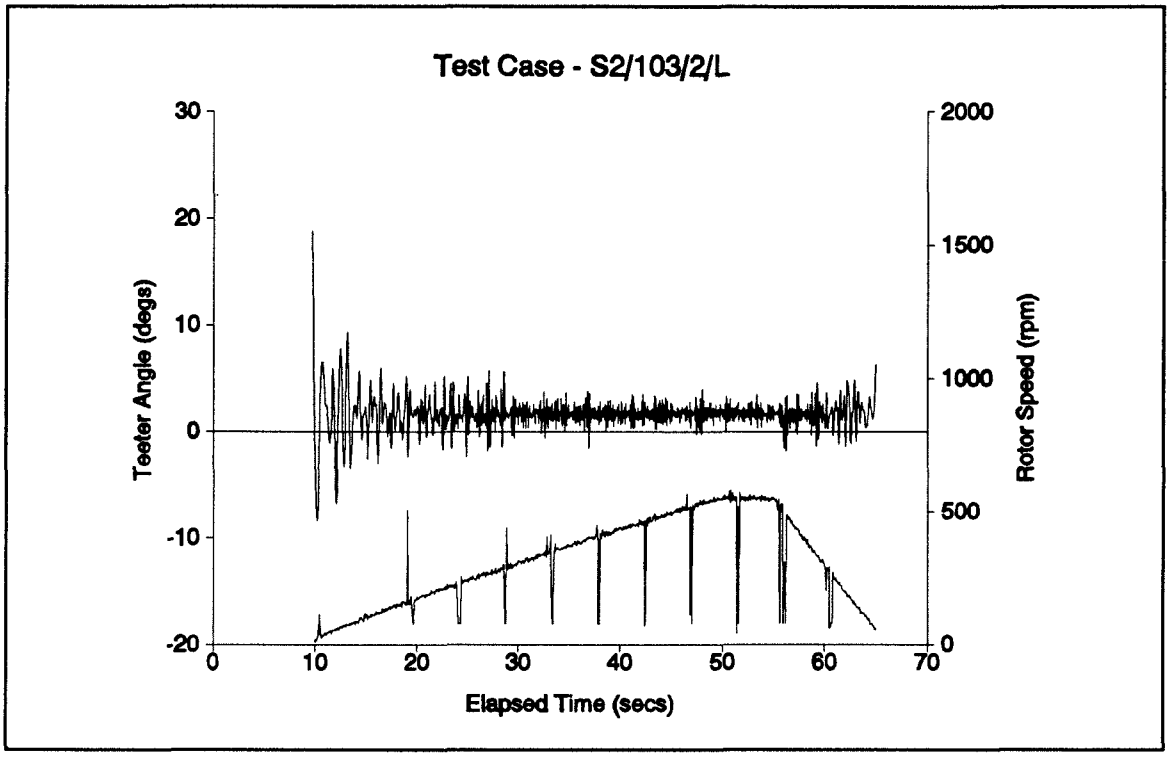

FigureIII.11.a - Wind Tunnel Test, 2 Blade, Deck Position D

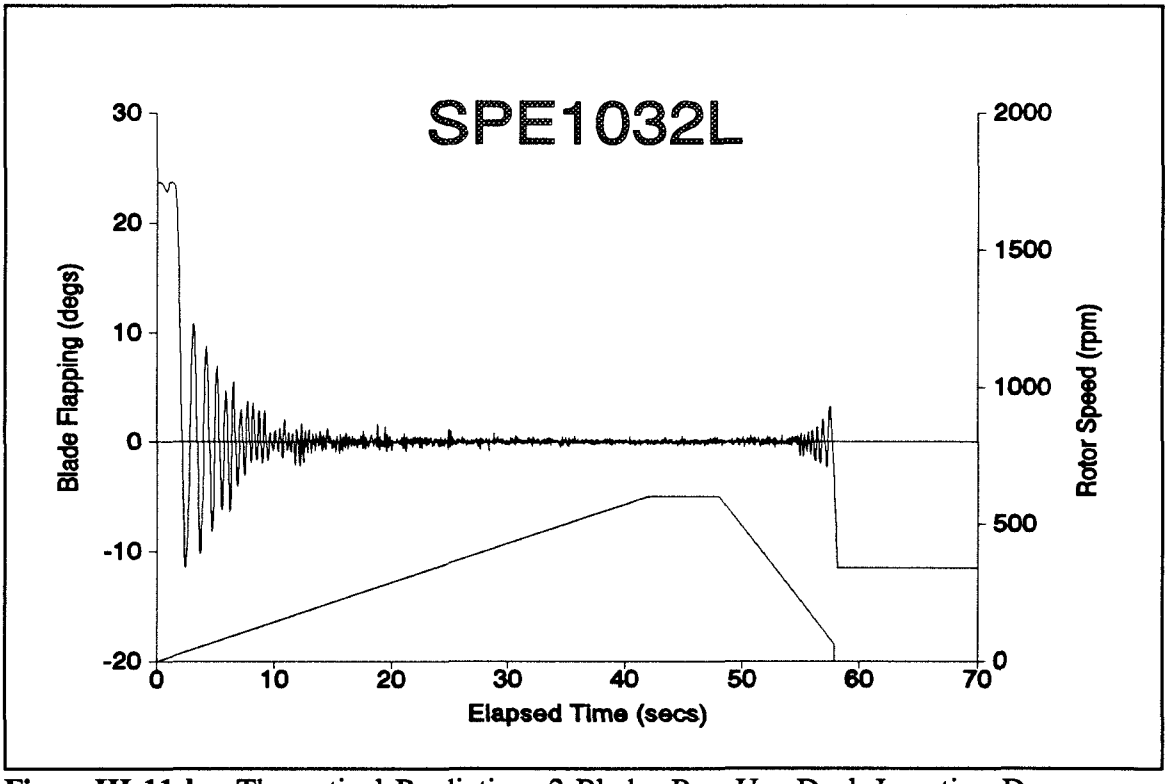

FigureIII.11.b - Theoretical Prediction, 2 Blade, Run Up, Deck Location D

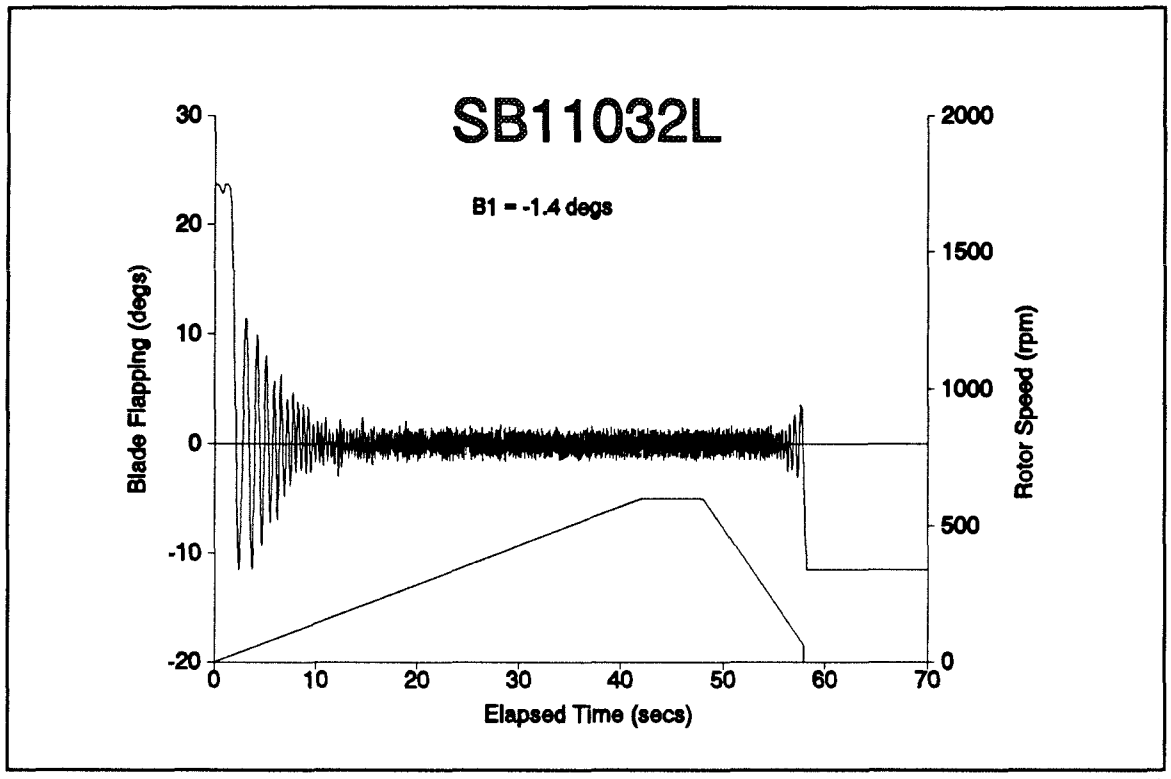

FigureIII.11.c - Theoretical Prediction. 2 Blade, Run Up, Deck Location D, B_1=-1.4°

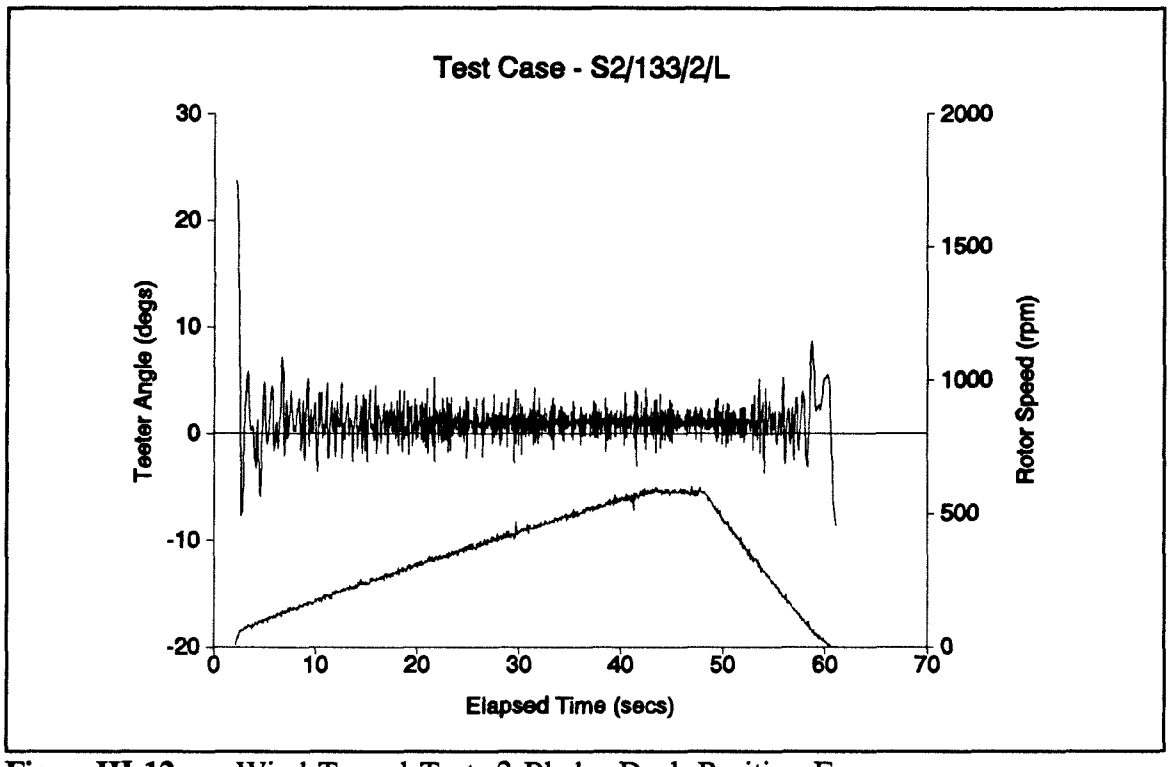

FigureIII.12.a - Wind Tunnel Test, 2 Blade, Deck Position E

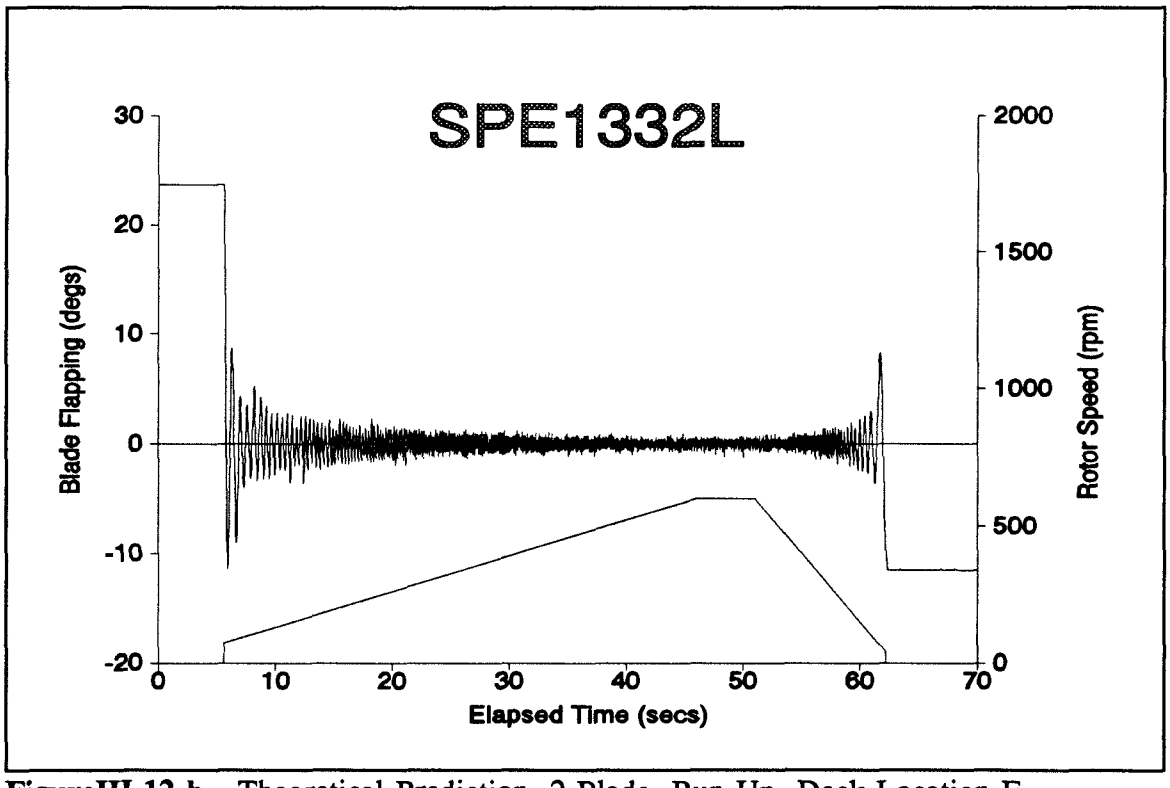

FigureIII.12.b - Theoretical Prediction, 2 Blade, Run Up, Deck Location E

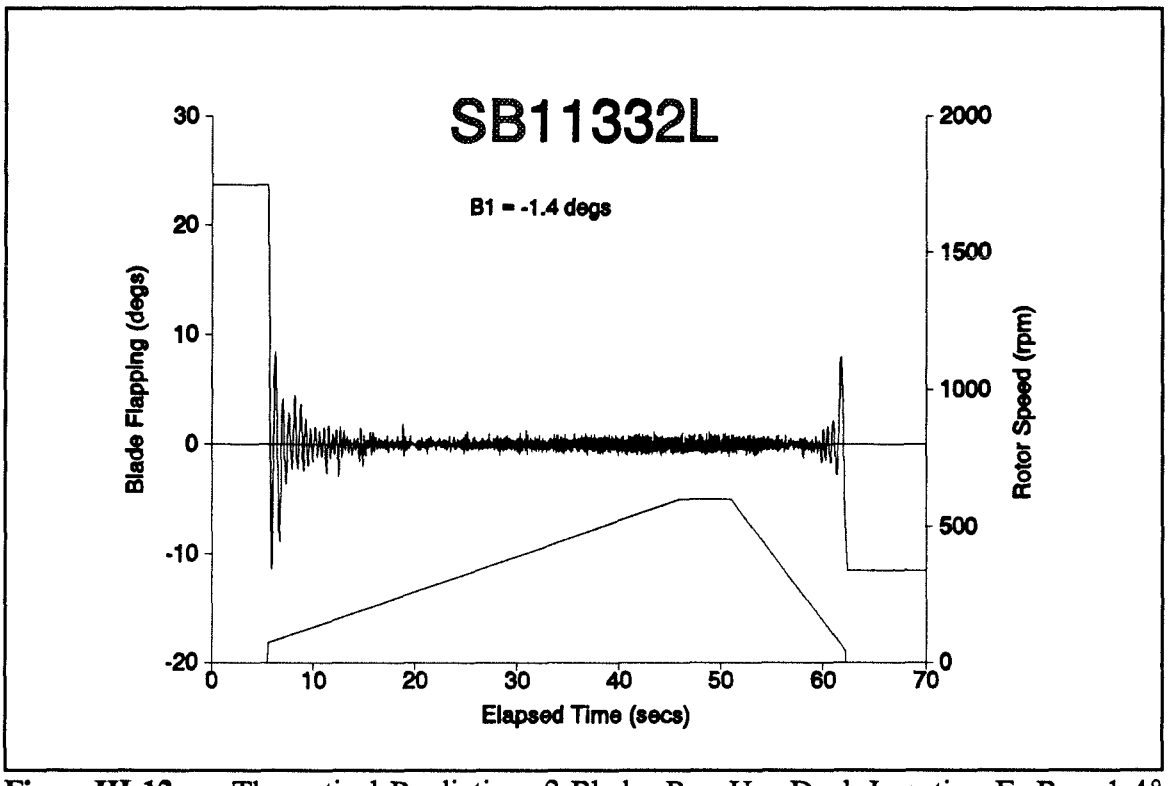

FigureIII.12.c - Theoretical Prediction. 2 Blade, Run Up, Deck Location E, B_1=-1.4°

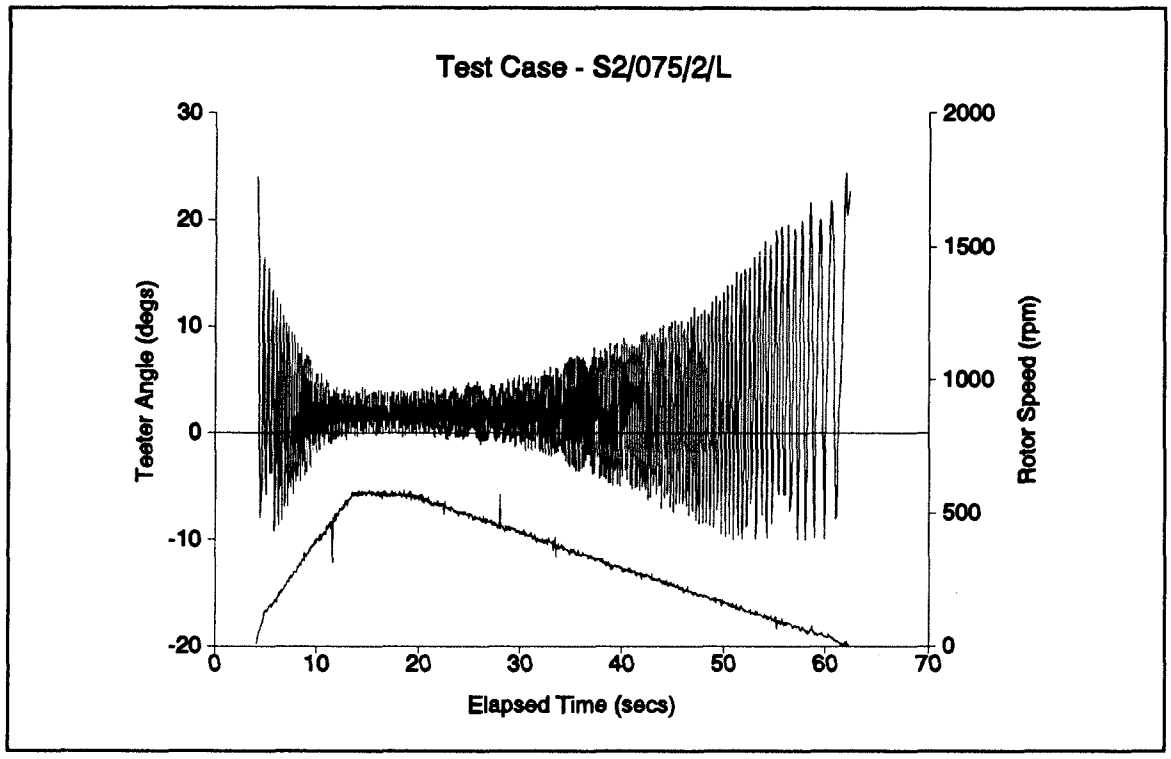

FigureIII.13.a - Wind Tunnel Tests, 2 blade, Deck Position A

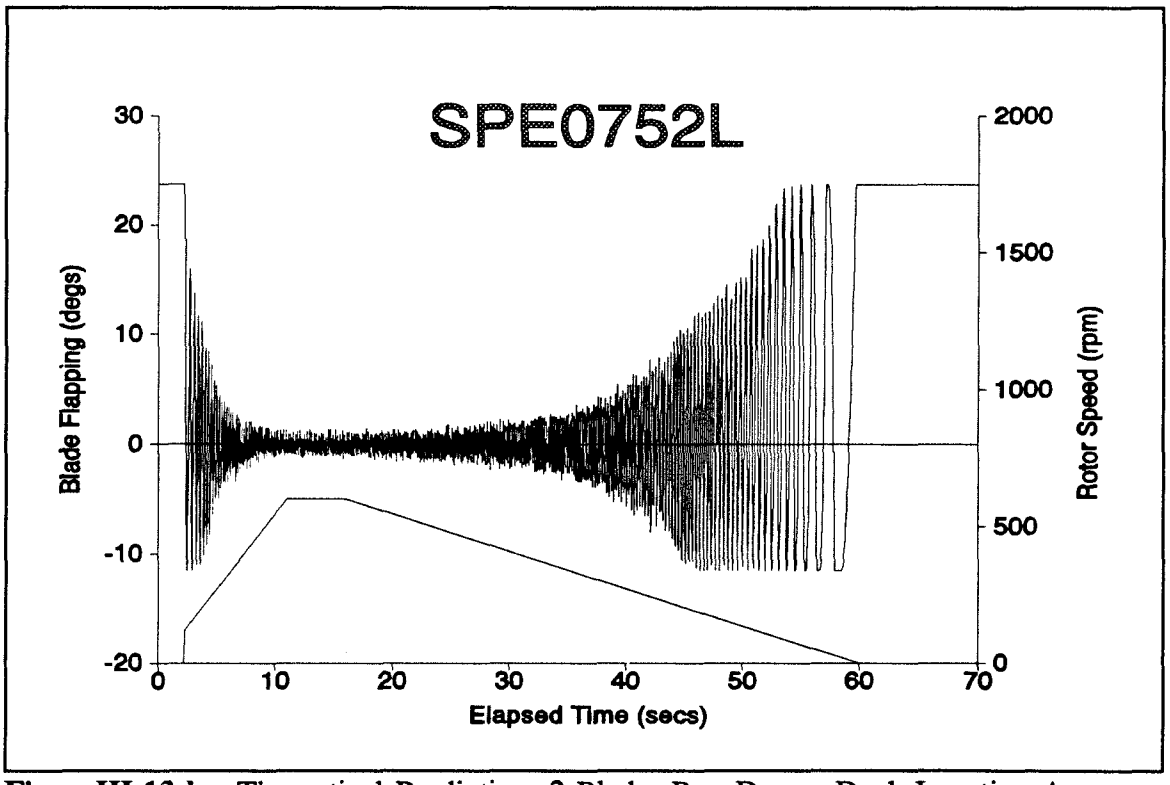

FigureIII.13.b - Theoretical Prediction, 2 Blade, Run Down, Deck Location A

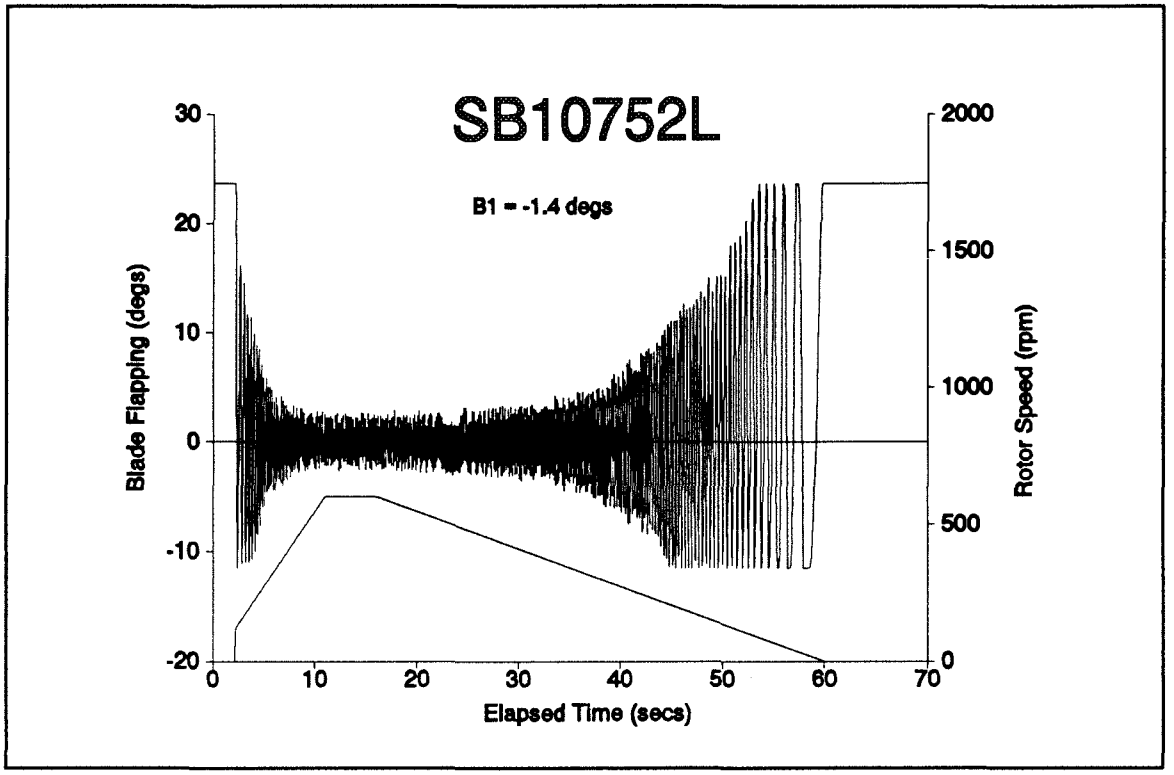

FigureIII.13.c - Theoretical Prediction. 2 Blade, Run Down, Deck Location A, B_1=-1.4°

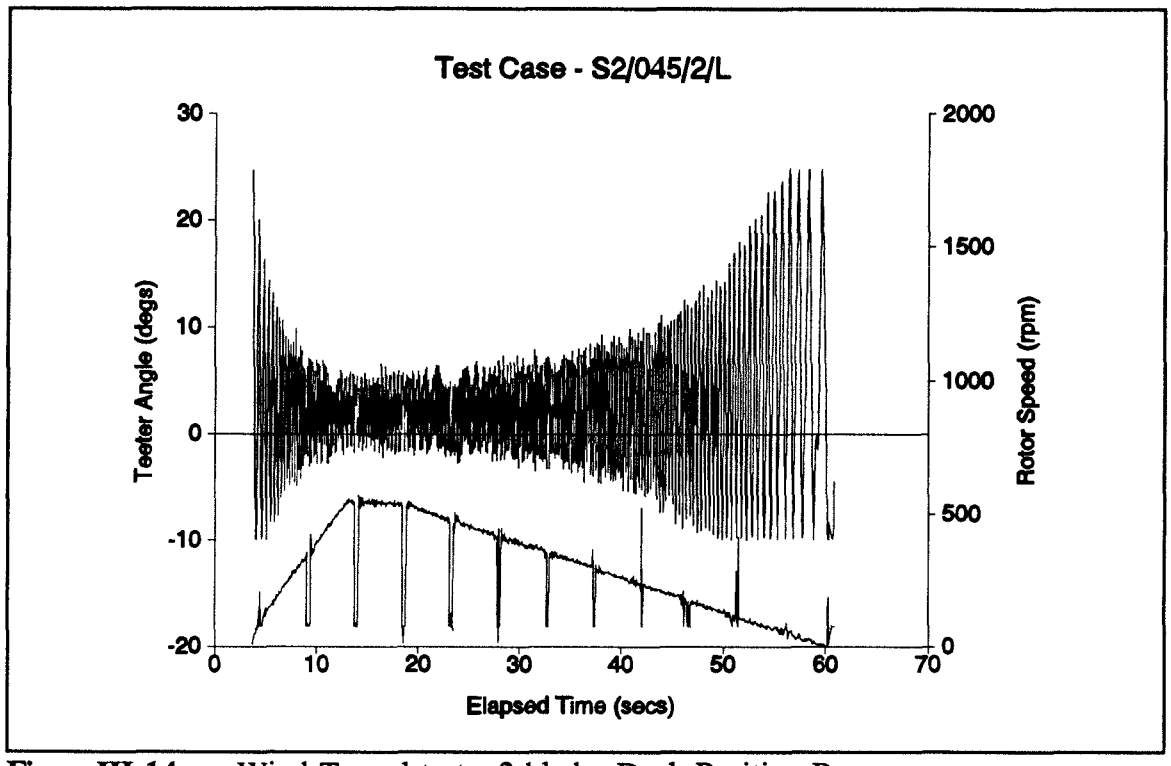

FigureIII.14.a - Wind Tunnel tests, 2 blade, Deck Position B

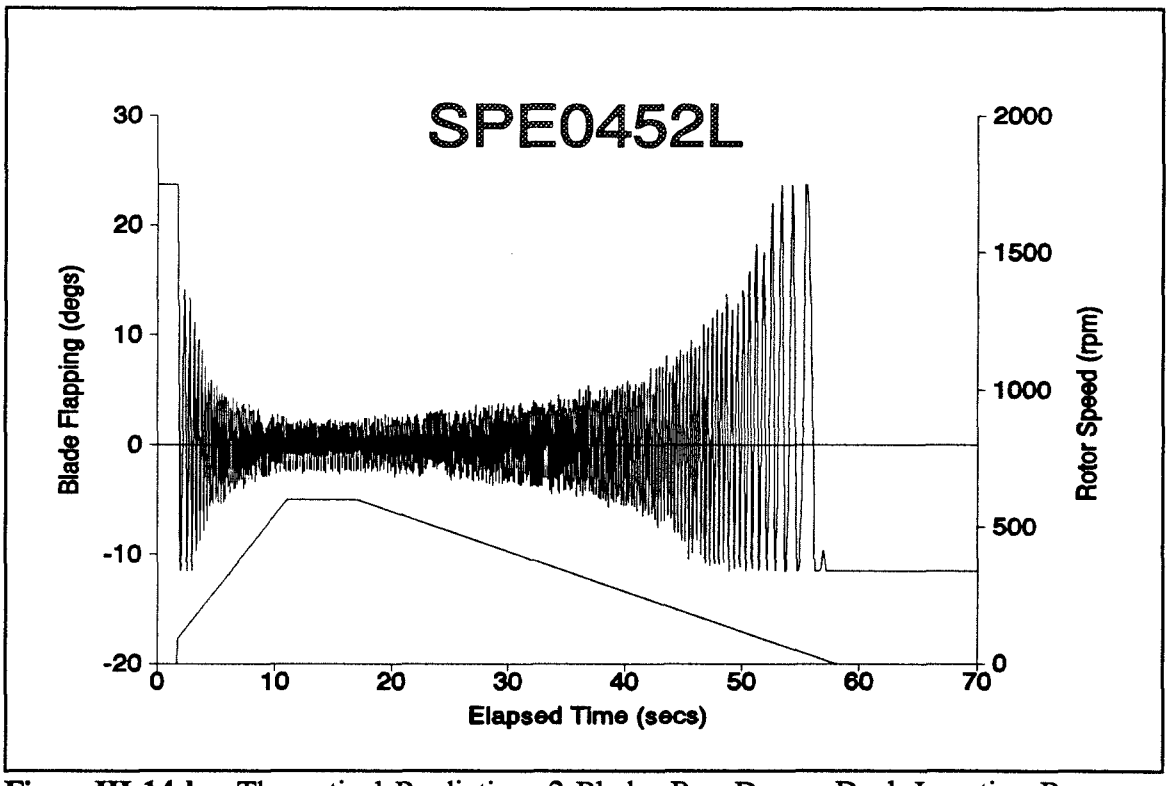

FigureIII.14.b - Theoretical Prediction, 2 Blade, Run Down, Deck Location B

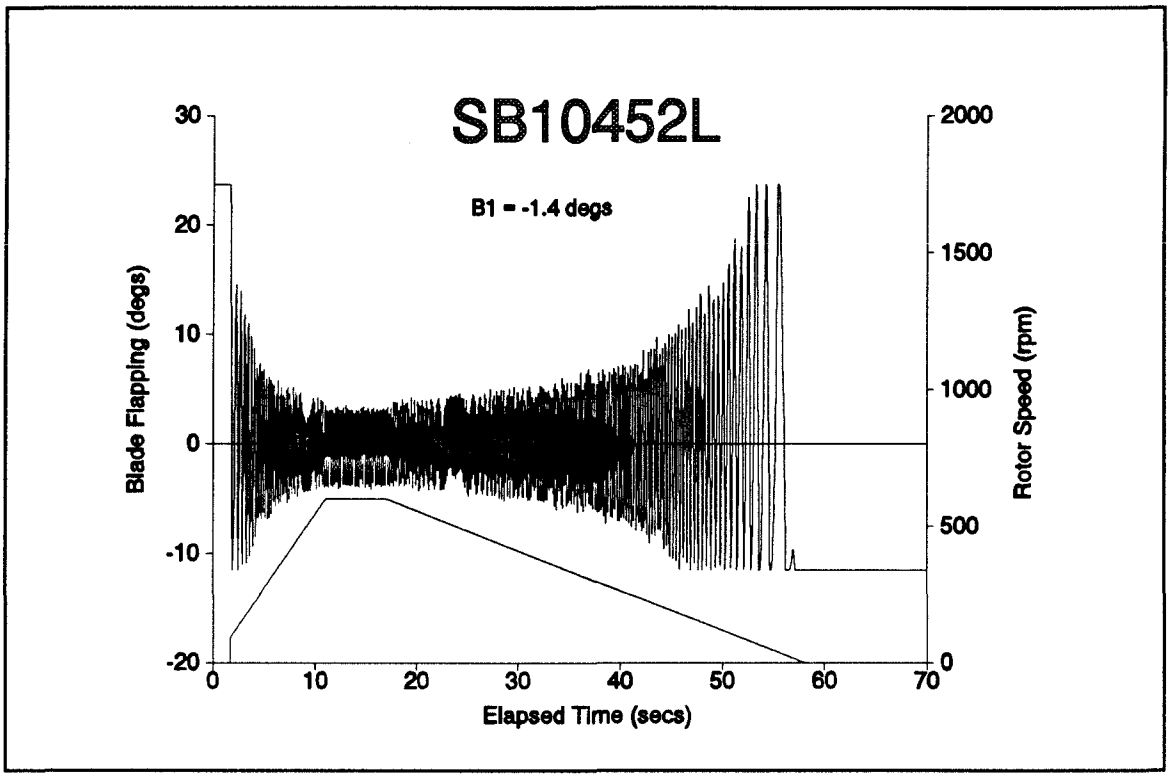

FigureIII.14.c - Theoretical Prediction. 2 Blade, Run Down, Deck Location B, B_1=-1.4°

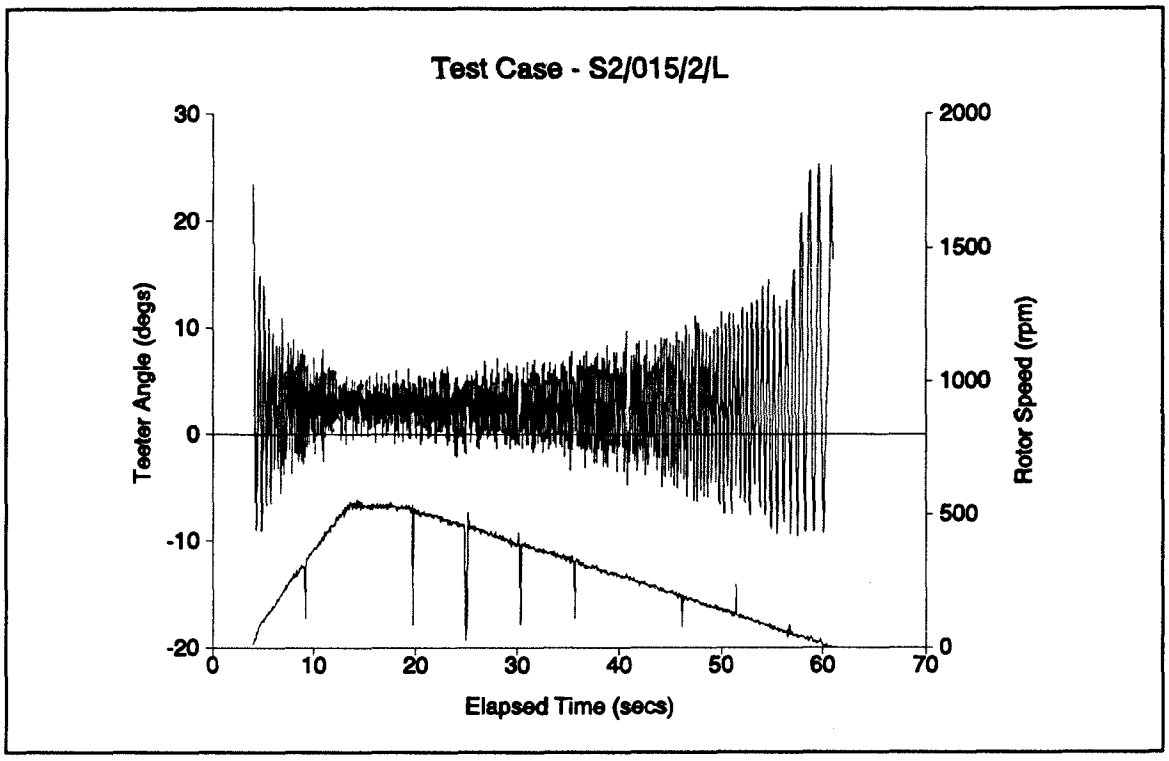

FigureIII.15.a - Wind Tunnel tests, 2 blade, Deck Position C

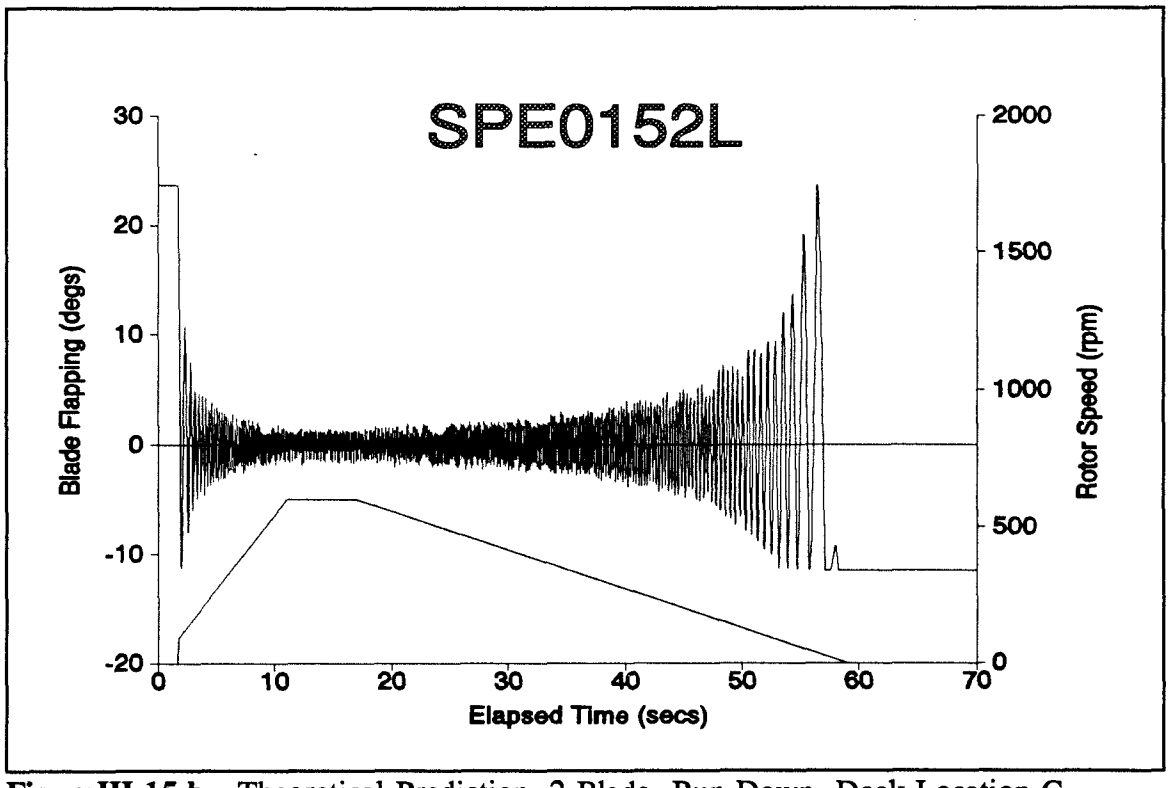

FigureIII.15.b - Theoretical Prediction, 2 Blade, Run Down, Deck Location C

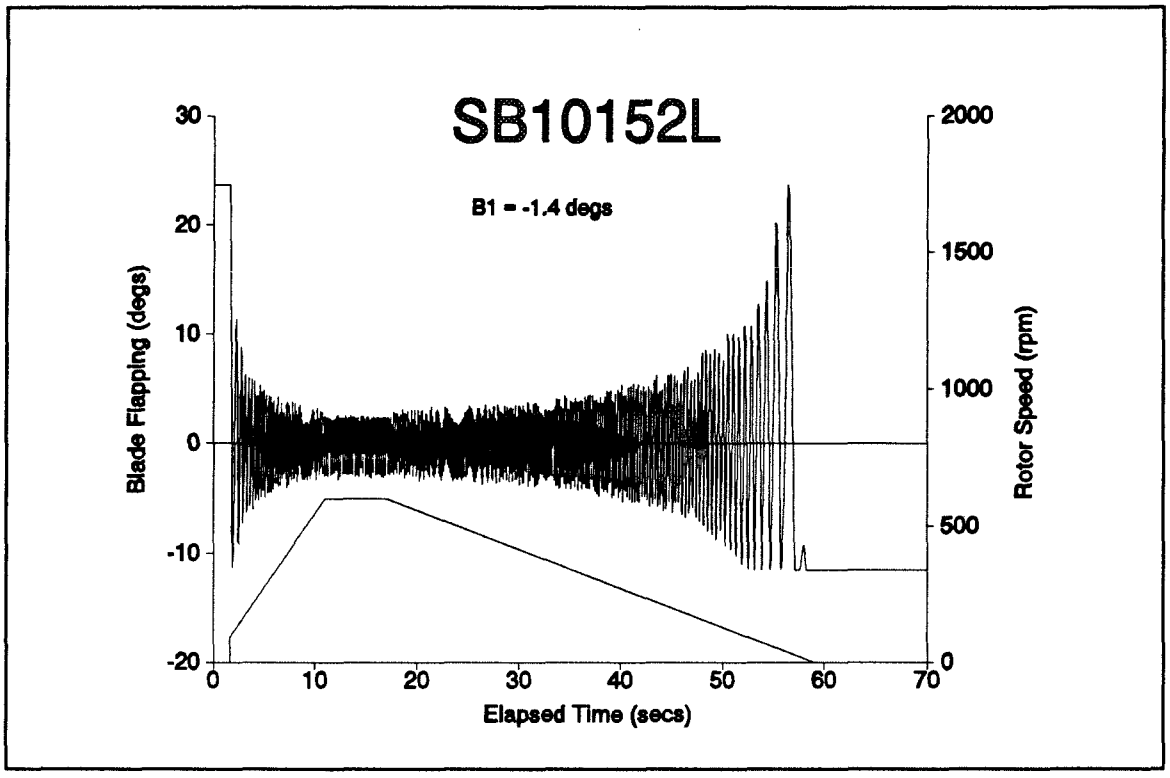

FigureIII.15.c - Theoretical Prediction. 2 Blade, Run Down, Deck Location C, $B_1 = -1.4°$

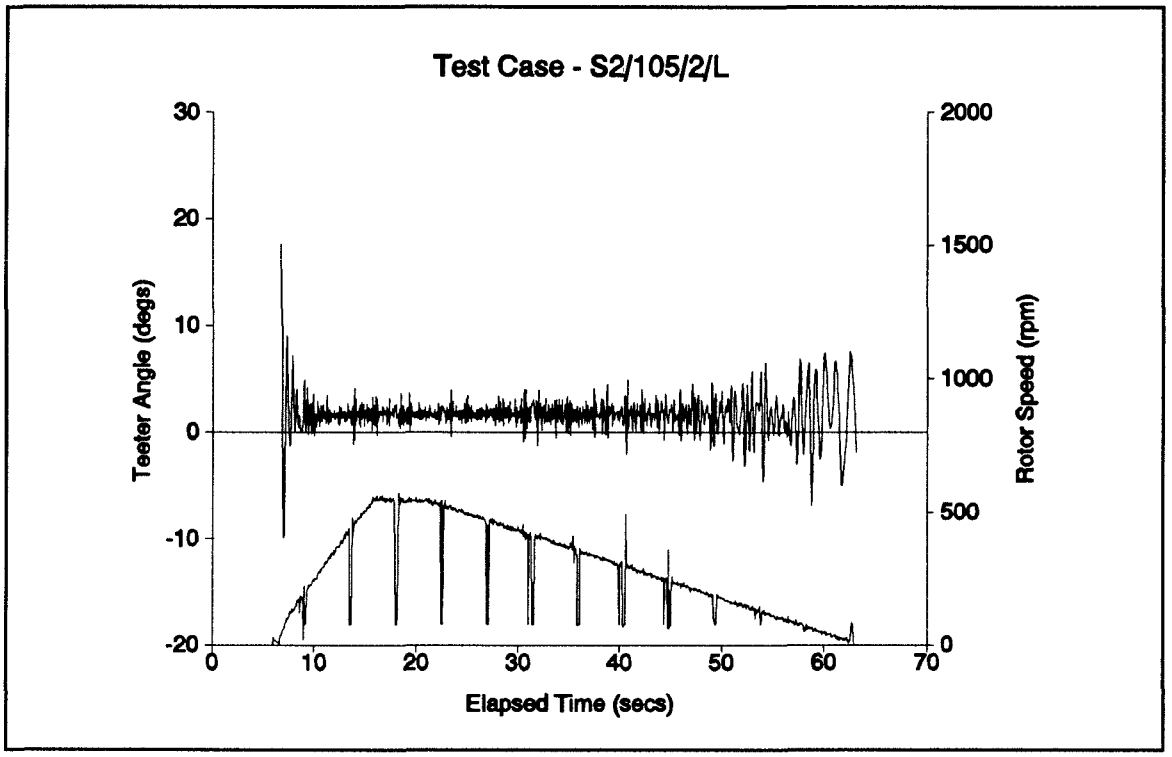

FigureIII.16.a - Wind Tunnel tests, 2 blade, Deck Position D

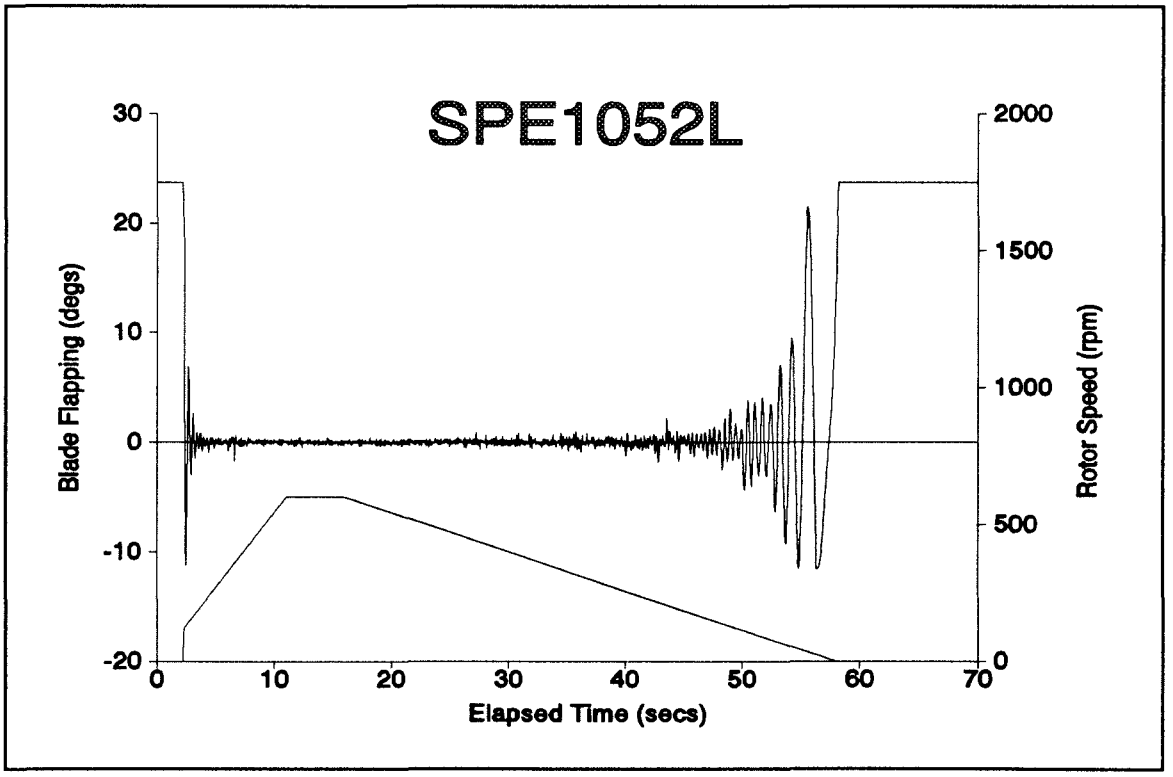

FigureIII.16.b - Theoretical Prediction, 2 Blade, Run Down, Deck Location D

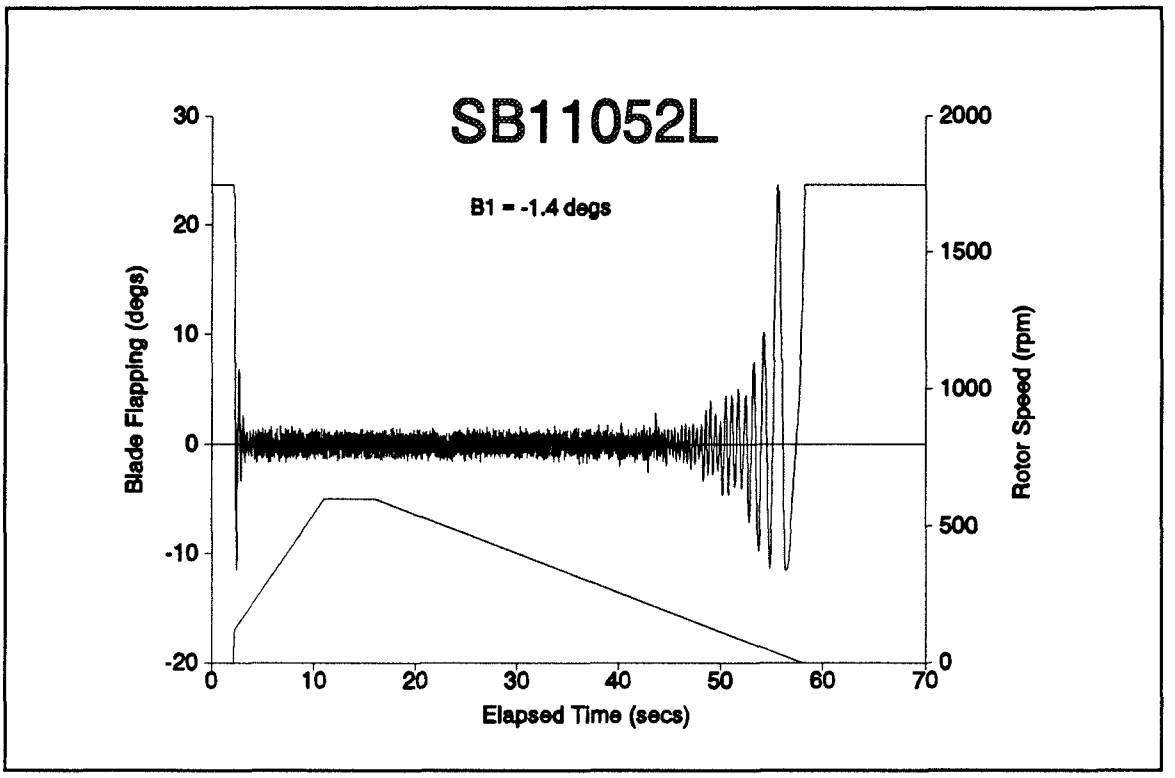

FigureIII.16.c - Theoretical Prediction. 2 Blade, Run Down, Deck Location D, B_1=-1.4°

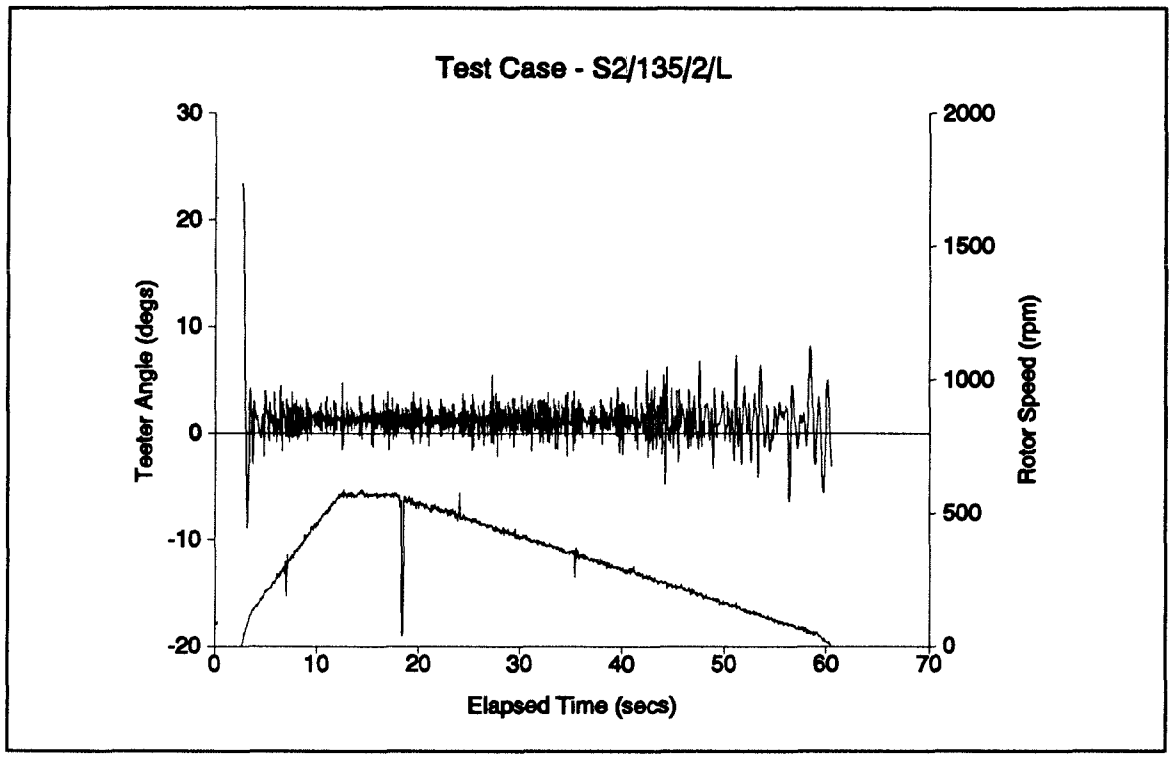

FigureIII.17.a - Wind Tunnel tests, 2 blade, Deck Position E

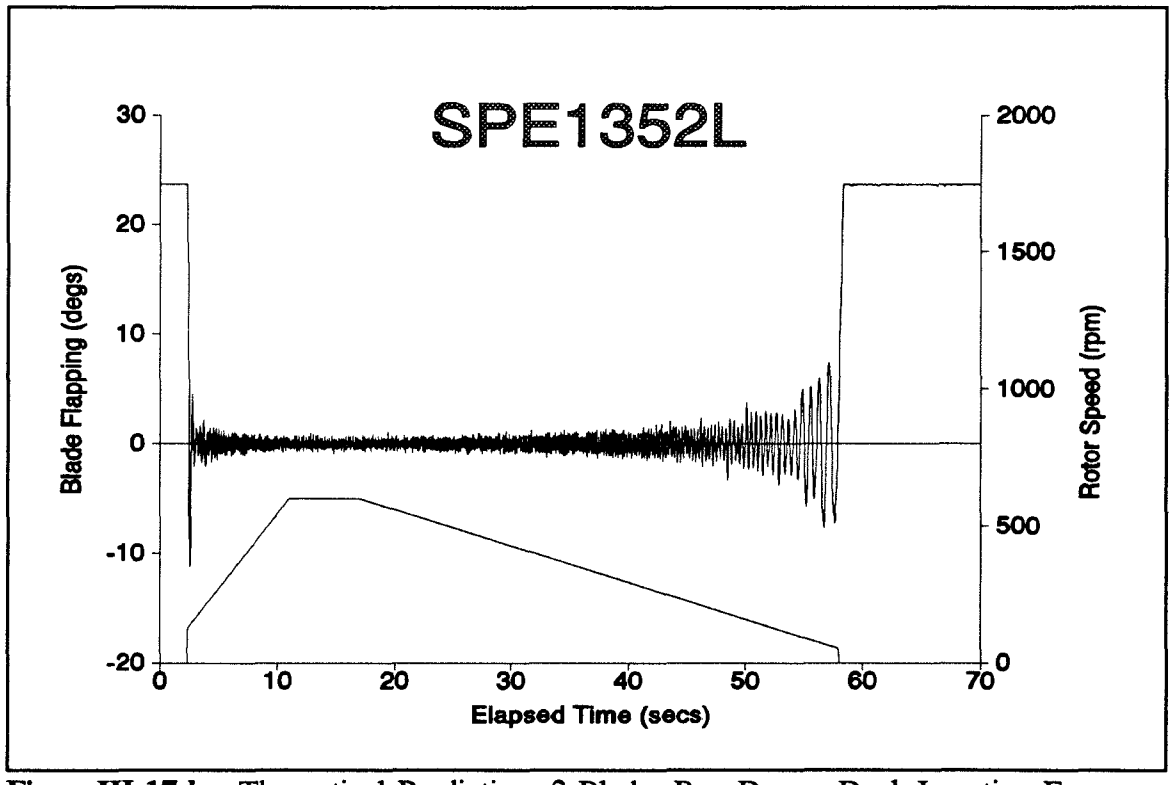

FigureIII.17.b - Theoretical Prediction, 2 Blade, Run Down, Deck Location E

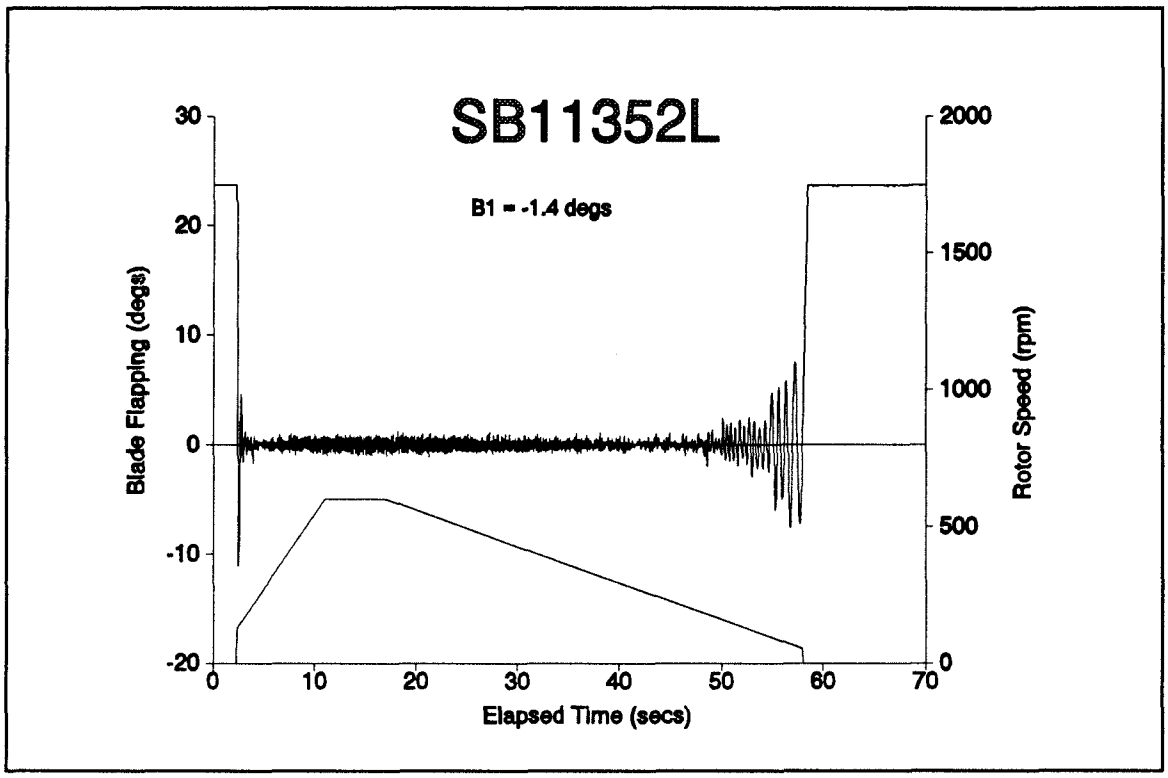

FigureIII.17.c - Theoretical Prediction. 2 Blade, Run Down, Deck Location E, B_1=-1.4°

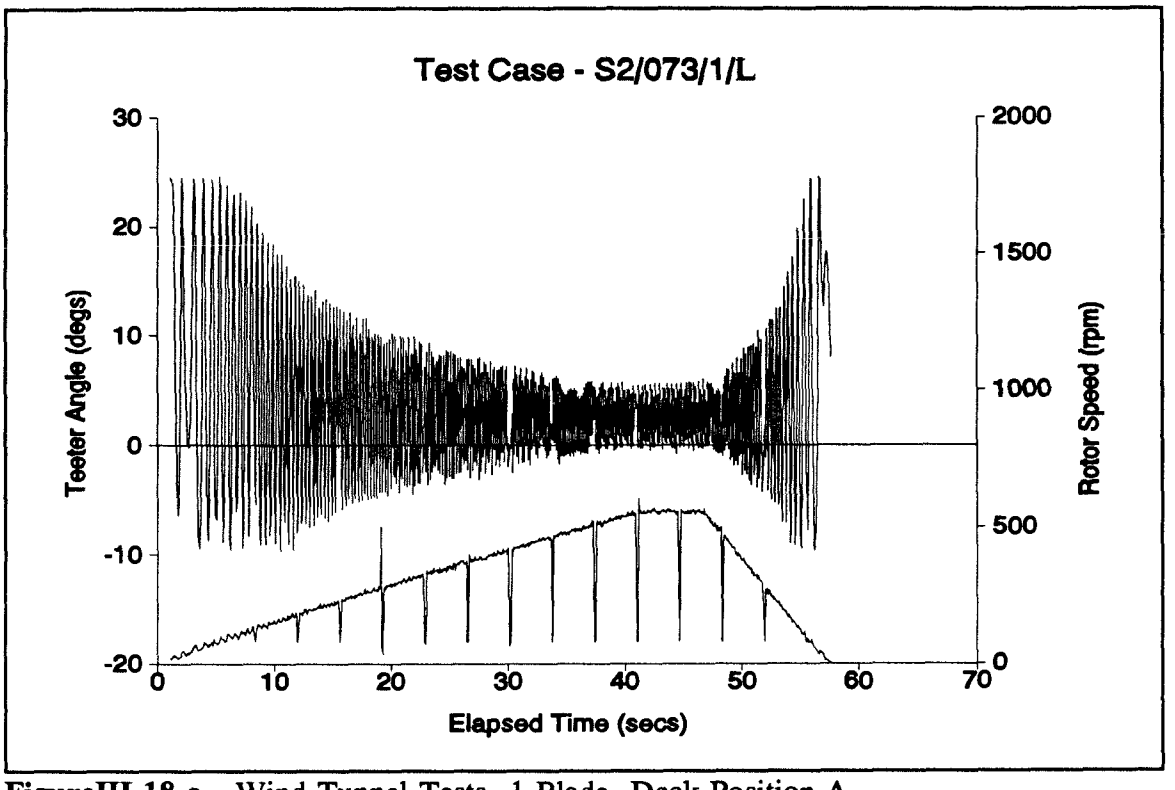

FigureIII.18.a - Wind Tunnel Tests, 1 Blade, Deck Position A

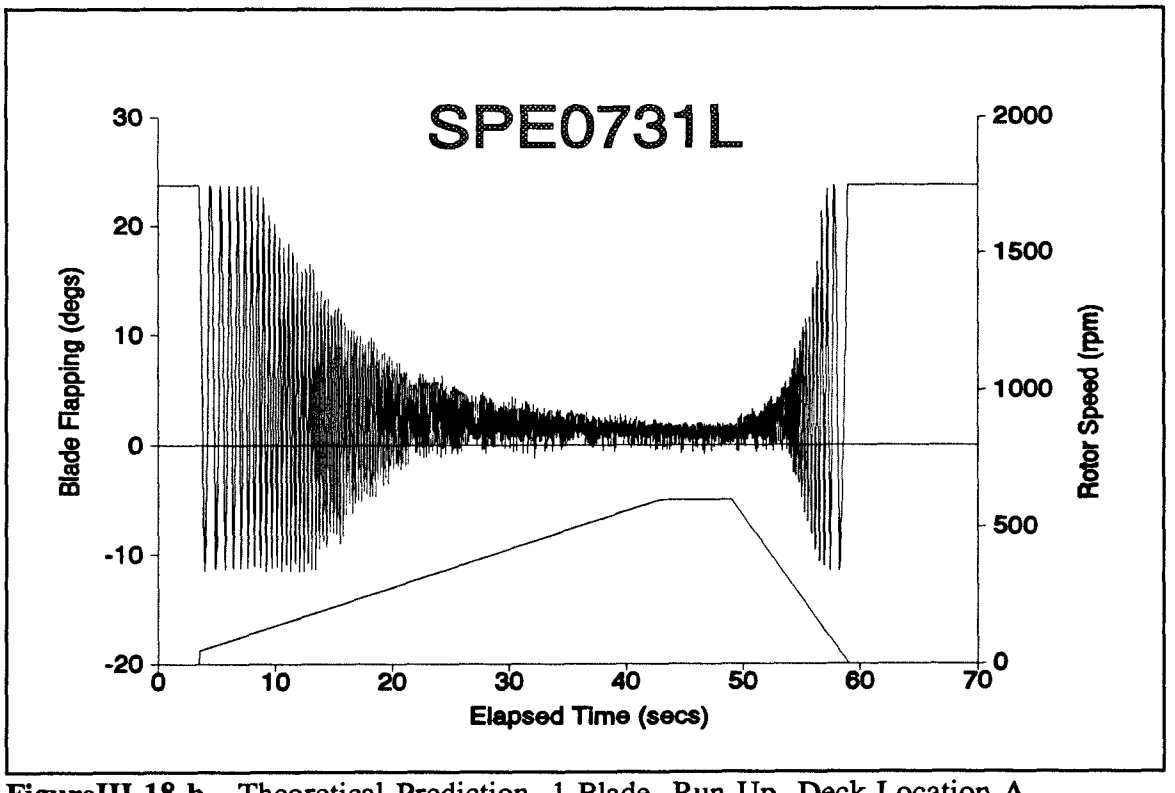

FigureIII.18.b - Theoretical Prediction, 1 Blade, Run Up, Deck Location A

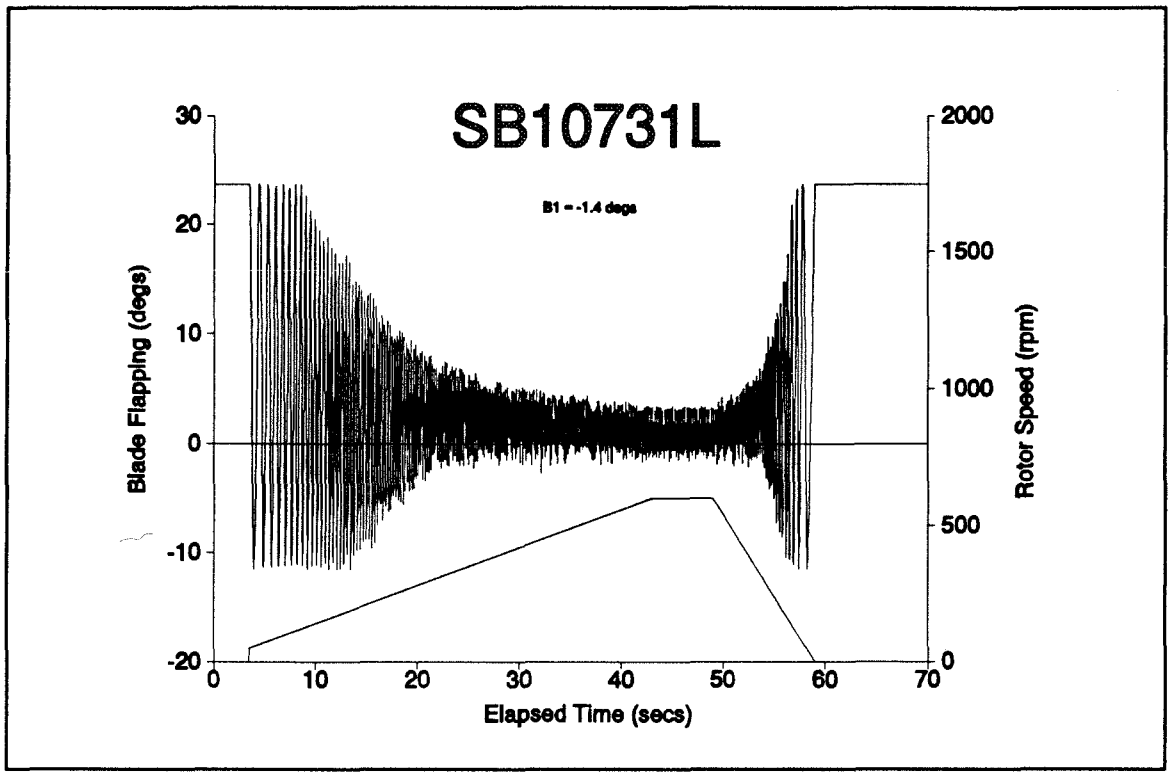

FigureIII.18.c - Theoretical Prediction. 1 Blade, Run Up, Deck Location A, B_1=-1.4°

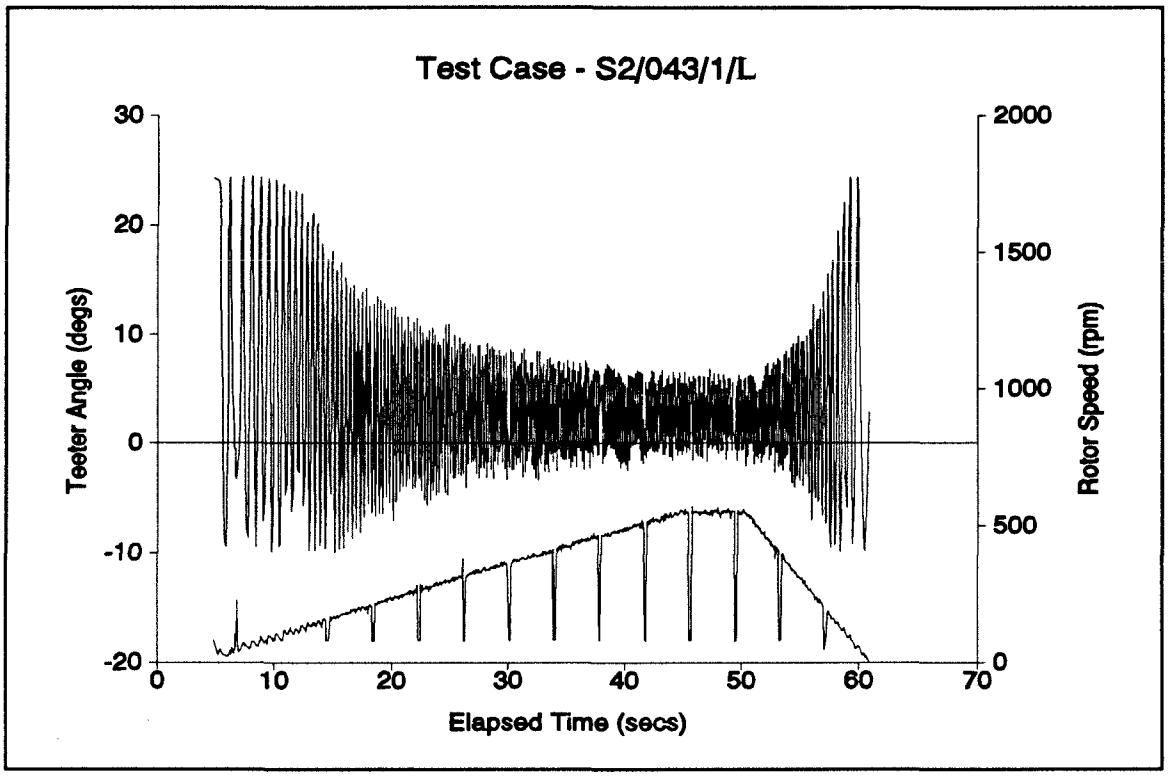

FigureIII.19.a - Wind Tunnel Tests, 1 Blade, Deck Position B

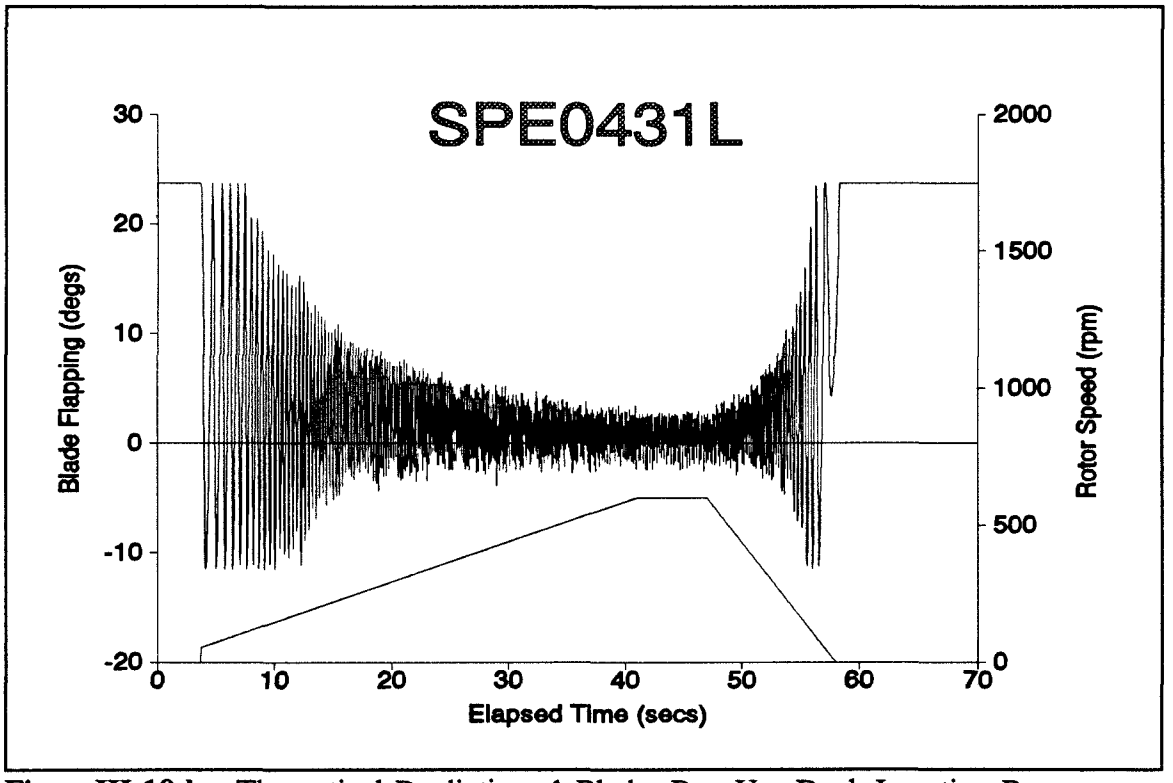

FigureIII.19.b - Theoretical Prediction, 1 Blade, Run Up, Deck Location B

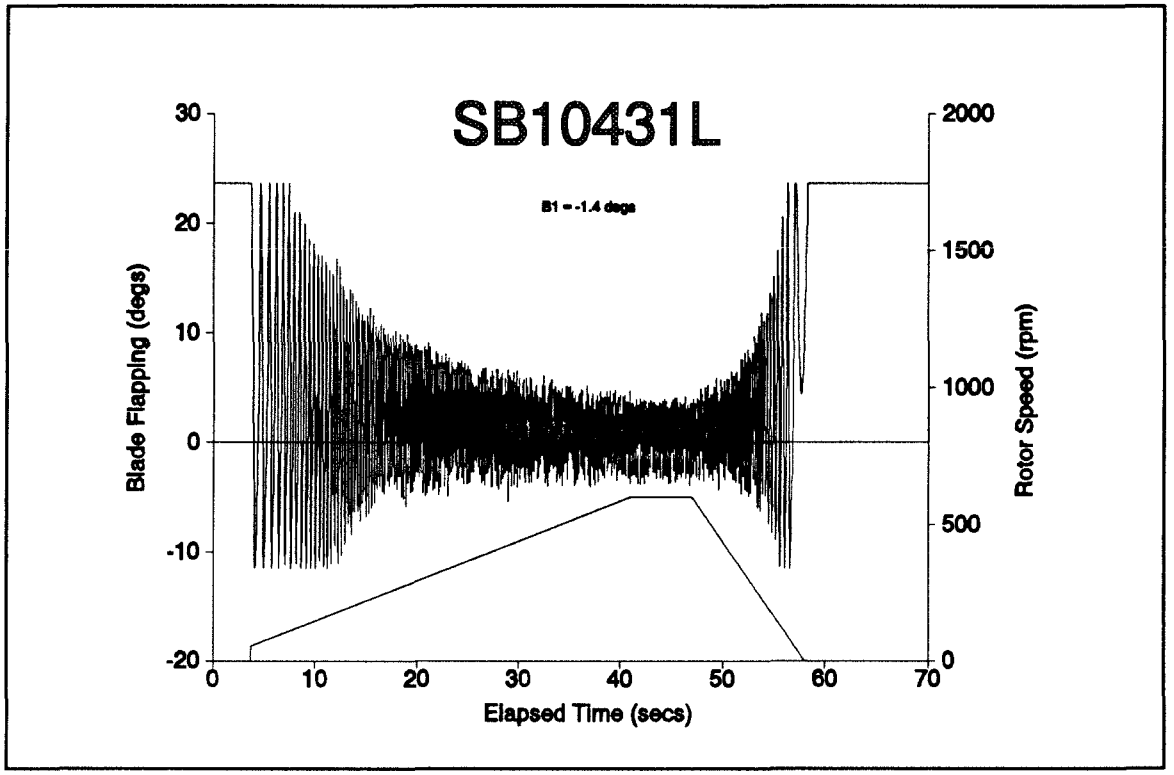

FigureIII.19.c - Theoretical Prediction. 1 Blade, Run Up, Deck Location B, B_1=-1.4°

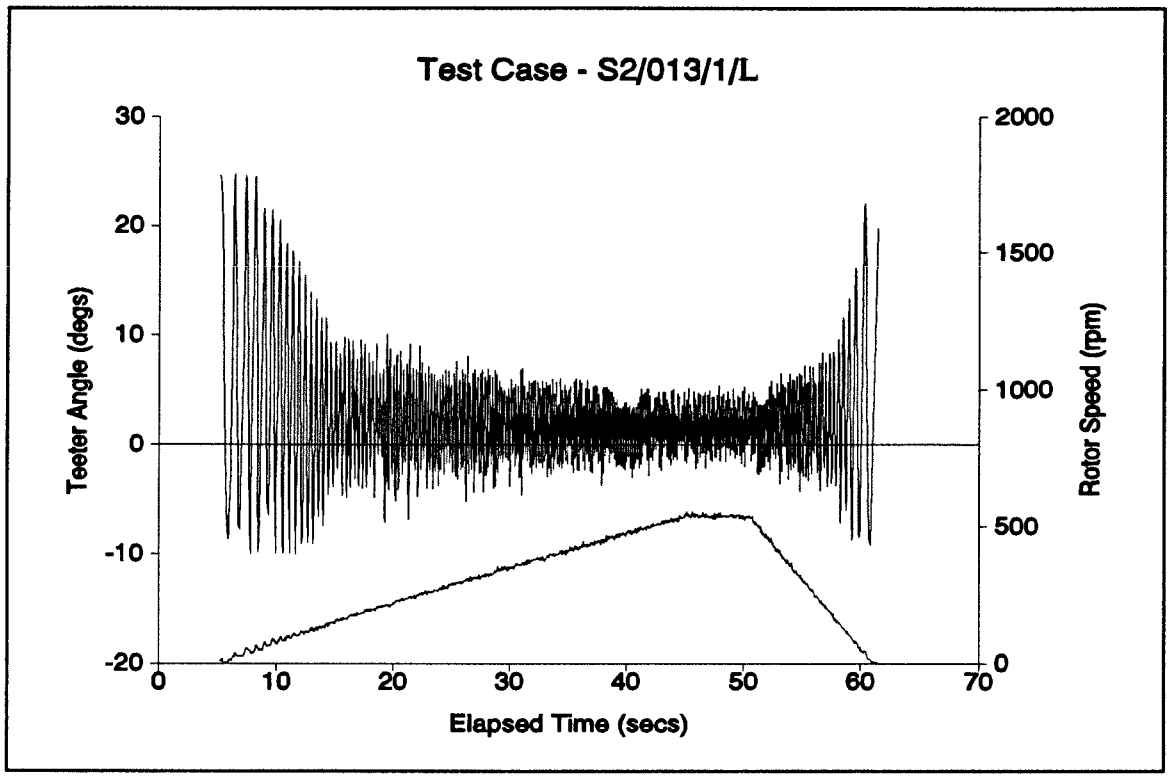

FigureIII.20.a - Wind Tunnel Tests, 1 Blade, Deck Position C

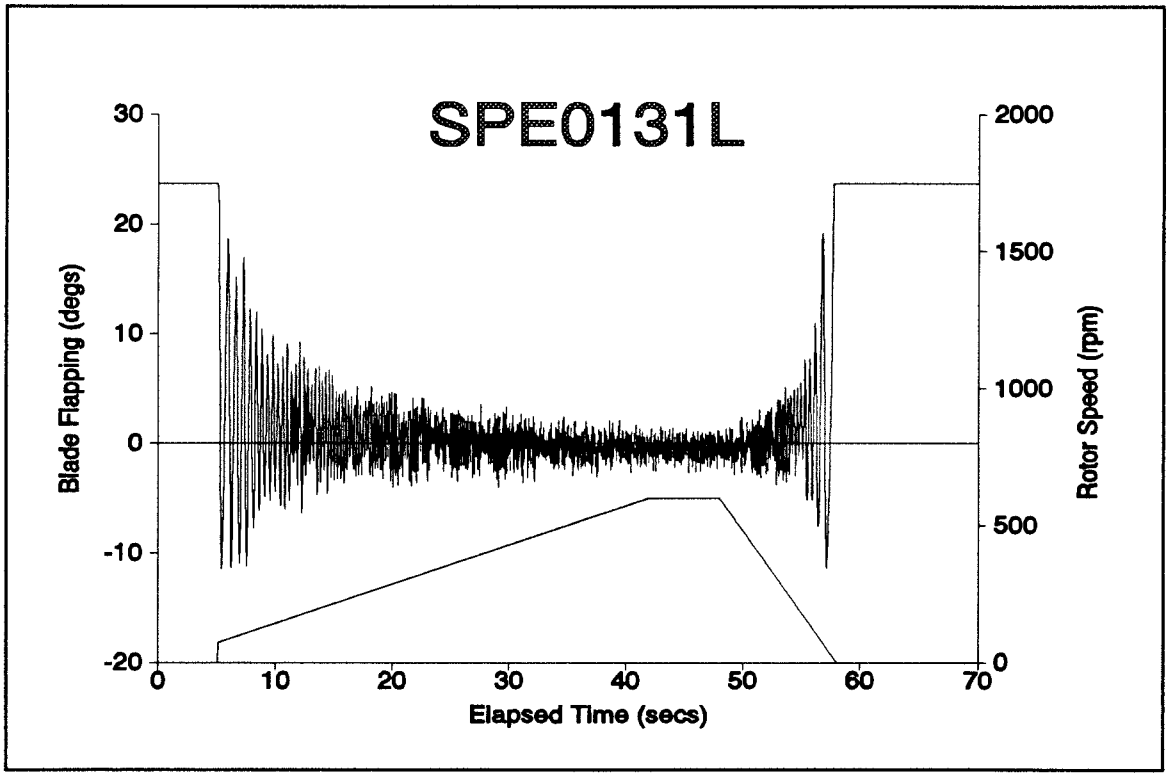

FigureIII.20.b - Theoretical Prediction, 1 Blade, Run Up, Deck Location C

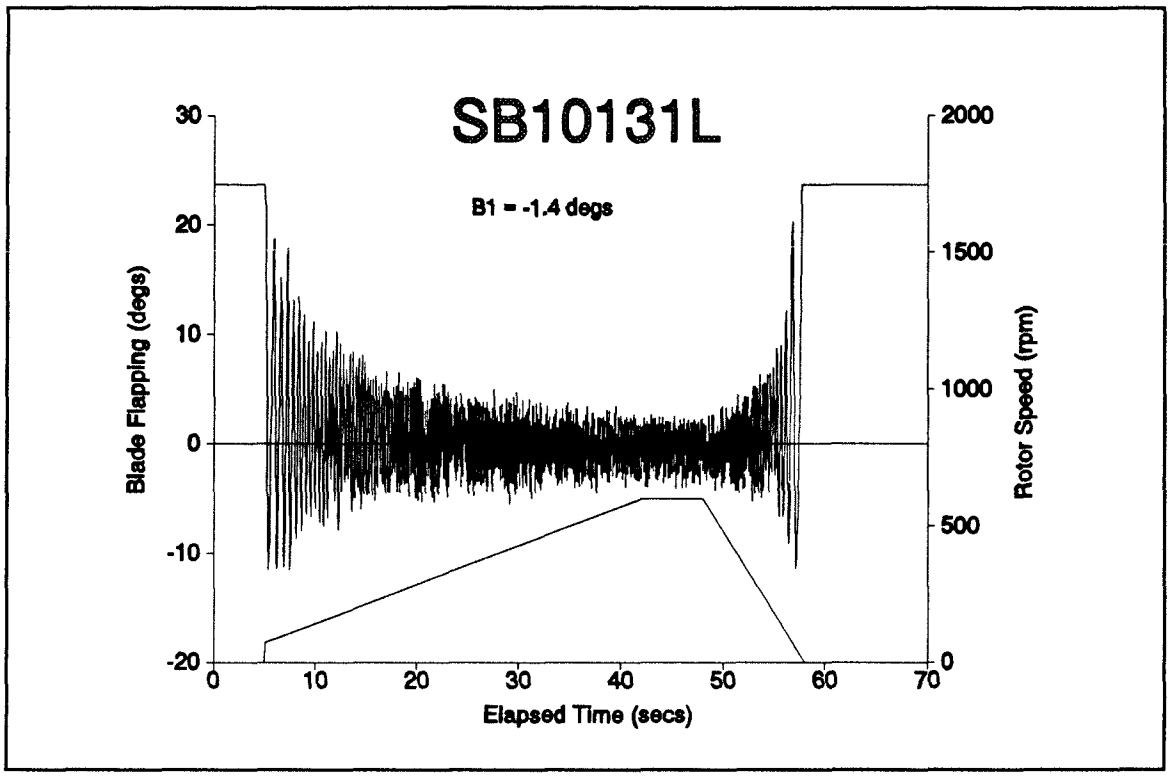

FigureIII.20.c - Theoretical Prediction. 1 Blade, Run Up, Deck Location C, B_1=-1.4°

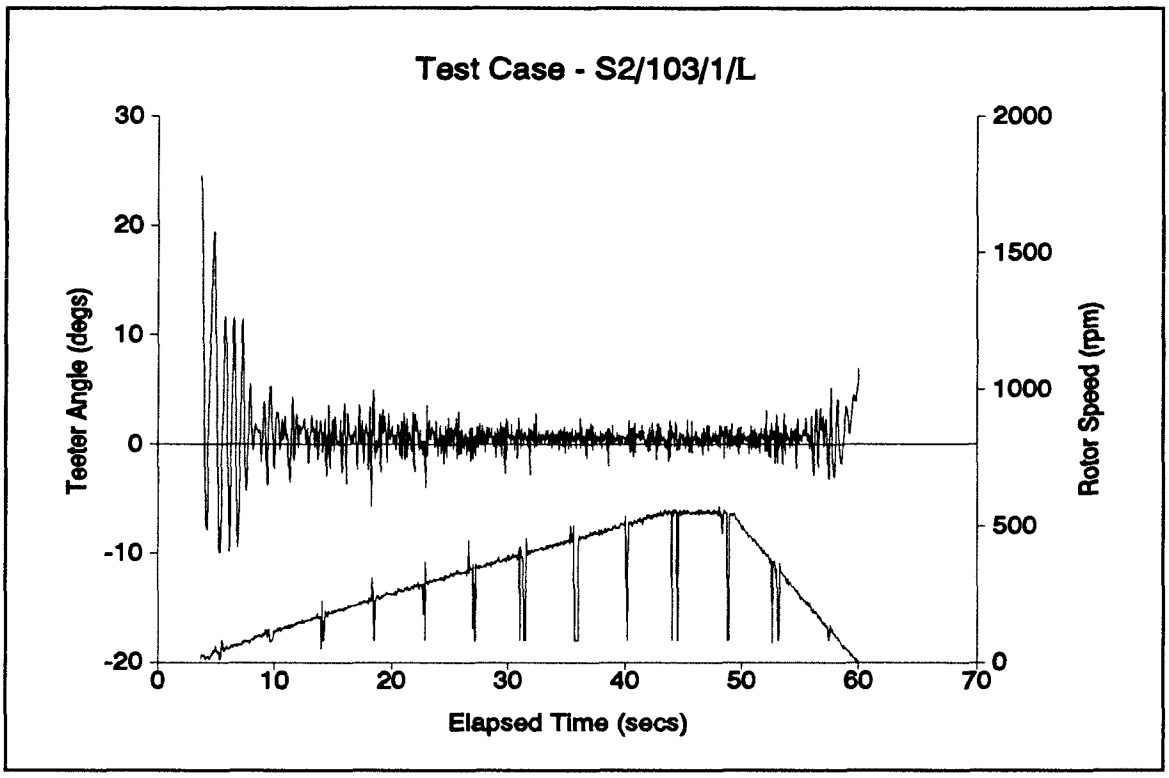

FigureIII.21.a - Wind Tunnel Tests, 1 Blade, Deck Position D

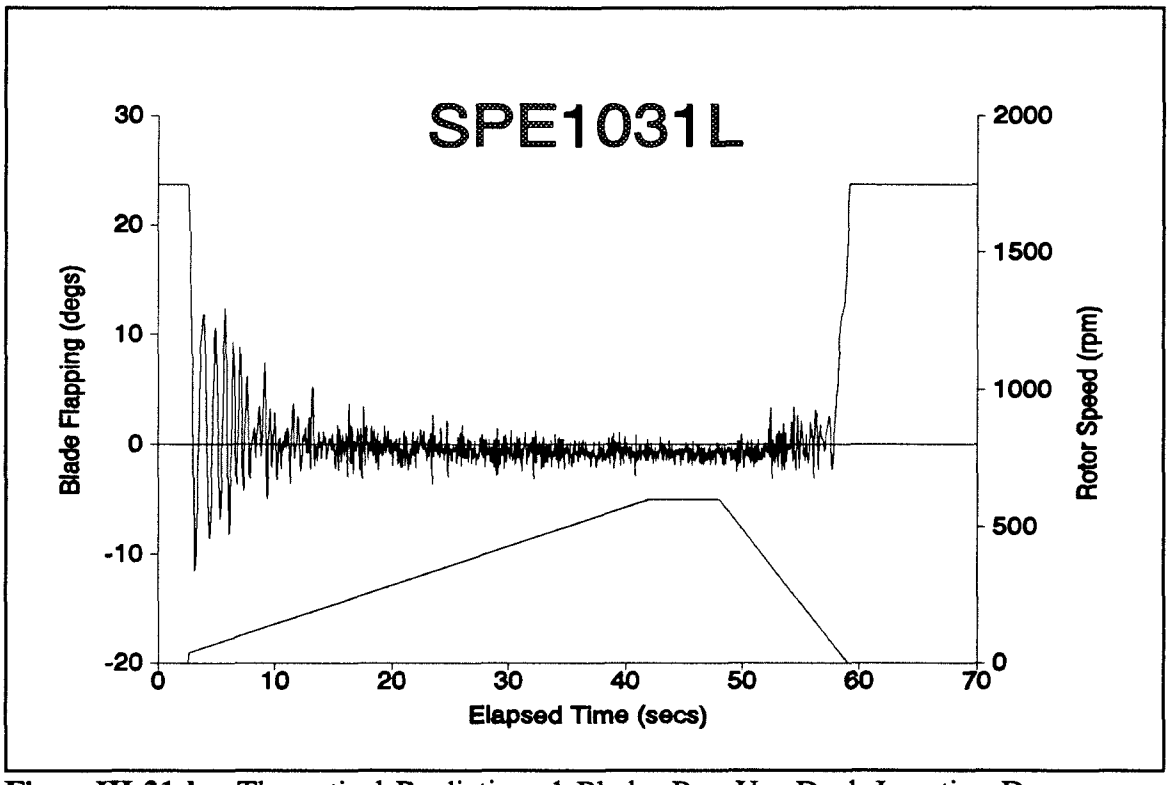

FigureIII.21.b - Theoretical Prediction, 1 Blade, Run Up, Deck Location D

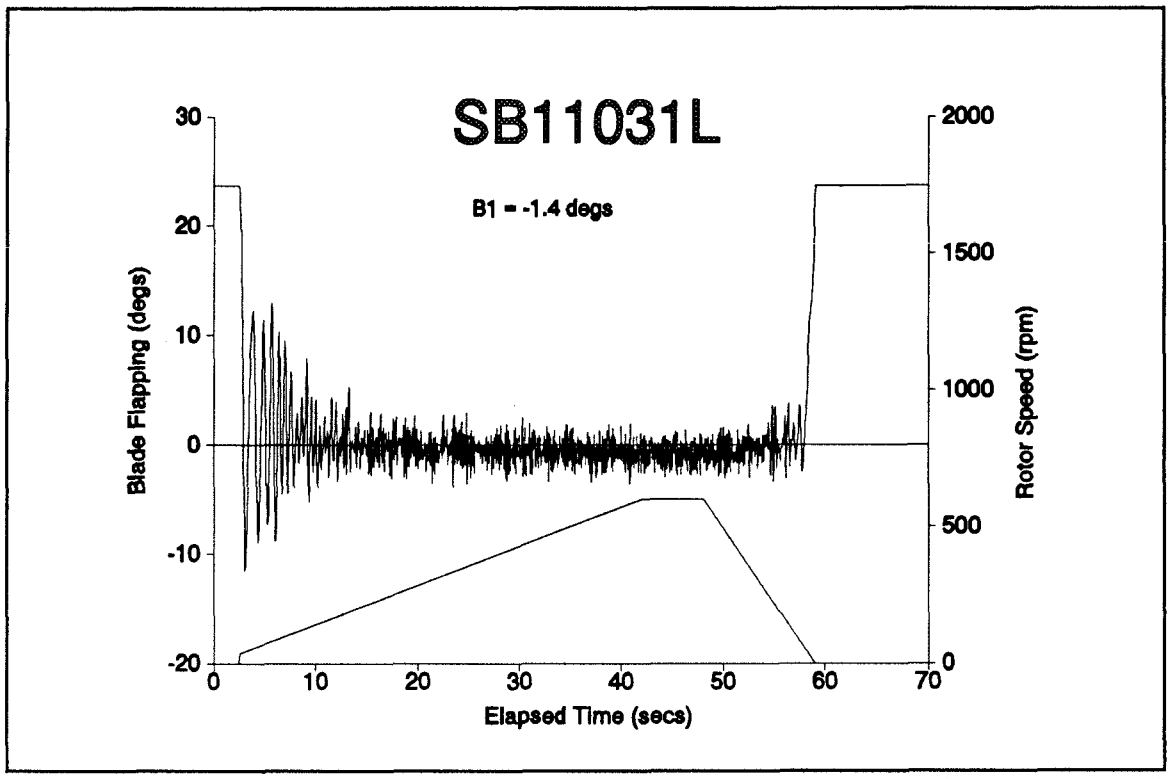

FigureIII.21.c - Theoretical Prediction. 1 Blade, Run Up, Deck Location D, B_1=-1.4°

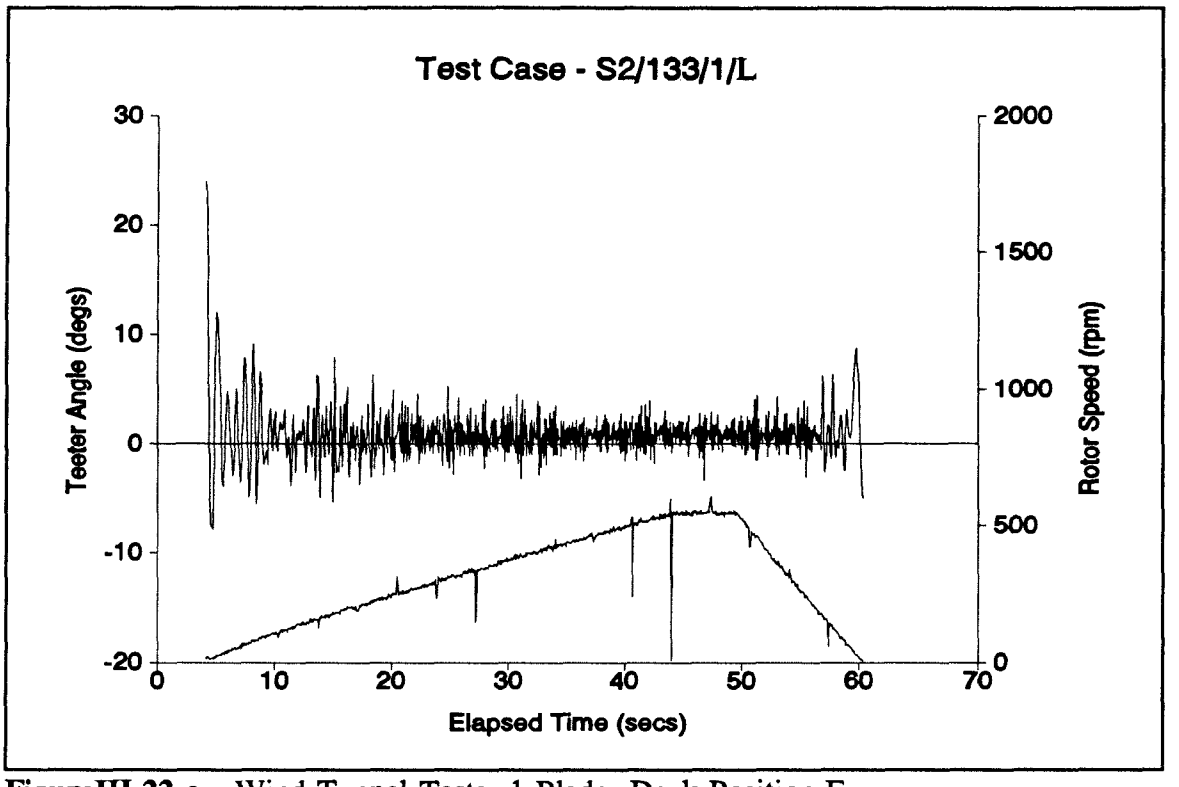

FigureIII.22.a - Wind Tunnel Tests, 1 Blade, Deck Position E

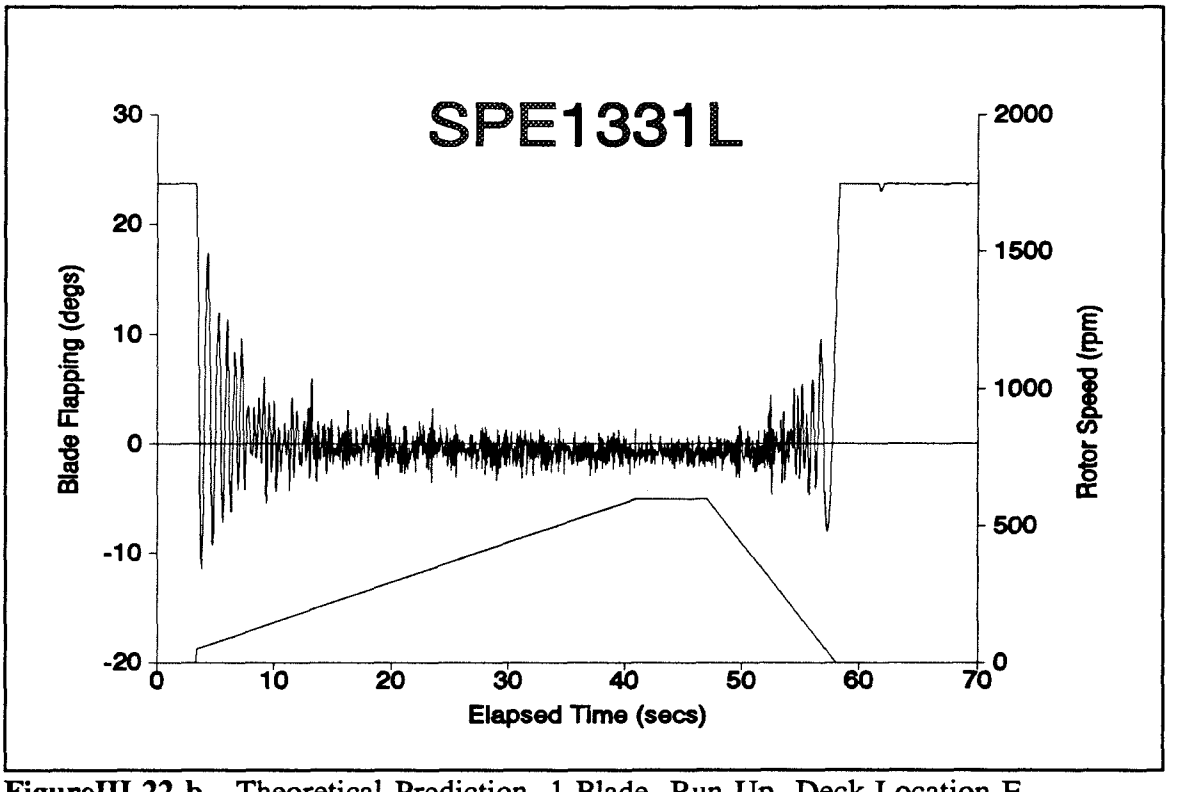

FigureIII.22.b - Theoretical Prediction, 1 Blade, Run Up, Deck Location E

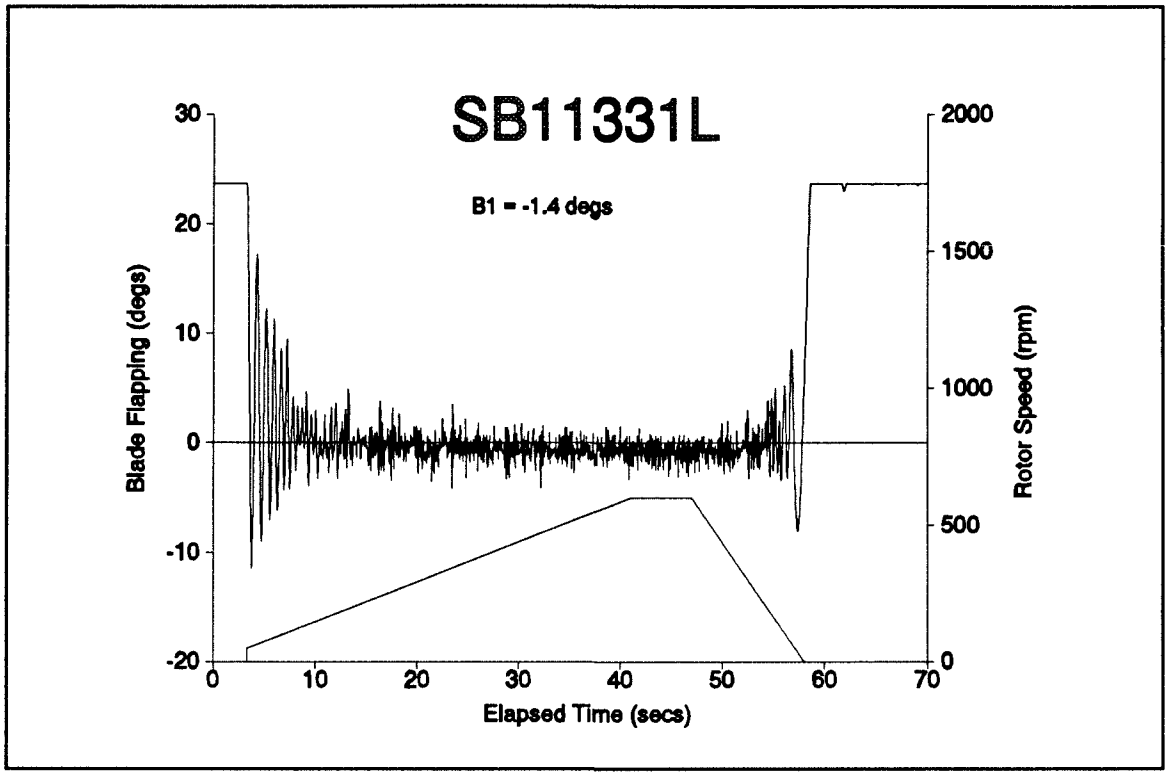

FigureIII.22.c - Theoretical Prediction. 1 Blade, Run Up, Deck Location E, B_1=-1.4°

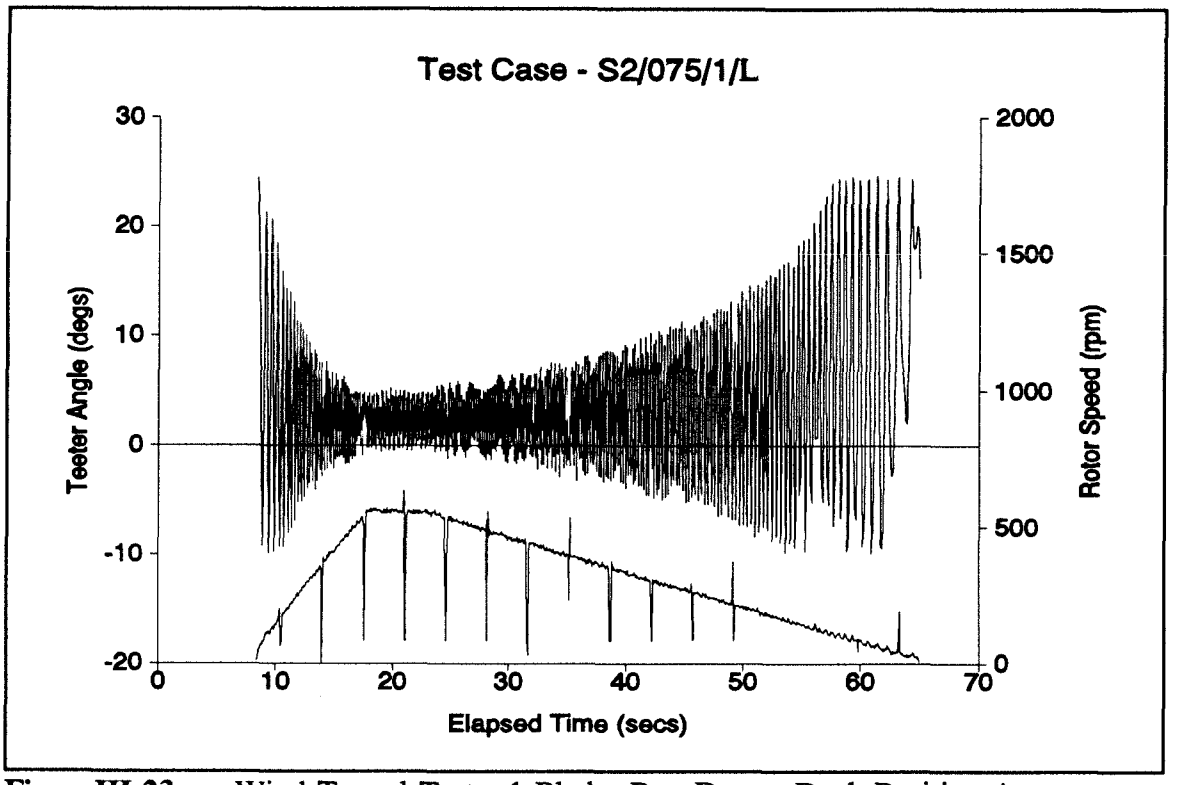

FigureIII.23.a - Wind Tunnel Tests, 1 Blade, Run Down, Deck Position A

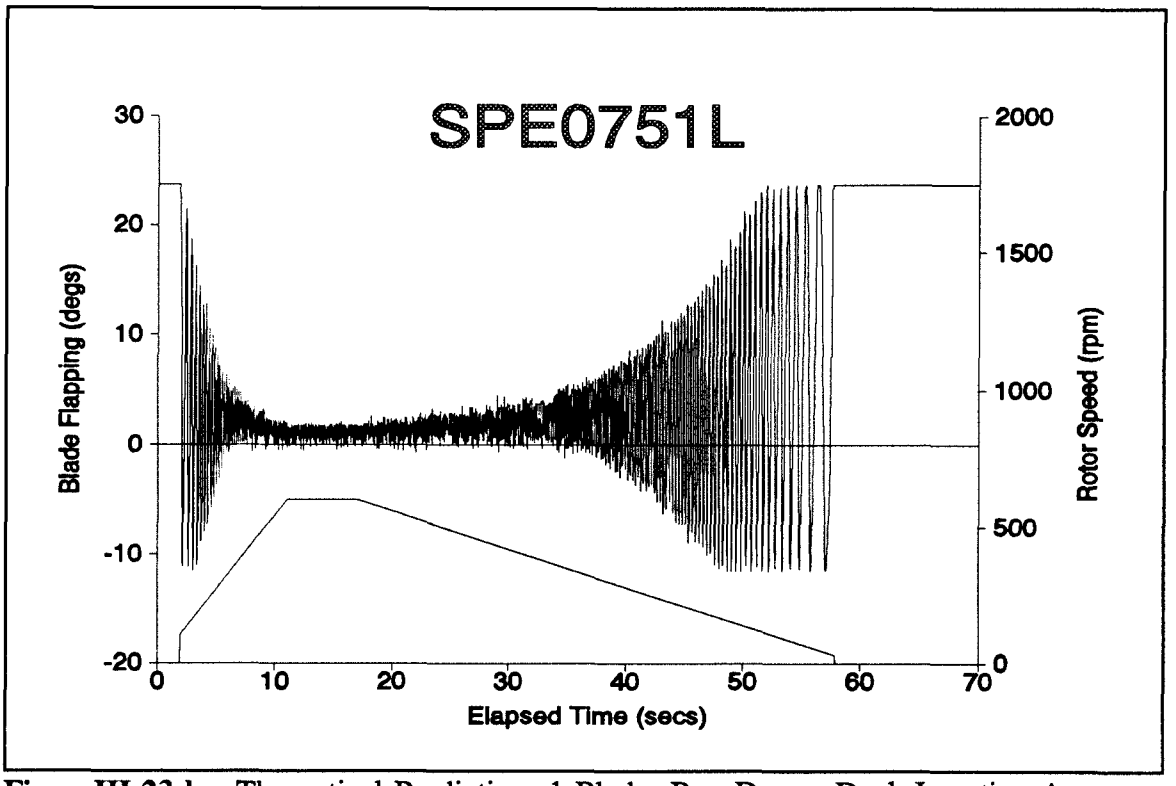

FigureIII.23.b - Theoretical Prediction, 1 Blade, Run Down, Deck Location A

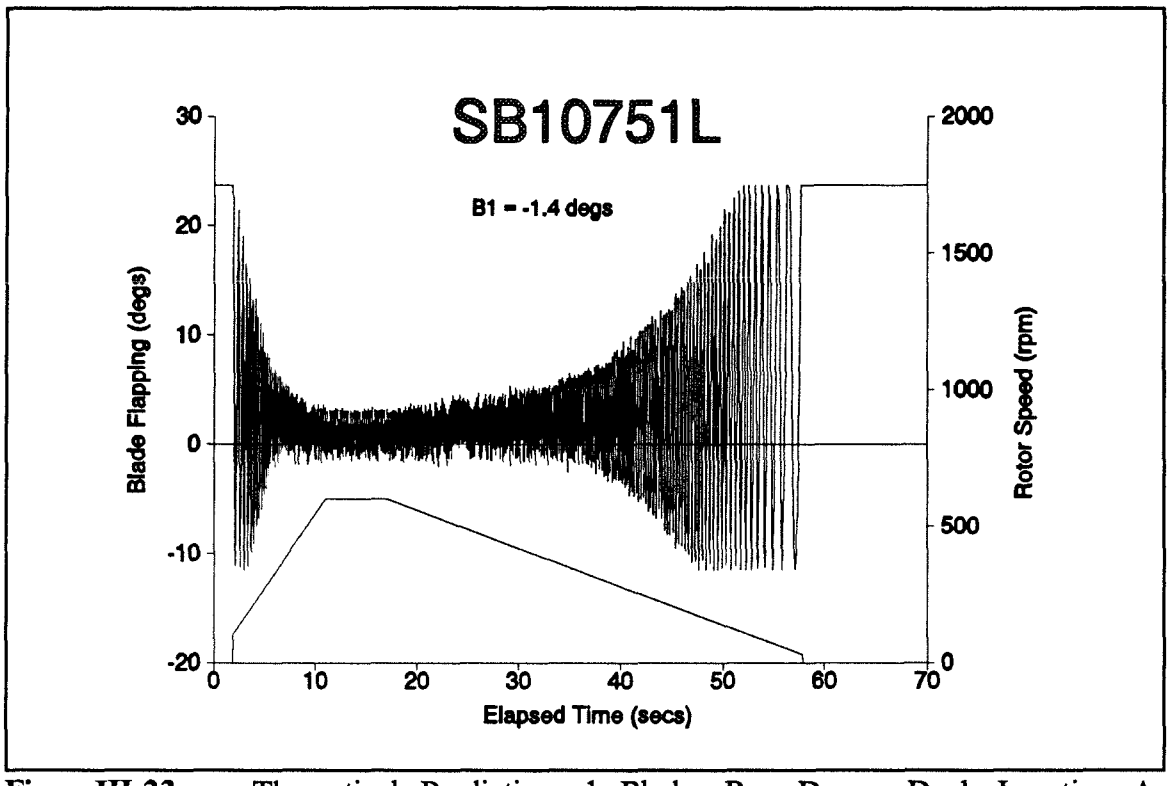

FigureIII.23.c - Theoretical Prediction. 1 Blade, Run Down, Deck Location A, $B_1 = -1.4°$

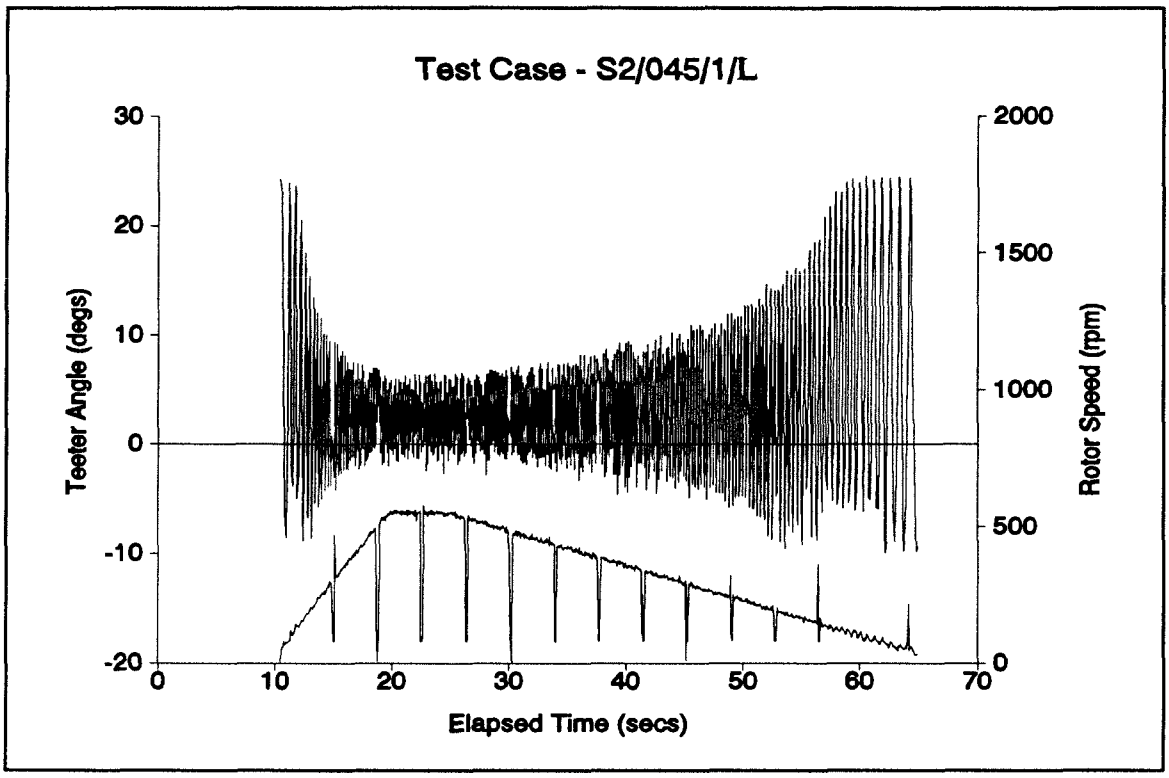

FigureIII.24.a - Wind Tunnel Tests, 1 Blade, Run Down, Deck Position B

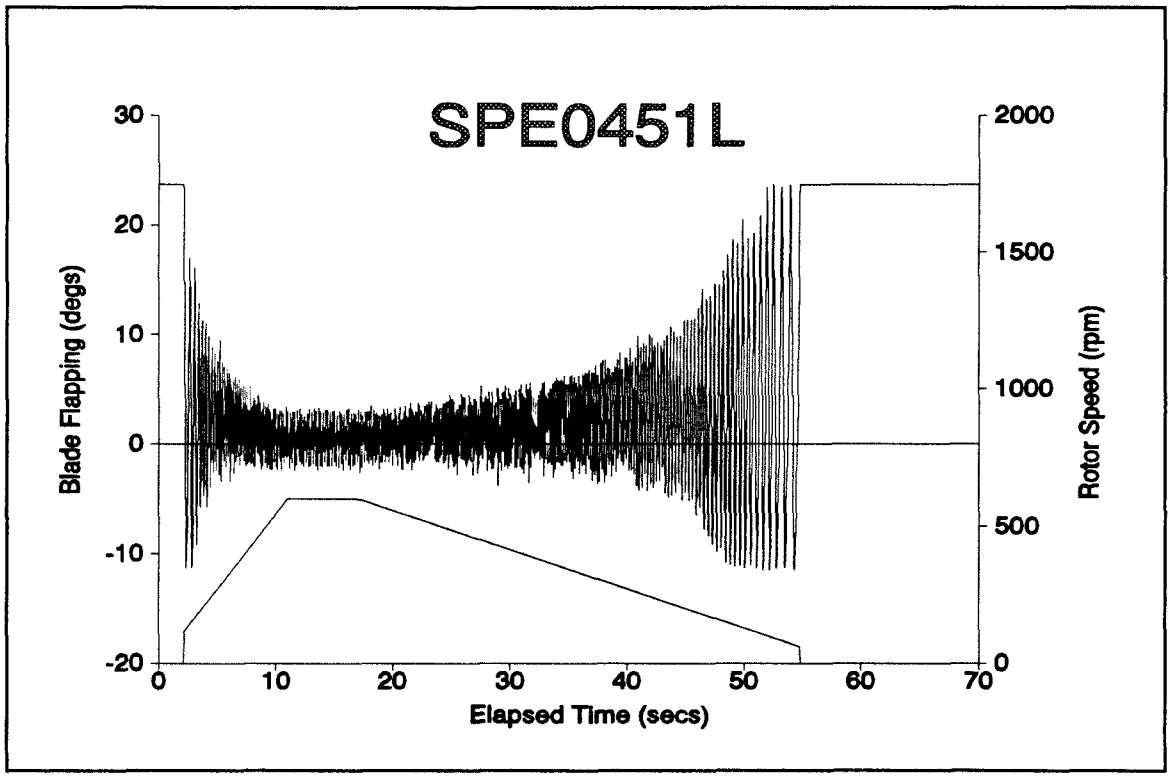

FigureIII.24.b - Theoretical Prediction, 1 Blade, Run Down, Deck Location B

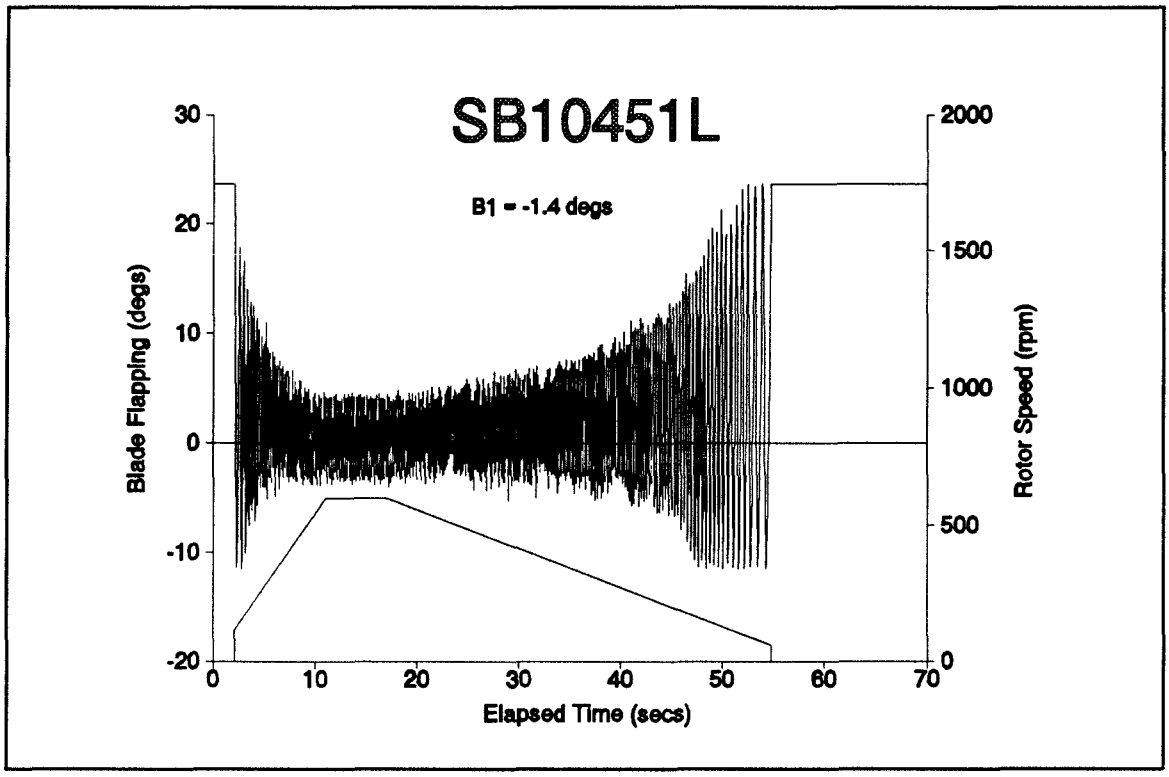

FigureIII.24.c - Theoretical Prediction. 1 Blade, Run Down, Deck Location B, B_1=-1.4°

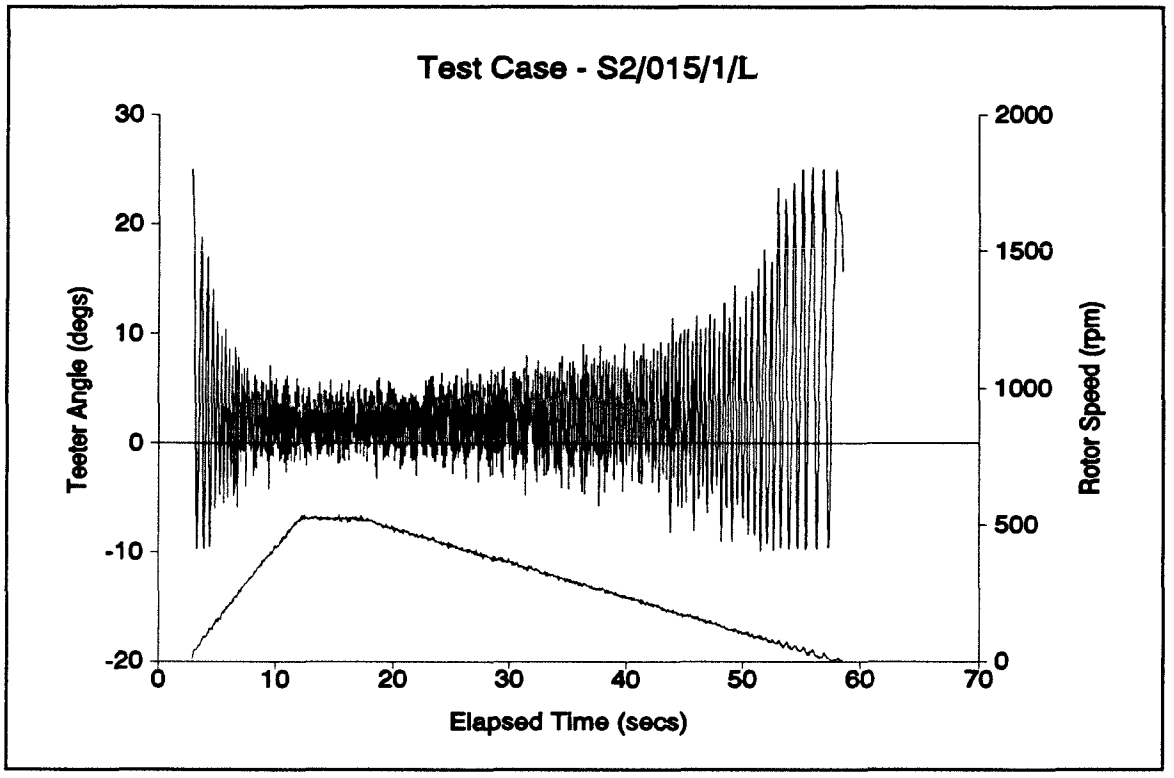

FigureIII.25.a - Wind Tunnel Tests, 1 Blade, Run Down, Deck Position C

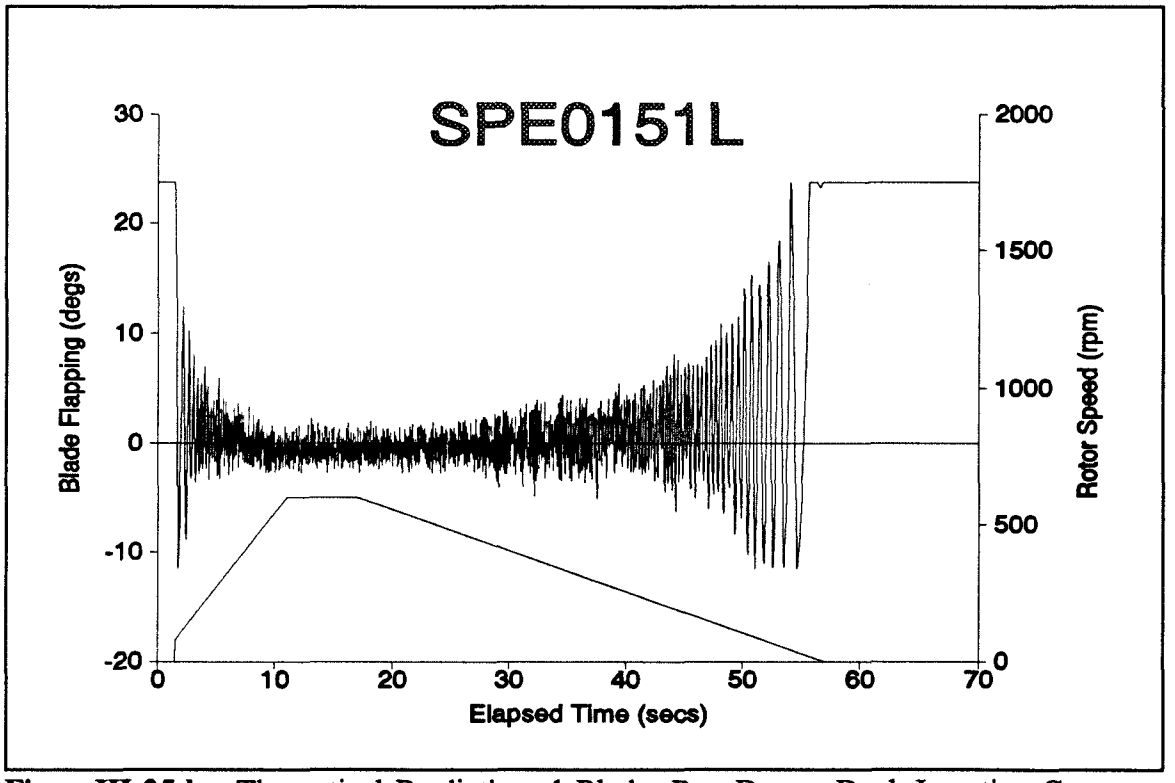

FigureIII.25.b - Theoretical Prediction, 1 Blade, Run Down, Deck Location C

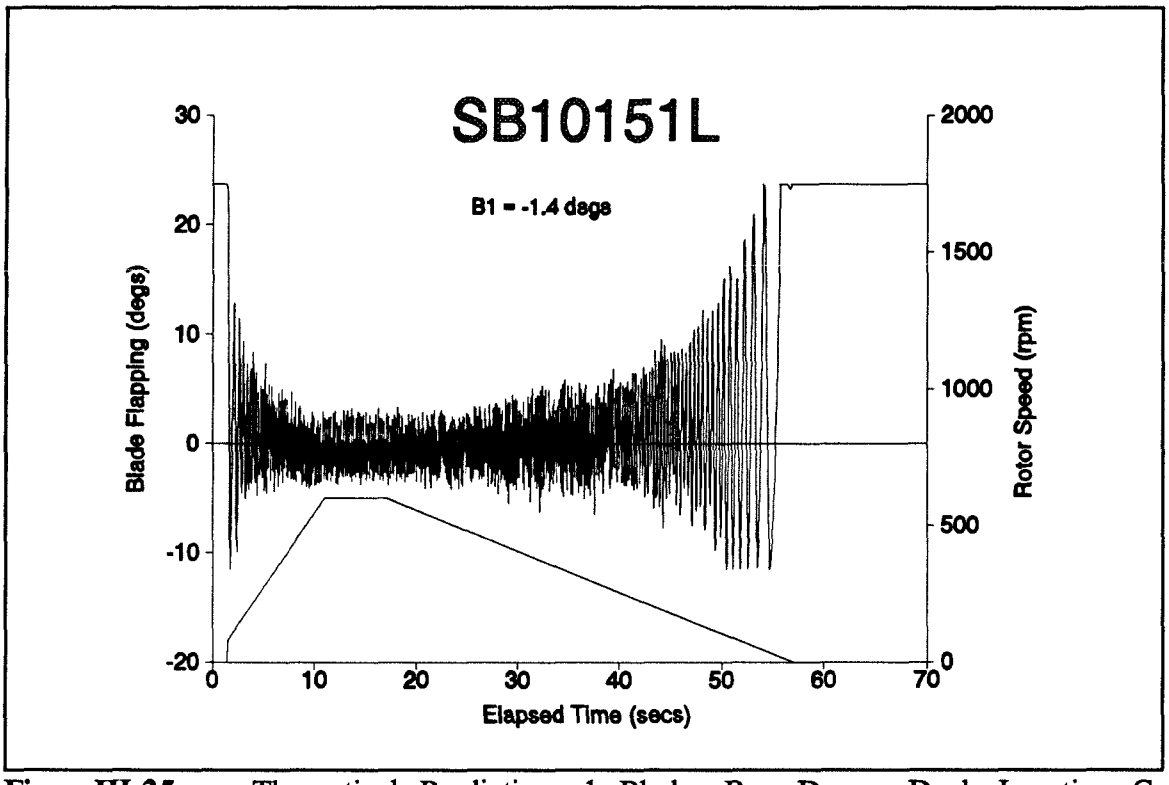

FigureIII.25.c - Theoretical Prediction. 1 Blade, Run Down, Deck Location C, B_1=-1.4°

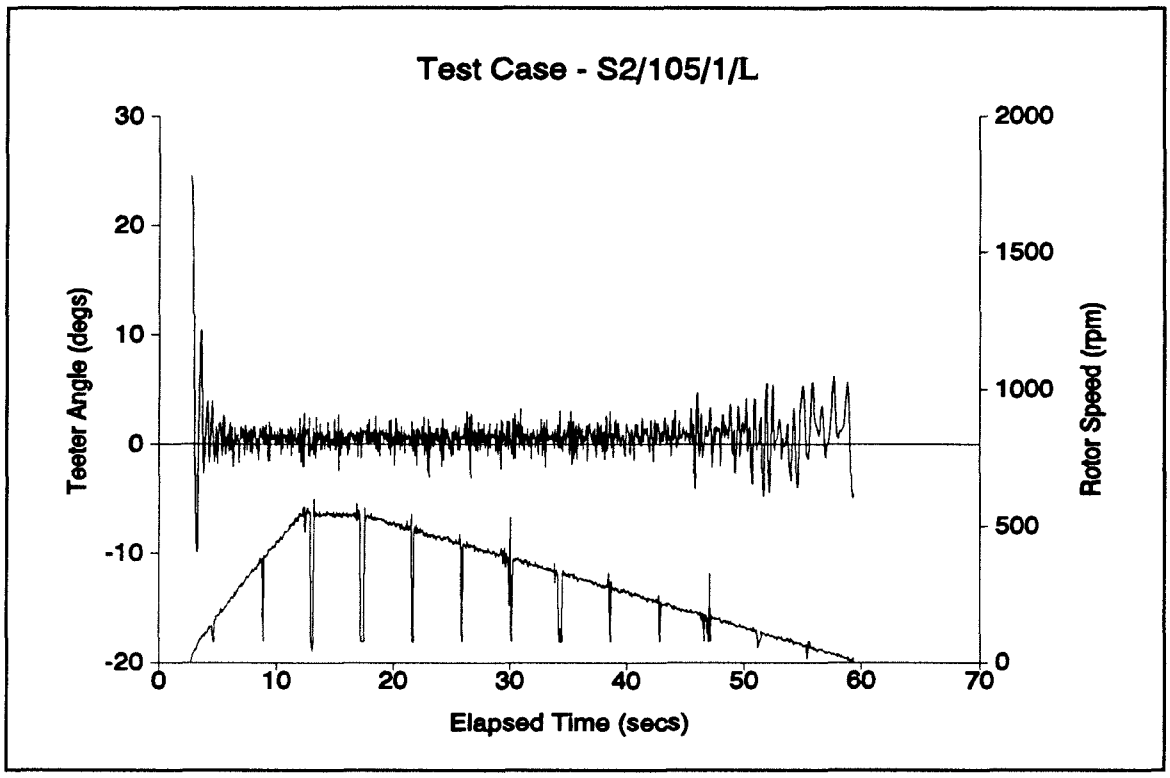

FigureIII.26.a - Wind Tunnel Tests, 1 Blade, Run Down, Deck Position D

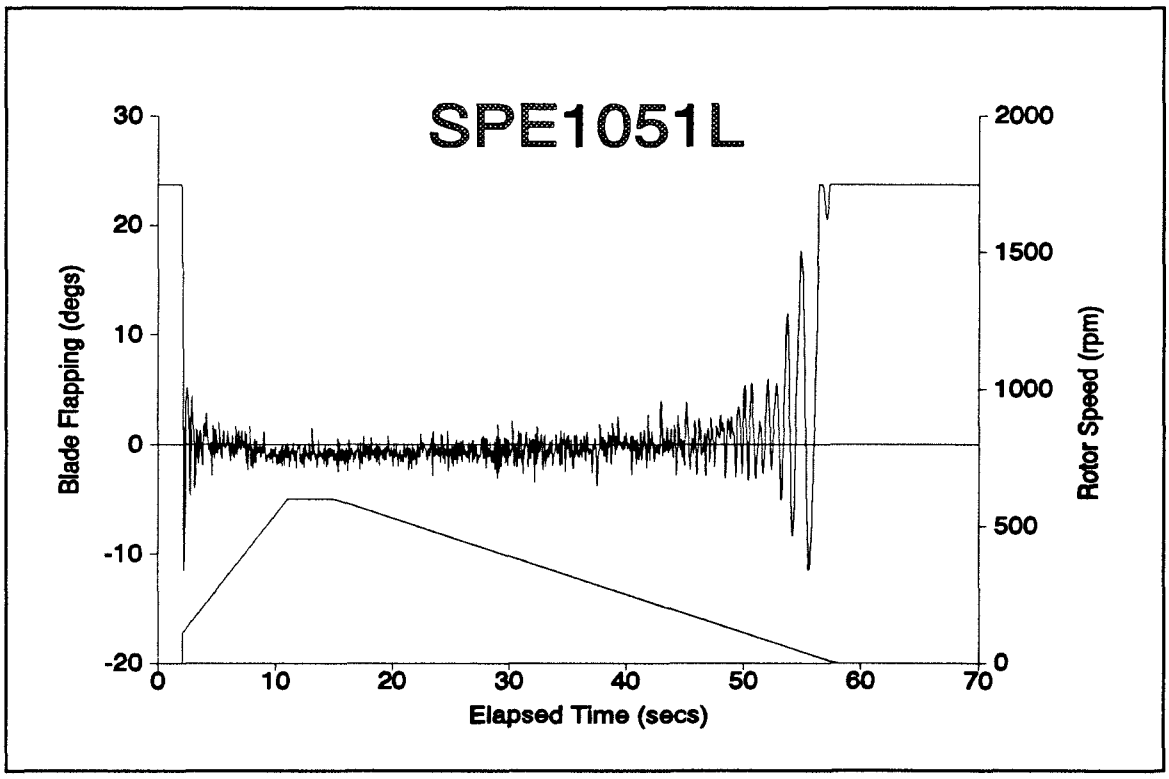

FigureIII.26.b - Theoretical Prediction, 1 Blade, Run Down, Deck Location D

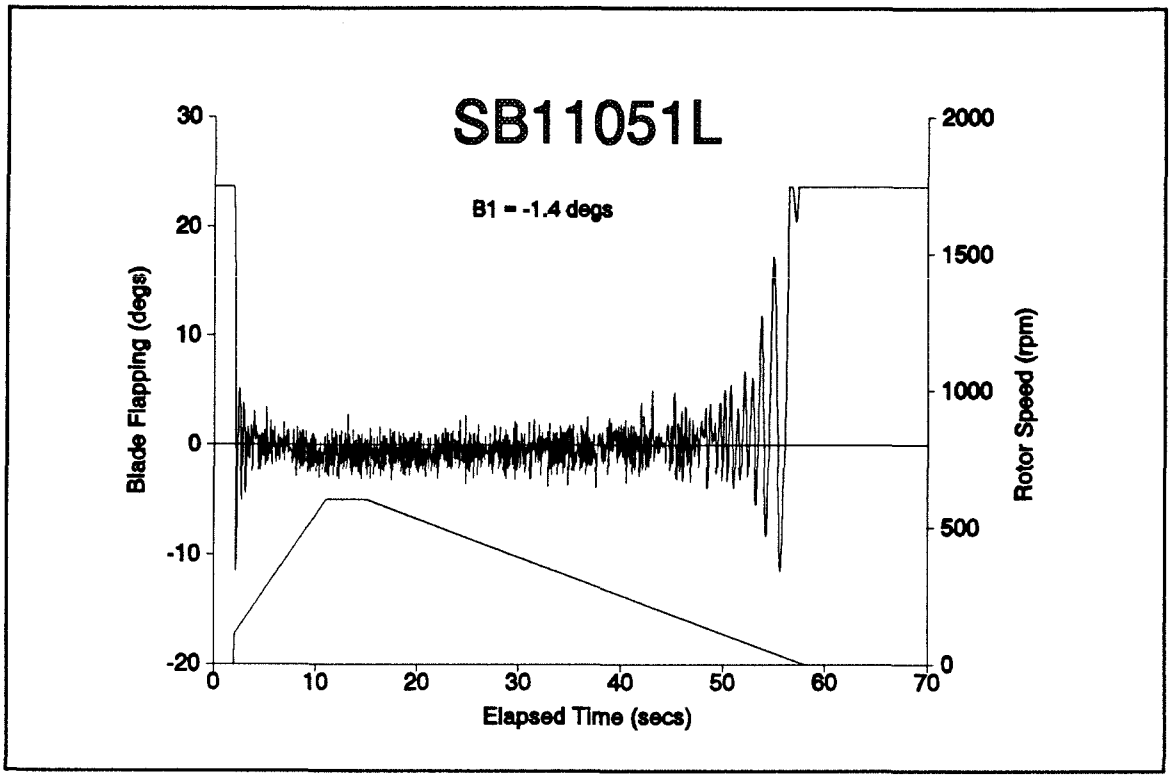

FigureIII.26.c - Theoretical Prediction. 1 Blade, Run Down, Deck Location D, B_1=-1.4°

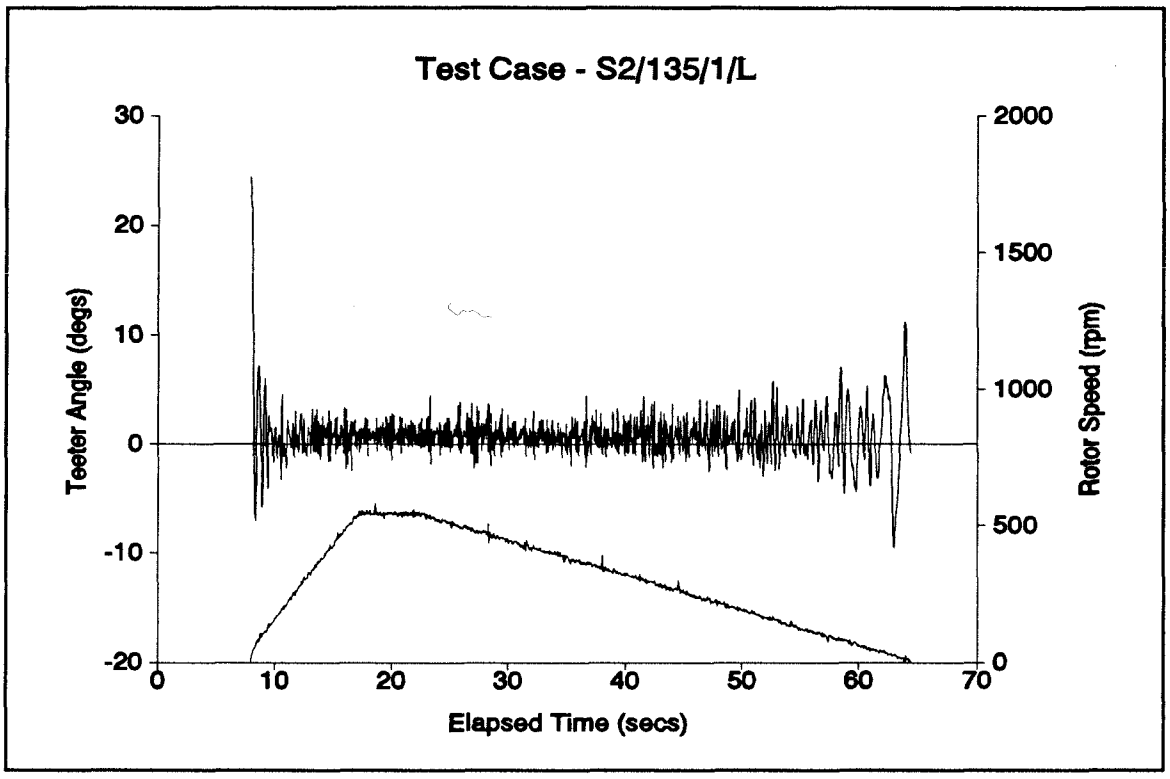

FigureIII.27.a - Wind Tunnel Tests, 1 Blade, Run Down, Deck Position E

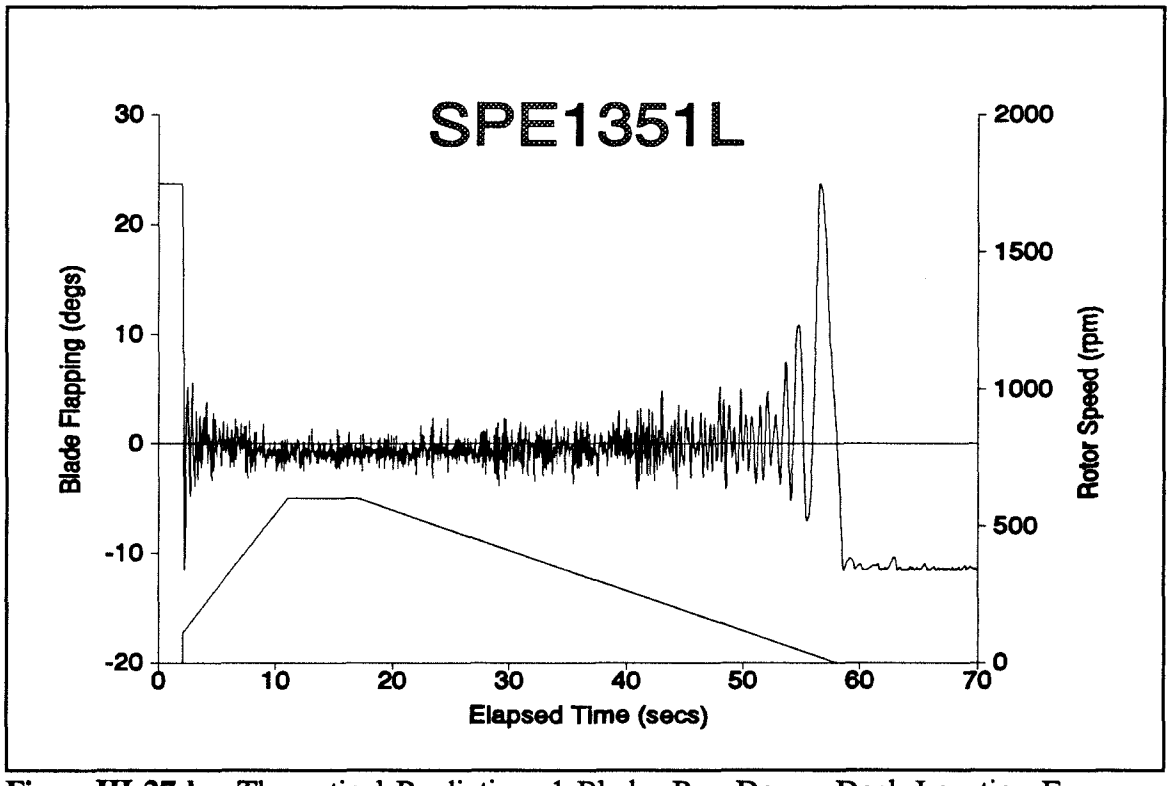

FigureIII.27.b - Theoretical Prediction, 1 Blade, Run Down, Deck Location E

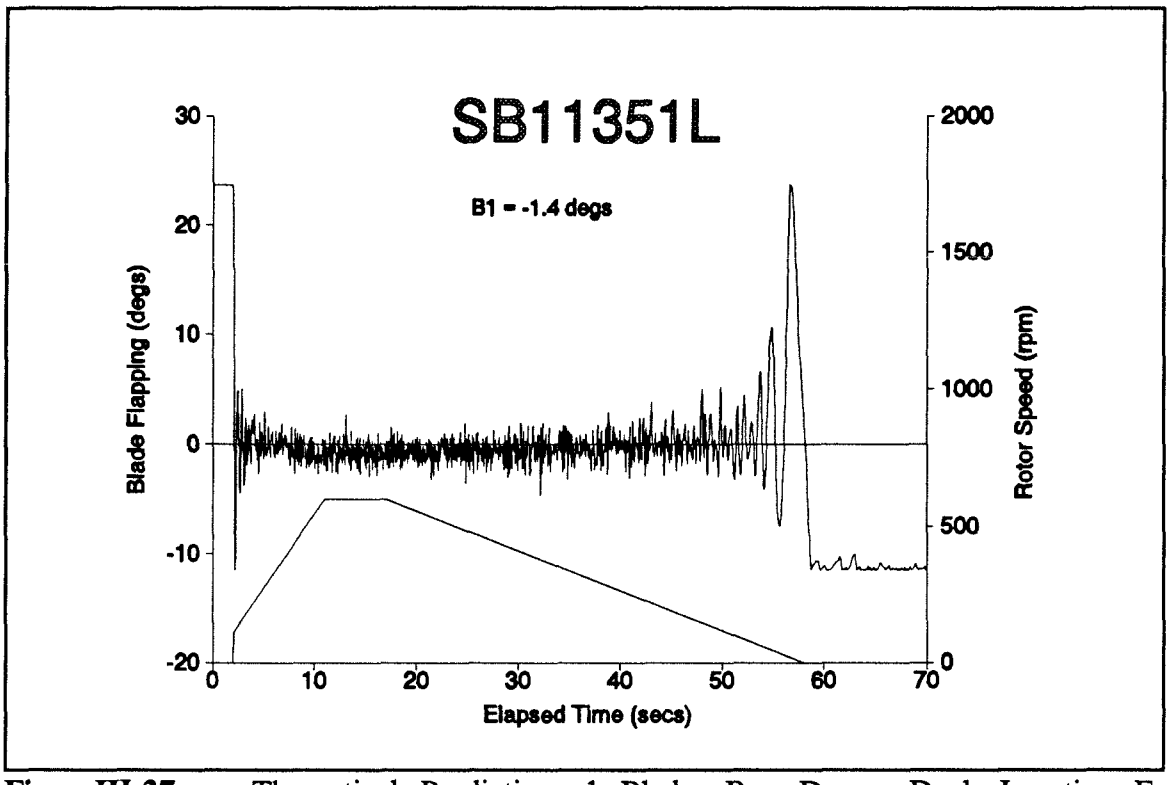

FigureIII.27.c - Theoretical Prediction. 1 Blade, Run Down, Deck Location E, B_1=-1.4°

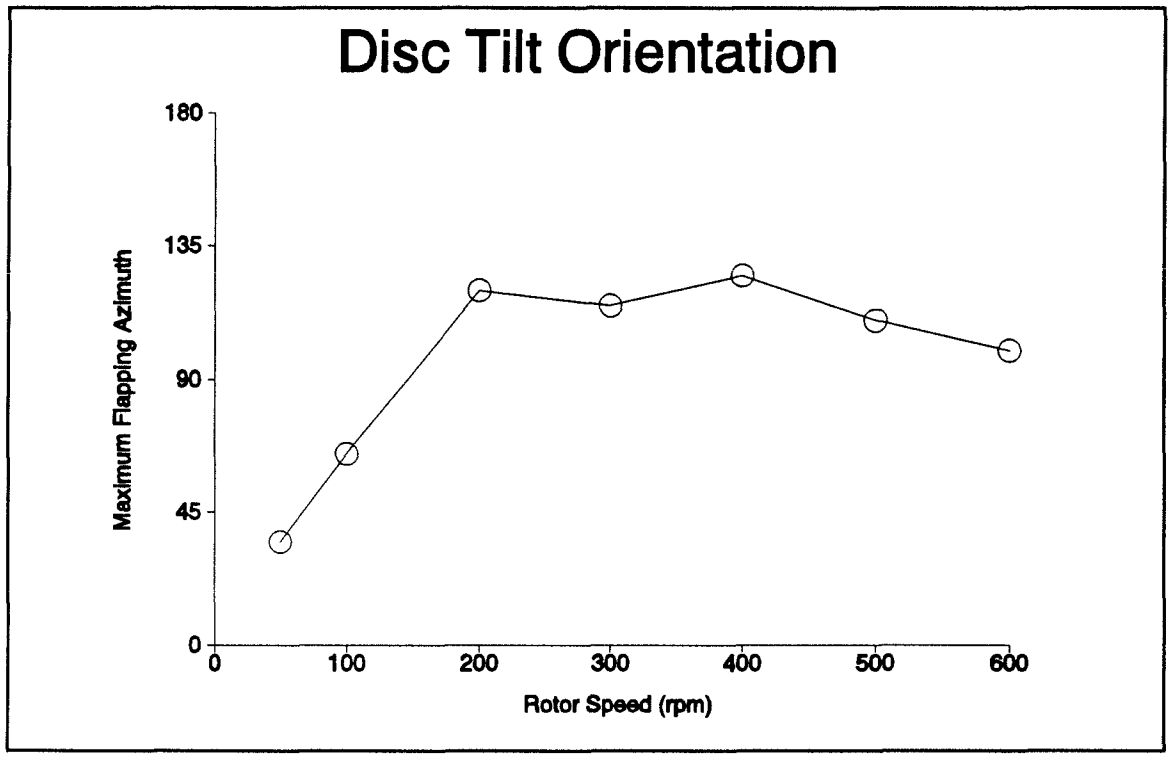

Figure III.28 - Maximum Flapping Azimuth Angle v Rotor Speed

CHAPTER 4

DEVELOPMENT OF THE BLADE MODAL METHOD

4.1 INTRODUCTION

The development of the theoretical method to model the teetering rotor blade(s) assumed that the blades were structurally rigid and any motion out of the rotation plane was pure flapping rotation. In reality the helicopter main rotor blade is flexible, particularly in the flatwise direction which is the main flapwise component. Under normal operation, the considerable centrifugal force generated by the rotation of the rotor causes considerable tension forces to be generated within the blade structure which effectively stiffens the blade. That is not to say that blade flexing does not occur since ample evidence is available that the overtone modes are of significance. The fundamental mode shape of the rotor blade is dominant and pure flapping rotation can be assumed with a high degree of confidence provided that the aircraft is operating away from the flight envelope boundaries. This is perhaps more obvious with an articulated rotor blade but even with a semi rigid rotor where the mode shape must include the flexible elements of the hub, the fundamental mode shape consists of the main elastic bending occurring on the hub elements and the rotor blade being virtually straight. In this case the concept of an effective flapping hinge can be introduced where the blade motion is effectively a rotation about a fixed, but virtual point. The blade dynamic behaviour will of course be influenced by the elastic energy transfer between the blade and the flexing rotor hub elements. This can be easily catered for by including a torsional spring at the effective hinge position. So why does the analysis of blade sailing require any further modelling? The important word in the above discussion is normal. The rotor will experience blade sailing when the rotor is operating in distinctly abnormal conditions. The rotor speed will be low which means that the tension forces within the blade are much reduced. This will allow elastic deformation of the blades to be more apparent. Also because the centrifugal force field is much smaller the blade weight must now be accounted for. Normal rotor operation will generate tip accelerations of the order of 500-750G which allows 1G to be justifiably ignored. However when rotor operation all the way from normal rotor speeds to stationary is to be analysed, the effects of gravity must be included. The variation in blade tension also brings a more fundamental dynamic problem. If the blade motion is to be expressed as a linear combination of mode shapes, because of the mathematical tractability of these concepts, then a difficulty arises in that the natural mode frequencies

and shapes will vary with the rotor speed. The modal properties are greatly influenced by the blade tension so as the rotor speed and hence tension distribution varies so the effects of these changes must be included in the analysis.

The initial work on this method was performed at Westland Helicopters Ltd and the mode details were obtained using the Dynamics Department's blade modal program J134.

4.2 EQUATIONS OF MOTION FOR A BLADE ELEMENT (FLAPWISE DEFLECTION ONLY)

The following analysis derives the equation of motion for a typical blade element when subjected to external forces normal to the plane of rotation (aerodynamic and gravity) and those along the blade length (centrifugal tension).

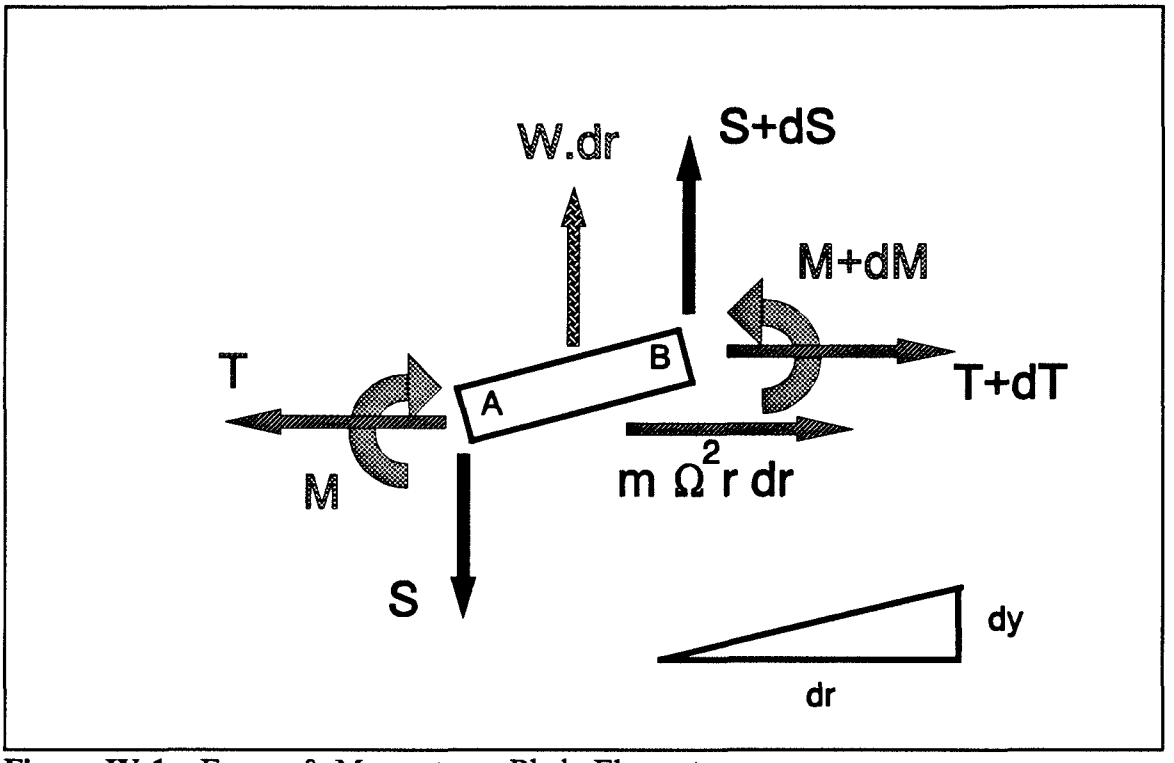

Figure IV.1 - Forces & Moments on Blade Element

With reference to Figure IV.1, the derivation of the blade aeroelastic equation is as follows:

Nomenclature:

T	tension
S	Shear force
M	bending moment
r	spanwise variable
y	flapwise deflection
m	blade mass/unit length
F	external force/unit length

Resolving vertically:

$$S+\delta S+F\delta r-S-m\delta r\ddot{y} = 0 \qquad \textbf{(IV.1)}$$

Clockwise moments about A:

$$M-(F\delta r-m\delta r\ddot{y})\frac{\delta r}{2}+(T+\delta T)\delta y-(M+\delta M)-(S+\delta S)\delta r = 0 \qquad \textbf{(IV.2)}$$

Ignoring second order terms the following is obtained after division by δr:

$$\frac{\delta S}{\delta r}+F-m\ddot{y} = 0 \qquad \textbf{(IV.3)}$$

and

$$T\frac{\delta y}{\delta r}-\frac{\delta M}{\delta r}-S = 0 \qquad \textbf{(IV.4)}$$

Proceeding to the limit (δr → 0) gives:

$$\frac{\partial S}{\partial r}+F-m\ddot{y} = 0 \qquad \textbf{(IV.5)}$$

and

$$T\frac{\partial y}{\partial r}-\frac{\partial M}{\partial r}-S = 0 \qquad \textbf{(IV.6)}$$

from the beam equation:

$$M = EI\frac{\partial^2 y}{\partial r^2} \qquad \textbf{(IV.7)}$$

whence on rearrangement:

$$\begin{aligned} EI\frac{\partial^2 y}{\partial r^2} &= M \\ \frac{\partial M}{\partial r} &= T\frac{\partial y}{\partial r} - S \\ \frac{\partial S}{\partial r} &= m\frac{\partial^2 y}{\partial t^2} - F \end{aligned} \qquad \textbf{(IV.8)}$$

these equations can be combined into one:

$$\frac{\partial^2}{\partial r^2}\left\{EI\frac{\partial^2 y}{\partial r^2}\right\} - \frac{\partial}{\partial r}\left\{T\frac{\partial y}{\partial r}\right\} + m\frac{\partial^2 y}{\partial t^2} = F \qquad \textbf{(IV.9)}$$

It was modified to permit the program to calculate the various arrays required by the method and derived as follows:

4.3 DERIVATION OF THE MODAL EQUATIONS OF MOTION

The previous section derived the basic equation of motion for a rotating beam. A particular beam will have a set of mode shapes ($g_n(r)$) and corresponding frequencies ρ_n and these are to be used as a basis for the solution of the blade sailing equations of motion. One problem to be addressed is that a set of mode shapes and frequencies is only applicable for a given tension distribution throughout the beam. This is equivalent to a specific rotor speed. Also, in order to model realistically a semi rigid rotor blade the existence of a precone angle must be reflected in the analysis. The blade dynamics is therefore governed by a set of modes, corresponding to a rotor speed of Ω_N and rotated, in flap, at the hub centre by a precone angle of β_0 see Figure IV.2. A semi rigid rotor hub will experience a steady state coning angle on the blades and in this respect is no different to an articulated rotor. However, if the rotor hub is constructed such that the flexible elements are perpendicular to the rotor shaft then the coning angle will generate a steady upward bending moment on these elements with the attendant fatigue problems. To combat this problem the elements are usually inclined and thereby remove this steady bending moment from the hub flexures. This angle is of the order of 3° and is known as *precone*. The precone angle will introduce extra centrifugal forcing terms (J_n) and the variation of the rotor speed will cause extra terms (C_{mn}) to be required to allow or the

changes in blade tension.

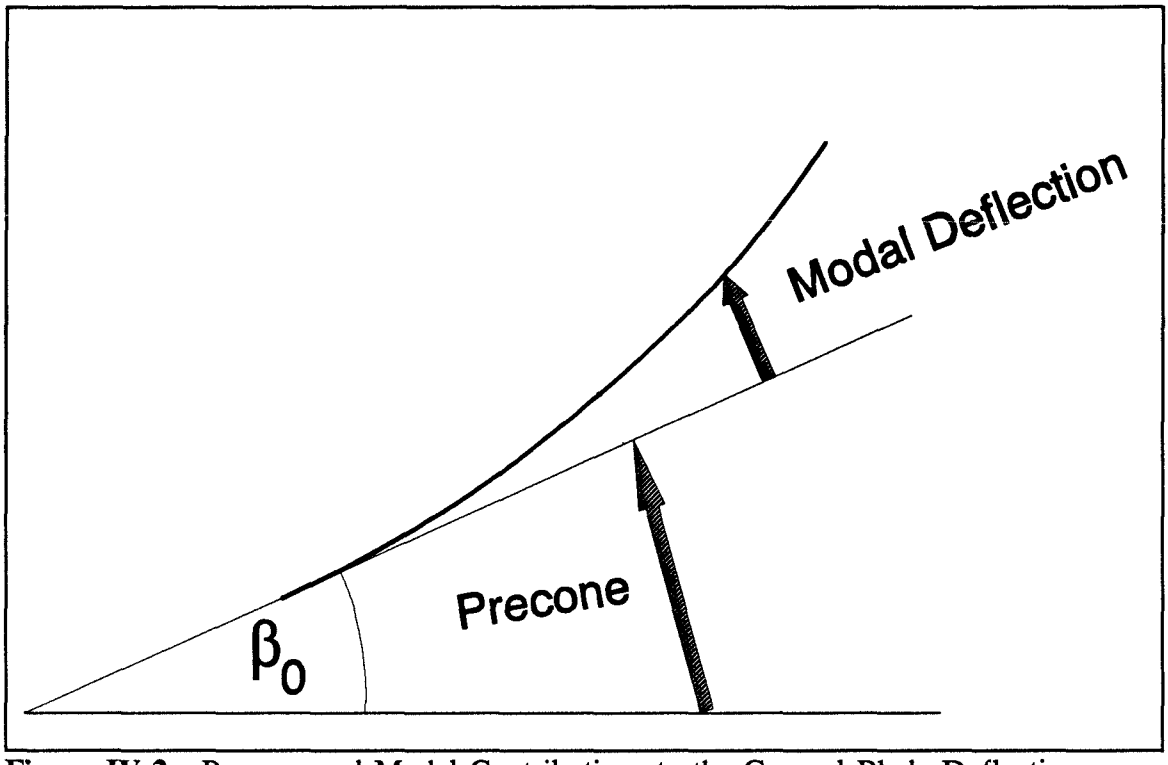

Figure IV.2 - Precone and Modal Contributions to the General Blade Deflection

For brevity the following shorthand is defined:

$$\frac{\partial}{\partial r} \equiv /$$
$$\frac{\partial}{\partial t} \equiv \cdot \qquad \textbf{(IV.10)}$$

As mentioned above, the mode shapes and frequencies are assumed to have no precone angle, i.e. as previously derived. The mode shapes and frequencies obey the usual orthogonal expressions, *(which can be proved by integration by parts)*. The basic modal equation of motion is:

$$\left\{EIg_n''\right\}'' - \left\{T_N g_n'\right\}' - m\rho_n^2 g_n = 0$$
$$T_N = \Omega_N^2 \int_r^R m\eta \, d\eta \qquad \textbf{(IV.11)}$$

The orthogonal properties are:

$$\begin{aligned} \int_0^R m g_m g_n dr &= I_n \delta_{mn} \\ \int_0^R \left[\left\{ EI g_n'' \right\}'' g_m - \left\{ T_N g_n' \right\}' g_m \right] dr &= \rho_n^2 I_n \delta_{mn} \end{aligned} \qquad \textbf{(IV.12)}$$

the mode shapes apply at $\Omega=\Omega_N$, the modal inertia is given by:

$$I_N = \int_0^R m g_n^2 dr \qquad \textbf{(IV.13)}$$

and the modal frequency is ρ_N

with a precone angle of β_0, the flapwise deflection is given by:

$$y(r,t) = \beta_0 r + \sum_m g_m(r)\, \zeta_m(t) \qquad \textbf{(IV.14)}$$

where each mode shape $g_m(r)$ has a timewise response $\zeta_m(t)$. *(For brevity, a double suffix will indicate a summation over the modes.)* The determination of $\zeta_m(t)$, $\forall m$ and t, will completely determine the blade flapping motion. The above results are now combined to form a set of second order equations of motion for the ζ_m modal responses.

(IV.14) is introduced into (IV.9) where F=L:

$$\zeta_m \left[EI g_m'' \right]'' - \left[T\left(\beta_0 + \zeta_m g_m' \right) \right]' + m \ddot{\zeta}_m g_m = L \qquad \textbf{(IV.15)}$$

which after rearrangement becomes:

$$\zeta_m \left[EI g_m'' \right]'' - \zeta_m \left[T g_m' \right]' + m \ddot{\zeta}_m g_m - \beta_0 T' = L \qquad \textbf{(IV.16)}$$

The aim is now to isolate the response of the nth mode ($\zeta_n(t)$). To do this, (IV.16) is now multiplied by g_n and integrated over the blade length:

$$\begin{aligned} &\zeta_m \int_0^R g_n \left[EI g_m'' \right]'' dr - \zeta_m \int_0^R g_n \left[T g_m' \right]' dr \\ &+ \ddot{\zeta}_m \int_0^R m g_n g_m dr - \beta_0 \int_0^R T' g_n dr = \int_0^R L g_n dr \end{aligned} \qquad \textbf{(IV.17)}$$

where the forcing term on the right hand side is L denoting the combination of the lift distribution and gravity.

Using (IV.11) the analysis gives:

$$\begin{aligned} &\zeta_m\left\{\rho_n^2 I_n \delta_{mn} - \int_0^R T_N g_m' g_n' dr\right\} \\ &-\zeta_m\left\{-\int_0^R T g_m' g_n' dr\right\} + \ddot{\zeta}_m I_n \delta_{mn} \\ &-\beta_0 \int_0^R T' g_n dr = \int_0^R L g_n dr \end{aligned} \tag{IV.18}$$

which becomes:

$$\begin{aligned} &I_n \ddot{\zeta}_m \delta_{mn} + I_n \rho_n^2 \zeta_m \delta_{mn} \\ &+\zeta_m \int_0^R (T - T_N) g_m' g_n' dr - \beta_0 \int_0^R T' g_n dr = \int_0^R L g_n dr \end{aligned} \tag{IV.19}$$

the tension terms obey the following:

$$\begin{aligned} T &= \Omega^2 \int_r^R m\eta\, d\eta \\ T_N &= \Omega_N^2 \int_r^R m\eta\, d\eta \\ T' &= -\Omega^2 m r \end{aligned} \tag{IV.20}$$

Defining the nth modal forcing F_n by:

$$F_n = \int_0^R L g_n dr \tag{IV.21}$$

the equation of motion becomes:

$$\begin{aligned} &I_n \ddot{\zeta}_m \delta_{mn} + I_n \rho_n^2 \zeta_m \delta_{mn} \\ &+\zeta_m \left(\Omega^2 - \Omega_N^2\right) \int_0^R \left\{g_m' g_n' \int_r^R m\eta\, d\eta\right\} dr \\ &+\beta_0 \Omega^2 \int_0^R m r g_n dr = F_n \end{aligned} \tag{IV.22}$$

now defining:

$$\begin{aligned} C_{mn} &= \int_0^R \left\{g_m' g_n' \int_r^R m\eta\, d\eta\right\} dr \\ J_n &= \int_0^R m r g_n dr \end{aligned} \tag{IV.23}$$

the final equation of motion is:

$$\begin{aligned} & I_n \ddot{\zeta}_m \delta_{mn} + I_n \rho_n^2 \zeta_m \delta_{mn} \\ & + \zeta_m \left(\Omega^2 - \Omega_N^2\right) C_{mn} \\ & + \beta_0 \Omega^2 J_n = F_n \end{aligned} \tag{IV.24}$$

To integrate the equations by a numerical method such as the Runge Kutta procedure, the second derivative of ζ_m is isolated thus:

$$\ddot{\zeta}_m = \frac{F_n - \beta_0 \Omega^2 J_n}{I_n} - \zeta_m \left[\rho_n^2 \delta_{mn} - \Omega_N^2 \frac{C_{mn}}{I_n} + \Omega^2 \frac{C_{mn}}{I_n} \right] \tag{IV.25}$$

Now:

$$\begin{aligned} F_n &= \int_0^R L_A g_n dr - G \int_0^R m g_n dr \\ &= \int_0^R L_A g_n dr - G H_n \\ H_n &= \int_0^R m g_n dr \end{aligned} \tag{IV.26}$$

where L_A is the aerodynamic lift distribution and G is the gravitational acceleration. this gives:

$$\begin{aligned} \ddot{\zeta}_n = & -\frac{G H_n}{I_n} - \beta_0 \frac{J_n}{I_n} \Omega^2 + \int_0^R \frac{L_A g_n}{I_n} dr \\ & - \zeta_m \left[\rho_n^2 \delta_{mn} - \Omega_N^2 \frac{C_{mn}}{I_n} + \Omega^2 \frac{C_{mn}}{I_n} \right] \end{aligned} \tag{IV.27}$$

with the following definitions:

$$\begin{aligned} \left[K_2 K_{0C}\right]_{ij} &= \rho_i^2 \delta_{ij} - \Omega_N^2 \frac{C_{ij}}{I_i} \\ \left[K_2 K_{0D}\right]_{ij} &= \frac{C_{ij}}{I_i} \\ \left[L_C\right]_i &= -G H_i \\ \left[L_D\right]_i &= \beta_0 J_i \end{aligned} \tag{IV.28}$$

the final equation to be solved becomes:

$$\ddot{\zeta}_n = \frac{[L_C]_n - [L_D]_n \Omega^2}{I_n} + \frac{\int_0^R L_A g_n dr}{I_n} - \sum_m \zeta_m \left\{ [K_2 K_{0C}]_{nm} + \Omega^2 [K_2 K_{0D}]_{nm} \right\} \qquad \text{(IV.29)}$$

the C_{mn} terms occur because the modes are appropriate to a particular rotor speed (Ω_N) but the analysis is required at a general rotor speed (Ω). These terms vanish at $\Omega=\Omega_N$, the rotor speed at which the modes apply because of the (Ω^2 - Ω_N^2) multiplier.

(As a point to note, the matrices are given names which are purely historical in the evolution of the method and correspond to the array names used in the computer program.)

The computer program allows the blade mass distribution and mode shapes only, to be specified and calculate the arrays directly. However, the Westland modal Program, J134, evaluates the various integrations with a radial increment of ¼ of an inch, which for the Lynx rotor blade corresponds to approximately 1000 incremental steps. To repeat this in the program directly would require a massive input specification and so as much use of this provision was made.

Semi rigid rotors have the distinct advantage in that the rotor hub element structural stiffnesses allow the blades to hang freely under gravity when the rotor is stationary but clear of the fuselage. The articulated rotor does not have this property and so restraint mechanisms have to be included in the hub design to keep the blades from falling to the ground. These droop stops are augmented by antiflap stops which prevent articulated blade motion in an upward direction. Again the semi rigid rotor flexible elements provide the necessary restraint for that problem. These stops are only of use for low speed rotor operation and hence retract as the rotor speed increases to the normal values. There is a distinct possibility of the blade cuffs contacting the stops during the rotor engagement or disengagement which will depend on the physical location of the stops. Because this will change the application of the loads on the blade cuff, the analysis will be further complicated. During rotor acceleration or deceleration the possibility exists for a stop to be retracted whilst the blade cuff is in contact with it. In such cases the stop is mechanically prevented from moving and must remain in position until the blade cuff

clears the stop sufficiently it can retract or extend as appropriate. This factor will cause a change in the boundary conditions applied to the blade. The method of its application will be discussed later in the Chapter.

The initial boundary conditions have now to be determined.

Their derivation is detailed below and entirely different approaches are used for rotor engagement and disengagement. For the former the stationary rotor blade position can be determined by setting the rotor speed and time derivatives of the modes to zero. This produces a straightforward matrix equation to solve.

4.4 CALCULATION OF INITIAL CONDITIONS

Rotor Run Up

The modal equation of motion is given by:

$$\begin{aligned} & I_n \ddot{\zeta}_m \delta_{mn} + I_n \rho_n^2 \zeta_m \delta_{mn} \\ & + \zeta_m \left(\Omega^2 - \Omega_N^2\right) C_{nm} \\ & + \beta_0 \Omega^2 J_n = F_n \end{aligned} \tag{IV.30}$$

where summing over m is implied.

with:

$$\begin{aligned} F_n &= \int_0^R (L_A - mG) g_n dr \\ &= \int_0^R L_A g_n dr - G H_n \\ H_n &= \int_0^R m g_n dr \end{aligned} \tag{IV.31}$$

with the rotor stopped, $\Omega=0$, implying $L_A=0$, and all time derivatives vanish. Under these initial conditions, equations (IV.30) reduce to:

$$\rho_n^2 I_n \zeta_n - \Omega_N^2 C_{nm} \zeta_m = -G H_n \tag{IV.32}$$

which can be re-expressed by:

$$\left\{\rho_n^2 I_n \delta_{mn} - \Omega_N^2 C_{nm}\right\} \zeta_m = -G H_n \tag{IV.33}$$

which is physically the static deflection under gravity.

this is a set of n equations which give the starting values for the modal responses ζ_n.

Rotor Run Down

To provide a realistic situation from which the rotor can commence its deceleration, a completely different approach to calculating the initial state is adopted.

In general, ζ_n will not be constant and so a pseudo-start position is used where $\forall n$:

$$\zeta_n = \dot{\zeta}_n = 0 \qquad \textbf{(IV.34)}$$

A stationary rotor blade hanging under gravity is a reasonable starting condition for a rotor engagement but is inappropriate for a rotor disengagement. The turning rotor blade will be experiencing a rapidly changing aerodynamic environment. consequently, to predict the actual blade position and velocity is a very difficult task. The method uses a settling period at the beginning of the calculation whereby the rotor blade is initially at zero deflection and velocity. This corresponds to the value and first timewise derivative of the modal deflections being set to zero. The rotor is now given a specified period to settle into a realistic blade motion, t_{pause}. A period of 1 second has so far been more than sufficient. After this period the initial conditions are established and the rotor deceleration can now commence.

Since the semi rigid rotor blade does not rely on hub restraints to hold it in position as does an articulated rotor, the tip droop for the hingeless rotor blade can be reasonably accurately reproduced. The yardstick for the comparison is the results of running the modal program of Westland Helicopters Ltd. for a stationary rotor. This highlights a major concern of the development of the method. That is, can a set of modes shapes at one rotor speed be used successfully to predict a blade deflection at another rotor speed? This can be mathematically assured if an infinite number of modes are used. However, can a finite number (4 say) be used with success? With a semi rigid rotor the blade will always be built in at the root and be a *fixed-free* dynamical system. With an articulated rotor at low rotor speed the blade will be moving on and off a stop and changing from a *pinned-free* to a *fixed-free* system. Therefore this changing of the blade characteristics must be handled by the method. Two avenues were identified:

(i) To use two sets of modes, one *fixed-free* the other *pinned-free* and switch between them as appropriate.

(ii) To use *pinned-free* modes throughout and model the droop and antiflap stops as high rate linear springs, applied when blade/stop contact occurs.

Whilst (i) has attractions, because a limited number of modes are in use the method of switching between the modes would cause parts of the blade position/velocity to be discontinuous. Because of this, option (ii) was considered safer and therefore this technique was adopted. There will be a difficulty of determining the initial blade position since a set of *pinned-free* modes with the addition of a point spring load has to model a *fixed-free* system hanging under gravity. The tip droop was again used as a basis for checking and whilst not all cases were able to produce precisely the correct values, those obtained were within 5% of overall values in the region of 30 inches.

The existence of the droop and antiflap stops now requires that when a contact is made an appropriate load is applied to the blade. This will be a point load and since the other blade loadings are distributed the spring load is expressed using the Dirac Delta Function. The blade position at the stop radial location is determined and knowing the stop contact positions the contact situation can be assessed. The mathematical expressions used for the load application is described below:

4.5 INCLUSION OF DROOP AND ANTI-FLAP STOPS

In the case of an articulated rotor the hub restraint mechanisms (namely the droop stop and anti-flap assembly) must be included. They are catered for by modelling as linear springs with a high spring rate as shown in Figure IV.3.

The springs will affect the equations only if contact is made between the blade cuff and either of the stops. Contact is dependent on rotor speed since the stop position changes at given rotor speeds and this will affect the possible blade/stop contact location. The restraints are extended at low rotor speed to control the blade cuff movement but retract as the rotor speed increases to become so called flight stops. It is still possible for the blade cuff to contact the droop stop in flight should a sufficiently severe manoeuvre be flown giving rise to the so called *droop stop pounding*.

For brevity, the effect of the droop stop is now explained and the anti flap stop analysis follows a similar course.

The right hand side of the model equation of motion is:

$$\int_0^R L g_n dr \qquad \textbf{(IV.35)}$$

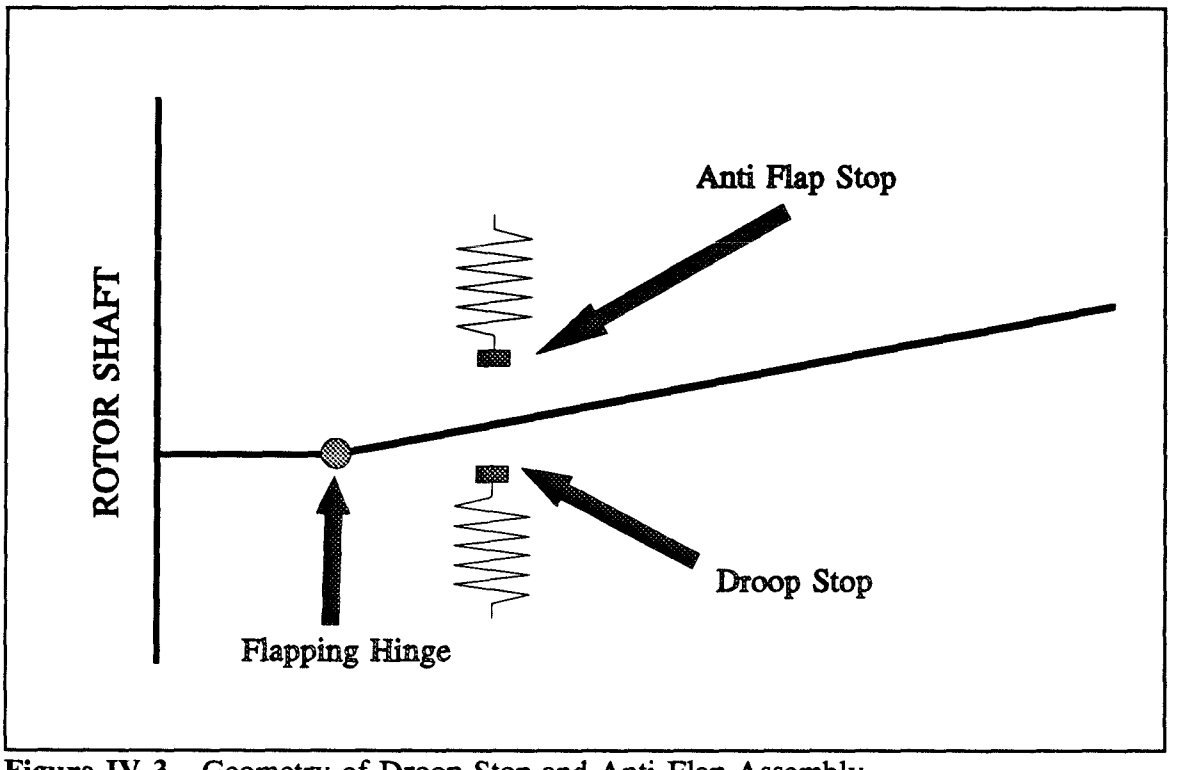

Figure IV.3 - Geometry of Droop Stop and Anti Flap Assembly

where L is the vertical force per unit length and g_n the nth mode shape.

Now:

$$L = L_A - mG + \delta(r - r_d)H(h_d - h)L_d \qquad \text{(IV.36)}$$

where

- δ is the Dirac Delta Function
- H is the Heaviside Step Function
- r_d is the radial position of the droop stop
- h_d is the vertical height of the droop stop above the hub plane
- L_d is the droop stop load

In equation (IV.36) the $\delta(r-r_d)$ term indicates a point load application. The Dirac Delta Function is used to apply a point load when a distributed load is under analysis. The $H(h_d-h)$ term only allows the load to be generated when spring contact is made by the blade cuff at the radial position r_d.

If k_d is the spring rate, then the extra term to be applied to the right hand side of the modal equation (IV.35) is:

$$\int_0^R g_n(r)\,\delta(r-r_d)H(h_d-h)k_d(h_d-h)dr = g_n(r_d)k_d(h_d-h)H(h_d-h) \quad \textbf{(IV.37)}$$

where:

$$h = \zeta_m g_m(r_d) \quad \textbf{(IV.38)}$$

(Note that the precone angle β_0 is inappropriate for an articulated rotor.)

For the initial state, which applies only to the rotor run up case, we must have the Heaviside function is unity, since the blade cuff will be resting on the droop stop under the influence of gravity. Also, there is normally a small amount of vertical play for the blade cuff between the droop stop and anti flap stop and in consequence, contact is only made with the droop stop for the initial condition. Therefore the initial state equations become:

$$\left\{\rho_m^2 I_m \delta_{mn} - \Omega_N^2 C_{nm}\right\}\zeta_m = -GH_n + \int_0^R g_n L_{DROOP} \quad \textbf{(IV.39)}$$

where:

$$L_{DROOP} = \delta(r-r_d)k_d\{h_d - \zeta_m g_m(r_d)\} \quad \textbf{(IV.40)}$$

whence:

$$\left\{\rho_m^2 I_m \delta_{mn} + k_d g_m(r_d)g_n(r_d) - \Omega_N^2 C_{nm}\right\}\zeta_m = -GH_n + k_d h_d g_n(r_d) \quad \textbf{(IV.41)}$$

which is solved as before.

The anti flap assembly loads are applied as for the droop stop when the transient motion is being calculated and the vertical position of the blade cuff is sufficient to cause contact. The load will be in the negative sense.

The method uses high rate springs to model the effect of the stops. However, as will be discussed in Chapter 6, provided a sufficiently large value is taken the actual value is not important. To allow a sensible blade position at the commencement of a rotor engagement

the method uses an iterative scheme to fix a value on the spring rate to give a realistic blade tip deflection.

The initial rotor stopped position is given by (IV.41). For a given value of k_d the above equations can be solved to give ζ_n. The tip deflection will then be given by:

$$\zeta_m g_m(R) \tag{IV.42}$$

If the required tip deflection is S_T (positive upwards) then the droop stop spring rate is adjusted via:

$$\Delta k_d = K\{S_T - \zeta_m g_m(R)\} \tag{IV.43}$$

where K is a tuning constant. As already discussed, the modes will be referenced to a particular rotor speed. For the initial condition before run up unless the modes are chosen for zero rotor speed there may be difficulty in obtaining an exact tip deflection. In cases run during the method's development, such errors were small, of the order of 1 or 2 inches.

One final comment is necessary concerning the extension or retraction of the droop and anti-flap stops. This can be accomplished at the respective rotor speeds only if there is no contact and adequate mechanical clearance for this to occur. Should this not be the case then the method must hold the respective stop in position until the clearance is achieved and the stop can then be moved. Such a situation is termed a *jammed stop*. (The time step is held constant throughout the calculation.)

The contact with a stop causes another but more subtle requirement. With an articulated rotor blade under free flapping motion the possibility of pitch flap coupling (δ_3) is present. Even though this is minimised by the geometry of the pitch control linkage arrangement some torsional motion is possible. The modal details also contain the torsional deflections of each mode and so this effect can be used in the calculation. As the blade cuff contacts the stop, the linkages will lock in place and the blade deflection is one of pure elastic bending which will have a different torsional behaviour. In most cases, with the placement of the flexural axis on the pitch axis, this will be virtually zero and so the application of torsional deflections will have to take due note of the blade/stop contact situation.

Having determined the blade motion at each time step, it is now possible to formulate a

method to calculate the instantaneous blade spanwise bending moment distribution. The modal program J134 gives the bending moment distribution for each mode, for a unit tip deflection. However, these modes and, more importantly, the bending moment distribution are heavily dependent on rotor speed. For this reason, the bending moments must be determined at each time step, the method being as follows:

4.6 BENDING MOMENT CALCULATION

The equations of motion of the blade are:

$$\begin{aligned} \frac{\partial S}{\partial r} &= -L_A + m\ddot{y} + mG \\ \frac{\partial M}{\partial r} &= T\frac{\partial y}{\partial r} - S \end{aligned} \qquad \textbf{(IV.44)}$$

since:

$$y = \beta_0 r + g_m(r)\,\zeta_m(t) \qquad \textbf{(IV.45)}$$

the following results are obtained:

$$\begin{aligned} \ddot{y} &= g_m \ddot{\zeta}_m \\ \frac{\partial y}{\partial r} &= \beta_0 + g_m' \zeta_m \end{aligned} \qquad \textbf{(IV.46)}$$

the tension is specified using:

$$T = \Omega^2 \int_r^R m\eta\, d\eta \qquad \textbf{(IV.47)}$$

In the Runge Kutta routine, used in the computer program, the aerodynamic lift force, L_A, is calculated.

The Runge Kutta solution method requires the equation of motion in the form:

$$\ddot{\zeta}_i = G\left(t, \zeta_i, \dot{\zeta}_i\right) \tag{IV.48}$$

with a time increment of δt[##], and considering the motion at time t, the following term is calculated:

$$\left[m_0\right]_i = \delta t \cdot G\left(t, \zeta, \dot{\zeta}\right) \tag{IV.49}$$

from which:

$$\ddot{\zeta}_i = \frac{\left[m_0\right]_i}{\delta t} \tag{IV.50}$$

whence we find:

$$\left.\frac{\partial S}{\partial r}\right)_r = -L_A)_r + \left\{\frac{1}{\delta t}\left[m_0\right]_m g_m + G\right\} m)_r \tag{IV.51}$$

this must be integrated with respect to r from the blade tip giving:

$$\begin{aligned} S(R) - S(r) &= \int_r^R \frac{\partial S}{\partial r} dr \\ S(R) &= 0 \\ S(r) &= -\int_r^R \frac{\partial S}{\partial r} dr \\ &= \int_0^r \frac{\partial S}{\partial r} dr - \int_0^R \frac{\partial S}{\partial r} dr \end{aligned} \tag{IV.52}$$

this shear force distribution is substituted into the moment equation which gives:

$$\frac{\partial M(r)}{\partial r} = T(r)\left\{g'_m(r)\,\zeta_m(t) + \beta_0\right\} - S(r) \tag{IV.53}$$

The choice of time step was made early in the development of the computer program by repeatedly running the calculation method with successively smaller steps until a satisfactory repeating of the blade tip behaviour was achieved. A typical value is 0.001 sec. The computer output was arranged so that only every 4th or 5th time step was recorded. The plots presented in this thesis will have typically 4 - 5 time steps between each data point. ##

$$M(r) = -\int_r^R \frac{\partial M}{\partial r} dr = \int_0^r \frac{\partial M}{\partial r} dr - \int_0^R \frac{\partial M}{\partial r} dr \qquad \text{(IV.54)}$$

CHAPTER 5

APPLICATION OF THE BLADE MODAL METHOD TO A SEMI RIGID ROTOR

5.1 INTRODUCTION

The blade sailing modal method developed in Chapter 4 is now applied to the semi-rigid main rotor of the Westland Lynx aircraft. Four flapwise modes were used to describe the blade deflection, the shapes and frequencies are shown in Figure V.1 and are referenced to a rotor speed of 34.1667 rads/sec. The rotor speed variations for run up and run down are presented in Figures V.2 and V.3. The run up rise time is 10, or 20 seconds for Figure V.21, whilst for the run down a 1 second pause is used, followed by a freewheel time of 17 seconds to a rotor speed of 47%NR and finishing with a braking time of 8 seconds. The initial test runs of the computer program were devoted to the results of the 3 axis hot wire anemometer survey of the flight deck of the Rover Class RFA model described in Chapter 1. The locations of the 13 measurement points are described in Appendix D. Before examining the predictions of the blade flapping behaviour, a brief analysis of the hot wire results is undertaken. For all cases, a collective pitch angle of 4° was assumed commensurate with the sub-minimum pitch setting of the Naval Lynx helicopter.

5.2 WIND TUNNEL DATA FOR WIND VELOCITY

As already discussed, the vertical velocity component seems to be the dominating theme and so Figure V.4 presents the vertical velocity variation for the 3 yaw angles (90°,135°,180°) normalised on the wind tunnel speed of 20 m/s. As can be seen, for the 90° and 135° yaw conditions the upflow on the starboard side is fairly well matched by a downflow on the port side, whilst at 180° yaw the upflow is virtually constant. The 90° yaw case has the greatest variation and this is the first evidence of this being the worst condition of those tested. Figure V.5 shows the total wind speed variation, again relative to the wind tunnel free stream speed. The dominance of the 90° yaw condition is reinforced. Figure V.6 shows the inclination angle of the incident flow vector, in the vertical plane and the results of Figure V.4 are repeated. The final Figure (V.7) plots the RMS turbulence variation. The peak turbulence is found in the 180° azimuth position, particularly for the 135° and 180° yaw angles. This is the effect of the ship superstructure, albeit downstream of the flight deck. For the 90° yaw condition the turbulence is uniformly high, peaking towards the leeward deck edge with the relatively sudden downward facing step of the port ship's hull. The previous discussion highlights

the potential severity of the 90° yaw condition when compared to 135° and 180°. For this reason all future work concentrated on the 90° yaw orientation of the wind to the ship. The 16 test cases considered are presented in Table V.1:

Table V.1 - Summary of Blade Sailing Predictions for the Westland Lynx

Figure No.	Rotor Operation	Gust Type	Blade Torsion	Run Up Time	Ship Roll Angle	Maximum Tip Deflection
7	UP	Wind Tunnel 180°	NO	10	0	28.8
8	DOWN	Wind Tunnel 180°	NO		0	27.7
9	UP	Wind Tunnel 135°	NO	10	0	32.4
10	DOWN	Wind Tunnel 135°	NO		0	31.4
11	UP	Wind Tunnel 90°	NO	10	0	64.9
12	DOWN	Wind Tunnel 90°	NO		0	55.9
13	UP	Simple	NO	10	0	40.5
14	DOWN	Simple	NO		0	50.8
15	UP	Linear	NO	10	0	31.7
16	DOWN	Linear	NO		0	31.8
17	UP	Linear	YES	10	0	41.6
18	DOWN	Linear	YES		0	41.6
19	UP	Linear	NO	20	0	33.4
20	UP	Linear	NO	10	7.5°	37.9
21	DOWN	Linear	NO		7.5°	43.1
22	DOWN	Linear	NO		-7.5°	41.2

The 180° cases with a rotor run up or run down are shown in Figures V.8,9, the 135° cases in Figures V.10,11 and the 90° cases in Figures V.12,13. The 180° case shows a very mild situation of a transfer from the 25 inch static tip deflection to the virtually zero flap deflection of normal operating rotor speed. The hub flexures keep the blade behaviour under tight control with a peak to peak amplitude of about 10 inches at full rotor speed to double that value as the rotor comes to rest. The 135° yaw condition produces an increased flapping deflection with the beginnings of isolated large flapping movements at low rotor speed. The 90° yaw condition shows a further increase in flapping behaviour with one instance of a large blade deflection. This must be a result of the random number generator used for the wind speed recreation producing an extreme event which for the 90° yaw case is more predictable in view of the increased turbulence for this situation. This occurrence is typical of comments made by pilots where excessive blade deflections can rapidly and unexpectedly build up. The blade tip deflection extrema are summarised in Figure V.14. The table lists the extreme downward tip deflection occurring in each case and it should be noted that a downward tip deflection of 75 inches is required for a blade to contact the aircraft tail boom. The 90° yaw case shows that 65 inches is obtained putting the blade tip uncomfortably close to the tail drive shaft cover.

Simple and Linear Gust Cases

Having observed the influence of ship yaw angle on the blade sailing behaviour, the dominance of the 90° yaw case has been highlighted. This situation has been used as a model for an investigation into the effect of various operational and theoretical influences. The 90° case can be likened to a horizontal flow (50 knots) over the ship's deck with an upflow and downflow ($\pm$15 knots) being superimposed on the windward and leeward rotor disc halves. The exact values are a 30% upgust on the windward side, a 24% downgust on the leeward side and a 19% horizontal supervelocity over the deck. Figures V.15,16 show what is termed a simple gust where the vertical wind components are applied uniformly over the entire half of the rotor disc. This will give a discontinuous change of the wind vertical velocity along the helicopter's centre line and is used only for comparison purposes since it is an extreme situation. Fairly severe motions are obtained. A more conceptually realistic situation is achieved, as described in chapter 3, whereby the vertical wind velocity varies linearly across the lateral rotor direction with value zero at the aircraft centre line. Figures V.17,18 show this situation and the

reduction in blade movement is shown. All the cases so far have not included any torsional motion of the blade.

Effect of Torsional Contribution to Modes

The previous 2 cases are repeated in Figures V.19,20 whereby the blade torsional motion in each flap mode is included. The increase in blade tip deflection is apparent and is of the order of a 30% increase over the results of Figures V.17,18.

Effect of Rise Time

The rotor run up is governed by the rise time and Figure V.21 shows the run up case of Figure V.17 only the rise time has been doubled to 20 seconds. An increase of 10% in the tip deflection is observed.

Effect of Ship Roll Motion

As can be appreciated, placing a helicopter on board a ship will require the helicopter rotor to endure any effects of ship motion. To observe any effects of ship motion, a 7½° ship roll behaviour is modelled. The roll oscillation, which is positive to port, has a time period of 10 seconds and the motion was centred at a point 30 feet below the ship's deck level. These values are considered typical for the Rover Class Royal Fleet Auxiliary type of vessel. The gyroscopic influence on the blade dynamics is ignored since the rotor speed is for most of the time much above the ship roll angular velocity. The ship's roll motion is modelled by the wind components being rotated about the aircraft's centre line at the appropriate angle with the horizontal component adjusted by the tangential flow velocity parallel to the deck surface caused by the rotation of the ship about the roll centre. Figures V.22,23 show such a situation with a blade tip deflection increase of about 12½%. Figure V.24 shows the equivalent run down with the phasing of the ship's roll motion being reversed, altering the phasing between the run down initiation and the ship's roll direction. Apart from the obvious reversal in the basic blade motion, only a marginal change in maximum tip deflection is observed.

The blade modal method was applied to the semi-rigid rotor of the Westland Lynx helicopter. The first calculation were made using data which was obtained by a hot wire anemometry survey of the flow over the flight deck of a Rover Class Royal Fleet Auxiliary vessel. The difficulty of the cone of acceptance of these probes meant that wind directions from the bow quarter were not sufficiently trustworthy. Therefore the flow data

from the rear quarter of the ship were used. The importance of wind direction was illustrated and since the abeam wind gave the greatest predictions for blade flapping excursions all of the further work was standardised on this condition.

The semi-rigid blade has advantages over the more common articulated rotor in that droop and anti flap stop restrainers are not required and the blade remains a cantilever at all times. Additionally, because an articulated rotor does not have the structural flapping stiffness of a semi-rigid hub it will have greater potential for large flapping excursions since the only flapping stiffness comes from the centrifugal forces induced by rotor speed. These problems are addressed in Chapter 6.

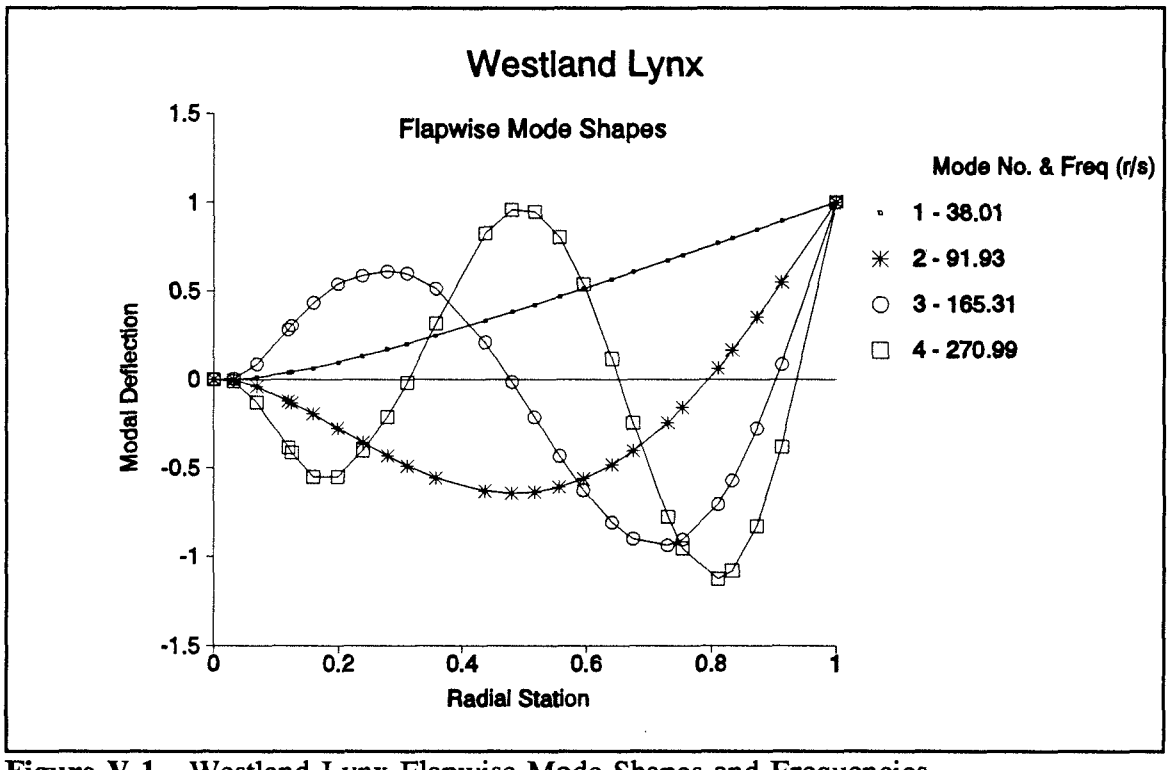

Figure V.1 - Westland Lynx Flapwise Mode Shapes and Frequencies

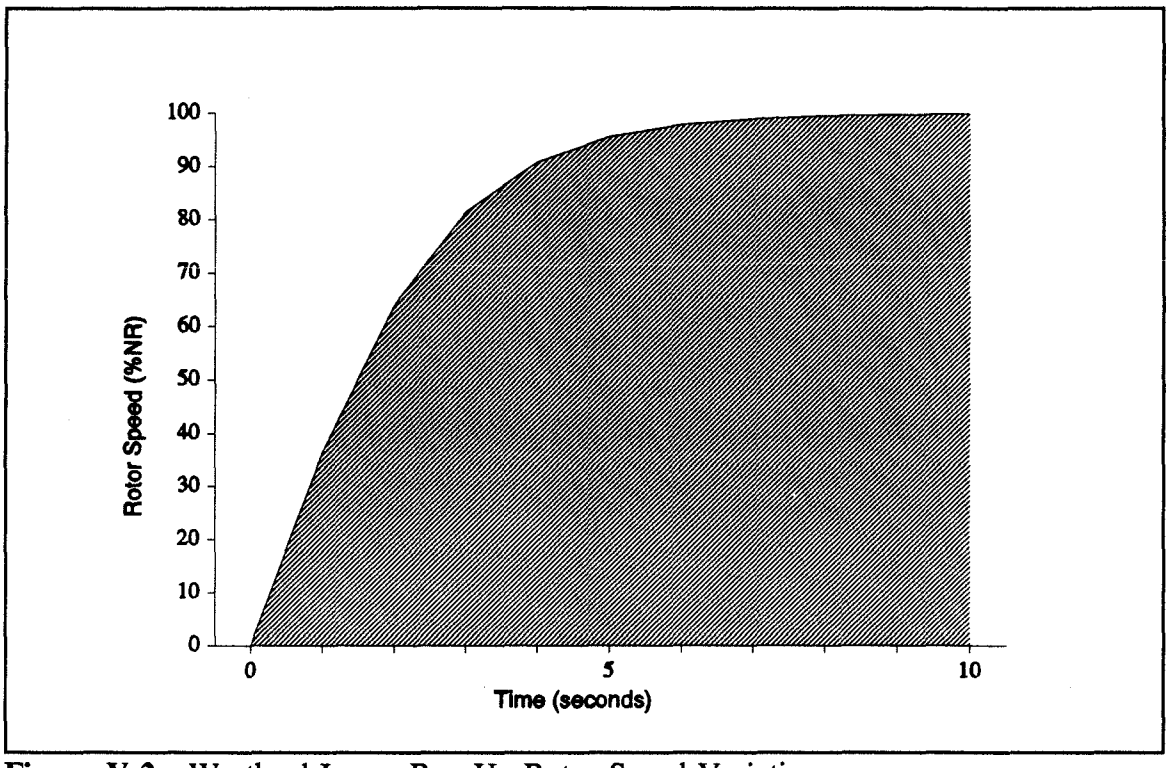

Figure V.2 - Westland Lynx, Run Up Rotor Speed Variation

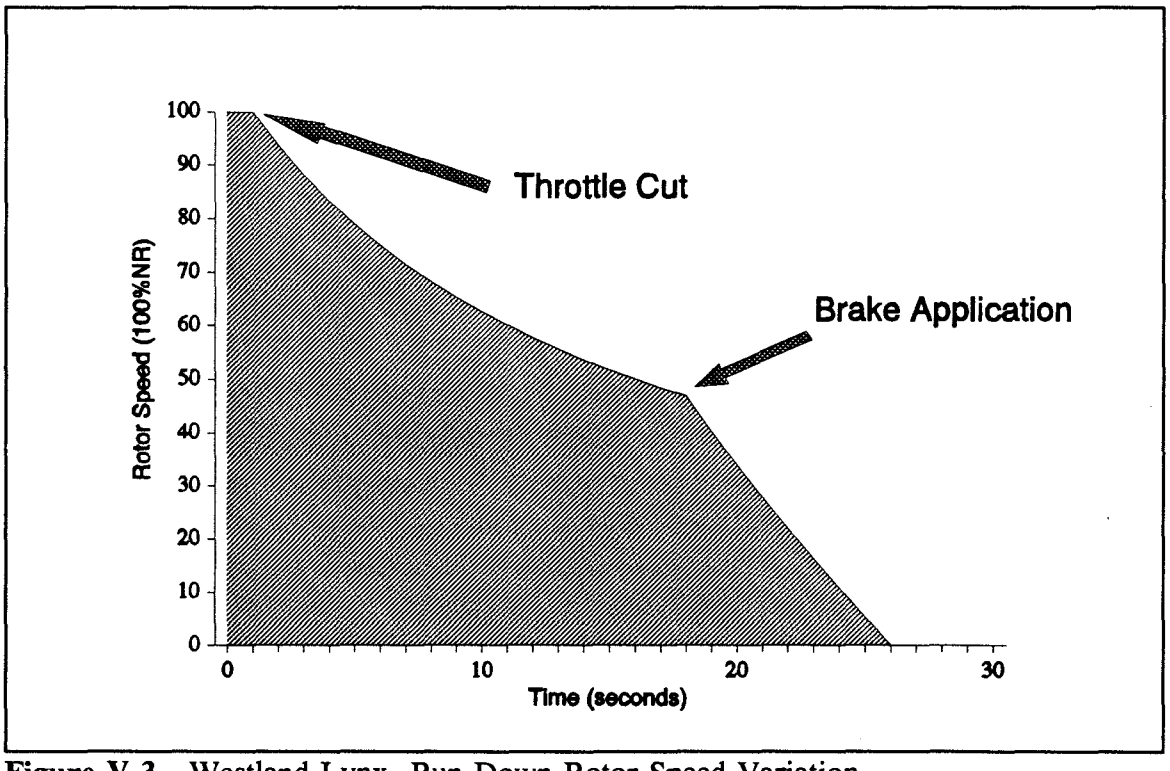

Figure V.3 - Westland Lynx, Run Down Rotor Speed Variation

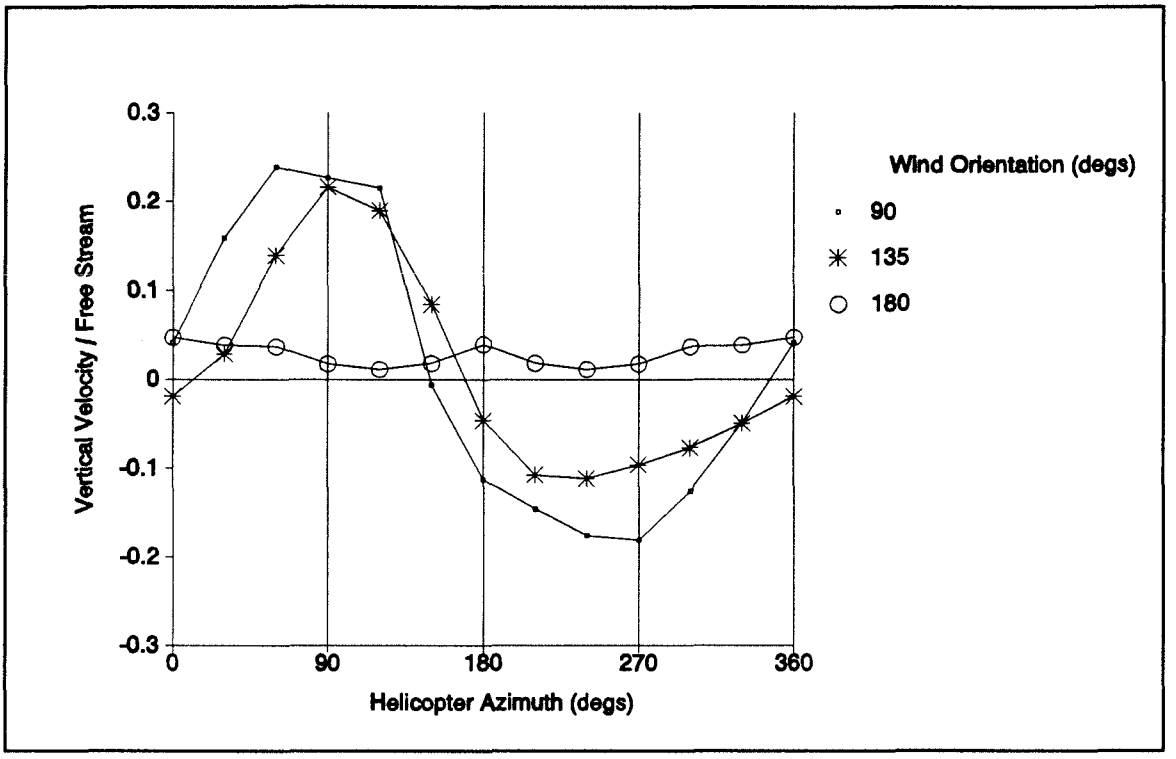

Figure V.4 - Mean Vertical Velocity around Rotor Disc

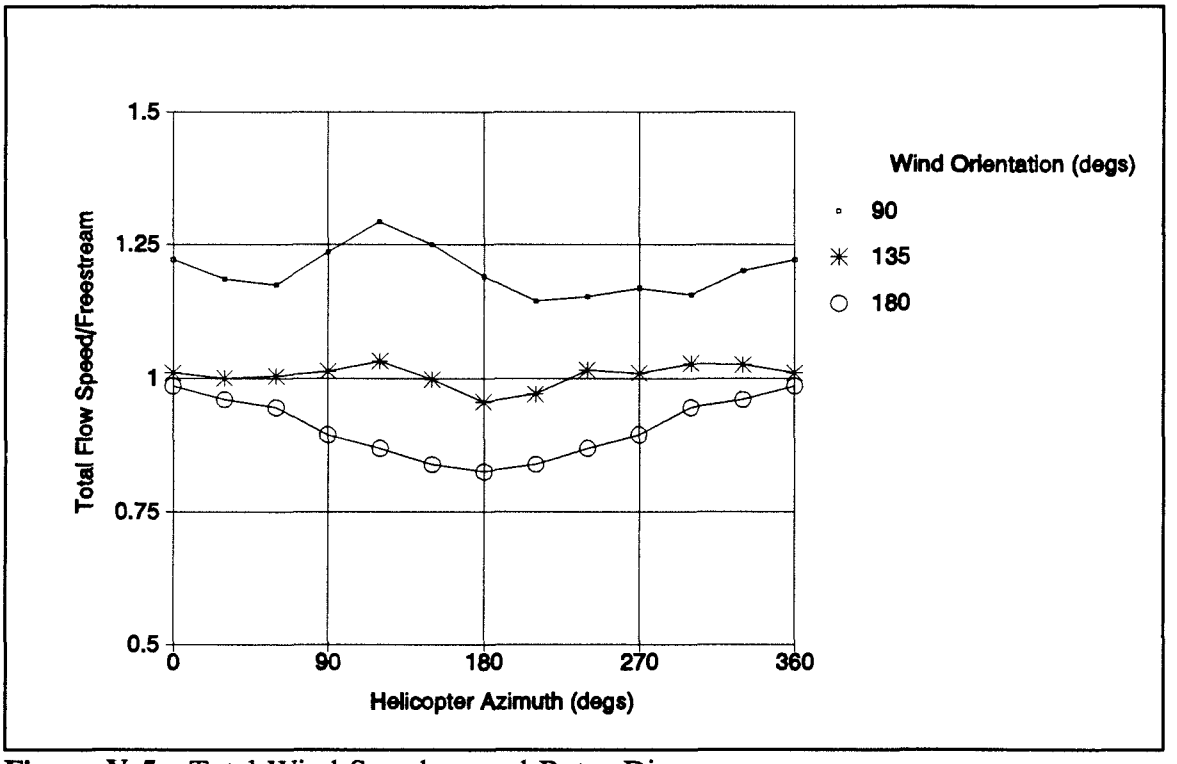

Figure V.5 - Total Wind Speed around Rotor Disc

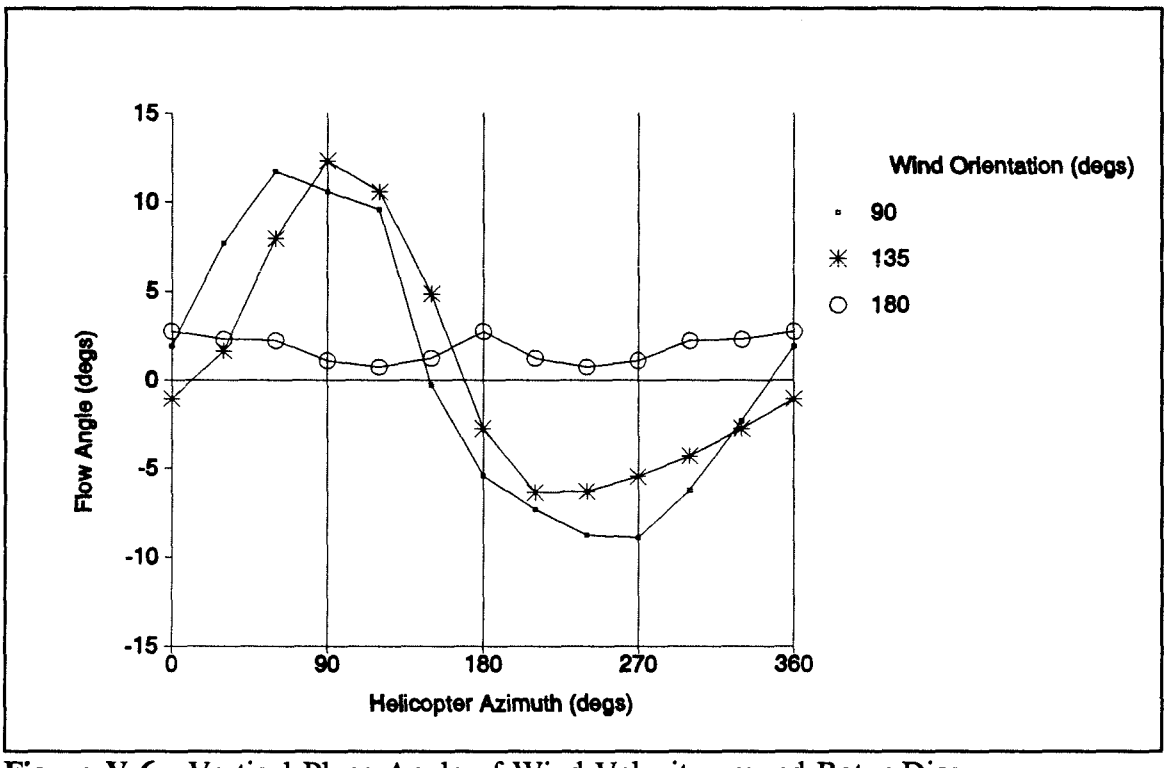

Figure V.6 - Vertical Plane Angle of Wind Velocity around Rotor Disc

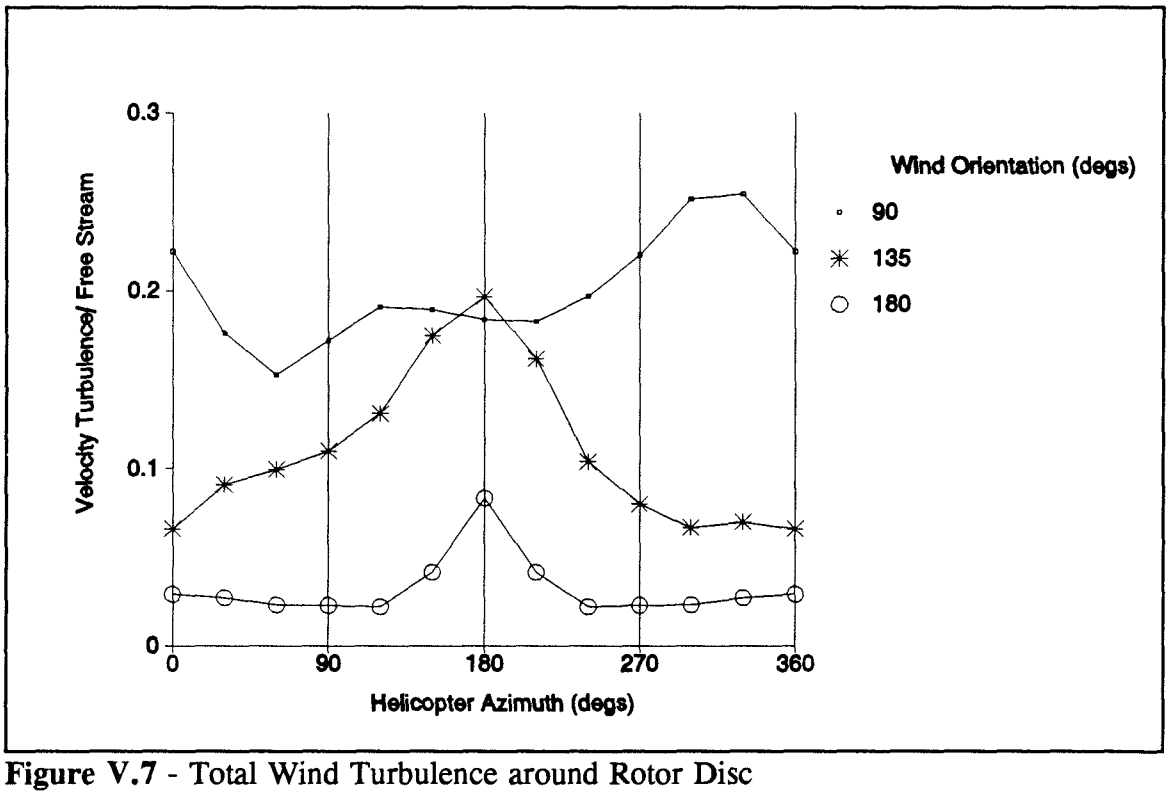

Figure V.7 - Total Wind Turbulence around Rotor Disc

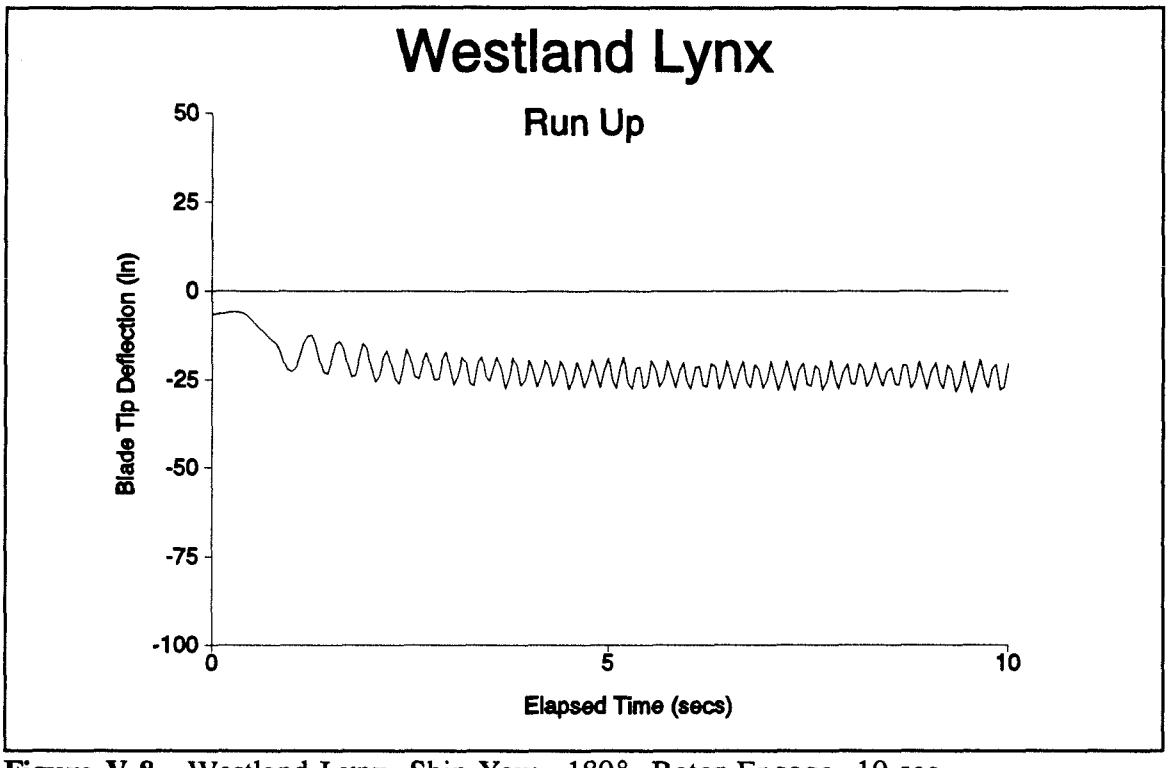

Figure V.8 - Westland Lynx, Ship Yaw=180°, Rotor Engage, 10 sec

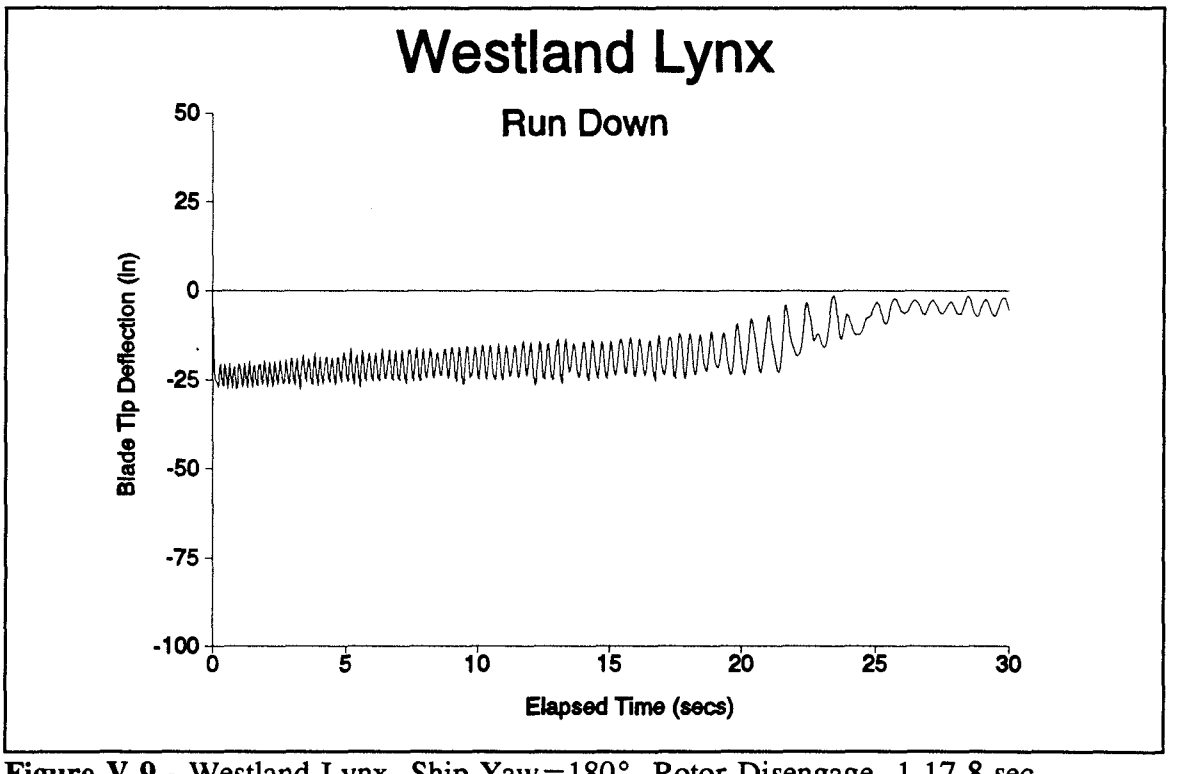

Figure V.9 - Westland Lynx, Ship Yaw=180°, Rotor Disengage, 1,17,8 sec

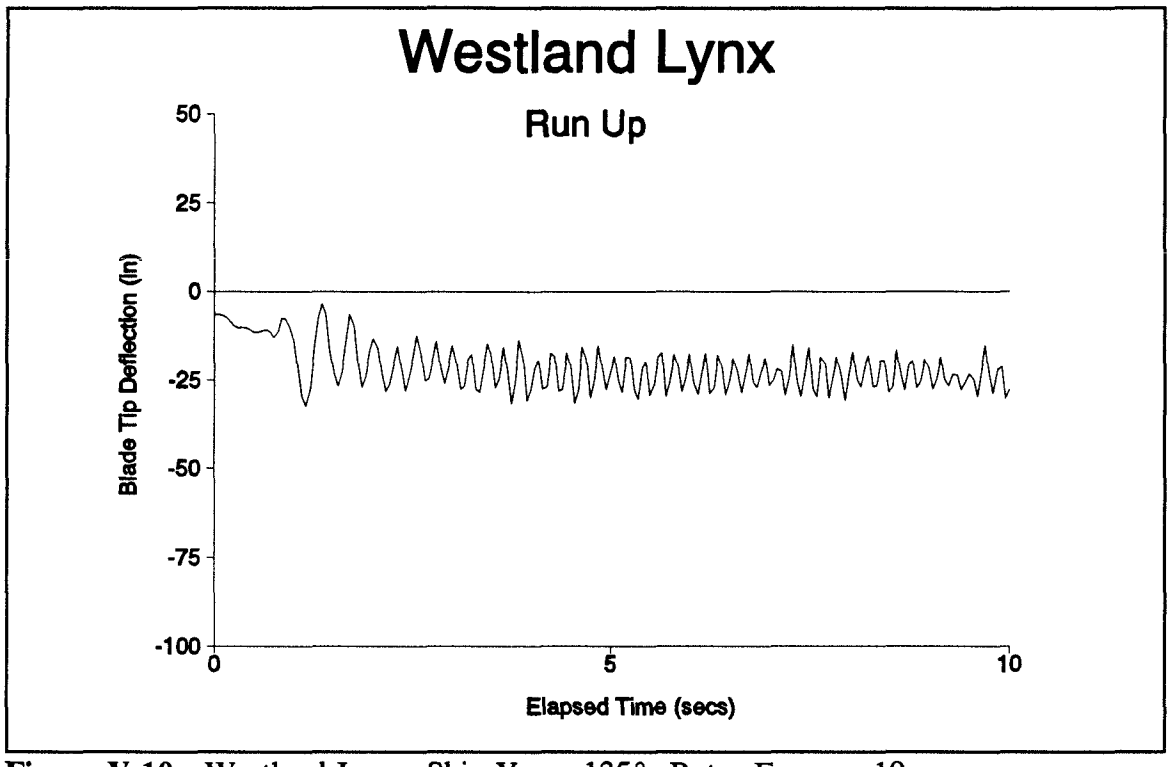

Figure V.10 - Westland Lynx, Ship Yaw=135°, Rotor Engage, 10 sec

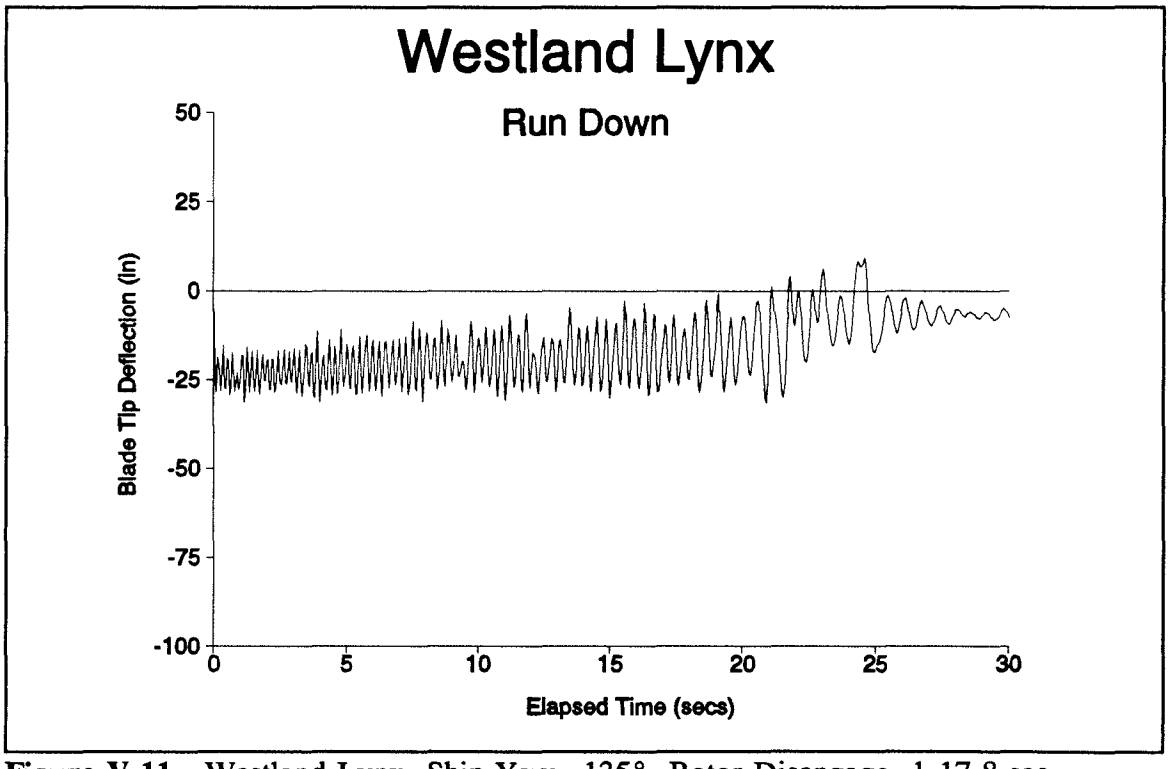

Figure V.11 - Westland Lynx, Ship Yaw=135°, Rotor Disengage, 1,17,8 sec

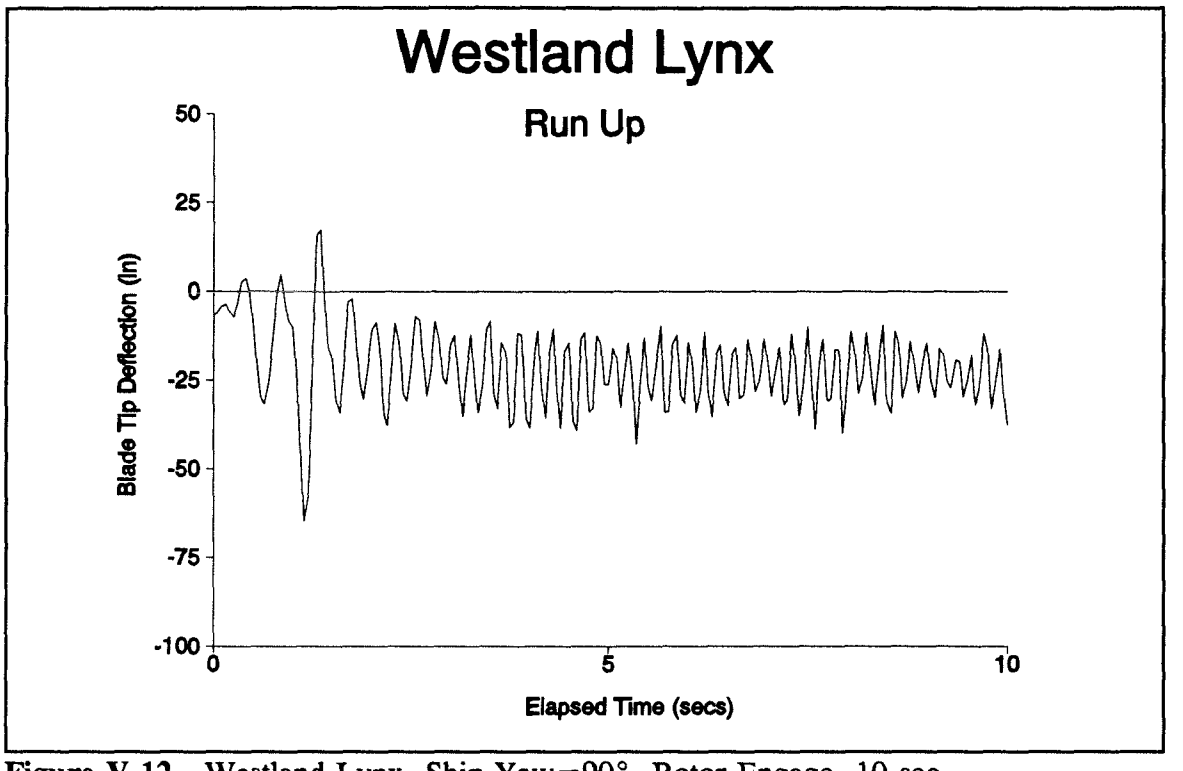

Figure V.12 - Westland Lynx, Ship Yaw=90°, Rotor Engage, 10 sec

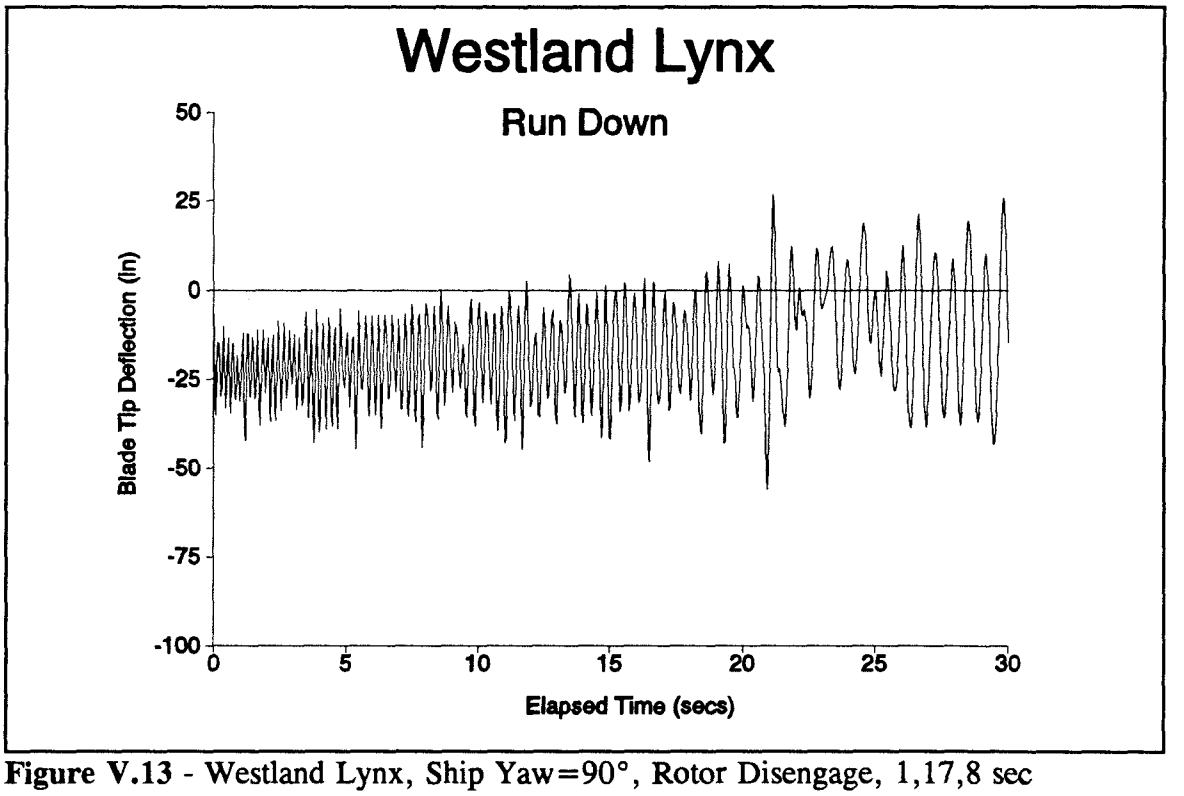

Figure V.13 - Westland Lynx, Ship Yaw=90°, Rotor Disengage, 1,17,8 sec

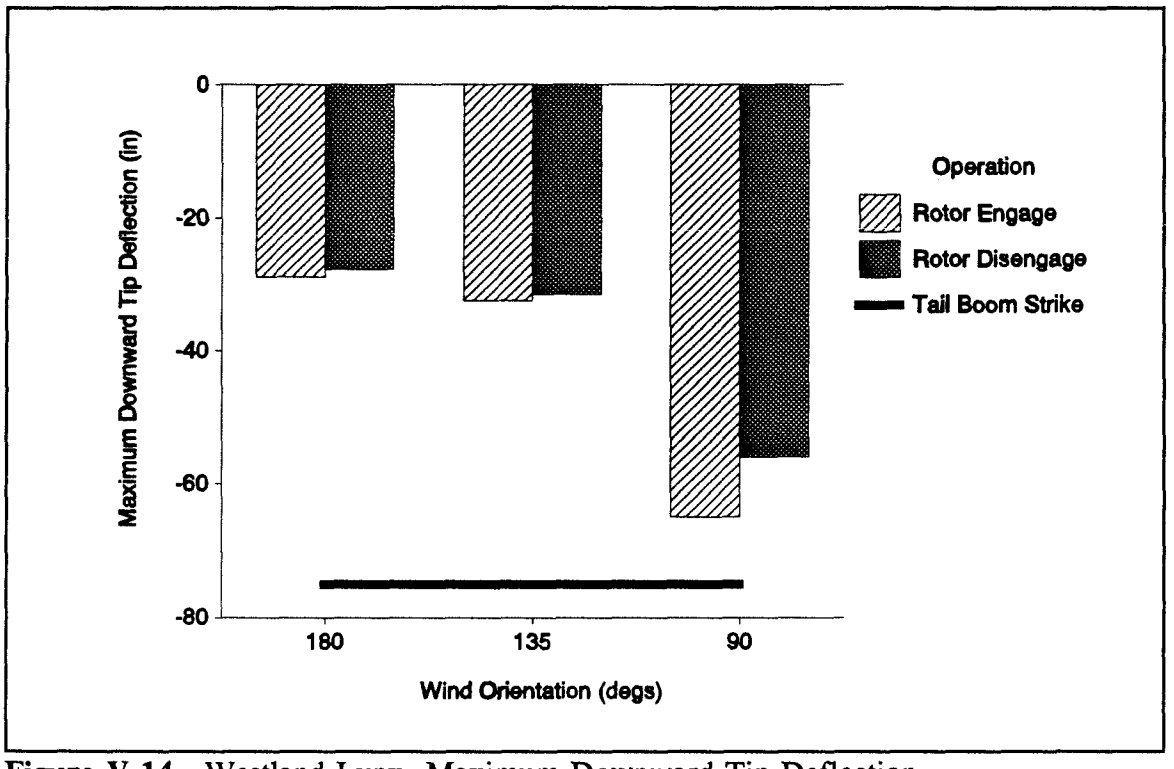

Figure V.14 - Westland Lynx, Maximum Downward Tip Deflection

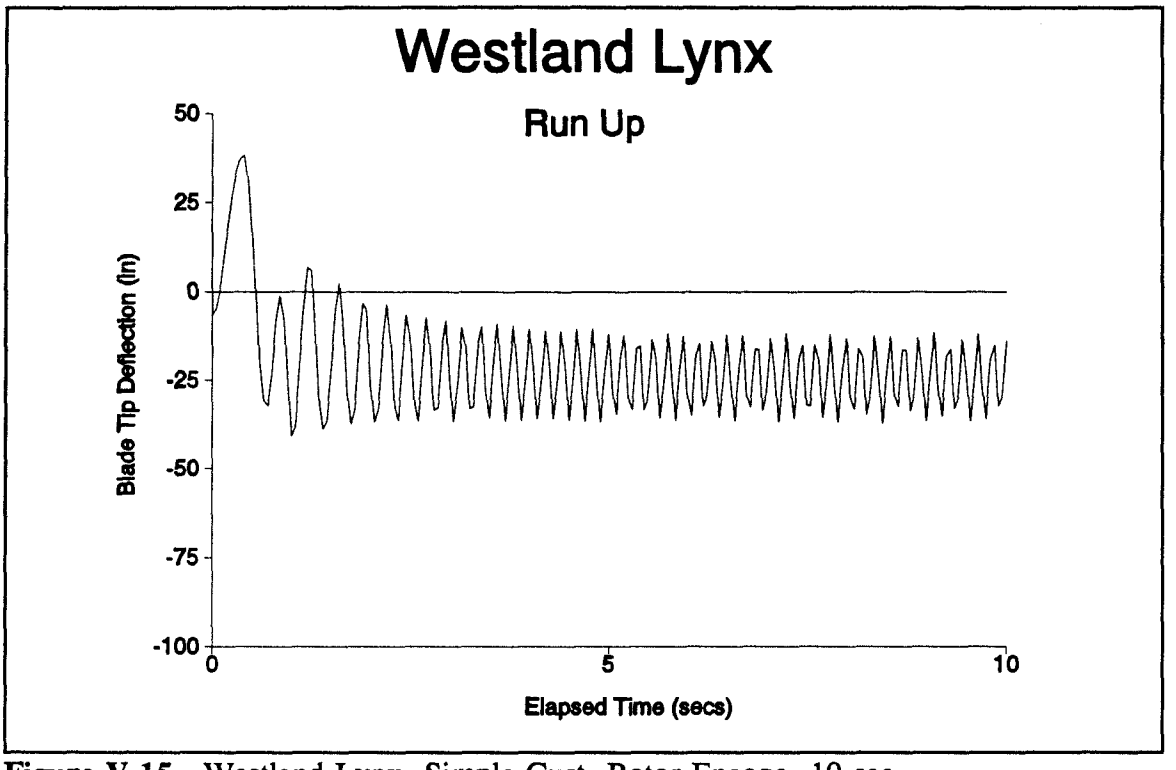

Figure V.15 - Westland Lynx, Simple Gust, Rotor Engage, 10 sec

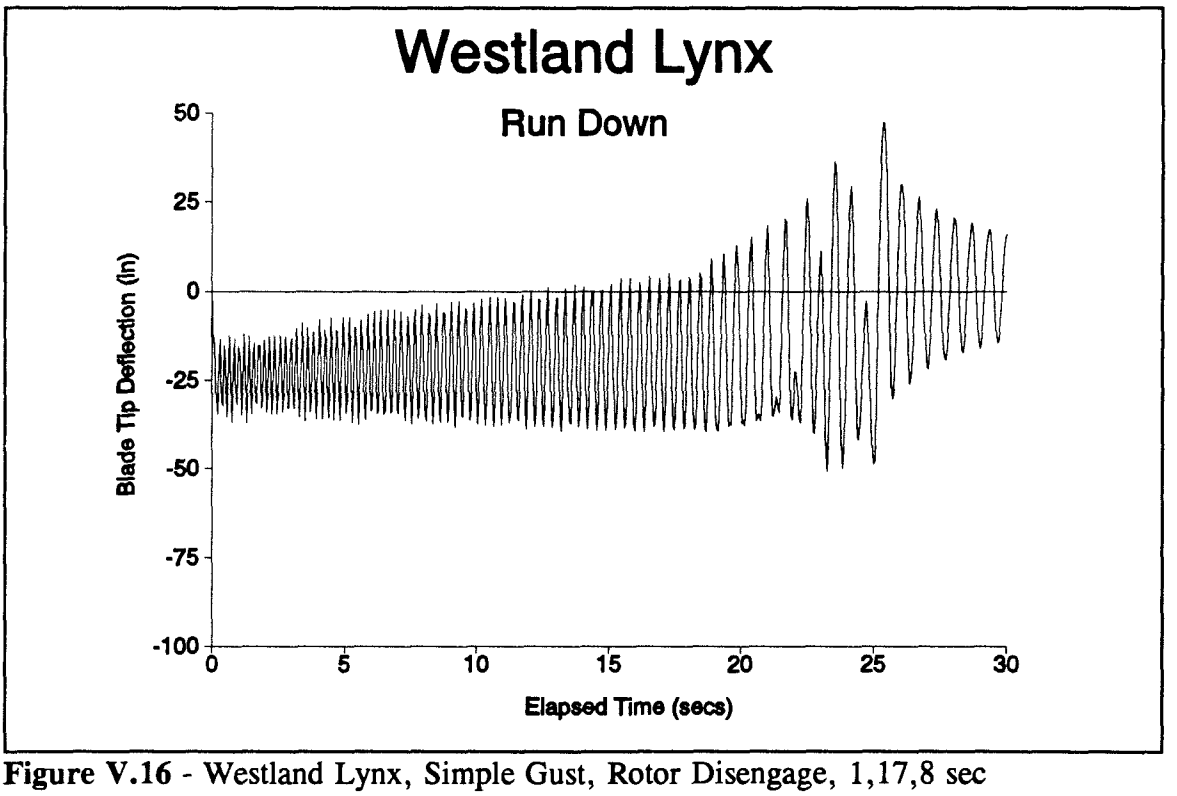

Figure V.16 - Westland Lynx, Simple Gust, Rotor Disengage, 1,17,8 sec

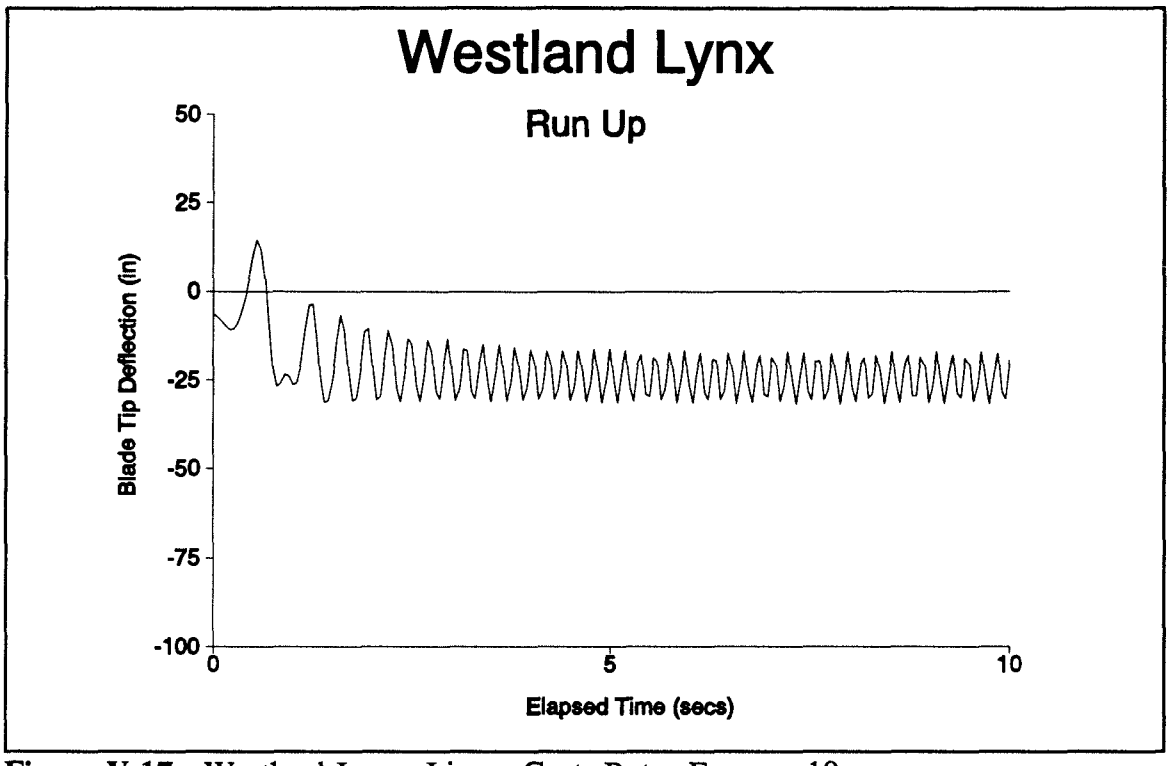

Figure V.17 - Westland Lynx, Linear Gust, Rotor Engage, 10 sec

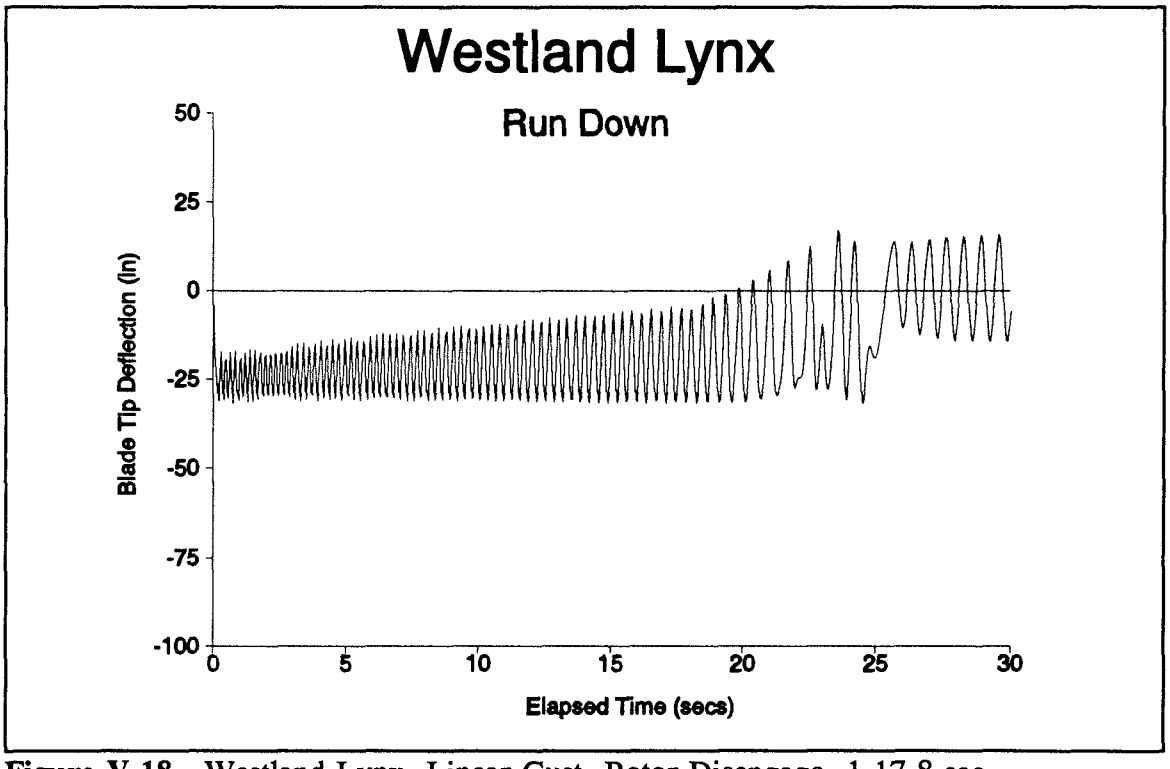

Figure V.18 - Westland Lynx, Linear Gust, Rotor Disengage, 1,17,8 sec

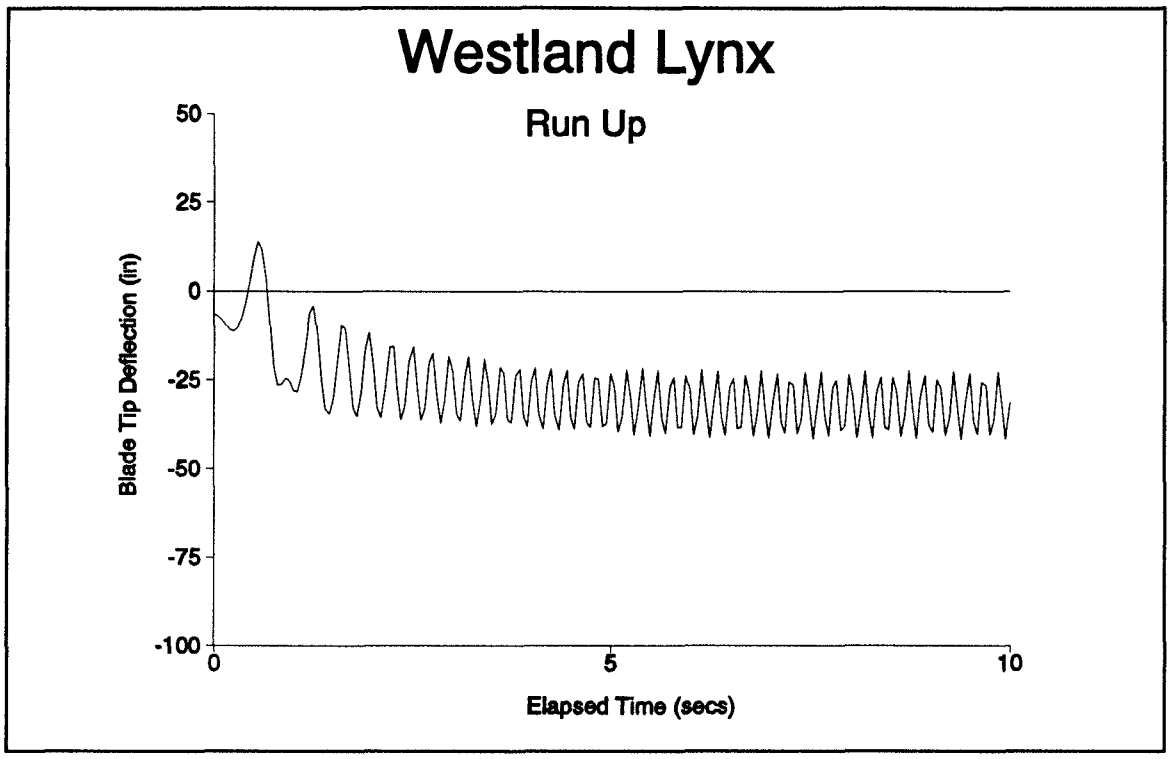

Figure V.19 - Westland Lynx, Linear Gust, Rotor Engage, 10 sec, Torsion Included

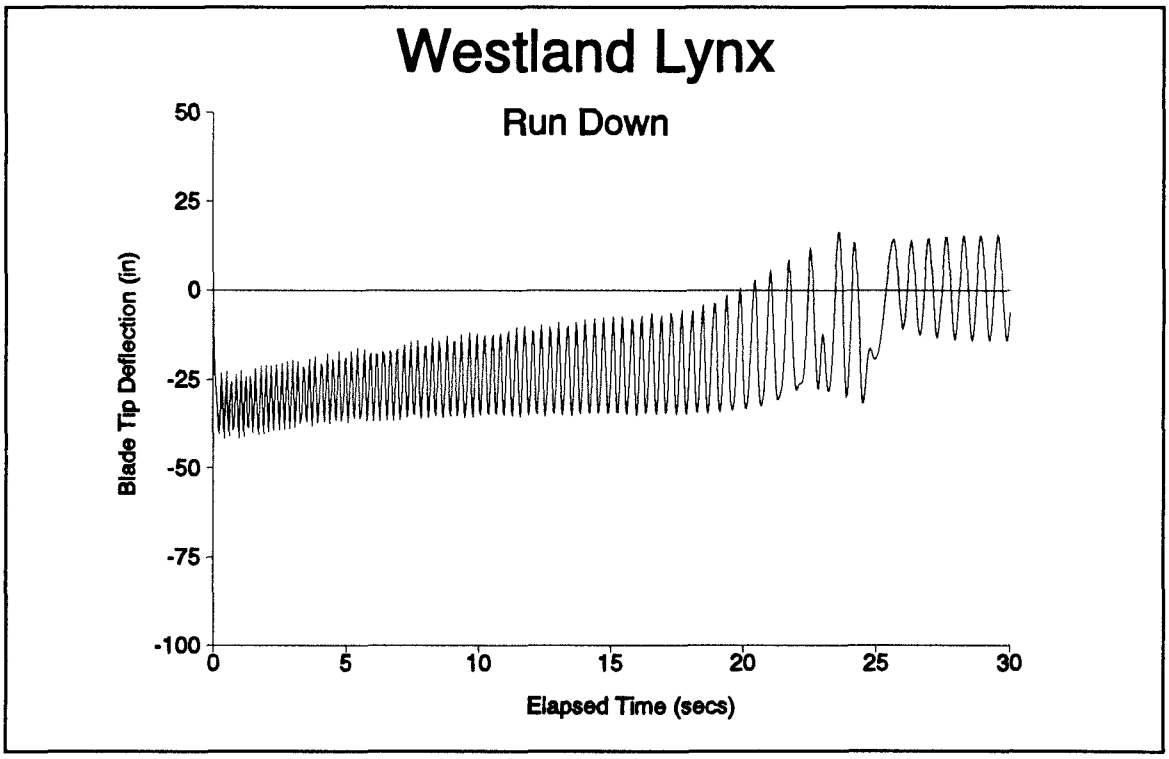

Figure V.20 - Westland Lynx, Linear Gust, Rotor Disengage, 1,17,8 sec, Torsion Included

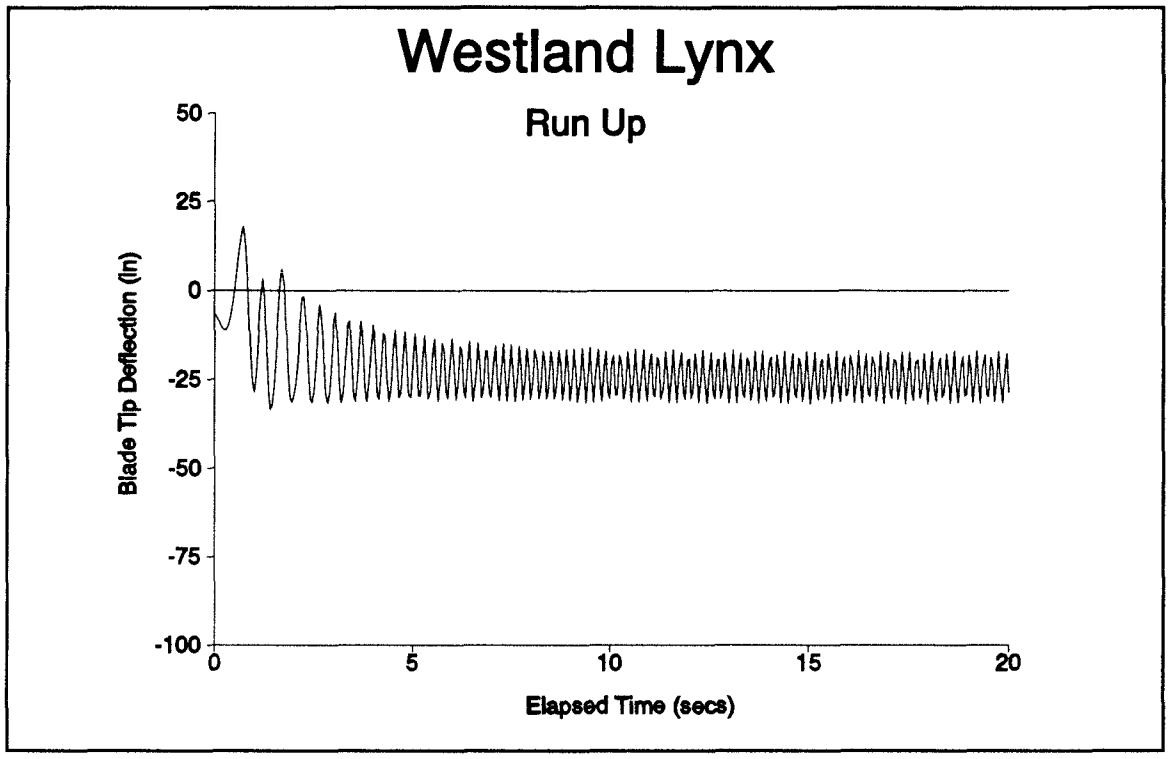

Figure V.21 - Westland Lynx, Linear Gust, Rotor Engage, 20 sec

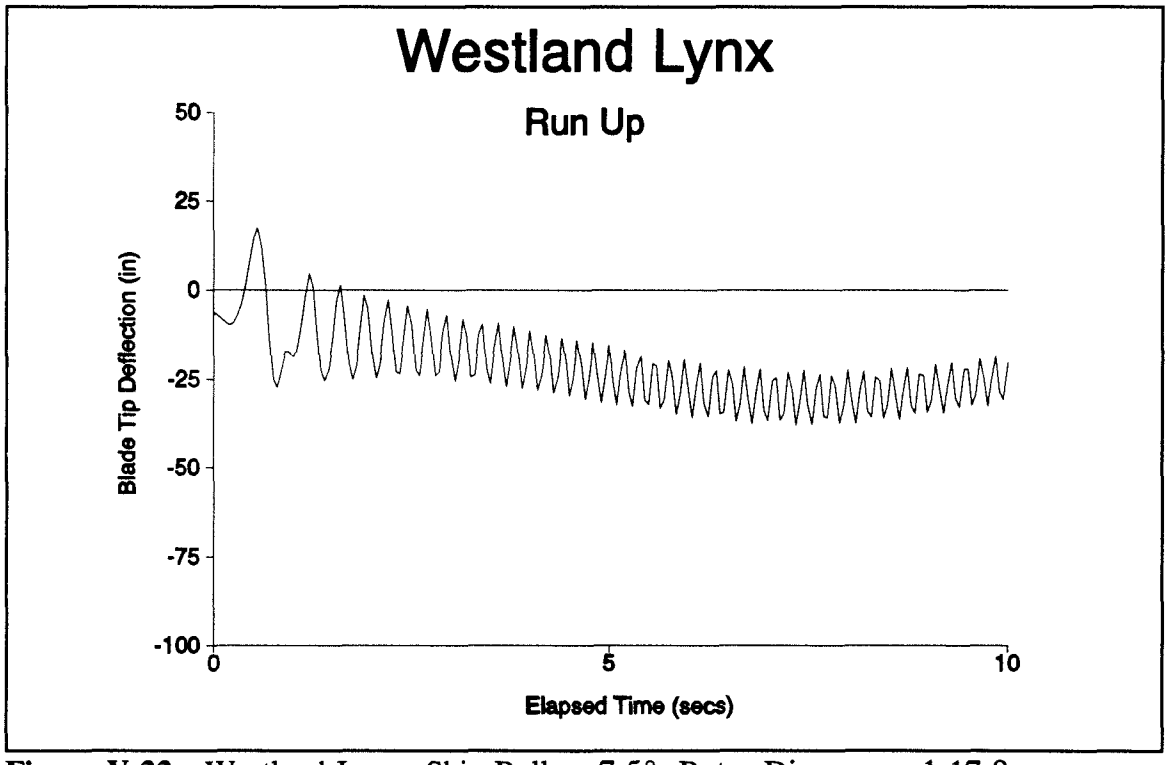

Figure V.22 - Westland Lynx, Ship Roll = 7.5°, Rotor Disengage, 1,17,8 sec

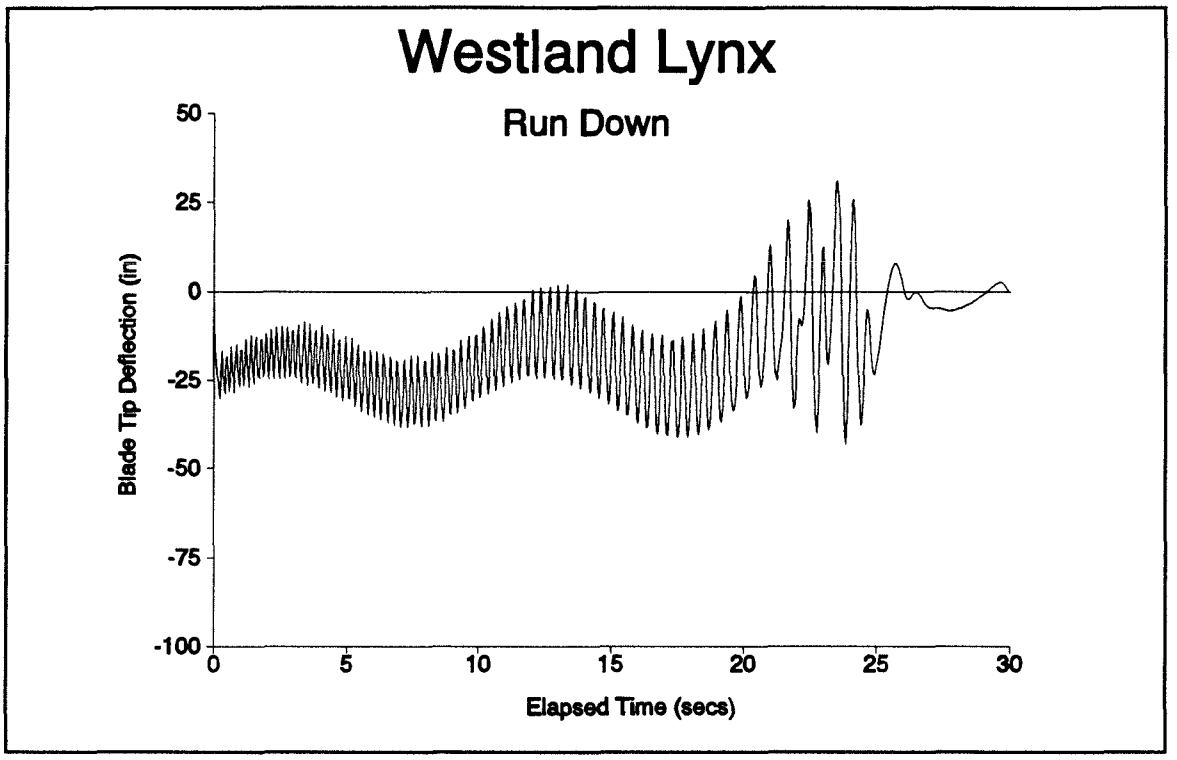

Figure V.23 - Westland Lynx, Ship Roll=7.5°, Rotor Disengage, 1,17,8 sec

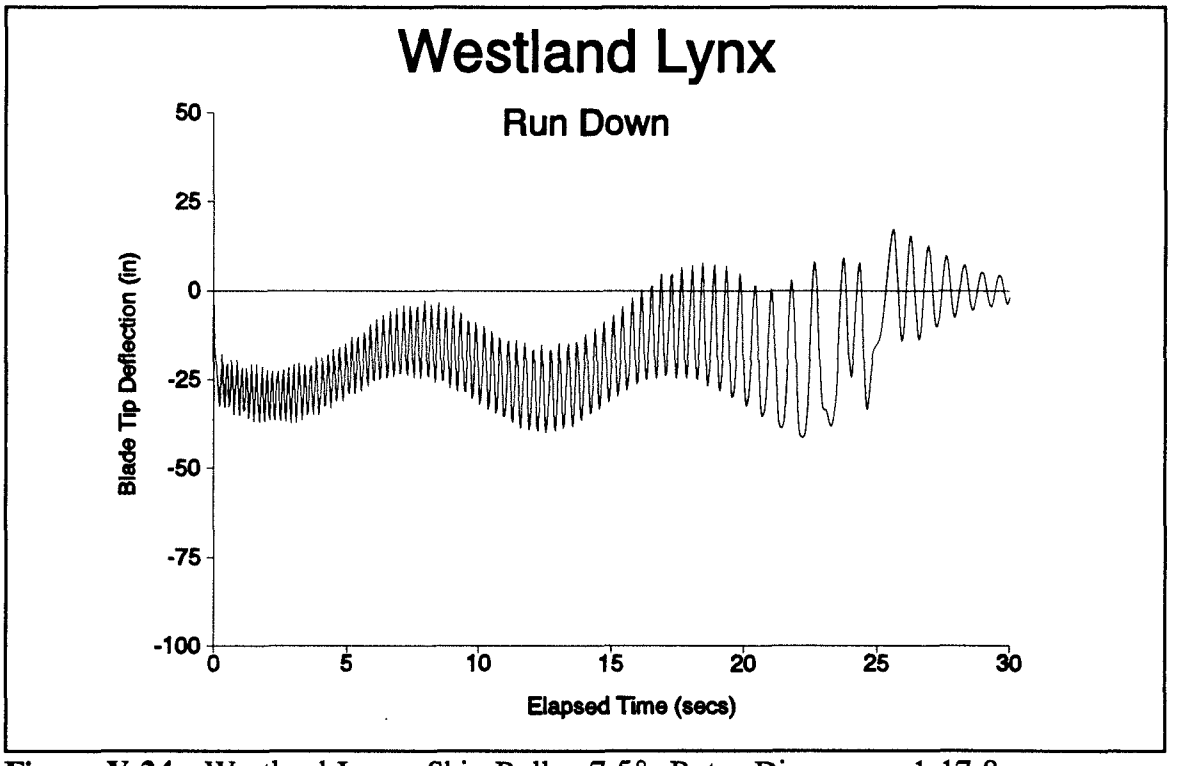

Figure V.24 - Westland Lynx, Ship Roll=-7.5°, Rotor Disengage, 1,17,8 sec

CHAPTER 6

APPLICATION OF THE BLADE MODAL METHOD TO AN ARTICULATED ROTOR

6.1 INTRODUCTION

The previous chapter showed the application of the blade modal method of Chapter 4 to semi-rigid rotors. In contrast, the present chapter applies the method to articulated rotors. An important difference between the rotor types is the rotor hub restraint mechanisms for controlling the blade flapping behaviour at low speed. The droop stop provides a limit for the downward movement of the blade cuff and a rest for the blades when the rotor is stationary. In this case, no support is provided by the centrifugal force and the blade is otherwise free to fall vertically. Upward blade flapping is, however, controlled by the anti-flap assembly. Both mechanisms retract under normal rotor operating conditions when a preset rotational speed is reached and extend by the action of a spring as the rotor speed is reduced. The extension of the theory to articulated rotors needed to include the forces derived from contacting these devices. The aircraft used for the study is the Westland Sea King helicopter.

6.2 DISCUSSION

The respect which must be paid to the problem of blade sailing can best be highlighted by a brief description of the technique of rotor engagement to normal operating rotor speed and deceleration to zero rotor speed. Before start up or run down it is usual to wait for a quiet period of the wind, if possible, by observation of the static blade behaviour and/or wind socks. For a fast rotor acceleration the throttle is opened before the rotor brake is released, at which point the throttle can be progressively opened as rapidly as possible. To minimise the danger of blade sailing, the periods of low rotor speed should be kept short. However, operational limitations can occur, and to illustrate this, the following two problems with the Sea King aircraft are described. Firstly, the engine governor has an input from the free turbine speed (N_F) and, if the throttle lever is advanced too quickly, the signals can be lost and the governor will freeze. To re-establish the N_F signal, the throttle lever must be returned to ground idle and then reopened, leaving the rotor in a possibly hazardous condition at low rotational speed. Secondly, if the traction between the tyres and the ground is reduced, on a wet ship's deck for example, a high torque condition can cause the fuselage to skid in the opposite rotational sense to the rotor. This tendency can be aggravated by a forward centre of gravity condition which will offload the tail wheel. High torque input to the rotor will also tend

to throw the blades onto the lag stops.

When decelerating the rotor in windy conditions, it is usual to slow the rotor until the droop stops extend, and when a quiescent period occurs the rotor can be decelerated to a halt using the rotor brake. Again this period should be as short as possible, but the rotor brake performance will be an obvious limit. The rotor brake tends to be a Cinderella item since its use is assumed and not perceived to be very glamorous. In fact it is a very necessary item of transmission system. This was tragically illustrated with the loss of the PP2 prototype of the EH101 aircraft.

Discussions with pilots, and consulting safety publications, indicate that blade sailing has occurred in the past with very serious consequences, both to the aircraft and to the operating personnel. Contact of the blade tips with the ground are reported and the tail boom is vulnerable to large blade excursions. Additionally, inboard parts of the blade are not without potential problems with the advent of weapon sights and engine intake filters positioned on top of the cockpit.

Linear springs of high rate are used for both the droop and anti-flap stops and are only invoked when the flapwise deflections of the blade at the respective spring positions are sufficient to cause contact with the appropriate stop. See Figure VI.1. The deflections required for a blade stop contact will change as the stops retract in a run up and extend in a run down. A further complication is that the rotor speed at which the extension or retraction occurs will be different for the droop and anti-flap stops. Furthermore, the mechanics of the stops is such that they cannot retract or extend with the cuff in contact with them. The logic of the method must allow for all these situations.

Since the method is based on a radially continuous loading distribution, the application of the point load must be applied via a Dirac delta function. The forcing to the nth mode has an additional term,

$$\Delta L = \int_{BLADE} L_s(r) g_n(r) \delta(r - r_s) dr \qquad \textbf{(VI.1)}$$

which reduces to:-

$$\Delta L = L_s(r_s) g_n(r_s) \qquad \textbf{(VI.2)}$$

where L_s is the spring load, r_s is the radius at which the spring stop is located, and δ is the Dirac delta function.

From this result, it can be seen that as the modal deflection $g_n(r_s)$ at the representative spring radial station increases relatively with respect to n, (the mode number), a given load will have a proportionately greater influence on the higher modes. The effect of this is discussed in the following section.

6.3 RESULTS

For the Sea King investigation, the variation of rotor speed is of identical form to that used for the Westland Lynx aircraft, as described in Chapter 5. Again four flapwise mode shapes are used and are shown in Figure VI.2. They are referenced to zero rotor speed. The run up is of hyperbolic tangent form (tanh) with an elapsed time of 40 seconds. The run down has a settling time of 1 second, a freewheel time of 26 seconds, and a rotor braking time of 21 seconds. (These Figures were obtained using stopwatch timing). The settling period is a computationally efficient means of obtaining the correct initial flapping behaviour of the rotor, the freewheel phase is when the rotor slows from operating rotor speed to a point when the rotor brake can be safely applied (45%NR). The final period sees the rotor coming to a halt whilst the rotor brake is applied. The commencement of the run down, the application of the rotor brake, and the final stopping of the rotor, will have elapsed times of 1, 27 and 48 seconds respectively. Throughout the analysis, a collective pitch of 6° was used which is the minimum pitch setting for the Sea King. The variation is shown in Figures VI.3 and VI.4. *Note that N_R is the notation for normal operating rotor speed.* For the Figures showing the theoretical blade tip deflection time histories, a collective pitch of 6° is used with no cyclic pitch applied. The rotor control angles consist of a collective pitch setting which gives a nominally zero thrust value, which is consistent with current operational practice. The absence of cyclic pitch is deliberately chosen to observe the blade flapping response due to wind conditions, without colouration from any applied disc attitude change via the cyclic pitch. The maximum downward deflection is indicated on each Figure with a horizontal arrow. The magnitude is indicated on each Figure.

As with the model development for a semi-rigid helicopter, the torsion content of the articulated blade modes is also included in the calculations. Articulated blade modes have a torsional component that will alter since contact with a hub restraint mechanism changes the kinematics of the pitch control mechanism. When the blade is clear of the stops, the

alignment of the push-pull rods governs the pitch-flap coupling irrespective of the elastic bending of the blade. When in contact with a stop, the flapping rotation and therefore the pitch control mechanism will lock and the blade deflection becomes purely bending. Consequently, in this situation, the blade torsion is zero. Within the computer program a torsion factoring of zero or unity is applied depending on whether the blade cuff makes contact with a hub restraint or not. The droop stop will extend/retract at a rotor speed of 68% N_R and the anti-flap stop at 30% N_R. Should the blade position at these rotor speeds mechanically interfere with the operation of the appropriate stop, then the method will hold the stop in its original position until the blade cuff moves sufficiently clear to allow the stop to change position *(jammed stop)*.

The investigation of the Westland Lynx helicopter in Chapter 5 included a wind tunnel experiment to determine the wind patterns over the flight deck of a Rover Class Royal Fleet Auxiliary ship. Because the wind tunnel data were taken at locations specifically tailored for the Lynx aircraft, they were not appropriate for the Sea King. The wind tunnel test results showed the overall effect of direction on the wind characteristics over the ship's deck and were used as a guide in constructing an alternative wind specification method for this analysis. This method is only applicable for winds normal to the ship's centre line, which the previous work of Chapter 5 predicted to be the most severe condition for blade flapping excursions. A basic wind speed of 50 knots was used, with no supervelocity over the deck of the ship, together with a vertical component of 15 knots which varies linearly from 15 knots upward to 15 knots downward across the disc between the windward and leeward sides respectively. (It should be noted that 15 knots is used for the Sea King as used for the Lynx. This was for reasons of consistency even though there are differences in the heights of the rotor above the deck.)

The initial results are shown in Figures VI.5 and VI.6. Only a droop stop restraint is included and four flapping modes define the blade motion. The wind direction is from starboard throughout. The rotor blade starts at zero azimuth angle, i.e. directly over the tail boom.As shown in Chapter 5, the semi-rigid rotor of the Lynx aircraft produces blade tip deflections of the order of 32 inches. However, Figures VI.5 and VI.6 show that the Sea King rotor is predicted to produce tip deflections far in excess of this. For the run up, Figure VI.5, the maximum tip deflection occurs early in the motion. With a run down, Figure VI.6, the greatest deflection is seen with the rotor almost at rest at

the end of the braking phase.

Figure VI.7 corresponds to Figure VI.5 except that the gust commences one second after the rotor engagement has started. The large initial downward movement has been removed and the value of starting the rotor in as low a wind as possible is demonstrated. Figures VI.8 and VI.9 show the introduction of the anti-flap stop and although the maximum upward tip deflection is reduced, little change in downward tip deflection is shown relative to Figures VI.5 and VI.6. The blade motion is biassed towards a downward movement and the droop stop is the major controlling blade cuff restraint. The effect of the anti flap stop only appears at the maximum upward tip movement. A notable effect is shown in these Figures which at first appears as something of a paradox. As the droop stop extends, the blade downward deflections increase, and conversely a droop stop retraction causes a decrease in the downward tip deflection. This at first unexpected behaviour is explained by the response of the higher modes relative to the fundamental. When not in contact with a stop, the blade's fundamental response dominates. However when a stop is encountered, the response of the overtone modes, the second in particular, is increased. As previously mentioned, modelling of the stops by a Dirac delta function causes a greater forcing contribution to the higher modes. Reference to equations (VI.1) and (VI.2) shows that the spring forcing to the nth mode contains a $g_n(r_s)$ term. As the mode number n increases, the value of $g_n(r_s)$ increases in magnitude, so for a given spring load the forcing will increase for increasing mode number n. The results show that the phasing of the blade deflection, at the stop location for the various modes, is such as to minimise the compression of the springs used to simulate the reaction of the stops on the blade cuff. In other words, the deflection contributions of the modes tend to cancel out at the stop location. This reduction in the blade cuff deflection requires the first and second mode contributions to be of opposite sign at the cuff. This phasing causes the modal contributions to the blade deflection at the tip to reinforce with the result of increasing the tip deflection. To justify the explanation of the effect, the cases were repeated for a smaller number of modes than the four used previously. Particular emphasis was placed on the single, *fundamental*, mode only.

The effect of the second mode response is shown by comparing Figures VI.10 and VI.11 with Figures VI.8 and VI.9. Figures VI.10 and VI.11 show the blade deflections when only the fundamental mode is used to describe the blade position. The drastic reduction

in blade deflection apparent is due to the fact that, with the single mode, any blade tip deflection must be accompanied by a corresponding compression of the stops by the cuff. The absence of the higher modes does not allow a high blade tip deflection to be built up without compression of the stops. Figures VI.10 and VI.11 show that the tip deflections are greater when a stop is retracted, which is the opposite effect to that obtained previously with 4 modes as shown in Figures VI.8 and VI.9. Figures VI.12 and VI.13 show the corresponding results for 2 modes, whilst Figures VI.14 and VI.15 for 3 modes. These results are summarised in Figure VI.16, and the change in maximum downward tip deflection with increase in the number of blade modes used is apparent. It can be seen that the inclusion of the second mode has a major influence on the response of the blade with the contributions of the third and fourth modes becoming progressively smaller.

6.4 COMPARISON WITH FULL SCALE AEROSPATIALE PUMA TESTS

During the formative period of the modal method, a comparison of the theoretical predictions with full scale experimental data was sought. To accomplish this, a test was conducted at DRA Bedford, with an Aerospatiale SA330 Puma helicopter for a rotor run up and run down in a 10 knot headwind over the nose of the aircraft. The blade flapping behaviour was used as a comparison for the model. The theoretical predictions of blade tip deflection with time are shown in Figures VI.17 and VI.18, whilst the flight test data are presented in Figures VI.19 and VI.20. The blade flapping modes used for the theoretical comparison were taken to be uncoupled, i.e. no torsion was included. The intention of doing this was to allow the comparison to be of the flapping motion only. The Puma data were obtained as flapping angles, which were converted to blade tip deflections assuming that the blade was rigid. Difficulty was experienced in extracting all the necessary data for the computer runs as the power generators on the aircraft did not activate some instrumentation at the lower rotor speeds. In consequence, the rotor speed variation at the lower rotor speeds has had to be interpolated. Some changes in cyclic pitch are indicated from the pilot inputs so a representative set of data for the rotor control angles was selected.

The comparison shows that the characteristics of the blade behaviour are reproduced. The blade flapping behaviour at normal (maximum) operating rotor speed shows good agreement between the results, but the coning angle is different by an amount corresponding to a flapping angle at the blade cuff of 1°. The coning error may be caused by the flow pattern over the top of the fuselage. The theoretical model at present contains no downwash representation, but this is not unreasonable since the collective pitch chosen gives nominally zero rotor thrust in order to conform with standard operational practice. In view of the problem of not acquiring data at the lowest rotor speeds, and the evidence of pilot input adjustments during the tests, it was not possible to guarantee specific values for the collective and cyclic pitch angles. Consequently, a detailed pursuit of the differences in coning angle did not appear justified.

The stationary blade deflection on the stops is also different, this being due to the fact that a cantilever blade is being modelled by several pinned blade modes. In the theoretical

model the stationary blade can only achieve equilibrium by compressing the spring which is modelling the droop stop. This gives rise to the observed increase in static blade droop. In reality the blade will cause essentially no deflection of the droop stop and behaves as a cantilever. The error can be reduced by not allowing bending of the second (or higher) modes, but the extra modes are required as previously explained to allow the large blade deflections when droop stop contact occurs.

This Chapter extended the blade modal method to articulated rotors. The expected increase in the blade motion was confirmed. The influence of the contacts with the droop and anti flap stops proved paradoxical at first but when the contribution of the overtone modes was considered the blade tip behaviour was entirely reasonable. The influence of ship rolling was seen to affect the blade motion considerably. This Chapter concludes the application of the method to conventional helicopter rotor systems.

6.5 SUMMARY OF FIGURES

A survey of the results presented in this Chapter is tabulated in Table VI.1:

Table VI.1 - Summary of Figures

Fig	Aircraft	Up or Down	Modes	DRP	A/F	Max Tip Defln	θ_0	A_1	B_1
5	SEA KING	Up	4	Y	N	63.8	6	0	0
6	SEA KING	Down	4	Y	N	77.4	6	0	0
7	SEA KING	Up	4	Y	N	45.3	6	0	0
8	SEA KING	Up	4	Y	Y	61.6	6	0	0
9	SEA KING	Down	4	Y	Y	83.2	6	0	0
10	SEA KING	Up	1	Y	Y	22.1	6	0	0
11	SEA KING	Down	1	Y	Y	21.9	6	0	0
12	SEA KING	Up	2	Y	Y	60.2	6	0	0
13	SEA KING	Down	2	Y	Y	74.6	6	0	0
14	SEA KING	Up	3	Y	Y	58.7	6	0	0
15	SEA KING	Down	3	Y	Y	80.5	6	0	0
16	PUMA	Up	4	Y	N		6.1	-0.4	-1.0
17	PUMA	Down	4	Y	N		6.1	-0.4	-1.0
18	PUMA	Up	EXPERIMENT						
19	PUMA	Down							

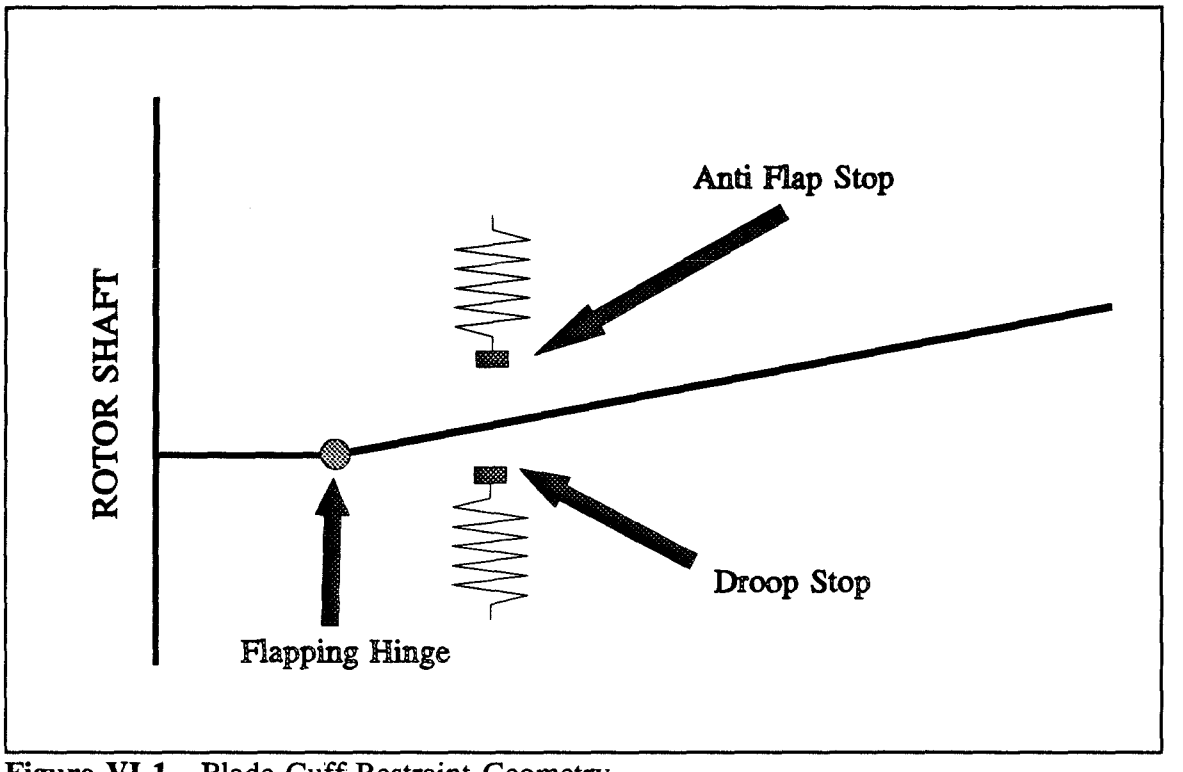

Figure VI.1 - Blade Cuff Restraint Geometry

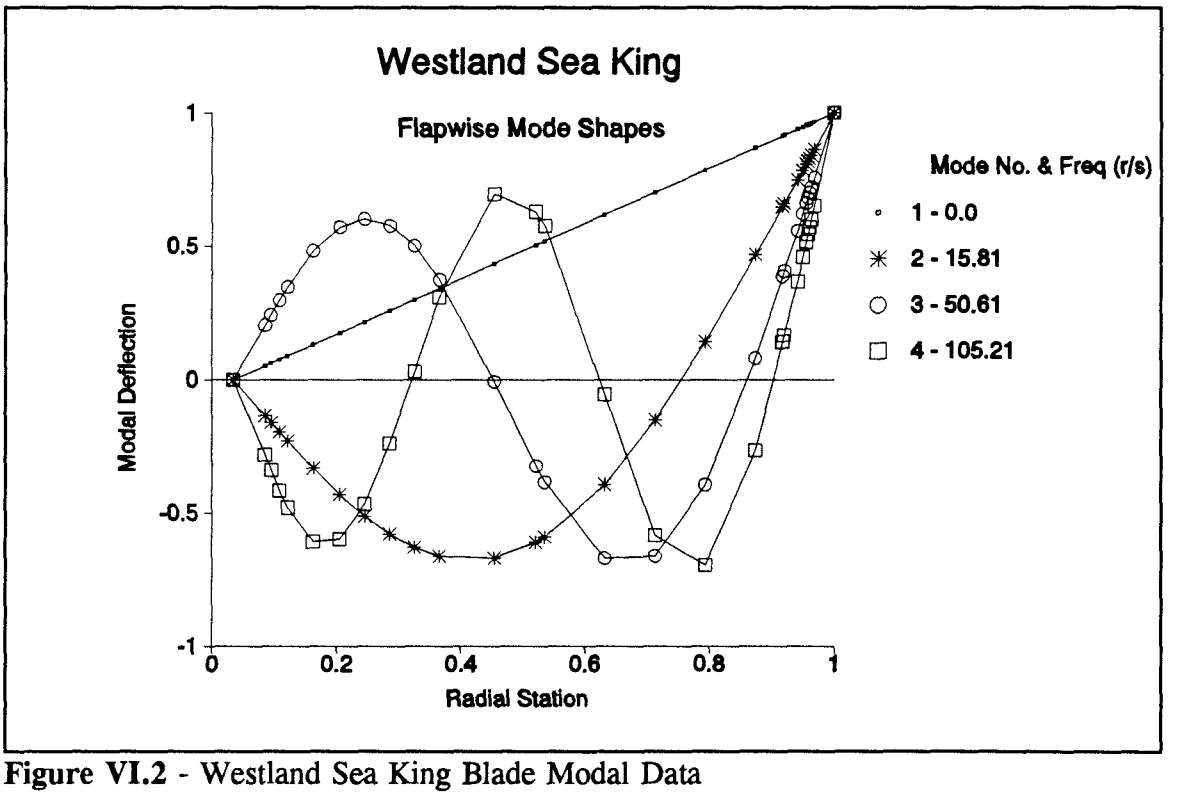

Figure VI.2 - Westland Sea King Blade Modal Data

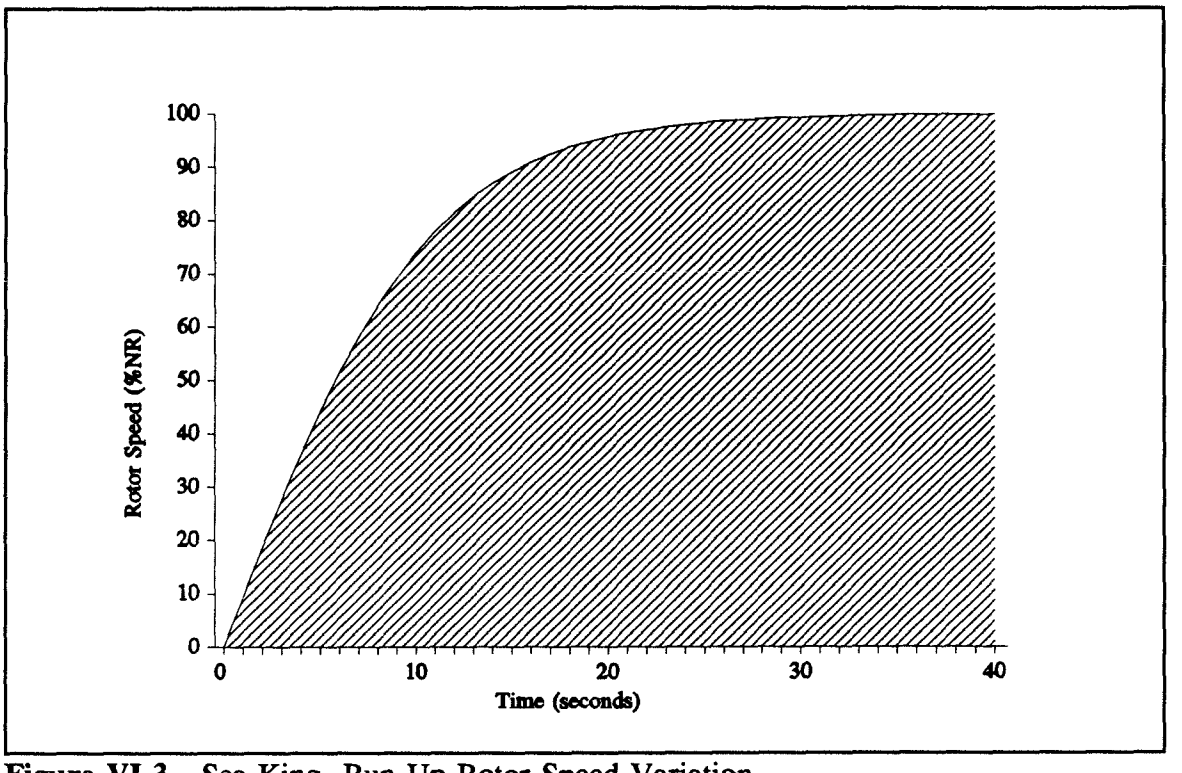

Figure VI.3 - Sea King, Run Up Rotor Speed Variation

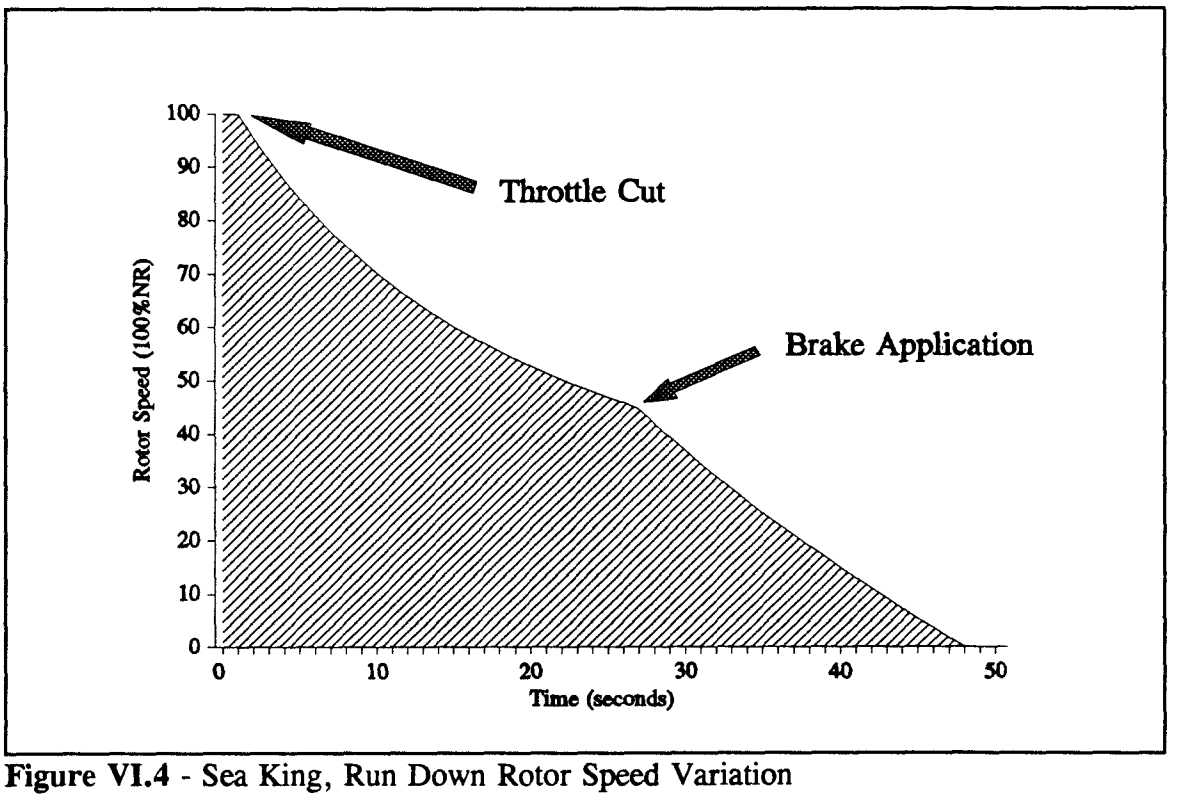

Figure VI.4 - Sea King, Run Down Rotor Speed Variation

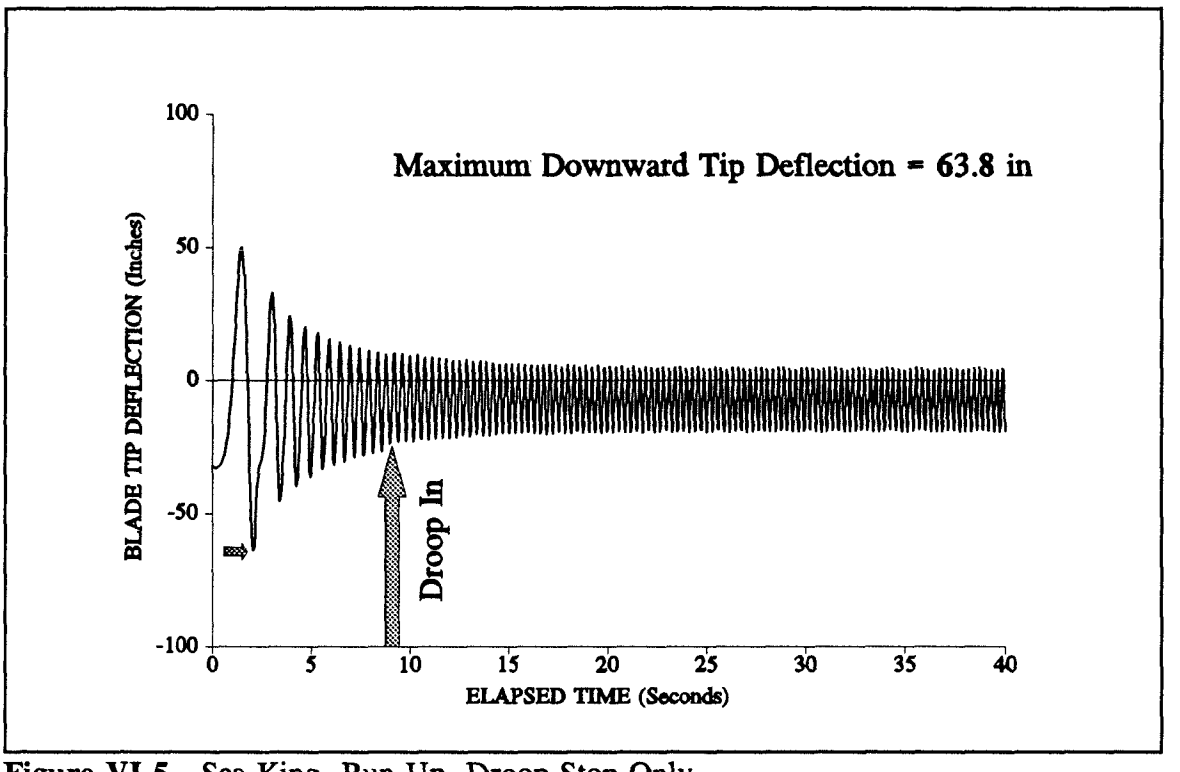

Figure VI.5 - Sea King, Run Up, Droop Stop Only

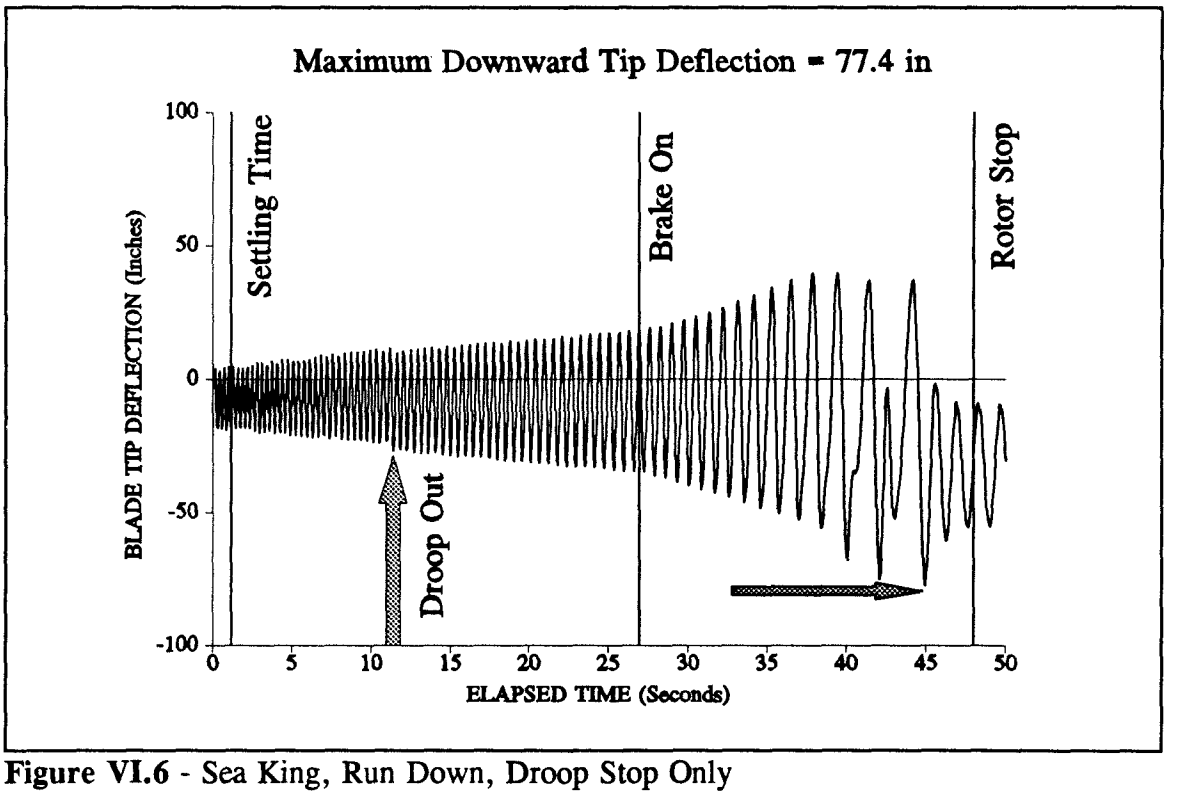

Figure VI.6 - Sea King, Run Down, Droop Stop Only

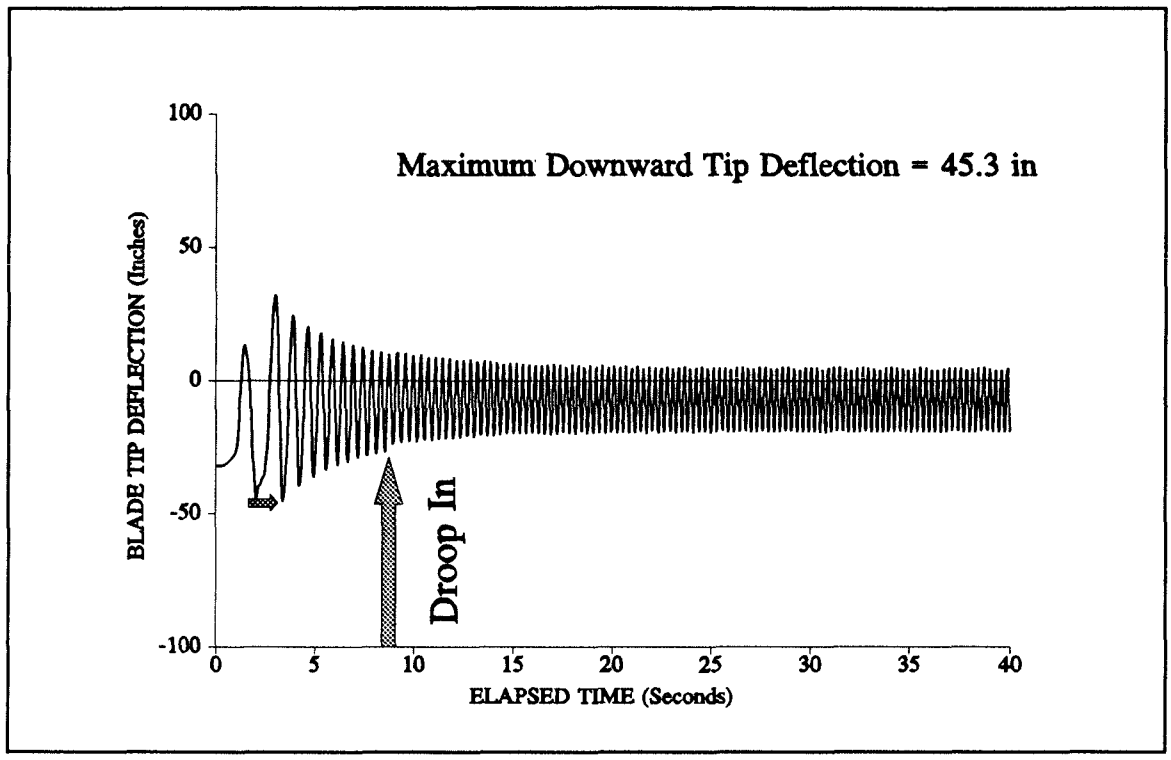

Figure VI.7 - Sea King, Run Up, Gust Delay of 1 second

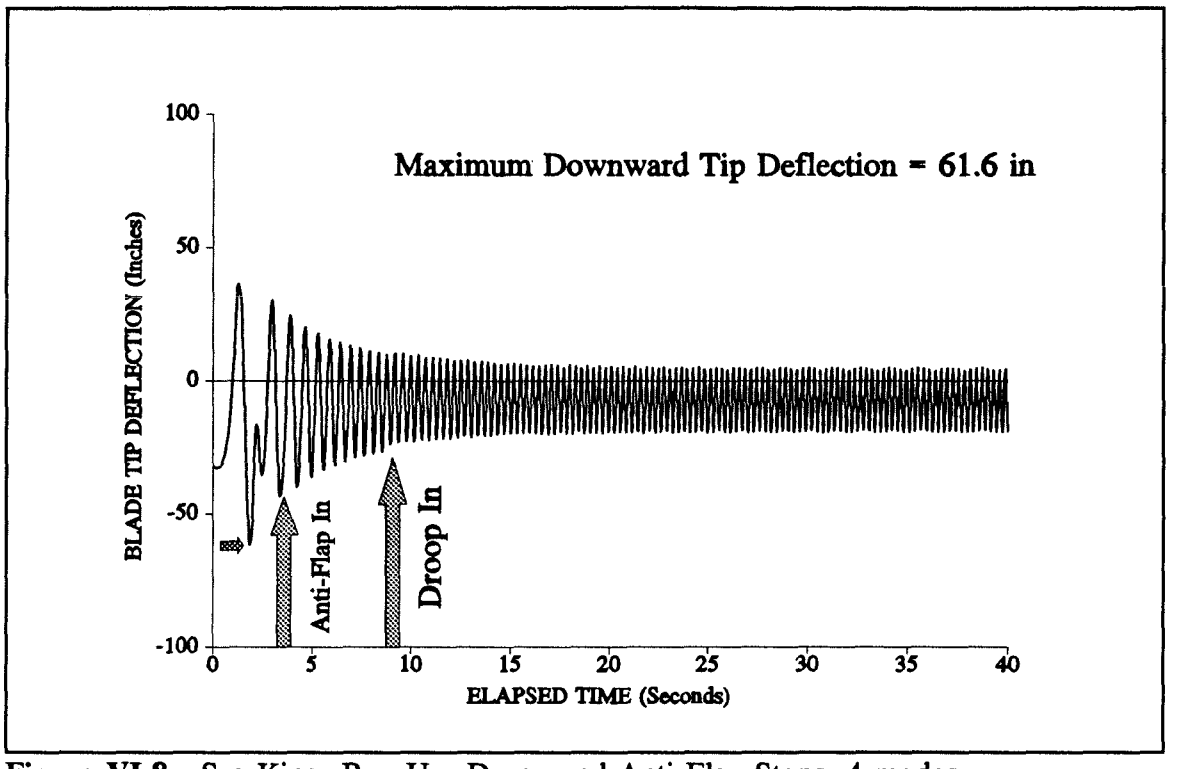

Figure VI.8 - Sea King, Run Up, Droop and Anti Flap Stops, 4 modes

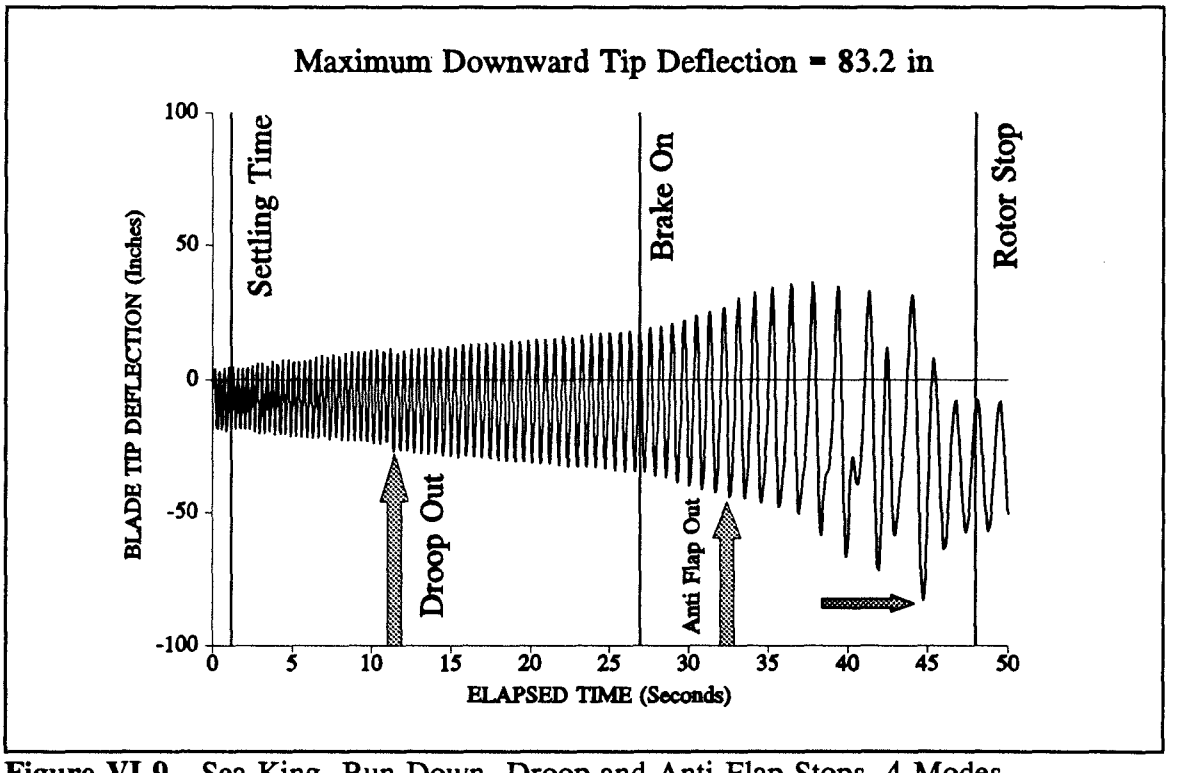

Figure VI.9 - Sea King, Run Down, Droop and Anti Flap Stops, 4 Modes

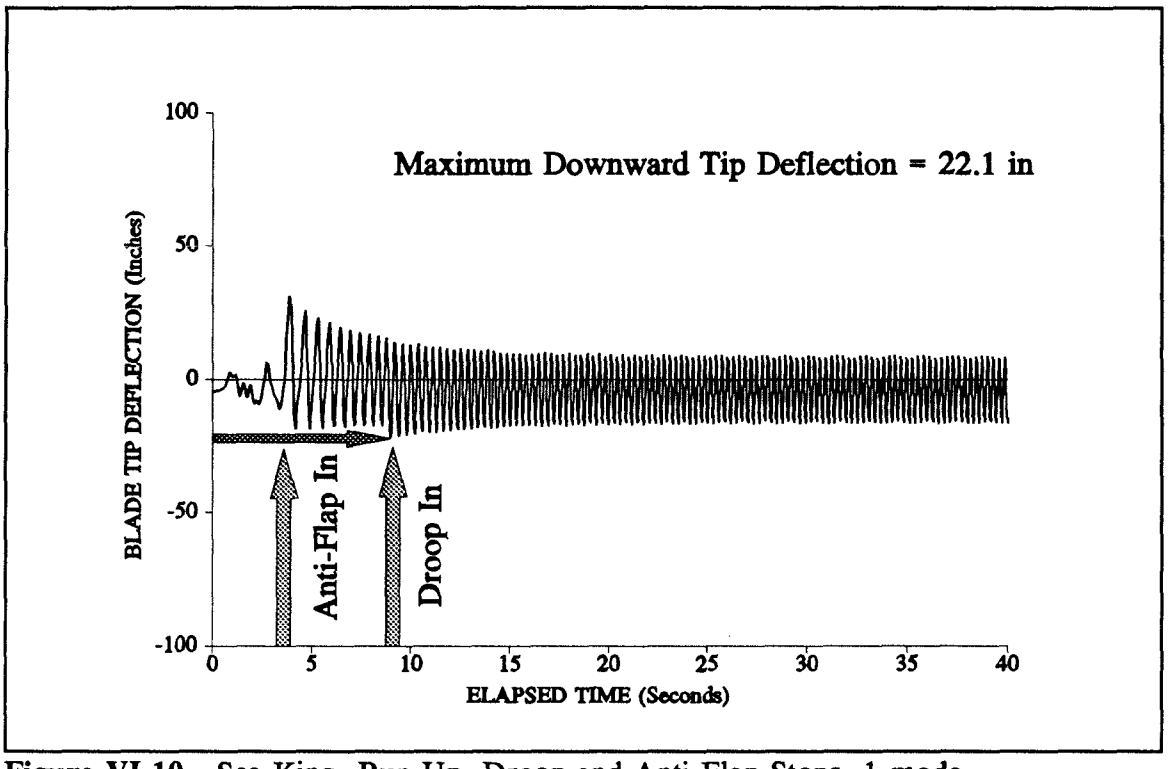

Figure VI.10 - Sea King, Run Up, Droop and Anti Flap Stops, 1 mode

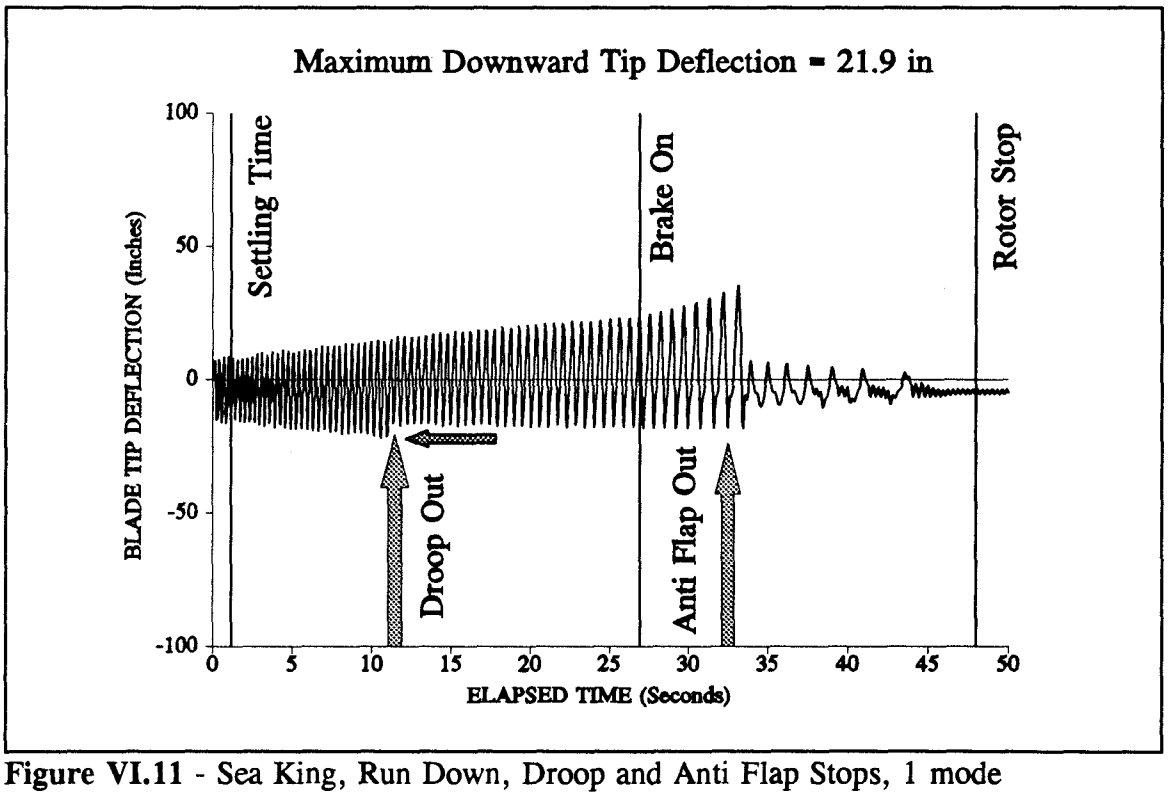

Figure VI.11 - Sea King, Run Down, Droop and Anti Flap Stops, 1 mode

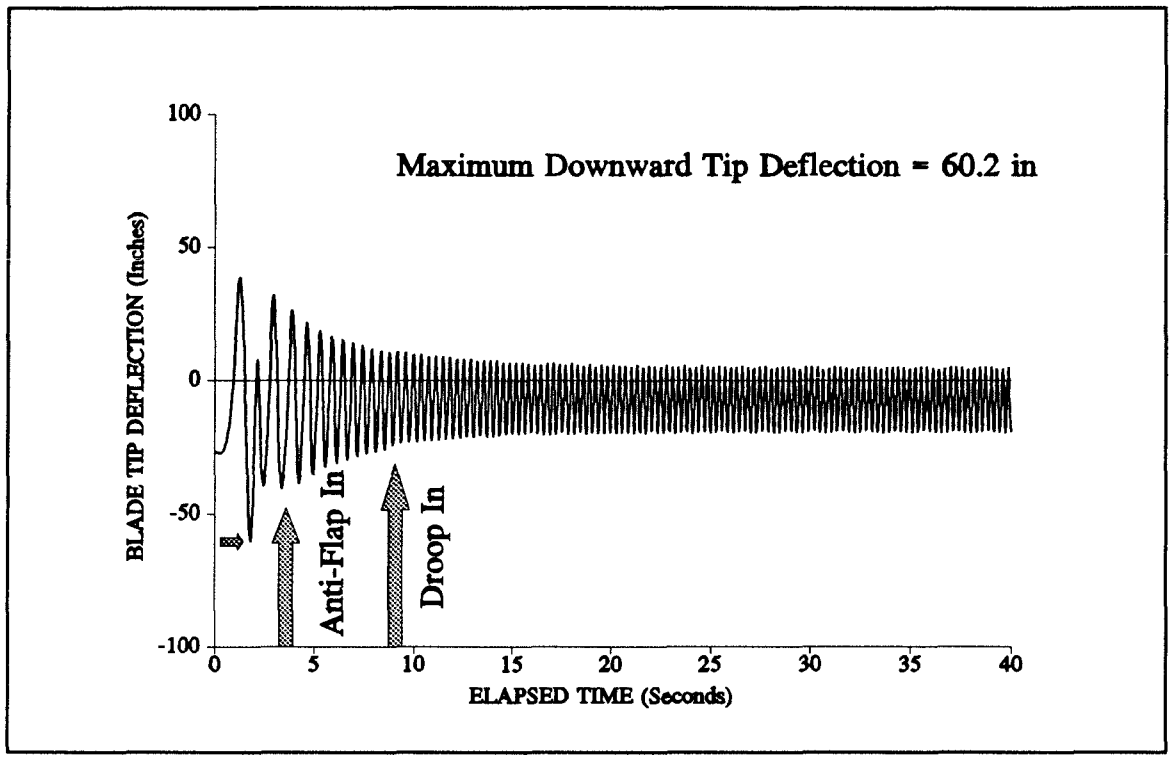

Figure VI.12 - Sea King, Run Up, Droop and Anti Flap Stops, 2 modes

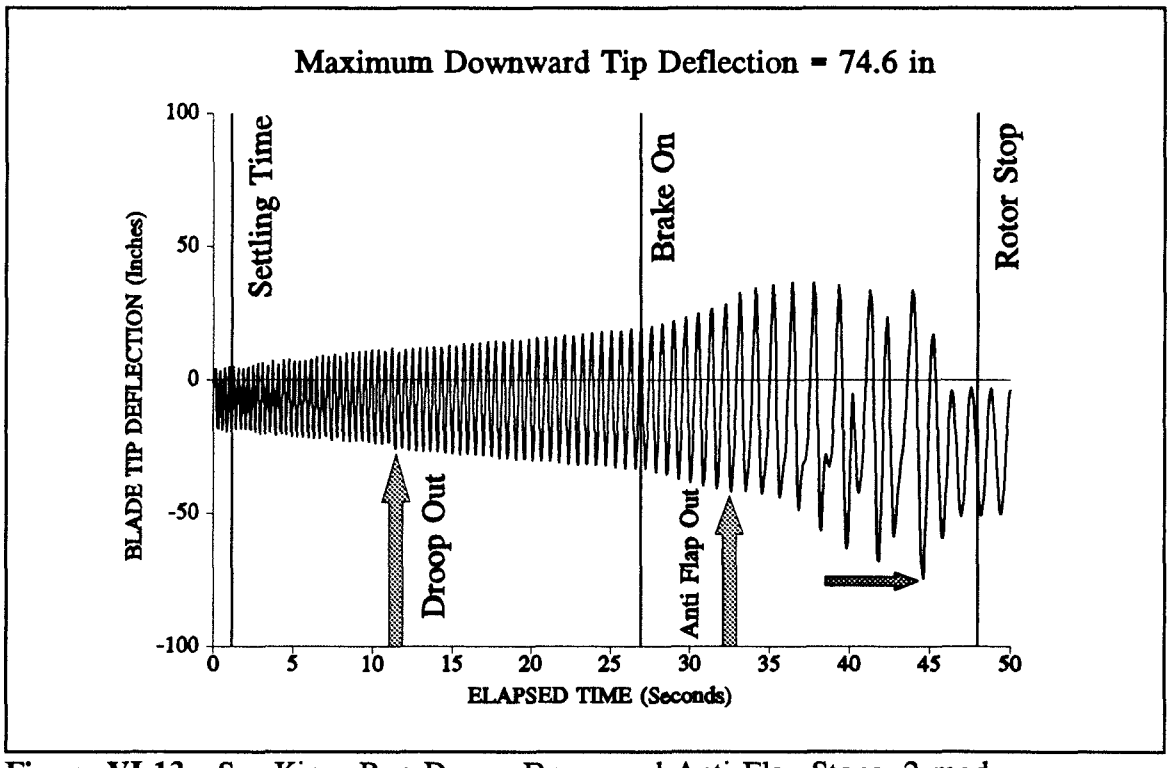

Figure VI.13 - Sea King, Run Down, Droop and Anti Flap Stops, 2 modes

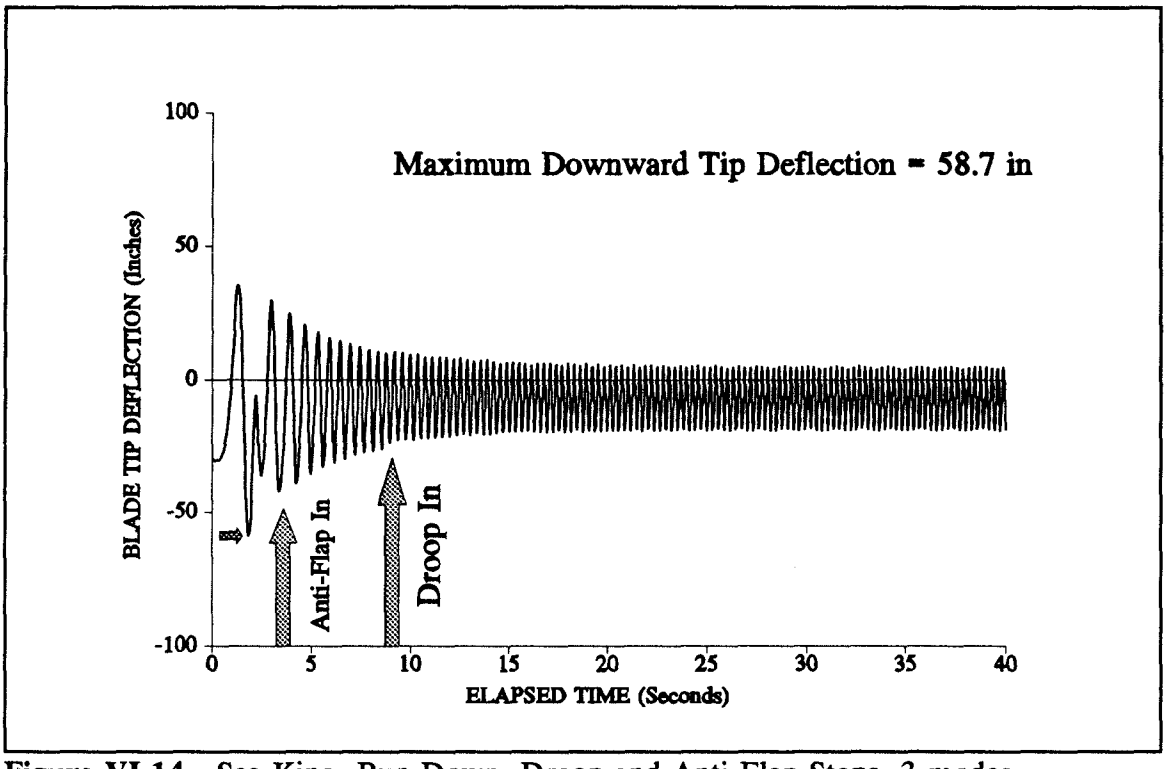

Figure VI.14 - Sea King, Run Down, Droop and Anti Flap Stops, 3 modes

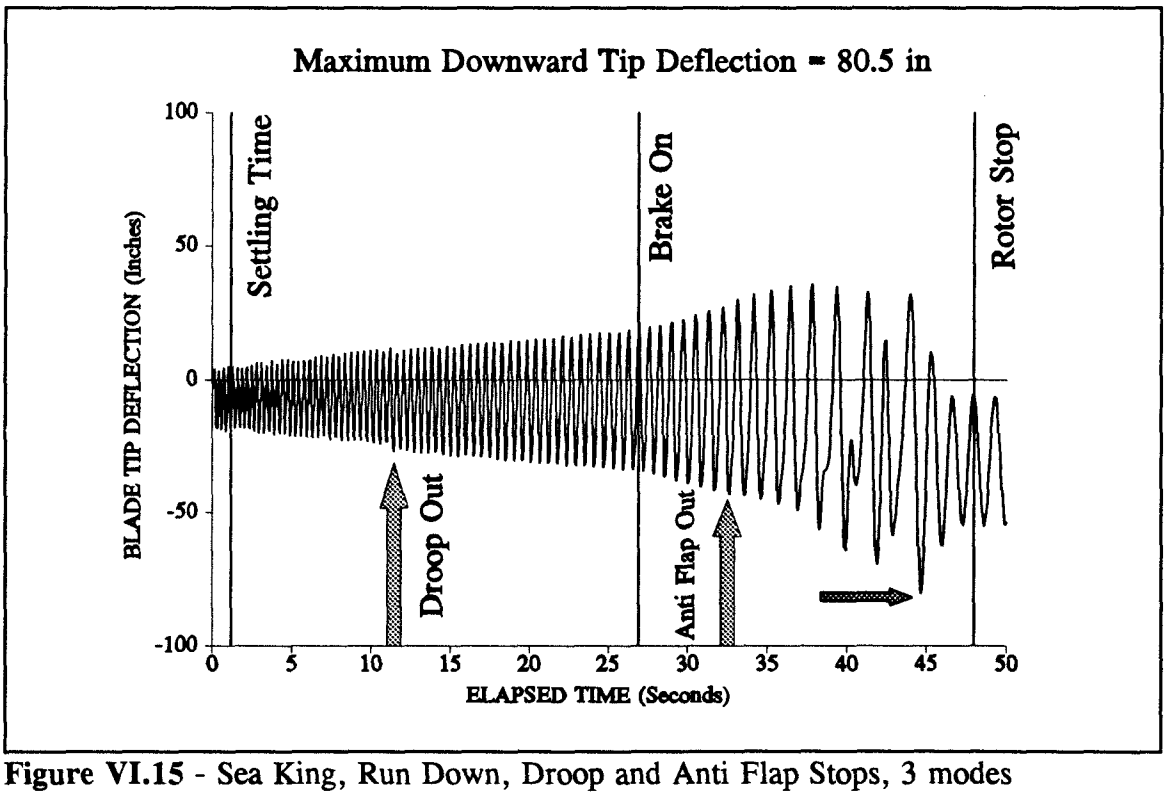

Figure VI.15 - Sea King, Run Down, Droop and Anti Flap Stops, 3 modes

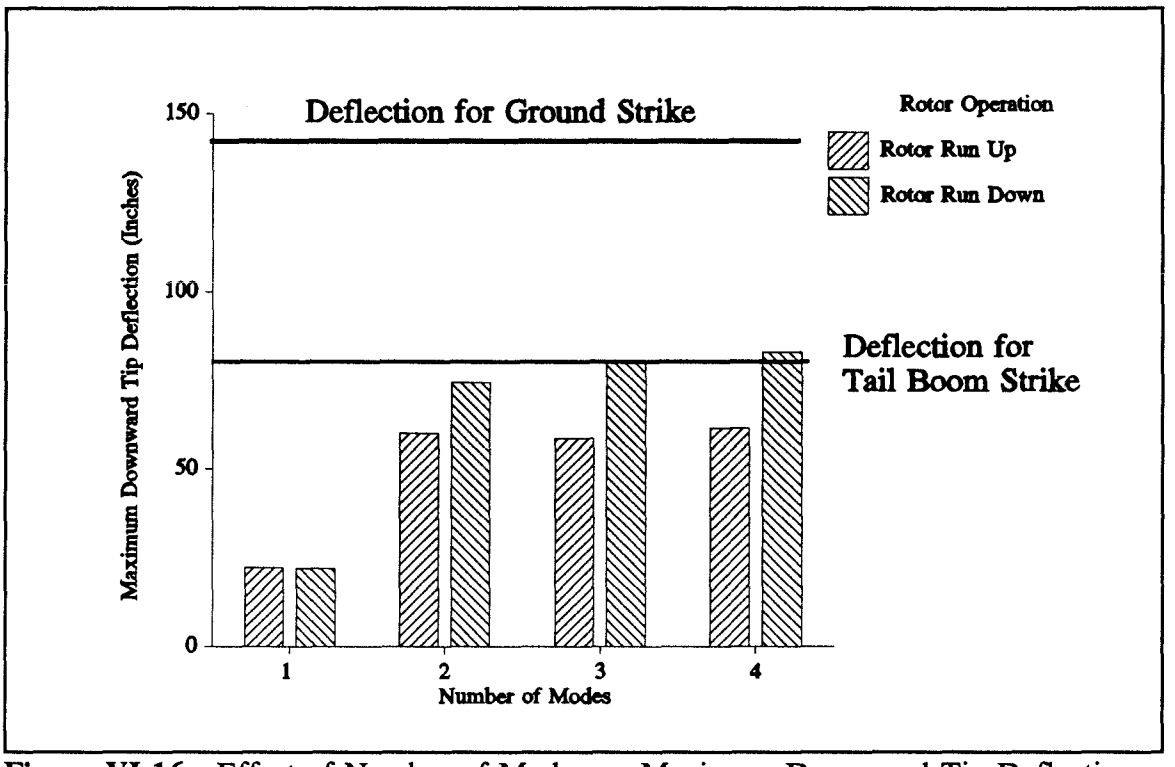

Figure VI.16 - Effect of Number of Modes on Maximum Downward Tip Deflections

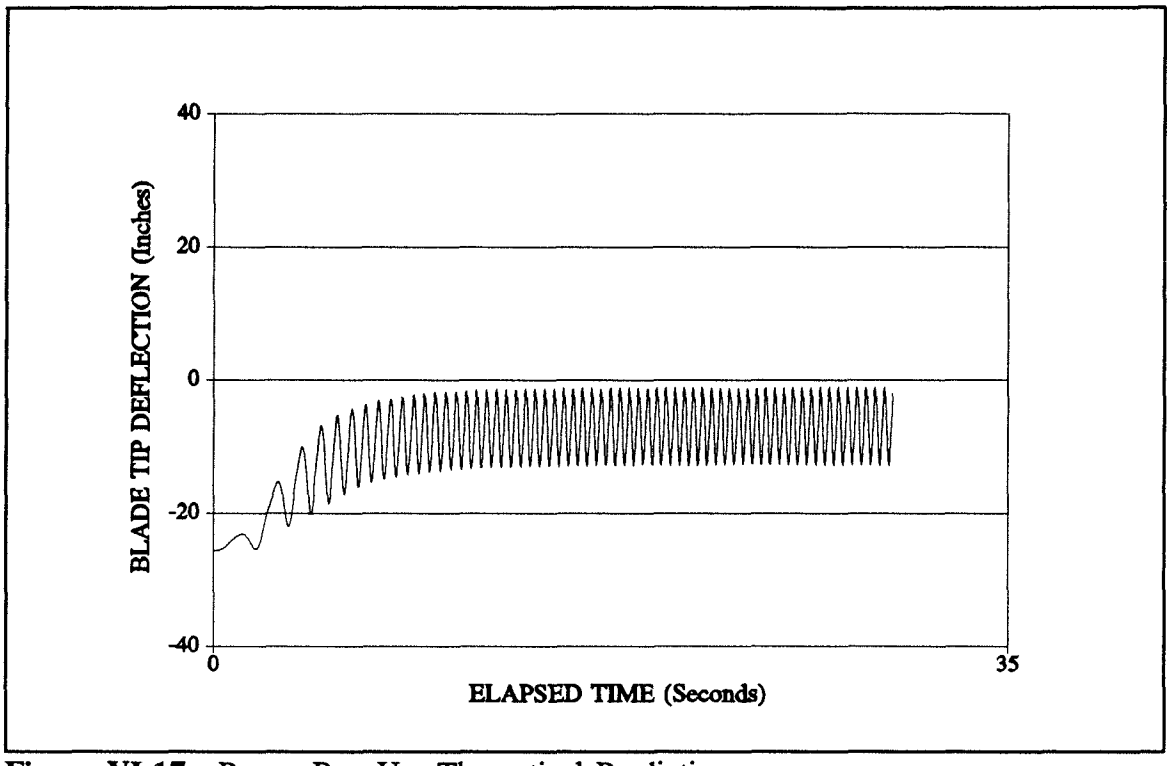

Figure VI.17 - Puma, Run Up, Theoretical Prediction

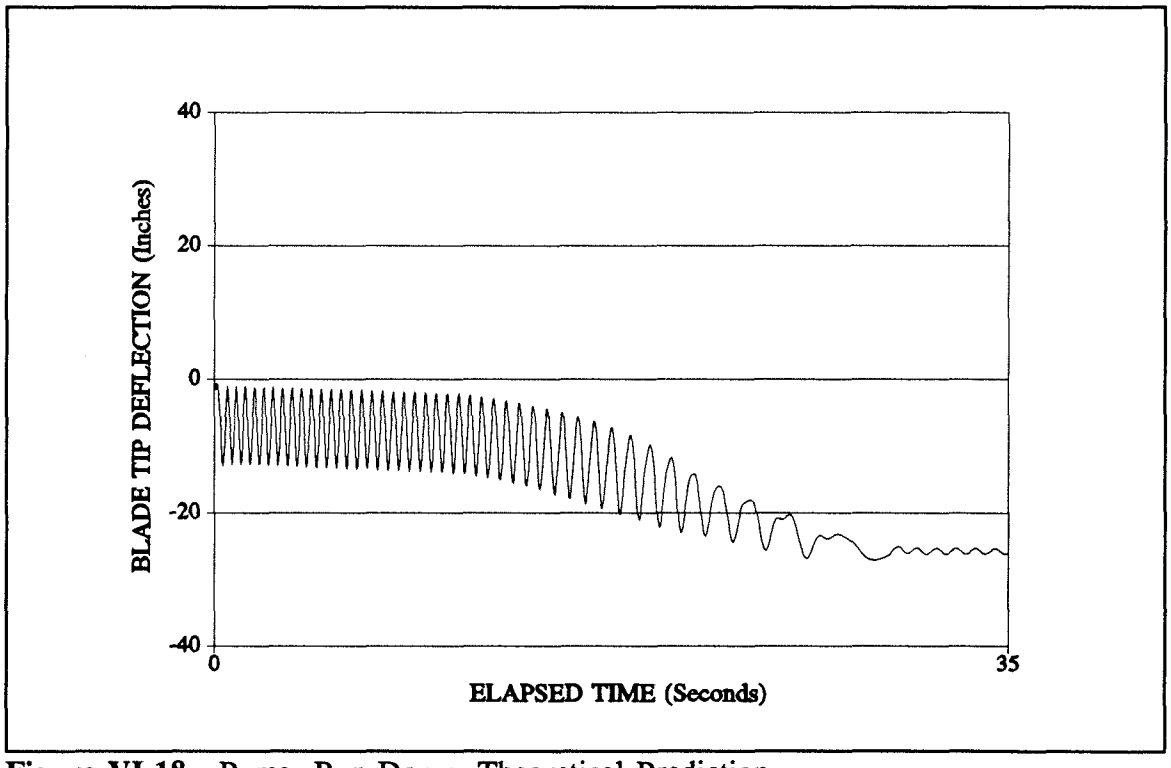

Figure VI.18 - Puma, Run Down, Theoretical Prediction

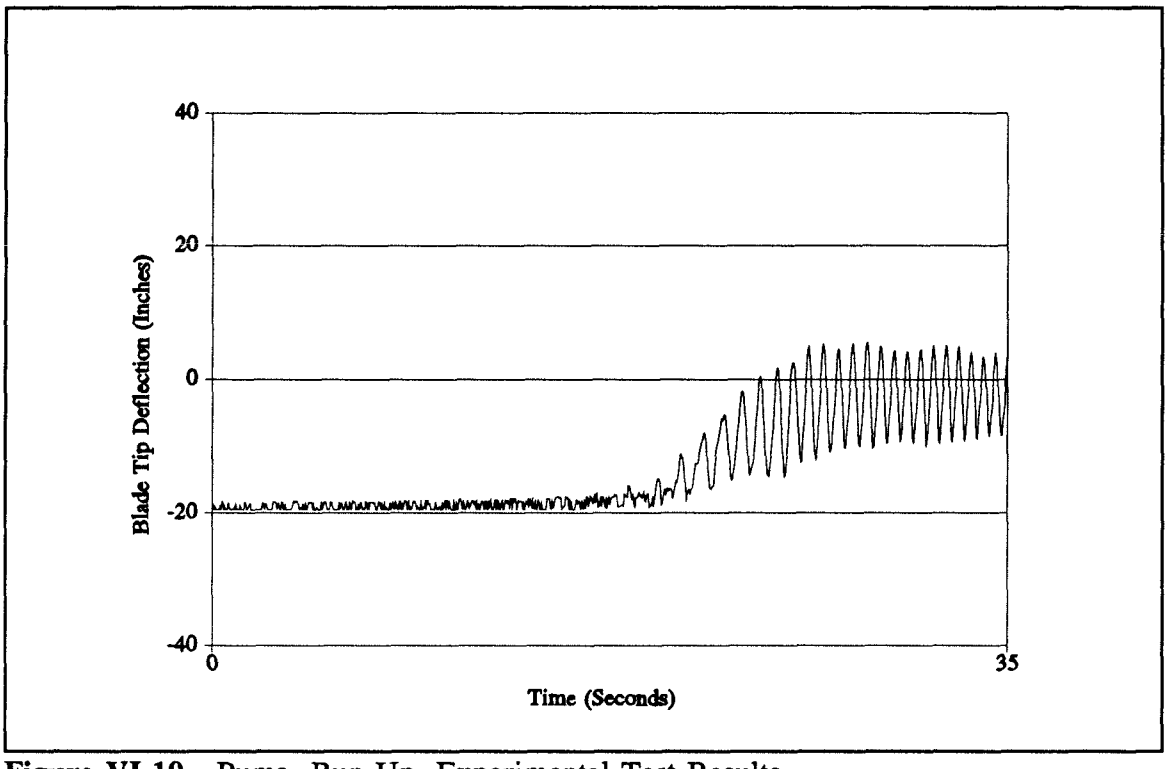

Figure VI.19 - Puma, Run Up, Experimental Test Results

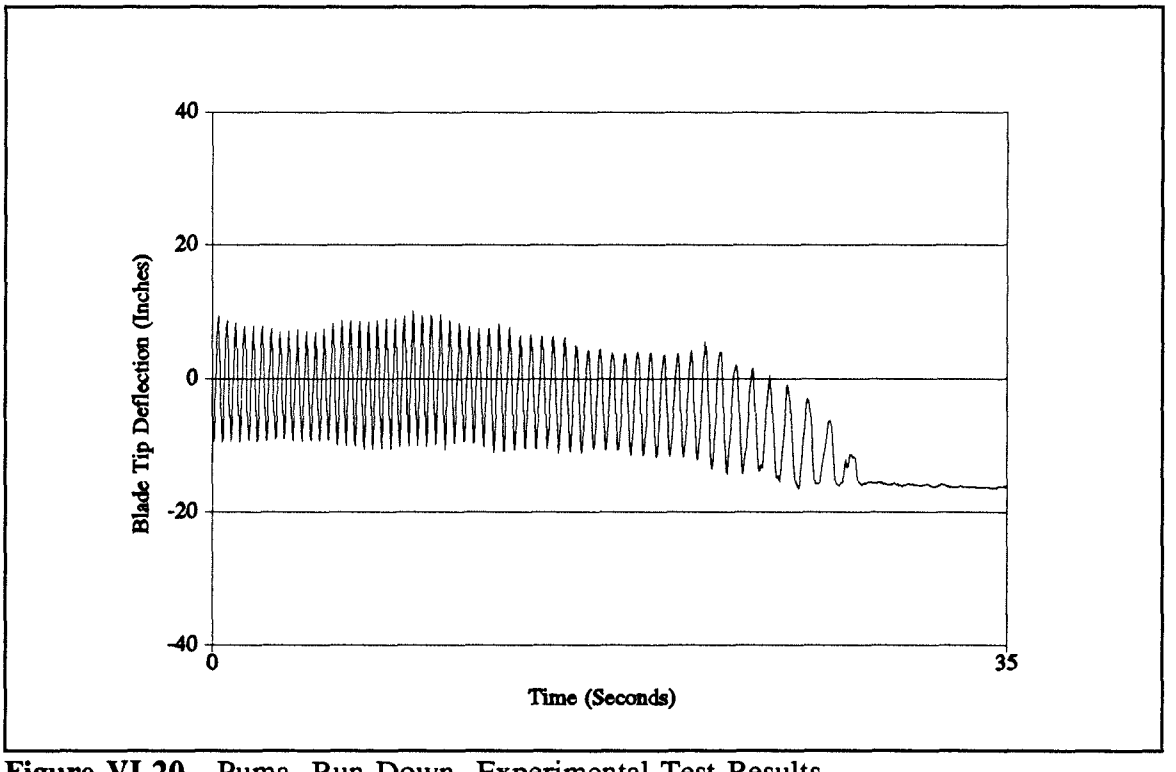

Figure VI.20 - Puma, Run Down, Experimental Test Results

CHAPTER 7

CONCLUSIONS AND FURTHER WORK

7.1 INTRODUCTION

The research described in this thesis has been conducted over a not inconsiderable period of time. The knowledge has tended to be of the slow release variety but as the blade sailing phenomenon was a completely undetermined quantity from the outset, efficient use of time resources and funding has required that a comprehensive appraisal of recently acquired results is made before the next stage of the work was planned.

This final chapter overviews the salient results of the work programme and discusses the potential directions which the research into blade sailing should prove the most beneficial. This final section could be a simple list of what should have been done in addition to that already completed. This is not the intention because the results obtained in this work have put the blade sailing problem in context and erroneous preconceived ideas about its occurrence have been put right. The influence of the ship's flight deck and superstructure is not just important but vital to the ultimate goal of accurate blade sailing prediction. The later reference surveys have shown that the airflow over a ship is the subject of work conducted in, particularly, America and Australia.

The complications of the flow over the ship needs careful study and, in addition, the unsteady character of these flow patterns also needs clarification. The effect of size and turbulence frequency on the wind tunnel results must be addressed. This last statement is a particularly important one as the occurrence of a blade sailing incident can *"come out of a blue sky"*. A rotor engagement or disengagement can be under way in an apparently innocuous manner when a sudden shift in the flow separation point or flow direction can trigger a large blade tip deflection to occur. This insidious nature of the blade sailing phenomenon makes it so potentially dangerous.

7.2 CONCLUSIONS

Wind Tunnel Tests - Chapter 2 describes a wind tunnel test which has shown that the flow induced by a ship's hull on a horizontal wind triggers considerable blade flapping behaviour on a helicopter operating from the flight deck. The location of the helicopter has a very important influence on the blade sailing behaviour of the rotor and the positions form two distinct groups. These groups exist because of the flow states over the flight deck are dominated by either the deflected freestream or the substantial region of turbulence caused by the separation off the windward deck edge.

Theoretical Rigid Blade Model Comparisons - To investigate blade sailing in a parametric manner, Chapter 3 describes a theoretical model and associated computer programme which have been constructed and which achieved very good agreement with the test results. The rotor controls were set to zero collective and cyclic pitch and the agreement was very successful at the low rotor speed parts of the rotor engagement and disengagement. There was a small degree of difference in the blade flapping amplitude at the maximum rotor speed which could be corrected by the introduction of approximately 1° of cyclic pitch. Comparing the results with and without the application of cyclic pitch shows the only differences occur at rotor speeds near the maximum and this indicates that the relative inability of cyclic pitch to control the sailing of a rotor blade. The good agreement was only achieved by using data obtained by a comprehensive LDA traverse and analysis of the velocity component data, over the ship's deck, into mean and standard deviation values. Use of a simplified wind specification model can only produce results of any value for deck locations towards the windward deck edge. However, it cannot cater for the blade behaviour at the two deck locations nearest the leeward deck edge.

The blade sailing behaviour obtained in the 7ft by 5ft wind tunnel was consistent with the first LDA velocity traverse conducted in the 11ft by 8ft facility, however, differences between the test results and the theoretical predictions were noted in the single blade behaviour at the A deck position. Here the differences were in the area of the amount of downward blade flapping which places the blade tip region close to the deck surface. In the LDA traverse a set of measurements were taken at approximately 1 foot above the deck and the theory interpolated between these values and an assumed value of zero at the deck surface (*no slip condition*) in its calculations. There will obviously be much activity in this region and a further test was conducted to examine more points in this important region. There is a discrepancy, albeit small, between the coning angles produced by the tests and the theory. The theoretical predictions make sense for a normal rotor system but for some reason one model blade is tracking high. The reasons for this have yet to be determined, but the problem is relatively minor compared to the overall success of the comparisons.

In Chapter 2, the set of wind tunnel tests investigated the blade sailing behaviour of the experimental model in more depth. The number of blades was one or two, and two

collective pitch settings were used. It was hoped to test a higher third value of collective pitch but the electric drive motor was marginal in power on some cases with the medium collective pitch value of 6° and so higher values were not tested. It proved difficult to isolate universal trends in the results which agree across the complete time history of the rotor operation. However, in order to assess, in a quantifiable manner, the time histories were examined in two areas.

Firstly, in order to gain a feel of the turbulence of the air surrounding the rotor at a given condition, and the response of the blades to it, the central maximum rotor speed behaviour was examined to produce mean and vibratory amplitudes. Secondly, the long run down phases were examined with the number of contacts with the blade flapping stops noted. This was seen as a measure of the severity of the blade sailing.

The conclusions of this set of tests are detailed below:

- *General comment on deck location.* The variations in blade behaviour between deck locations A-C and D-E are again highlighted.
- *Rotor at maximum rotor speed.* For the two bladed rotor configuration, deck location B appears to be the worst case for low collective pitch, whilst the windward deck edge location A becomes the worst as the collective pitch increases. It would seem that the large upward flow velocities at this location can influence a higher collective pitch setting.
- *Differences in behaviour between rotor configurations.* Medium collective pitch gives the single blade rotor configuration a not unexpected but substantial increase in coning angle. However, the vibratory rotor flapping is also markedly increased. A lowering of maximum rotor speed with a fixed wind tunnel speed gives the anticipated increase in vibratory blade flapping which for deck location C was virtually pro rata with the consequent increase in advance ratio. At deck location B a halving of the wind tunnel speed reduces the coning angle of the single bladed rotor and the vibratory flapping amplitude, for both rotor configurations, reduces by about 40%.
- *Run down behaviour.* Generally the single blade rotor configuration strikes the stops more frequently than the two blade teetering rotor. This may be affected by the fact that the counterbalance weight, of necessity, matches the first moment of the blade it replaces but will have a lower value of inertia giving an increase in

effective Lock number.

- *Blade/stop strikes.* The two blade teetering rotor strikes the upper stop most at deck location B whilst the single bladed rotor is worst at A. Downward stop strikes are worst at B for two blades but marginally C for a single bladed rotor.
- *Variation of collective pitch.* As regards blade/flapping stop contacts, increasing the collective pitch has a detrimental effect on the single bladed rotor.
- *Variation of rotor speed.* Halving the rotor speed, at deck location C causes an increase in stop contacts.
- *Variation of wind speed.* Halving the wind tunnel speed for deck location B dramatically reduces the severity of the blade sailing behaviour.

The dangers of deck locations A and B are now apparent and with the advent of the EH101 Merlin helicopter operating from Type 23 frigates, the interaction of the rotor blades with the incoming flow from an abeam wind has the potential to be very hazardous. Wind tunnel experiments can now be considered to see whether devices such as deck projections can be used to minimise the damaging effect of the wind.

Finally, the tests to date have only considered zero cyclic pitch. A recent library search has highlighted attempts to devise a control philosophy to predict and respond to a potential blade sailing incident and avoid it using the pitch controls. The ability of the rotor to respond must be limited by the aerodynamic pressure obtained at low rotor speeds. The effectiveness of cyclic pitch can be readily observed with the model and this would be a valuable addition to the results.

The rerun of the wind tunnel tests with the LDA set up was conducted using an improved seeding arrangement and a more extensive grid structure for the test point locations. More confidence in the results has been achieved together with a greater understanding of the flow behaviour surrounding the ship.

The agreement between the first tests and the predictions with the coarser grid data was good, however, the agreement with the finer grid data is better. The variation of the lowest blade positions has been improved during the run up or run down manoeuvres. This aspect was noted in the first set of test comparisons and provided evidence that the ship flow velocity data was deficient close to the deck surface and that a more detailed survey of this area would be advantageous. All of these factors vindicates the decision to conduct the second set of LDA tests.

These two sets of tests have produced data which is a consistent explanation of the existence of helicopter blade sailing. Theoretical modelling can accurately predict the blade behaviour in virtually every case. For the other cases, the differences are small but further work will aim to eliminate these as well. The methods employed in the theory have been used in a second calculation method which allows the blade freedom in flapwise bending which has been described in Chapter 6. The success of the rigid blade modelling generates confidence in the more involved calculations for the flexible blade.

Introduction of Blade Flexibility to Theoretical Model - Chapter 4 describes the derivation of a method allowing for blade flexibility. This is achieved by using flapwise blade modes to decide the flapping motion. The equations are not compatible with a closed form solution, particularly because of the inclusion of highly non-linear aerodynamics and the possible impacts of an articulated blade with a droop or anti-flap stop. For this reason, a fourth order Runge Kutta method was used to integrate the equations of motion.

Application of Flexible Model to a Semi-Rigid Rotor - In Chapter 5, the method is applied to the Westland Lynx semi-rigid rotor. Hot wire anemometer results conducted in the Department's 7ft by 5ft wind tunnel were used to evaluate the blade sailing using the modal method of Chapter 4. The importance of ship yaw angle was demonstrated. Unfortunately due to the directional characteristics of the hot wire probe only rearward incident wind directions could be reliably investigated. The effect of rotor geometry and other inputs to the blade motion were also investigated. The results showed that a downward tip deflection of 32 inches was achievable which is 43% of that required to strike the tail cone.

Application of Flexible Model to an Articulated Rotor - Chapter 6 discusses the blade sailing theoretical model, described in Chapter 4 and its application to articulated blades with the mechanical hub restraints found on such rotor heads.

The blade deflections produced are substantially in excess of those for semi-rigid rotors, and for the Westland Sea King are of the order of 85 inches in a steady 50 knot wind. A figure of 146 inches is required for blade tip contact with the ground in front of the cockpit, and with a more adverse wind condition this amount of blade flapping seems attainable, particularly if the second flapwise modal response is increased. A downward flapping angle of 13°, corresponding to a tip deflection of 81 inches, is required for a

blade strike on the tail boom, which is within the predicted results obtained. The importance of including higher order modes in the representation is demonstrated.
A comparison has been made with a test using a full size Puma aircraft. The basic characteristics of the response are accurately modelled, but small differences are seen in the steady state coning angle and the stationary blade position against the droop stop. The former indicates that inaccuracies in the specification of collective pitch angle or rotor inflow may be present. The latter is a result of the spring approximation of the hub restraints and a possible solution of this problem is the introduction of two sets of modes allowing the modal description to vary from cantilever to pinned during the motion. Whether this is necessary for blade sailing purposes requires further evidence, but the modelling of the hub using spring restraint mechanisms shows encouraging agreement as far as the oscillatory response is concerned.

7.2 FURTHER WORK

It is the author's hope that the research described herein provides an important statement concerning the ability to determine the possible occurrence of helicopter blade sailing and to predict its magnitude. As is usual, many questions are answered but to fulfil the continuity equation many more are posed! This final section aims to highlight the most appropriate course of future action to answer these questions and to enable blade sailing to be fully understood and in consequence avoided, if at all possible.

- The wind tunnel tests showed the large variation in flow patterns over the flight deck. The literature search has shown the importance which the helicopter community puts on this problem and its full implications. Consequently it is vital that this is fully explored. A considerable amount of work has been performed already and a full appraisal of the results would seem a prudent place to start. Further LDA work on the flow characteristics over various types of ship (and perhaps oil rig) together with the ensuing turbulence would seem a proper course of further study. Because of the hazards of blade sailing occurrences, model testing would form the most sensible way of pursuing the potentially worst conditions. To do this accurately the effects of scale on separation behaviour and turbulence frequency would also need to be addressed.

- The modelling of the blade modes and in particular the change in characteristics when contacting mechanical stops need further investigation. The blade sailing method

should be applied to a greater number of existing and proposed blade designs. Their susceptibility to blade sailing would provide useful design pointers for the immediate future.

■ As already mentioned, the aerodynamic theories used to calculate the blade forcing require the effect of Reynold's Number to be examined. The large changes in incidence will generate stall and the influence of dynamic stall modelling will need to be determined. This thesis takes the airflow problem and applies it to the rotor aeroelastic equations of motion to model the blade behaviour. The driving force is, naturally, of aerodynamic origin and the incorporation of realistic predictions of lift is an important area in which blade sailing could be effectively studied. The differences between a sailing rotor blade and one operating at normal rotor speeds is highlighted by two aerodynamic phenomena. Firstly, that of Reynold's Number. The quantitative input to the method was of the N.A.C.A. 0012 aerofoil operating at a Reynold's Number applicable to normal operating rotor speed. At the low rotor speeds where blade sailing can be expected, the low Reynold's Number behaviour of aerofoil sections must be studied and incorporated into the method. Secondly, is the interpretation of the blade aerodynamics in a dynamic sense. The present model caters for high incidence stall effects but in a quasi-steady manner. The large variation in incidence angle and the frequency of its changing is sufficient evidence for the study of the dynamic stall behaviour of suitable rotor blade aerofoil sections to be undertaken and to determine the effect of these phenomena on the lift generated.

■ The deficiency in the blade dynamics structural modelling where the non-linear effects of large modal deflections are not considered will need to be examined. The relatively colossal blade flapping excursions must require that the method allows for the foreshortening of the blade in an axial sense and the combination of the modal contributions.

■ The aspect of rotor downwash has for a number of years struck fear into the author's heart. The difficulty of predicting downwash distributions in the most benign situations is well known. The assumption of zero collective pitch, giving nominally zero rotor thrust, is perhaps reasonable but with the blades generating considerable lift forces, localised downwash cells must occur. A quick fix has been tried with success, but an in depth look at the downwash problem must be addressed, no matter how daunting.

To conclude, the connection between bridge trusses and rotor blade flapping hinges was drawn. The autogyro was the original generator of these mechanical devices, and the structural engineer in the shape of Juan de la Cierva provided the link, see Townson[41]. Blade sailing has been a puzzle in that its importance and potential dangers have been highlighted by many conversations with naval helicopter pilots, but there does not seem to be a commensurate amount of work conducted on the subject, at least in the public domain. Full scale comparisons with the emerging theories would be a much needed fillip.

The only full scale data obtained to date has been with a Puma aircraft engaging and disengaging its rotor in winds of 10 knots. The agreement, see Newman[5], was good. This gave confidence but it felt hollow as a victory in that this was hardly a severe situation. It is the author's hope that a detailed description of instances of blade sailing can be compiled for later comparison. This may be viewed as a tall order considering the perversity of its occurrence. However, using aircraft for dedicated testing is seen as impractical. Perhaps Boeing Vertol's Internal Memo[42] will provide a good starting point, however, such information is sensitive and is not normally in the public domain.

Recent contacts with Aeronautical Research Laboratory, Melbourne, Australia, and The University of Pennsylvania have shown that the blade sailing phenomenon is now being actively pursued elsewhere in the world. These contacts must and this work will be maintained.

APPENDIX A

AERODYNAMIC MODEL

A.1 INTRODUCTION

Two aerodynamic models were used for the analysis. The first is the simple constant lift curve slope assumption where the incidence multiplied by an input constant provides the appropriate lift coefficient. This was used only in the formative development of the method. The second aerodynamic model is described in Beddoes[36] and a brief description follows.

It is an empirical model using a series of parameters to specify the variation of normal force coefficient with incidence for a series of Mach numbers. For a given Mach number the parameter values are determined by linear interpolation.

A.2 METHOD

The method is a quasi-steady theory developed from a method by Kirchoff which admits a trailing edge stall. The model specifies the normal force coefficient (C_N) below and above the stalling angle appropriate to the respective Mach number. As the incidence increases, the separation point starting at the trailing edge progressively moves forward until at an incidence of α_1 it is positioned at the 70% chordwise station (from the leading edge), and at this point the aerofoil section is considered to have stalled. The set of parameters defined are α_1 (the stalling angle), $C_{L\alpha}$, S_1, S_2.

The trailing edge separation point is defined by:

$$f = 1.0 - 0.3e^{\frac{\alpha - \alpha_1}{S_1}} \tag{A.1}$$

for $|\alpha| \leq \alpha_1$ *(i.e. unstalled)*

$$f = 0.66e^{\frac{\alpha_1 - \alpha}{S_2}} + 0.04 \tag{A.2}$$

for $|\alpha| > \alpha_1$ *(i.e. stalled)*

from this value of f the normal force coefficient is given by:

$$C_N = \frac{1}{4} C_{L_\alpha} \sin \alpha \left(1 + \sqrt{f}\right)^2 \tag{A.3}$$

and the lift coefficient is obtained using the pitch angle θ:

$$C_L = C_N \cos\theta \qquad \textbf{(A.4)}$$

The NACA 0012 aerofoil section was used for the investigation. It is appropriate to the Westland Sea King and at low Mach numbers to the Westland Lynx NPL 9615 section which is itself based on NACA 0012 for the rearward 70% and a drooped nose for greater Mach number penetration on the advancing side. The rotor rig used in the wind tunnel tests used a cambered section, but these types of rotor blades are normally based on NACA 0015 type sections and so use of NACA 0012 data for the low Mach numbers found during the tests were considered justified. The camber was allowed for by using an appropriate no lift angle.

The data for this is tabulated in Table A.1:

Table A.1 - Aerodynamic Model Input Data for NACA 0012 Aerofoil

Mach Number	$C_{L\alpha}$	α_1	S_1	S_2
0.30	6.188	0.2443	0.02443	0.02443
0.35	6.388	0.2204	0.02758	0.04302
0.40	6.589	0.2025	0.02967	0.05585
0.45	6.772	0.1868	0.03002	0.06144
0.50	7.019	0.1710	0.02793	0.06283
0.55	7.334	0.1580	0.02443	0.06161
0.60	7.706	0.1449	0.02094	0.05760
0.65	8.251	0.1297	0.01745	0.04974
0.70	9.053	0.1065	0.01396	0.04014
0.75	10.227	0.0750	0.01047	0.02967
0.80	12.748	0.0401	0.00698	0.01745

The variation of the separation point, f, with incidence is plotted in Figure A.1 and the corresponding variation of C_L in Figure A.2.

As can be seen the data is supplied at Mach numbers from 0.3 to 0.8 in steps of 0.05. For Mach numbers below 0.3, the values at 0.3 are used. For Mach numbers in excess of 0.8 the accuracy cannot be guaranteed and so the method aborts.

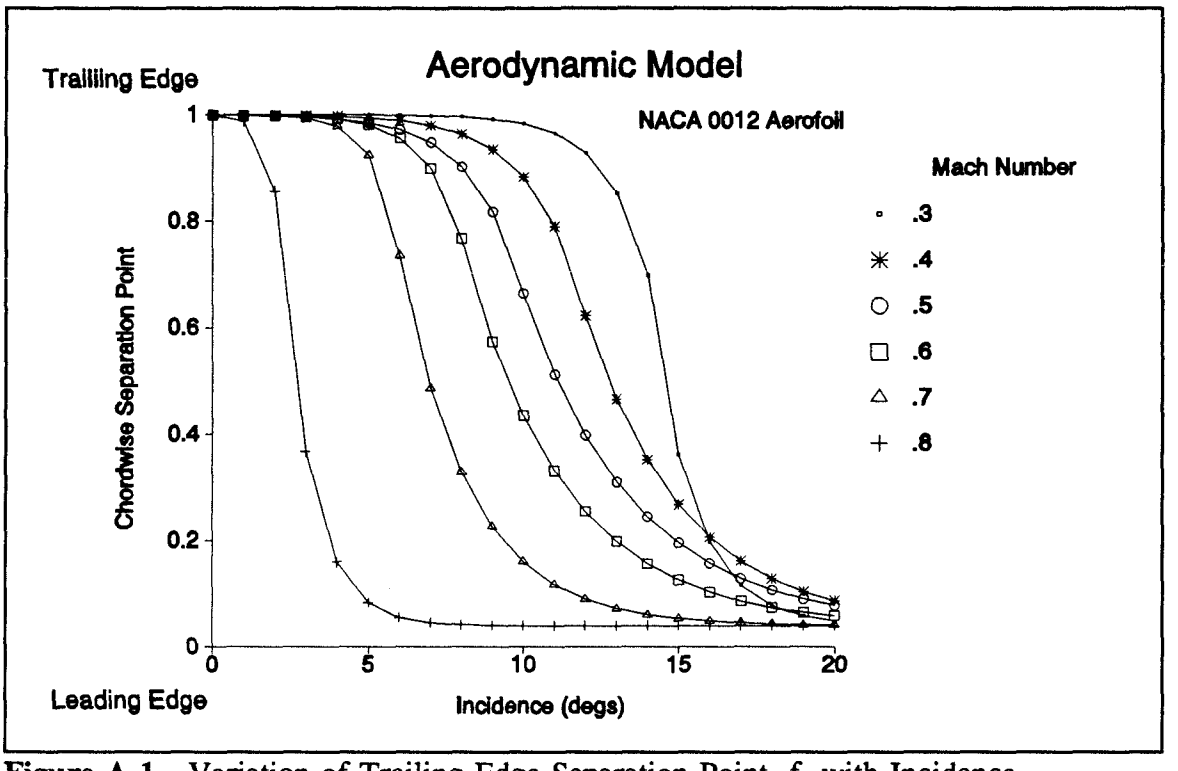

Figure A.1 - Variation of Trailing Edge Separation Point, f, with Incidence

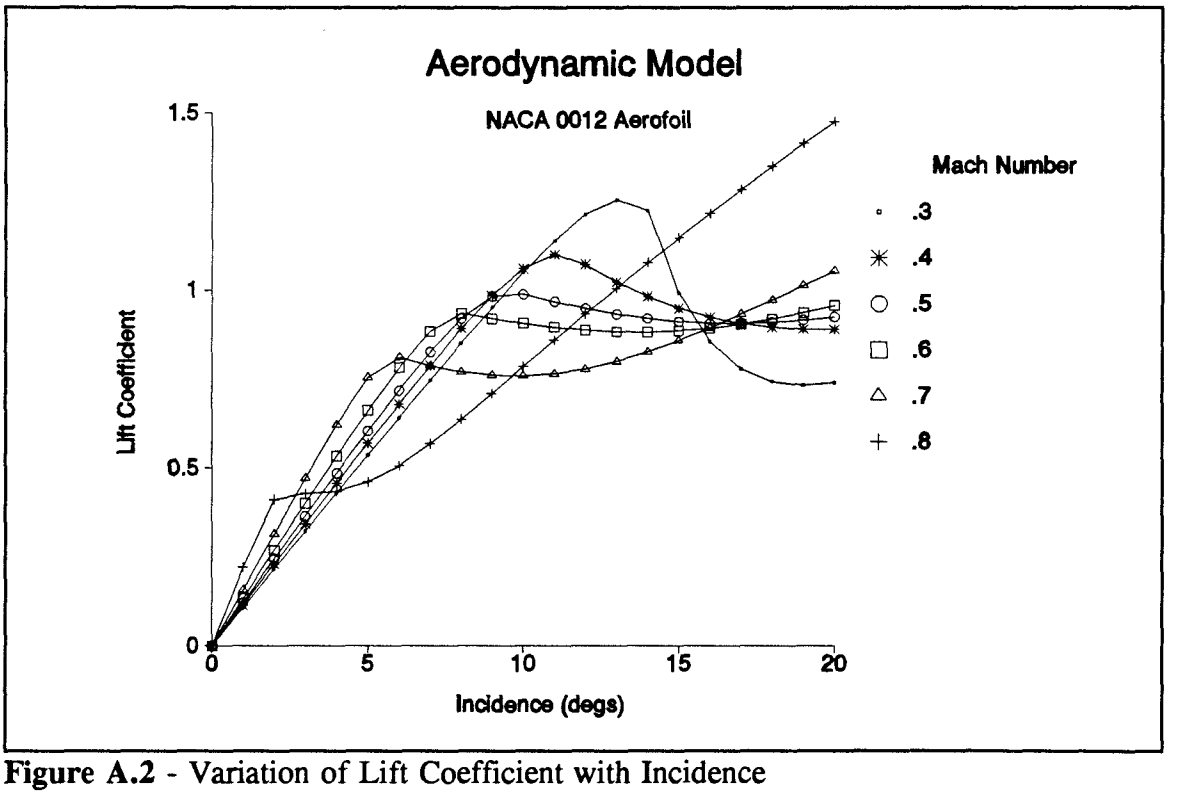

Figure A.2 - Variation of Lift Coefficient with Incidence

APPENDIX B

ROTOR SPEED VARIATION

B.1 INTRODUCTION

The variation of rotor speed was determined by an idealised theoretical model. The underlying assumptions for the method are:

(i) The rotor aerodynamic torque slowing the rotor is of the form

$$a + b\Omega^2 \tag{B.1}$$

where a and b are constants

This requires:

(ii) During run up the engine torque remains constant

(iii) During run down the rotor brake torque also remains constant

(iv) The blade control angles (collective and cyclic pitch) remain constant

(ii) and (iii) justify taking a as a constant, (iv) means that the profile drag distribution will remain unchanged with time. This is not strictly true when high Mach number effects are considered, however, it is the low rotor speed behaviour which is under consideration and so this is not considered unreasonable.

In addition to the profile torque there will also be a thrust induced contribution to the aerodynamic drag. This has been ignored since the procedure for run up or down of the rotor is to avoid a thrust on the rotor and hence minimise any blade flapping excursions. with these considerations and ignoring any effect of the gust on the C_D distribution assertion (iv) justifies taking b as a constant.

B.2 ROTOR RUN UP

The aerodynamic torque, Q_A, is given by:

$$Q_A = k\Omega^2 \tag{B.2}$$

if Q is the engine torque and I the rotor inertia, the equation of motion becomes:

$$I\frac{d\Omega}{dt} = Q - k\Omega^2 \tag{B.3}$$

using the result

$$Q = k\Omega_M^2 \tag{B.4}$$

where Ω_M is the rotor speed at which there is no net torque on the rotor. (Normally $\Omega_M=\Omega_N$, the normal operating rotor speed); (B.3) becomes:

$$I\frac{d\Omega}{dt} = k\left(\Omega_M^2 - \Omega^2\right) \tag{B.5}$$

It is evident that $\Omega \leq \Omega_M$ so equation (B.5) may be integrated to give:

$$\Omega = \Omega_M \tanh\left\{\frac{k}{I}\Omega_M t\right\} \tag{B.6}$$

i.e. the rotor speed build up is of hyperbolic tangent form. As $t\rightarrow\infty$, $\Omega\rightarrow\Omega_M$, i.e. to ultimately attain a rotor speed of Ω_M, an infinite time must elapse. This is unrealistic so a modification to (B.6) is made by saying that the rotor speed attains 99.9% of its normal operating value (ΩN) after a specified time (called the rise time). With this definition, (B.6) becomes:

$$\Omega = \Omega_N \tanh\left\{3.8\frac{t}{RISE\ TIME}\right\} \tag{B.7}$$

As an example, Figure B.1 shows a typical result of the method.

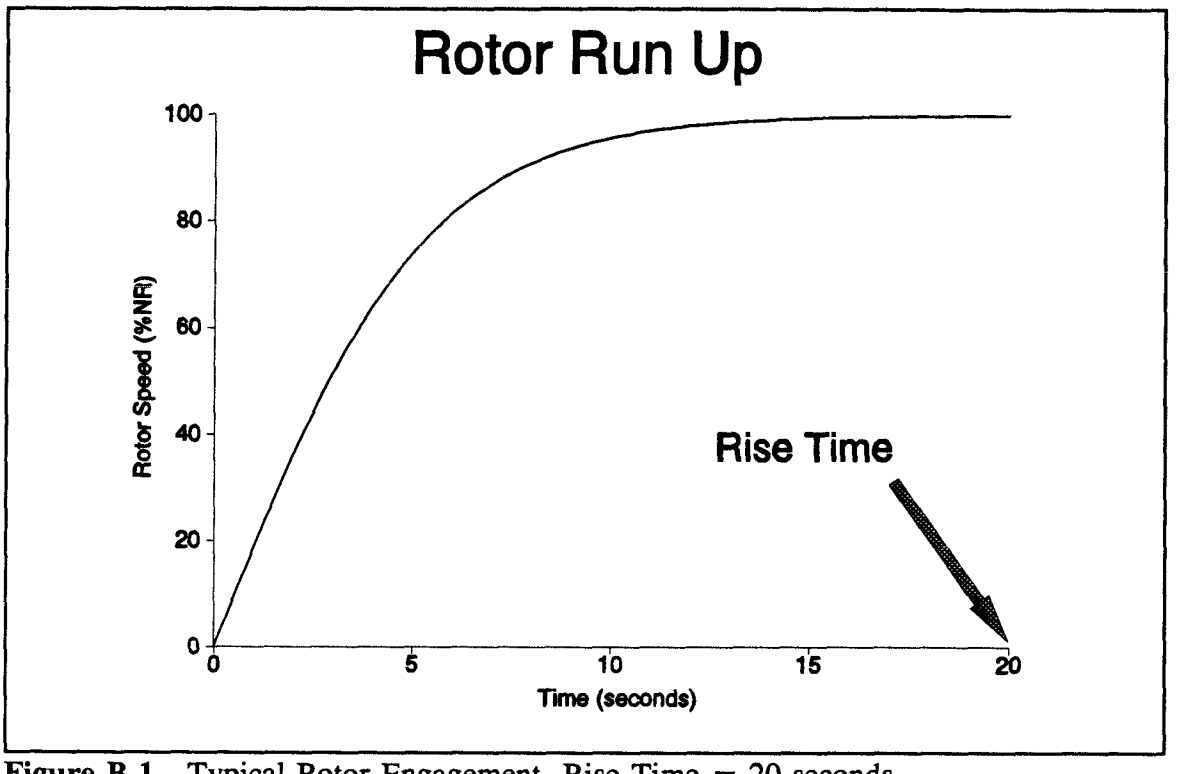

Figure B.1 - Typical Rotor Engagement, Rise Time = 20 seconds

B.3 ROTOR RUN DOWN

If Q_B is now the braking torque, the equation of motion now becomes:

$$I\frac{d\Omega}{dt} = -Q_B - k\Omega^2 \qquad \textbf{(B.8)}$$

using the definition (B.4) the following is obtained:

$$I\frac{d\Omega}{dt} = -k\left(\Omega^2 + \Omega_M^2\right) \qquad \textbf{(B.9)}$$

(it must be noted that in this case Ω_M is the rotor speed at which the aerodynamic torque equals the braking torque.)

which integrates to:

$$-kt\frac{\Omega_M}{I} = \tan^{-1}(\omega) + constant \qquad \textbf{(B.10)}$$

where:

$$\omega = \frac{\Omega}{\Omega_M} \tag{B.11}$$

the boundary conditions are $\Omega=\Omega_B$ at t=0, from which:

$$\begin{aligned} constant &= -\tan^{-1}(\omega_B) \\ \omega_B &= \frac{\Omega_B}{\Omega_M} \end{aligned} \tag{B.12}$$

then defining τ by:

$$\tau = \frac{k\Omega_M}{I}t \tag{B.13}$$

(B.10) becomes:

$$\begin{aligned} -\tau &= \tan^{-1}(\omega) - \tan^{-1}(\omega_B) \\ -\tau &= \tan^{-1}\left\{\frac{\omega - \omega_B}{1 + \omega\,\omega_B}\right\} \end{aligned} \tag{B.14}$$

from which:

$$\omega = \frac{\omega_B - \tan\tau}{\omega_B \tan\tau + 1} \tag{B.15}$$

This analysis hold only when the rotor brake is applied. With a freewheeling rotor Q=0), therefore $\Omega_M=0$ and the mathematics breaks down.

For zero braking torque a separate analysis is required. With zero braking torque, the equation of motion becomes:

$$I\frac{d\Omega}{dt} = -k\Omega^2 \tag{B.16}$$

which integrates to:

$$\frac{1}{\Omega} = \frac{kt}{I} + constant \tag{B.17}$$

if the rotor speed is Q_A when time t=0:

$$constant = \frac{1}{\Omega_A} \tag{B.18}$$

from which:

$$\frac{1}{\Omega} - \frac{1}{\Omega_A} = \frac{kt}{I} \tag{B.19}$$

which becomes after rearrangement:

$$\frac{\Omega}{\Omega_A} = \frac{1}{1+\bar{\omega}t} \qquad \bar{\omega} = \frac{k\Omega_A}{I} \tag{B.20}$$

Equations (B.15) and (B.20) are now used to define the rotor run down model.

The run down procedure is as follows:

At time t=0 the rotor is rotating at Ω_N when the engine power is cut and the rotor freewheels to a rotor speed of Q_B at time t_1. At this point, the rotor brake is applied and the rotor decelerates, stopping after a further time t_2.

Two possibilities exist:

(i) The profile drag coefficient, rotor blade data and rotor brake torque are specified and t_1, t_2 values are therefore determined.

(ii) The run down segment times t_1, t_2 are specified with the rotor blade data, and the profile drag coefficient and rotor brake torque are then calculated to provide the correct values for t_1 and t_2.

Procedure (i)

With the assumption of constant C_{D0} value:

$$Profile\ drag\ torque = \frac{1}{2}\rho N C_{D0}\int_0^R cr^3 dr\Omega^2 = k\Omega^2 \tag{B.21}$$

which gives:

$$k = \frac{1}{2}\rho N C_{D0}\int_0^R cr^3 dr$$
$$\Omega_M = \sqrt{\frac{Q_B}{k}} \qquad \textbf{(B.22)}$$

if the rotor is decelerating from normal operating rotor speed, i.e. $\Omega_A=\Omega_N$, then:

$$\overline{\omega} = \frac{k\Omega_N}{I} \qquad \textbf{(B.23)}$$

and for $\Omega_N \geq \Omega \geq \Omega_B$ *(brake off / freewheeling phase)*:

$$\Omega = \frac{\Omega_N}{1+\overline{\omega}t} \qquad \textbf{(B.24)}$$

for $\Omega_B \geq \Omega \geq 0$ *(brake on phase)*:

$$\omega_B = \frac{\Omega_B}{\Omega_M}$$
$$\tau = \frac{k\Omega_M}{I}(t-t_B) \qquad \textbf{(B.25)}$$

where t_B is the elapsed time when the rotor brake is applied and can be found by putting $\Omega=\Omega_B$ in equation (B.24).

Finally taking (B.15) and using (B.11) and (B.12) the following is obtained:

$$\Omega = \Omega_B\left(\frac{1-\frac{\tan\tau}{\omega_B}}{1+\omega_B\tan\tau}\right) \qquad \textbf{(B.26)}$$

Procedure (ii)

The actual calculations are identical, the difference in the methods is that the profile drag coefficient and rotor brake torque are now determined by the deceleration timing rather than being specified as input data.

t_1 is the time from engine shut down to when the rotor speed equals ΩB and the rotor brake is applied.

t_2 is the time from brake application ($\Omega=\Omega_B$) to the rotor actually stopping ($\Omega=0$). referring to (B.17):

(brake off phase)

$$\frac{1}{\Omega_B}-\frac{1}{\Omega_N}=\frac{kt_1}{I} \tag{B.27}$$

whence:

$$k=\frac{I}{\Omega_N t_1}\left(\frac{1}{n_B}-1\right) \tag{B.28}$$

where:

$$n_B=\frac{\Omega_B}{\Omega_N} \tag{B.29}$$

from (B.21), the required profile drag coefficient is given by:

$$C_{D0}=\frac{k}{\frac{1}{2}\rho N\int_0^R cr^3 dr} \tag{B.30}$$

(brake on phase)

referring to (B.15) and using the fact that $\Omega=0$ at $t=t_1+t_2$:

$$\begin{aligned}\omega_B &= \tan\tau \\ &= \tan\left(\frac{k\Omega_M}{I}t_2\right) \\ &= \frac{\Omega_B}{\Omega_M}\end{aligned} \tag{B.31}$$

if ω_N is defined:

$$\omega_N=\frac{\Omega_N}{\Omega_M} \tag{B.32}$$

(B.31) can be re-expressed as:

$$n_B \omega_N = \tan\left\{\frac{k\Omega_N t_2}{I} \cdot \frac{1}{\omega_N}\right\} \tag{B.33}$$

or:

$$\omega_N \tan^{-1}\{n_B \omega_N\} = \frac{k t_2 \Omega_N}{I} \tag{B.34}$$

(B.34) can be solved for ω_N and Newton Raphson has been used successfully.

Now:

$$\Omega_M = \frac{\Omega_N}{\omega_N} \tag{B.35}$$

whence the required rotor brake torque is given by:

$$Q_B = k\Omega_M^2 \tag{B.36}$$

As an example, Figure B.2 shows a typical result of the method.

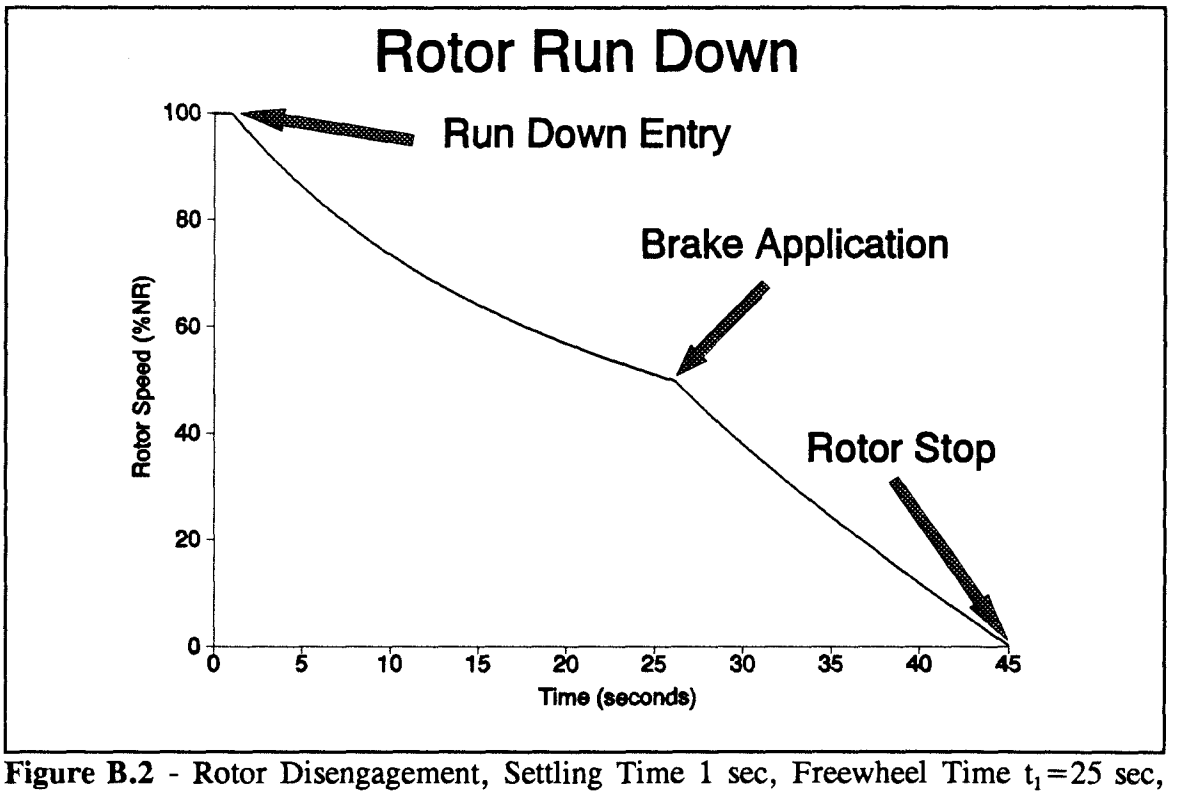

Figure B.2 - Rotor Disengagement, Settling Time 1 sec, Freewheel Time t_1=25 sec, Braking Time t_2=19 sec.

The commencement of the run down manoeuvre follows a 1 second settling period.

APPENDIX C

THE FOURTH ORDER RUNGE KUTTA METHOD APPLIED TO A SECOND ORDER DIFFERENTIAL EQUATION

The analysis outlined herein is derived from Hildebrand[34]

The equation to be solved is of the form:-

$$\frac{d^2y}{dx^2} = y'' = G(x,y,y') \tag{C.1}$$

From the point (x,y,y'), the marching increment terms are calculated thus:-

$$\begin{aligned} m_0 &= hG(x_n\ ,\ y_n\ ,\ y_n') \\ m_1 &= hG(x_n+\frac{1}{2}h\ ,\ y_n+\frac{1}{2}hy_n'\ ,\ y_n'+\frac{1}{2}m_0) \\ m_2 &= hG(x_n+\frac{1}{2}h\ ,\ y_n+\frac{1}{2}hy_n'+\frac{1}{4}hm_0\ ,\ y_n'+\frac{1}{2}m_1) \\ m_3 &= hG(x_n+h\ ,\ y_n+hy_n'+\frac{1}{2}hm_1\ ,\ y_n'+m_2) \end{aligned} \tag{C.2}$$

From which the variables are advanced with the following steps:-

$$\begin{aligned} x_{n+1} &= x_n+h \\ y_{n+1} &= y_n+hy_n'+\frac{h}{6}(m_0+m_1+m_2) \\ y_{n+1}' &= y_n'+\frac{1}{6}(m_0+2m_1+2m_2+m_3) \end{aligned} \tag{C.3}$$

APPENDIX D

RESOLUTION OF WIND TUNNEL VELOCITIES

D.1 INTRODUCTION

The following discussion outlines the wind tunnel data specification and the transformations and reflections necessary to use this data in the blade modal method.

D.2 LOCATION OF HOT WIRE MEASUREMENT POINTS

The wind data from the wind tunnel tests consists of three components aligned with the undisturbed freestream direction. The points are numbered as shown in Figure D.1:

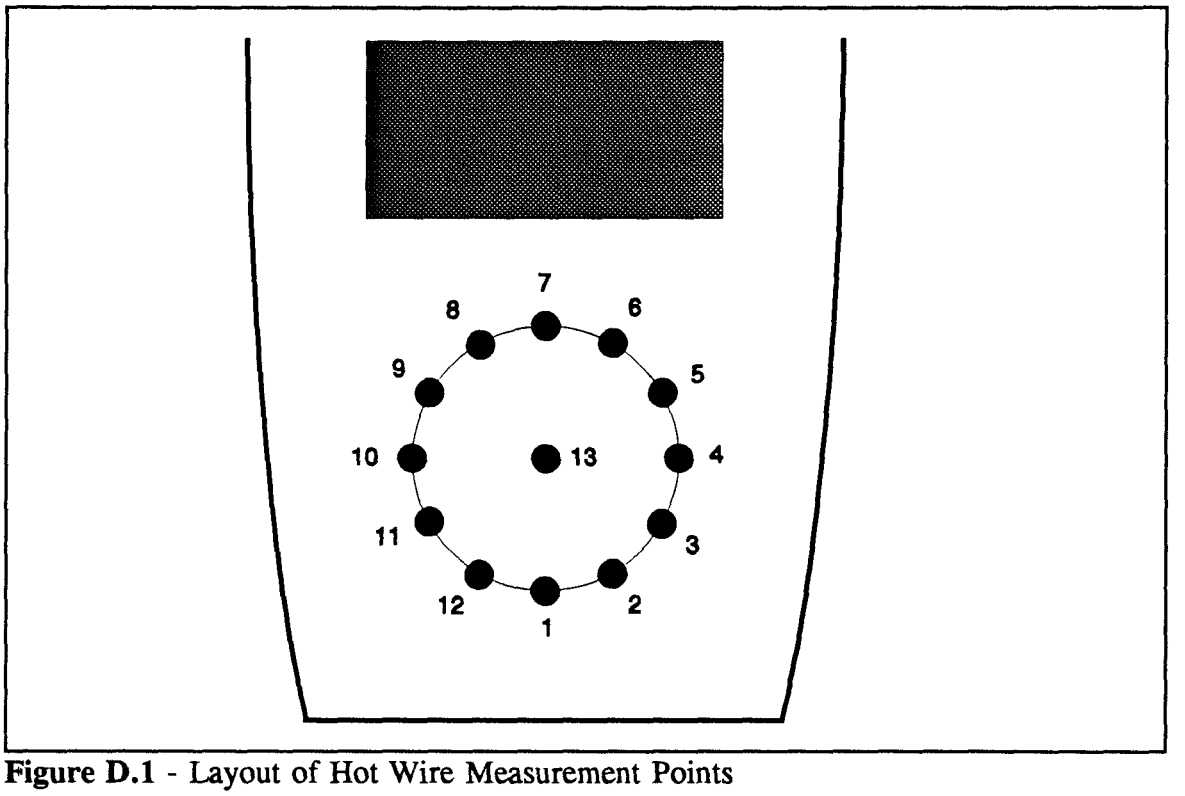

Figure D.1 - Layout of Hot Wire Measurement Points

Twelve of the points are laid out in an anticlockwise sense every 30° of azimuth with the remaining point at the centre. The radial distance between the 12 points and the 13th point (the rotor centre) is 75% of the scaled Lynx rotor radius. This radial location is a good representative point to describe the blade aerodynamics if only a single point is available. The 13 points are located vertically at the scaled height above the deck surface. The helicopter is assumed to be facing the bow of the ship.

D.3 WIND/SHIP ORIENTATION TRANSFORMATION

The wind tunnel tests were only performed for winds from the starboard direction.

Provision for winds coming from the port side are incorporated into the computer program. (The results of running the program have been limited to starboard winds only.) The transformation assumes the wind character is symmetric with respect to the ship's centreline and to obtain the port wind components requires a renumbering of the points. For all non ahead winds, resolution from wind tunnel to ship axes will be required. The convention is the wind from starboard. With reference to Figure D.2, for a point with such a wind the input data is as presented and needs no transformation.

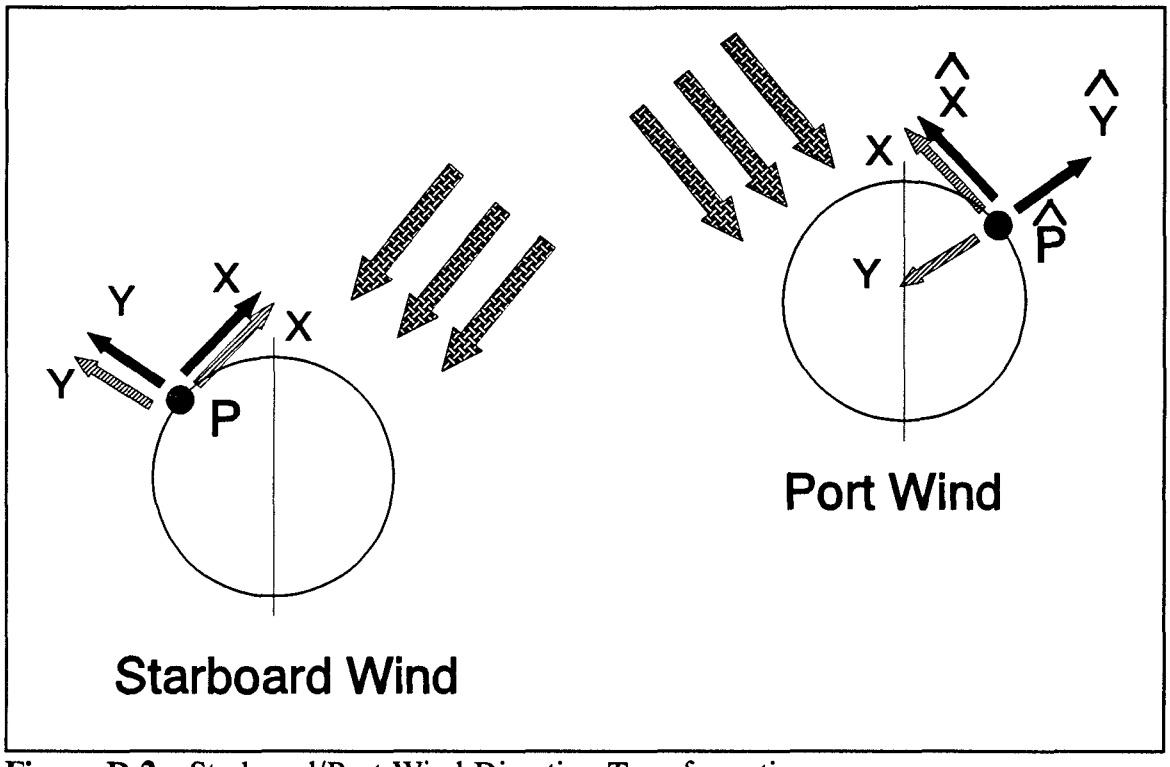

Figure D.2 - Starboard/Port Wind Direction Transformation

However, to cater for a wind from the port direction, a mirror image situation must be selected. Point P will now refer to P and the velocities X and Y become $\hat{X}$ and $\hat{Y}$. However, the axes system assumed at P and P is shown dashed.
Whence if the wind is required at $\hat{P}$ (for a port wind) then the velocities are:

$$\begin{aligned} \hat{U}_x^P &= U_x^P \\ \hat{U}_y^P &= -U_Y^P \end{aligned} \qquad \textbf{(D.1)}$$

the indices will require interchanging as given by:

$$i_p = 14 - \hat{i}_p \tag{D.2}$$

with the exception:

$$i_p = \hat{i}_p = 1 \tag{D.3}$$

D.4 RESOLVING VELOCITIES

Figure D.3 shows the orientation of the wind tunnel axes and the ship axes which is used in the program. The angle between the two axes systems is given by θ_W.

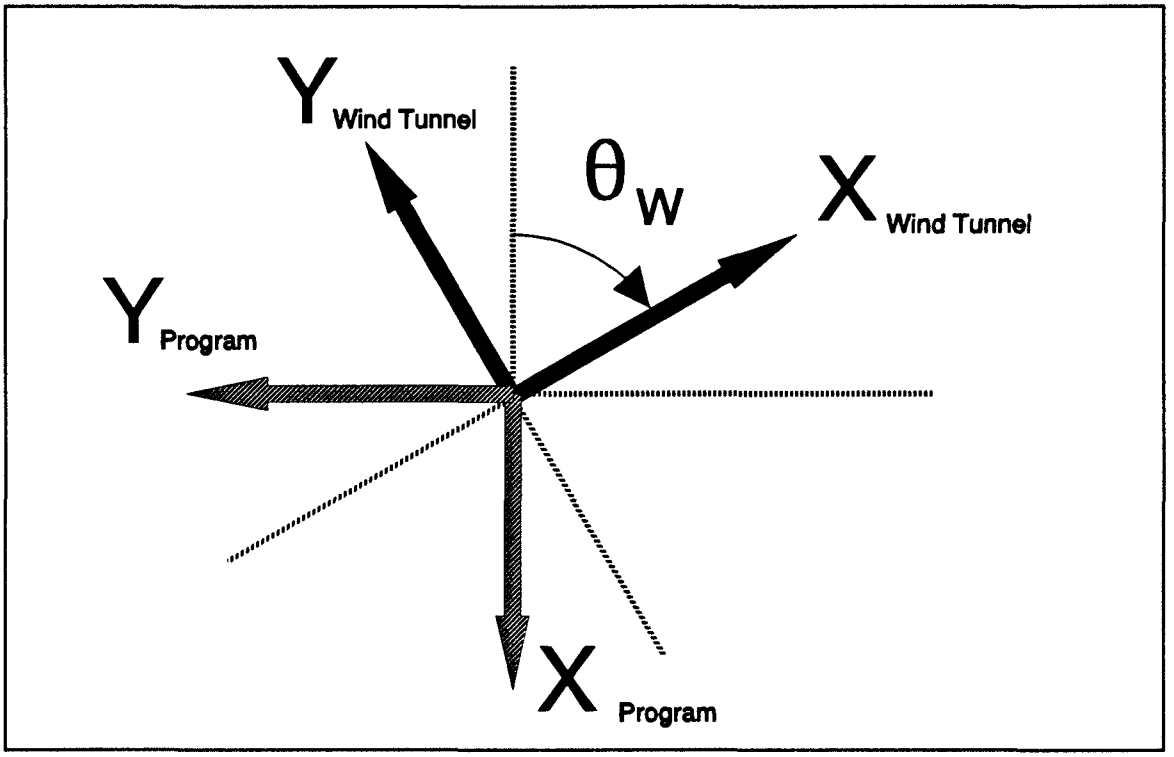

Figure D.3 - Axes for Resolving Wind Velocities from Wind Tunnel Axes to Ship Axes

The transformation between the two sets of axes is given by:

$$\begin{aligned} X_{PROG} &= -X_{WTT}\cos\theta_W - Y_{WTT}\sin\theta_W \\ Y_{PROG} &= -X_{WTT}\sin\theta_W + Y_{WTT}\cos\theta_W \end{aligned} \tag{D.4}$$

D.4 INTERPOLATING VELOCITIES

The three wind components at each of the 13 points are known at any instant of time. In order to establish those values for a general point of the rotor disc, interpolation is

required in both radial and azimuthal senses. For simplicity, a linear interpolation scheme is used.

The given azimuth is converted to the clock face numbering scheme and the wind component values at the radius of the circle defined by the measuring points can be determined by the interpolation. This data together with the values at the rotor centre enables a radial interpolation to be performed to give the values required at the point of the rotor disc in question.

The gust/wind is calculated at the given azimuth angle and radius; using ψ_D is the azimuth angle and r the radius, ψ_D is reduced to the range [0,360°] by:

$$\hat{\psi}_D = \psi_D - 360 \times int\left\{\frac{\psi_D}{360}\right\} \tag{D.5}$$

The azimuth angle $\hat{\psi}$ is converted to the numbering scheme on the clock face with 13 at the centre via:

$$\begin{aligned} \psi_N &= \frac{\hat{\psi}_D}{30} \\ \tilde{\psi}_N &= \psi_N + 1 \end{aligned} \tag{D.6}$$

The clock points either side are given by:

$$\begin{aligned} \psi_{N\ lower} &= int(\psi_N) + 1 \\ &= int(\tilde{\psi}_N) \\ \psi_{N\ upper} &= \psi_{N\ lower} + 1 \end{aligned} \tag{D.7}$$

with the special case of:

$$\begin{aligned} &if \quad \psi_{N\ lower} = 12 \\ &then \quad \psi_{N\ upper} = 1 \end{aligned} \tag{D.8}$$

we thus have the following situation, with reference to Figure D.4:

$$\begin{aligned} D\psi_{NL} &= \tilde{\psi} - \psi_{N\ lower} \\ D\psi_{NU} &= 1 - D\psi_{NL} \end{aligned} \tag{D.9}$$

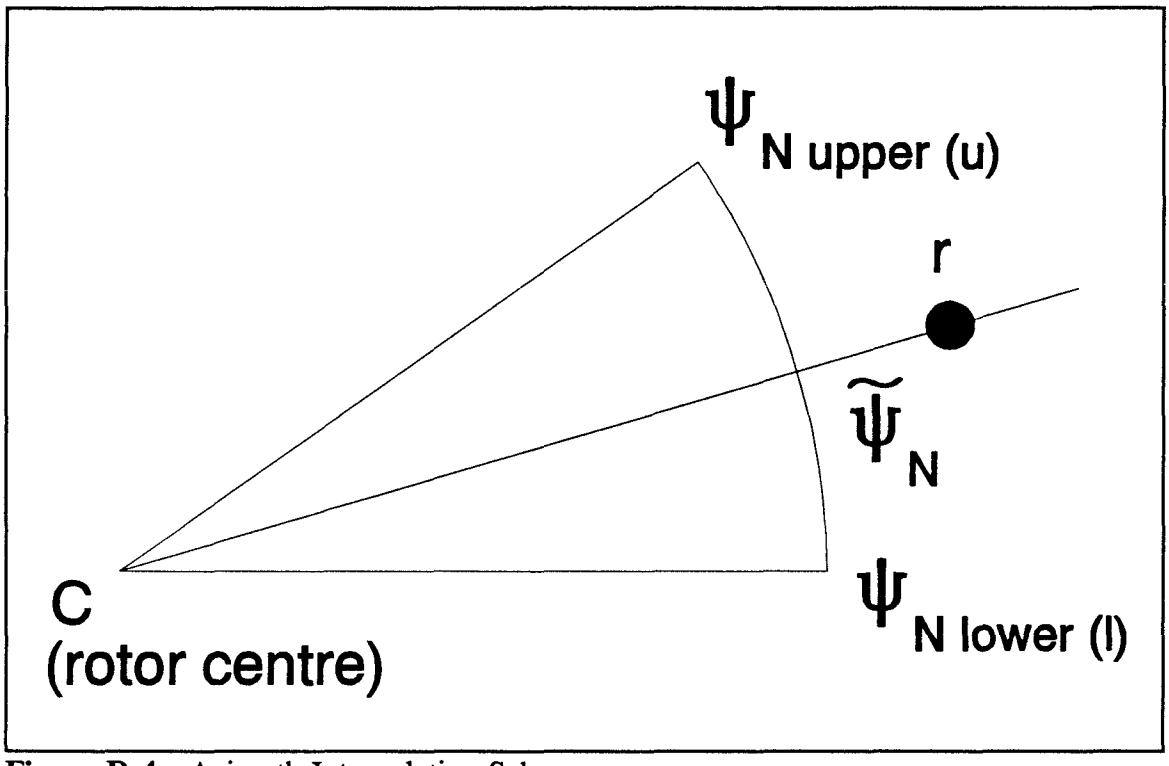

Figure D.4 - Azimuth Interpolation Scheme

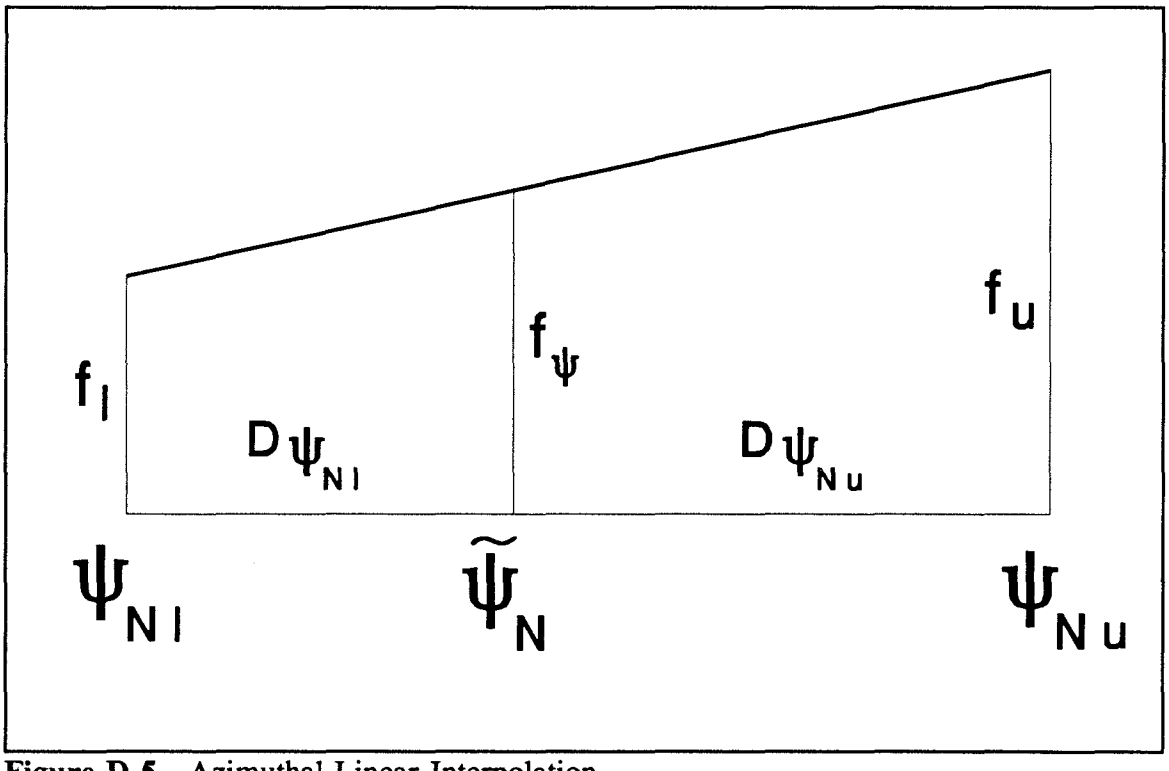

Figure D.5 - Azimuthal Linear Interpolation

Then, with reference to Figure D.5, the quantities at $\psi_{N\ lower}$ and $\psi_{N\ upper}$ are interpolated to ψ_N by:

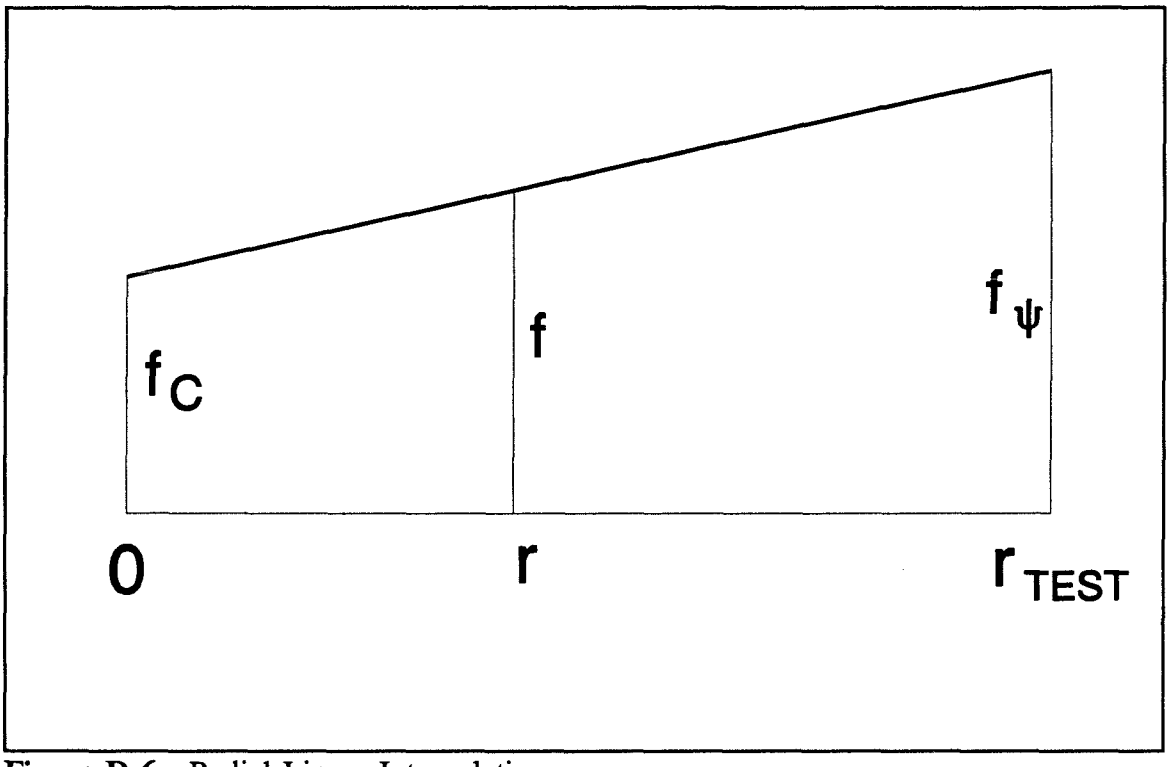

Figure D.6 - Radial Linear Interpolation

$$f_{\psi N} = f_u D\psi_{Nl} + f_l D\psi_{Nu} \tag{D.10}$$

which is equivalent to a linear interpolation via:

$$\begin{aligned} f_\psi - f_l &= \left\{\frac{f_u - f_l}{D\psi_{Nl} + D\psi_{Nu}}\right\}(\psi_N - \psi_{Nl}) \\ f_\psi &= f_l + (f_u - f_l) D\psi_{Nl} \\ &= f_u \cdot D\psi_{Nl} + f_l \cdot D\psi_{Nu} \end{aligned} \tag{D.11}$$

Having obtained the value at r_{test} rotor radius and correct azimuth we now wish to interpolate radially.

Using Figure D.6 we have:

$$\begin{aligned} f - f_C &= \left\{\frac{f_\psi - f_C}{r_{test}}\right\} r \\ f &= \frac{f_C r_{test} + (f_\psi - f_C) r}{r_{test}} \\ &= \frac{f_\psi r + f_C (r_{test} - r)}{r_{test}} \end{aligned} \tag{D.12}$$

combining the two linear interpolations gives finally:

$$f = \frac{(f_u D\psi_{Nl} + f_l D\psi_{Nu})r + f_C(r_{test} - r)}{r_{test}} \qquad \textbf{(D.13)}$$

D.6 RE-CREATING WIND TUNNEL VELOCITY TIME HISTORIES

The method used implements a random number generator routine which produces a Gaussian (or normal) distribution for a specified mean and standard deviation.

The wind tunnel data in question was processed to give a mean value and standard deviation for all three velocity components at each of the 13 measuring points. From this data the component values were recreated using the random number routine. The values are reset every time the routine is called. The frequency of updating the wind velocity model must be geared to the correctly scaled frequency of the velocity excursions. The basic hot wire output used to assess the accuracy of the model consists of 1000 samples, at a rate of 1kHz, thus representing a model scale time period of 1 sec. To convert that to a representative full scale time period, constancy of Strouhal number is used.

The Strouhal number, S, is defined by:

$$S = \frac{fl}{V} \qquad \textbf{(D.14)}$$

where f is the frequency
1 is the length
V is the velocity

If suffix F refers to full scale and M to model scale the following applies:

$$f_F \frac{l_F}{V_F} = f_M \frac{l_M}{V_M}$$
$$f_F = f_M \left\{\frac{V_F}{V_M}\right\} \cdot \left\{\frac{l_M}{l_F}\right\} \qquad \textbf{(D.15)}$$

The wind tunnel model is 1/120th scale, the wind tunnel speed is 20 m/s. So if a full scale wind speed of 50 knots is used then:

$$f_F = \frac{1}{100} f_M \tag{D.16}$$

in which case the full scale timebase is 100 times the model scale, i.e. the above 1000 samples represents 100 seconds at full scale.

The methods of assessing the validity of the time history recreation was to compare, subjectively, the actual time history of a predominant wind component with a history produced by the routine. (This was a NAG routine for the first analysis, although the later versions of the program uses a random number generator given in Press et al[35].) A possible time expansion/compression was allowed for and the most faithful reproduction was obtained with the synthesis being updated at one half of the frequency of the model data. The comparison of this situation is shown in Figure 2.4 of Newman & Hurst[7]. This corresponds to 500 updates reflecting 100 seconds. In other words each update should be every 0.2 of a second. If δt is the time step (in seconds) for the Runge Kutta routine, then the wind model will need to be updated every:

$$\frac{1}{5\delta t} \tag{D.17}$$

passes round the loop. For the program runs $\delta t = 0.01$ sec whence the updates will need to occur every 20 passes.

REFERENCES

1. Newman. Simon, **The Foundations of Helicopter Flight**, Edward Arnold, April 1994.
2. Burton. K.W., **Blade Sailing**, Dynamics Dept. Report 146N, Westland Helicopters Ltd., March 1978.
3. Newman. S.J., **A Theoretical Model for Predicting the Blade Sailing Behaviour of a Semi-Rigid Rotor Helicopter**, Paper 47, 15th European Rotorcraft Forum, Amsterdam, 1989
4. Newman. S.J., **A Theoretical Model For Predicting The Blade Sailing Behaviour Of A Semi Rigid Rotor Helicopter**, Vertica Vol 14, No.4, pp 531-544, 1990
5. Newman. S.J., **The Application of a Theoretical Blade Sailing Model to Predict the Behaviour of Articulated Helicopter Rotors**, Journal of The Royal Aeronautical Society, June/July 1992
6. Newman. S.J. and Hurst. D.W., **Helicopter Blade Sailing Characteristics**, Final Report, AASU Memo 86/4 February 1986
7. Hurst. D.W. and Newman. S.J., **Wind Tunnel Measurements of Ship Induced Turbulence and the Prediction of Helicopter Rotor Blade Response**, Vertica Vol 12, No.3, pp 267-278, 1988
8. Newman. S.J. and Hurst. D.W., **Wind Tunnel Measurements of Ship Induced Turbulence and the Prediction of Helicopter Rotor Blade Response**, Paper 3, The Royal Aeronautical Society/The Royal Institute of Naval Architects Symposium on Helicopters and the Marine Environment. London, 1982
9. Hurst. D.W. & Newman. S.J., **Wind Tunnel Measurements of Ship Induced Turbulence and the Prediction of Helicopter Rotor Blade Response**, Paper 99, 11th European Rotorcraft Forum,, London, September 1985
10. Porteous. T.C., **Commercial Chinook - First Year of Operation**, Paper 5, Proceedings of the Twenty - Sixth Symposium, Society of Experimental Test Pilots Sept 1982
11. Carico. D., McCallum, Lt Cdr K.E., Higman. J., **Dynamic Interface Flight Test and Simulation Limitations**, Paper 100, 11th European Rotorcraft Forum,, London, September 1985
12. Hofman. C.F.G.M. and Fang. R., **Determination of Limitations for Helicopter**

Ship-Borne Operations, Paper 79, 10th European Rotorcraft Forum, The Hague 1984

13. Roades M.M. and Val Healey. J., **Flight Deck Aerodynamics of a Non Aviation Ship**, Journal of Aircraft, Vol. 29, No. 4, July-Aug 1992
14. Johnston. J.B.B., **The Operation of Helicopters from Small Ships**, R.A.E. Tech. Memo. Aero 1348, Aug 1971
15. Johns. M.K. and Healey. J.V., **The Airwake of a DD-963 Class Destroyer**, Naval Engineers Journal, Vol 101, No. 3, May 1989, pp 36-42.
16. Narveson. M.L., **Flow Modification over a Backward Facing Step**, Naval Postgraduate School, Monterey, California. NPS AD-A241 351, September 1990.
17. Healey. J.V., **Simulating the Helicopter/Ship Interface as an Alternative to Current Methods of Determining Safe Operating Envelopes**, Naval Postgraduate School, Monterey, California. NPS 67-86-003, September 1986.
18. Woolman .S.G., **Control of Flow over a Backward Facing Step**, Naval Postgraduate School, Monterey, California. NPS AD-A238 638, September 1990.
19. Moran R.D., **Simulation of a Rotorcraft in Turbulent Flows**, Naval Postgraduate School, Monterey, California. NPS AD-A245 742, September 1991.
20. Lloyd. A.R.J.M., **Ship Motions, Wind and the Helicopter**, Paper 2, Royal Aeronautical Society/ Royal Institute of Naval Architects Symposium on "Helicopters and the Marine Environment", 2nd June 1982
21. Val Healey. J., **Establishing a Database for Flight in the Wakes of Structures**, Journal of Aircraft, Vol. 29, No. 4, July-Aug 1992
22. Healey. J.V., **The Prospects for Simulating the Helicopter/Ship Interface**, Naval Engineers Journal, Vol 99, No. 2, 1967, pp 45-63
23. Renirie. L.T. & Hoekstra. Tj., **Helicopter - Ship Qualification Testing**, Fifth European Rotorcraft and Powered Lift Aircraft Forum, Amsterdam 1979
24. Newman. S.J., **A Wind Tunnel Investigation into the Blade Sailing Behaviour of a Model Teetering Rotor Operating from the Simulated Flight Deck of a Rover Class Royal Fleet Auxiliary Vessel**, AASU 91/2, September 1991
25. Newman. S.J., **A Continuation of the Wind Tunnel Investigation into the Blade Sailing Behaviour of a Model Teetering Rotor Operating from the**

Simulated Flight Deck of a Rover Class Royal Fleet Auxiliary Vessel, AASU 93/1, January 1993

26. Newman. S.J., **The Wind Tunnel Investigation into the Blade Sailing Behaviour of a Model Teetering Rotor Operating from the Simulated Flight Deck of a Rover Class Royal Fleet Auxiliary Vessel**, Final Report, AASU 94/6, August 1994
27. Newman. S.J., **An Investigation into the Phenomenon of Helicopter Blade Sailing**, The Institute of Mathematics and its Applications/ The Royal Aeronautical Society Conference on Aerospace Vehicle Dynamics and Control. Cranfield Institute of Technology, September 1992.
28. Newman. S.J., **An Investigation into the Phenomenon of Helicopter Blade Sailing**, pp 225-244, Proceedings of the Conference on Aerospace Vehicle Dynamics and Control. The Institute of Mathematics and its Applications Conference Series No. 47, 1994.
29. Newman. S.J., **The Problems of Rotor Engagement and Disengagement of a Shipborne Helicopter**, Journal of Naval Science, Volume 20, No. 1, pp 56-64, 1994
30. Newman. S.J., **A Theoretical and Experimental Investigation into the Rotor Blade Aeroelastic Behaviour of a Shipborne Helicopter during Rotor Engagement and Braking**, Paper 32, 75th AGARD Fluid Dynamics Panel Meeting, Aerodynamics and Aeroacoustics of Rotorcraft, Berlin 1994.
31. Newman. S.J., **The Verification of a Theoretical Helicopter Rotor Blade Sailing Method by means of Wind Tunnel Testing**, S.J. Newman, submitted to The Journal of The Royal Aeronautical Society, *expecting publication 1995.*
32. Willmer. M.A.P., **The Motion of Helicopter Blades at Low Rotor Speeds in High Winds**, Royal Aircraft Establishment (Bedford), Technical Memorandum No. Naval 181, September 1963.
33. King. S.P., **An Analytical Investigation of Blade Sailing**, Dynamics Dept. Report 214N, Westland Helicopters Ltd., January 1981.
34. Hildebrand. F.B., **Introduction to Numerical Analysis**, McGraw-Hill, 1956
35. Press. W.H., Flannery. B.P., Teukolsky. S.A. and Vetterling. W.T., **Numerical Recipes - The art of scientific computing**, Cambridge University Press 1986.

36. Beddoes. T.S., **An Analytical Model for Trailing Edge Stall**, RP 637, Westland Helicopters Ltd., April 1981.

37. Schafer. J., **Basic Helicopter Maintenance**, International Aviation Publishers, Inc., 1980

38. Leone. P.F., **Analytic Correlation with Mishap Report of a CH46D Aft Rotor Blade Tunnel Strike Induced by a Wind Flow up through the Aft Rotor Disk During a Startup Operation while Shipboard at Sea**, Boeing Vertol Company, IOM 8-7450-PFL-06, April 21, 1982

39. Leone. P.F., **Theoretical and Experimental Study of the Flap Droop Stop Impact Transient Aero Elastic Response of a Helicopter Rotor Blade**, Journal of the American Helicopter Society, Vol 9, Jan 1964

40. Piercy. N.A.V., **Aerodynamics**, The English Universities Press Ltd., 1937

41. Townson. G., **Autogiro, The Story of the Windmill Plane**, Aero Publishers Inc., 1985

42 **H-46 Tunnel Strike Mishap History**, Inter Office Memo. 107, April 1983